SEPARATION OF SUCCINIC ACID FROM FERMENTATION BROTHS AND ESTERIFICATION BY A REACTIVE DISTILLATION METHOD

By

Alvaro Orjuela Londono

A DISSERTATION

Submitted to
Michigan State University
in partial fulfillment of the requirements
for the degree of

DOCTOR OF PHILOSOPHY

Chemical Engineering

2010

ABSTRACT

SEPARATION OF SUCCINIC ACID FROM FERMENTATION BROTHS AND ESTERIFICATION BY A REACTIVE DISTILLATION METHOD

By

Alvaro Orjuela Londoño

Because of the scarcity of fossil resources, high crude oil prices, and the environmental benefit of using renewable feedstock, fermentation technologies applied to the production of chemicals have arisen as a feasible alternative to traditional processes. One of the most promising commodities in the chemical industry is succinic acid, which currently has a market of over \$0.4 billion per year and the potential to increase up to \$1.3 billion per year. Petrochemical derived succinic acid has a lower production price (\$1.05 to 1.29 US/Kg) compared with that derived by fermentation (\$1.66 to 2.2 US/Kg, sold at \$5-9 US/Kg). Therefore, efforts must be done to decrease processing costs in bio-based succinic acid production.

Owing to the majority of processing costs in fermentation are accounted for the separation and purification of the desired product (50 - 80% of the final cost), many attempts to improve and reduce separation steps have been made, but to date there is not a successful technology scaled up to industrial production. Despite the fact that several separation processes have been proposed to overcome this problem (precipitation, ion exchange resins, membranes, reactive extraction, and liquid-liquid extraction), none addresses the main limiting barriers of large energy and material requirements as well as waste generation.

One of the most promising alternatives is the direct conversion of succinic acid to esters using hybrid reactors, mainly reactive distillation. This process has shown remarkable

advantages in similar applications (i.e. acetates production, ethyl lactate, fatty acids, etc.) by reducing processing costs, and could provide esters as intermediate products for the synthesis of other chemicals from succinic acid. Although this is a well understood technology, research focused on the performance of the operation for succinic acid compounds must be conducted, in order to create the tools required for design and scale up to large scale production.

In this work a recovery process of succinic acid through esterification with ethanol is studied. Although it is particularly applied for succinic acid, this approach could be used for other acids and alcohols.

In the first part an experimental study on phase equilibria of esterification mixtures and reaction kinetics is presented.

In a second stage, succinic salts are recovered by precipitation and esterification using synthetic and actual culture broth mixtures. Recovery of succinic species higher than 90% was obtained.

In a next stage, experiments on esterification using a pilot plant reactive distillation column proved that high conversion of succinic acid (> 98%) and high selectivity to diethyl succinate (>98%) can be obtained. Simulations of reactive distillation unit using Aspen plus process design software (Version 7.1, AspenTech) were validated using pilot scale experiments. Good agreement of the model was observed.

Finally, using the model previously developed, a complete conceptual design of a process for the recovery of succinic acid from a fermentation broth was developed in Aspen Plus including a preliminary economic study. Results indicated that the process is feasible under different conditions. Economic analysis indicates that the process is a feasible alternative to compete with current technologies for succinic acid recovery.

Dedicated to my beloved Angélica, my family, my dear friends and all the people who supported me in this effort. This work is the product of many hands and thoughts in collective construction.

ACKNOWLEDGMENTS

I would like to thank Dr. Dennis J. Miller and Dr. Carl T. Lira for their guidance as my advisors through my Ph. D. studies. I am especially grateful for their unconditional support, trust and friendship during all these years, and also for giving me the opportunity to work in their group. I also wish to thank Dr. Martin Hawley, Dr. Kris Berglund and Dr. Chris Saffron for serving on my committee. Special thanks to Dr. Lars Peereboom and Dr. Aspi Kolah without whom this work would not have been possible. Thanks to my sister Andrea who gave me a hand to reach the last step. I am also grateful with Michigan Biotechnology Institute (MBI) at MSU and Working Bugs ™ for providing fermentation samples.

I want to extent my appreciation for my group colleagues and future doctors Krishna Sai, Abu Hassan and Xi Hong. Also I thank all undergraduate students for their assistance: Jonathan Evans, Peter K. Rossman, Nathan Hanna, and especially to my friend Abraham J. Yanez.

I would like to express gratitude for financial and administrative support of my sponsors: Fulbright Commission, the Colombian Administrative Department of Science, Technology and Innovation (COLCIENCIAS), the Colombian National Planning Department (DNP), and specially the National University of Colombia (Universidad Nacional de Colombia, Bogota).

Special thanks to all my family, friends, classmates, and all members of the Latin American Community at MSU for their help, support, good moments and unconditional love. Thanks to Cerati, Robi Draco, and Pearl Jam for providing the perfect sound track. Thanks also to all staff members of the MSU Chemical Engineering Department. And finally, I want to thank my beloved Angelica for supporting me at every moment, for having me in her thoughts and prayers, for being my partner in this trip.

PREFACE

Succinic acid (1,4-butanedioic acid), a four-carbon dicarboxylic acid, is recognized as a potential bio-based substitute for petrochemical-derived maleic anhydride as a major commodity for the synthesis of many chemicals of commercial interest. However, current prices of succinic acid obtained by fermentation are higher than those achieved using the maleic anhydride petrochemical pathway.

Several alternatives have been proposed to recover succinic acid form fermentation media: extraction with amines and/or solvents, ion exchange, membrane separation, electro-dialysis, adsorption with solids, precipitation and other techniques. None of them have overcome major challenges associated with intensive energy and materials consumption and waste generation.

Taking into account that succinic acid derivatives of commercial interest can also be produced from succinate esters, this project presents a new recovery process that by-passes succinic acid purification and produces succinate esters directly as major products. This novel process comprises reactive extraction of succinate salts obtained from the broth by esterification with ethanol (or other alcohol) followed by a reactive distillation unit to drive the reaction to completion.

As outcomes of this study, several contributions have been made to the field of downstream processing of products obtained by fermentation. Among them we can recognize:

- Development of a new recovery process for recovery of succinic acid by reactive extraction and reactive distillation.

- Experimental evaluation of vapor-liquid, liquid-liquid and solid-liquid equilibria data for binary and ternary mixtures including succinate species.
- Generation of thermodynamic models to accurately describe phase equilibria required for modeling of the recovery process.
- Development of complete activity-based and mole-fraction based kinetic models to describe esterification of mixed succinic acid and acetic acid with ethanol using an ion exchange resin as catalyst.
- Experimental evaluation and computational modeling of a pilot-plant scale reactive distillation unit for esterification of mixed succinic acid and acetic acid with ethanol.
- Conceptual design and modeling of the complete recovery process including preliminary economic evaluation.

This document is divided in four main sections which follow the path from conception to economic evalutation. The major steps include measurement of the mixture properties and reaction kinetics, development of a recovery scheme, preliminary process, evaluation in a pilot-scale column, validation of the operation using process simulation and then economic evalutation. Chapters 1 to 4 in Part 1 describe experimental evaluation of phase equilibria in mixtures containing succinate species, and development of thermodynamic models to describe non-idealities observed in reactive mixtures studied. Also in Part 1, Chapter 5 describes kinetic models for esterification of mixed succinic acid and acetic acid with ethanol. All this fundamental information is used in modeling developed in subsequent chapters.

Chapter 6 of Part 2 describes the novel recovery process developed to retrieve succinic acid from fermentation broths by reactive extraction with ethanol.

Chapters 7 and 8 of Part 3 describe experiments on a pilot plant scale reactive distillation unit for esterification of mixed succinic and acetic acid with ethanol. Additionally, computational models are developed and validated against experimental results using process design software (Aspen Plus®).

Finally chapter 9 included in Part 4 depicts the complete conceptual design of the process including reactive extraction and reactive distillation stages, and a preliminary economic evaluation of the technology is presented.

TABLE OF CONTENTS

LIST OF TABLES

LIST OF FIGURES

PART 1: PHASE EQUILIBRIA AND CHEMICAL KINETICS

Included in this section is a copy of the paper: Phase equilibria for reactive distillation of diethyl succinate. Part I. System diethyl succinate + ethanol + water, by A. Orjuela, A. J. Yanez, D. T. Vu, D. Bernard-Brunel, D. J. Miller, C. T. Lira. Published in Fluid Phase Equilibria, 290 (1-2) (2010) 63-67.

The paper is reformatted and figures and tables are enlarged to fulfill edition requirements for the dissertation document.

1. Phase equilibria for reactive distillation of diethyl succinate. Part I. System diethyl succinate + ethanol + water

1.1 Summary

Liquid-liquid equilibrium data for the ternary system water-ethanol-diethyl succinate were measured at 303.15 K and 313.15 K and atmospheric pressure. The reliability of the LLE data was confirmed using the Othmer-Tobias correlation. *P-x* data for the vapor-liquid equilibrium for the binary system ethanol-diethyl succinate at 323.15 K and ethanol + water at 101.3 kPa were also measured. Data were fitted using the modified UNIQUAC and NRTL equations for the liquid phase and the Hayden-O'Connell (HOC) equation for the vapor phase. The models agree reasonably well with the experimental data and can predict reported azeotropic conditions. The NRTL-HOC is capable of fitting the LLE data better than the UNIQUAC-HOC.

1.2 Introduction

Processes to recover carboxylic acids from fermentation broths have been studied for many years in order to reduce separation costs, which in general account for 50 - 80% of the final cost of commercial chemical processes [1-3]. Amongst carboxylic acids available by fermentation, succinic acid and its derivatives have enormous potential as commodities in the chemical market [1-5]. Diethyl succinate (DES) is used as a solvent, as an additive in fragrance formulation, as chemical intermediate and even as an additive for biodiesel and if produced economically could be a future route to PBS polymers. Succinates and other dibasic esters can be used as green solvents to extract carboxylic acids (i.e. acetic) even succinic acid from dilute solutions [9-17]. DES is currently produced by direct esterification of the acid or anhydride with ethanol. Several alternatives to recover succinic acid from dilute aqueous solutions have been proposed, primarily solvent-amine extraction, salt precipitation, membrane separation and ion exchange. Esterification of diluted solutions has gained attention because direct recovery and production of derivatives is accomplished. However, esterification extend is limited by chemical equilibrium, and product separation is required to drive the reaction forward.

Reactive distillation is an emerging technology with significant commercial potential for a wide range of bio-based ester manufacturing [6-8]. Because reactive distillation integrates the reaction and separation into a common process unit, significant thermodynamic data are needed for process design, but the resulting process is significantly more economical than a conventional reactor/separator system. Diethyl succinate exhibits a heteroazeotrope with water and thus reliable thermodynamic models must be of representing both liquid-liquid equilibrium (LLE) and vapor-liquid equilibrium (VLE). Published efforts to utilize generalized group contribution methods are unreliable in predicting experimental data for DES systems [13, 14] justifying the need for experimental measurements and correlation. The traditional approach of extending binary measurements to multicomponent VLLE systems remains challenging. Quantitative models of multicomponent mixtures predicted from fitted binary VLE data must be adjusted to simultaneously represent multicomponent VLE and LLE [18-20]. In this study experimental LLE data for the systems diethyl succinate + ethanol + water, and VLE data for the system diethyl succinate + ethanol were obtained. These data, together with others reported in the open literature were correlated with a modified UNIQUAC equation [18] and the NRTL equation [21] using a regression tool included in Aspen Plus®. A comparison with predictions using UNIFAC [22, 23] is also shown.

1.3 Materials and methods

1.3.1 Materials

Diethyl succinate (DES, 99%, Sigma-Aldrich), ethanol (EtOH, 200 proof, Decon Labs), water (H_2O, HPLC grade, J.T. Baker), *n*-butanol (99.9%, Mallinckrodt), and acetonitrile (HPLC grade, EMD). Traces of methyl red (Reagent grade, EM science) were used to enhance observation of the liquid-liquid interface during LLE measurements. The stated chemical purities of solvents were confirmed using gas chromatography and Karl-Fischer titration using Hydranal-coulomat E solution (Riedel-de Haën). The only impurities detected were traces of water. The chemicals were used without further purification for LLE. For VLE, the ethanol was dried using $CaCl_2$. For VLE, DES was purified by vacuum distillation. Only 85-90 % of the pre-distilled volume was used for the experiments, discarding the first overhead fraction (5-10 %) and the reboiler residue (5 %).

1.4 Experimental procedures

1.4.1 Experimental procedures for LLE

LLE data for ternary mixtures were determined on a mass basis, using glass vials (10 cm^3) stirred with magnetic bar. These vials were placed in an isothermal bath equipped with a circulator pump and temperature control (Isotemp immersion circulator 730, Fisher Scientific, ± 0.1 K). The temperature was measured with an ASTM certified glass thermometer (model 64 C, ± 0.1 K). The total mass for all the experiments was about 10g. Experiments were performed to measure the tie lines and separate experiments were performed to locate a wider range of binodal points.

1.4.2 LLE Tie Lines

Equilibrium tie lines were obtained by preparing ternary mixtures of known overall composition within in the two phase region. The liquid mixtures were stirred at constant temperature for 12 h. After equilibration the vial was centrifuged for 20 minutes at 4000 rpm and returned to the isothermal bath for 12 more hours without stirring. The bottom phase was removed with a syringe and the weight of every phase was recorded. After analysis, the recovered masses were compared to the initial masses and the difference was less than 1% (mass) for all the experiments. Both phases were analyzed for each experiment. The H_2O + EtOH + DES system was measured at 303.15 K and 313.15 K (± 0.1 K).

1.4.3 Binodal Curve

The binodal envelope was measured at 303.15 K and 313.15 K (± 0.1 K) to confirm the tie line measurements. Fixed amounts of binary mixtures of H_2O + DES and EtOH + H_2O were prepared gravimetrically using an analytical balance (Sartorius R 300 S, ± 0.1 mg). Weighted amounts of EtOH or DES were added in stages to each binary mixture using a syringe (0.1 cm^3). After every addition the mixture was stirred for 10 minutes and checked for the phase boundary. In order to enhance visual observation of the two phases, traces of methyl red were added to the mixture. The organic phase preferentially dissolves methyl red causing the ester-rich phase to have an orange color and the aqueous phase remained colorless or slightly red. Accuracy of this method to measure binodal lines within 1% (mass) was reported in a previous work [24].

1.4.4 Experimental procedures for VLE

P-x experiments were carried out using the apparatus and analytical methods described in detail by Vu *et al.* [25, 26]. The equilibrium pressure was measured using a Baratron® model

PDR 2000 (MKS instruments). To assure degassing, after the initial pressure stabilized, the pressure was lowered to approximately half the equilibrium pressure and the vacuum valve was closed and the equilibrium pressure re-stabilized. Following re-equilibration, variations in pressure of ± 0.2 kPa in between repetitions were considered acceptable. Reported pressure is an average of three measurements obtained for every composition. Isothermal VLE of the DES-EtOH were measured at 323.15 K (± 0.05 K).

T-*x*-*y* data for the binary EtOH + H_2O were measured in a recirculating apparatus (Fischer America VLE 100D, Inc.). Temperature measurements were within ± 0.05K and pressure control was within ± 0.1 kPa. Though data for this system are plentiful, this system was measured to validate the apparatus and methods which will be used in subsequent studies.

1.5 Analysis

Samples from VLE experiments on the systems DES + EtOH and EtOH + H_2O were analyzed as described in [25]. LLE samples were analyzed using a gas chromatograph (HP 5890 series II), equipped with a thermal conductivity detector, *n*-butanol was used as internal standard and acetonitrile as solvent. A 15 m long Alltech EC-WAX column (0.53 mm i.d., 1.20 µm Film thickness) was used with a temperature programmed analysis: Column initial temperature 313.15 K (3 min), ramp rate 30 K/min, final temperature 523.15 K (0.5 min). The injection port was maintained at 543.15 K in a splitless mode. Detector temperature was 523.15 K. Helium was used as carrier (0.25 cm^3/s) and volume injections of 5×10^{-4} cm^3 were used. Samples of known composition in the range of interest were used for calibration, and injected by triplicate to obtain repeatability within 0.5% by mass. Data integration was done using a Peaksimple

Chromatography Data System (SRI Model 302) with Peaksimple software version 3.59. Karl-Fisher analysis (Aquacount coulometric titrator AQ-2100) was used to measure and confirm water content in reagents and samples.

1.6 Results and discussion

1.6.1 Experimental Results

LLE experimental data for the system H_2O + EtOH + DES are listed in Table 1-1 (tie lines) and Table 1-2 (binodal curve) where w_i represents mass fraction of each component. These data agree well with data trends reported at 297 K [24].

Table 1-1. Tie lines compositions for H_2O + EtOH + DES in weight fractions.

	Aqueous Phase (Aq.)			**Organic Phase (Org.)**		
***T* (K)**	**w EtOH**	**w H2O**	**w DES**	**w EtOH**	**w H2O**	**w DES**
303.15	0.145	0.822	0.033	0.051	0.044	0.905
	0.202	0.749	0.049	0.089	0.071	0.840
	0.236	0.693	0.071	0.144	0.098	0.758
	0.260	0.641	0.099	0.161	0.134	0.705
	0.281	0.587	0.132	0.197	0.157	0.646
	0.280	0.580	0.140	0.212	0.171	0.617
313.15	0.031	0.950	0.019	0.021	0.032	0.947
	0.060	0.894	0.046	0.051	0.049	0.900
	0.128	0.837	0.035	0.096	0.076	0.828
	0.184	0.758	0.058	0.119	0.104	0.777

As expected, the area of phase splitting is reduced as temperature and ethanol concentration increase. The consistency of LLE data was checked with the Othmer-Tobias method [27] as shown in Figure 1-1, and a linear relation was obtained at both temperatures. *P-x* data for the binary EtOH + DES are listed in Table 1-3. Previously [25] the lab was able to measure the vapor composition in the static apparatus. However, due to the low volatility of DES the vapor sampling was not used in this work.

Table 1-2. Binodal curve data for H_2O + EtOH + DES in weight fractions.

T = 303.15 K			T = 313.15 K		
w EtOH	w H2O	w DES	w EtOH	w H2O	w DES
0.081	0.049	0.870	0.145	0.090	0.765
0.156	0.096	0.748	0.193	0.135	0.672
0.204	0.145	0.651	0.210	0.159	0.631
0.234	0.196	0.570	0.242	0.229	0.529
0.257	0.245	0.498	0.261	0.294	0.445
0.295	0.435	0.270	0.274	0.364	0.362
0.289	0.579	0.132	0.278	0.570	0.152
0.272	0.643	0.085	0.256	0.639	0.105
0.237	0.712	0.051	0.222	0.707	0.071
0.228	0.718	0.054	0.167	0.792	0.041
0.218	0.739	0.043	0.047	0.930	0.023
0.220	0.740	0.040	0.000	0.979	0.021
0.203	0.758	0.039			
0.14	0.833	0.027			
0.051	0.926	0.023			
0.045	0.934	0.021			

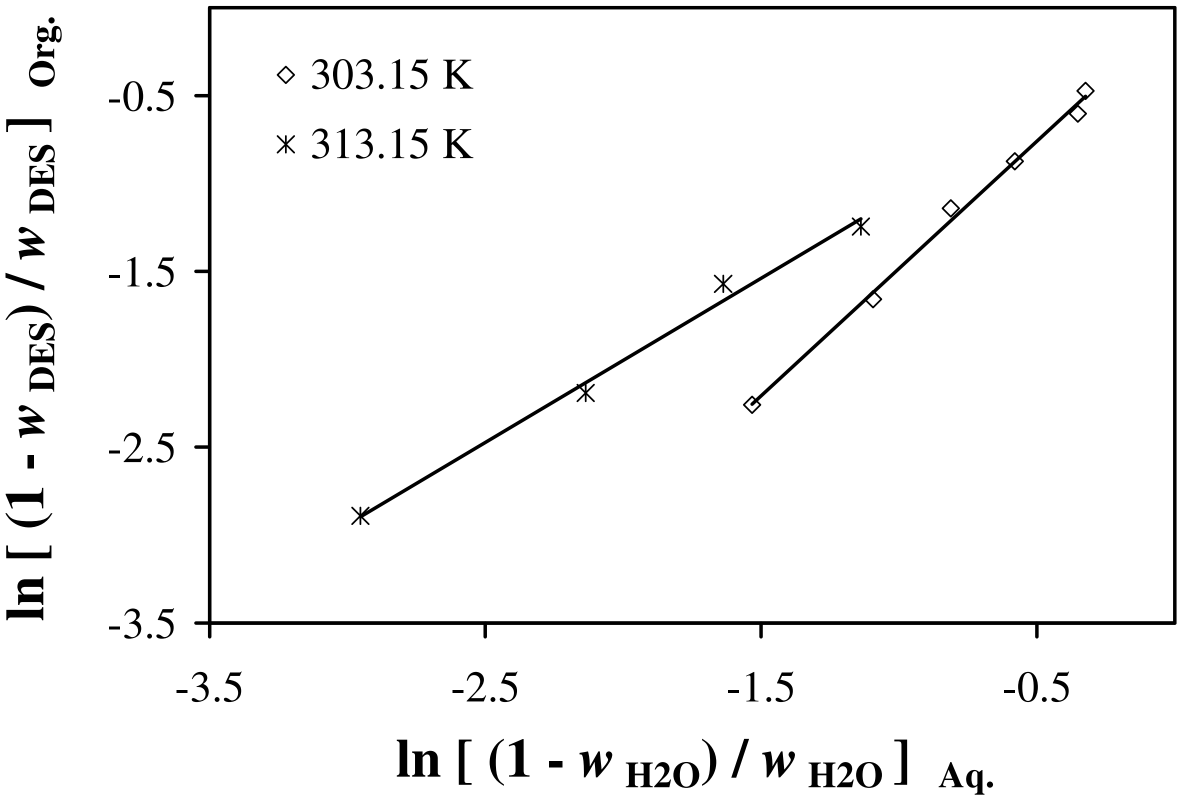

Figure 1-1 Othmer-Tobias plots for the H_2O + EtOH + DES ternary system.

The EtOH:DES relative volatility was too large to collect data for this system using the recirculating Fischer *T-x-y* apparatus. However, *T-x-y* data for the binary EtOH + H_2O system collected on the Fischer apparatus listed in Table 1-4 agree with literature [30-34].

Table 1-3. *P-x* data for EtOH + DES at 323.15 K.

P **(kPa)**	x_{EtOH}	***P*** **(kPa)**	x_{EtOH}	***P*** **(kPa)**	x_{EtOH}	***P*** **(kPa)**	x_{EtOH}
0.07	0.000	8.19	0.150	17.83	0.423	27.00	0.851
3.04	0.045	9.68	0.192	20.40	0.516	28.06	0.903
4.11	0.065	12.88	0.276	22.93	0.624	28.20	0.911
5.11	0.084	12.97	0.284	24.33	0.704	29.53	1.000
6.84	0.118	15.03	0.331	25.46	0.769		

Table 1-4. ***T-x-y*** **data for EtOH + H_2O at 101.325 kPa.**

T (K)	x_{EtOH}	y_{EtOH}	T (K)	x_{EtOH}	y_{EtOH}
373.15	0.001	0.005	354.65	0.326	0.605
371.75	0.006	0.072	353.35	0.463	0.652
369.65	0.014	0.154	352.65	0.541	0.675
367.35	0.0234	0.230	351.75	0.686	0.745
365.65	0.031	0.285	351.55	0.776	0.801
363.45	0.049	0.356	351.35	0.840	0.846
361.45	0.065	0.418	351.45	0.904	0.901
359.55	0.097	0.453	351.55	0.972	0.972
357.55	0.139	0.531	351.65	0.980	0.977

1.6.2 Model Fitting

In order to develop comprehensive models for the reactive distillation process, the mutual solubility data of the binary H_2O + DES reported by Stephenson [28] were included in the parameter estimation. The formats of the model equations and parameter arguments correspond to those implemented in ASPEN PLUS® (Aspen) [29]. Vapor pressures of the pure components were evaluated using extended Antoine equation [29] with default Aspen Plus parameters (DAPP). Calculated data were consistent with vapor pressure and boiling point for the components reported in literature.

To represent LLE data using the UNIQUAC equation, the modified UNIQUAC equation is used. For the residual activity coefficient contribution, the molecular surface parameter q' for

H_2O and EtOH is implemented as suggested by Anderson [18, 19] and the values were taken from that work. For DES q' was not modified. Values for surface area q and the molecular volume r were taken from the DAPP as calculated by the van der Waals data. Experimental data to correlate the binary EtOH + H_2O were obtained from *T-x-y* experiment and from literature. For application of the NRTL equation, only binary parameters for H_2O + DES and EtOH + DES were evaluated. Binary parameters for EtOH + H_2O were taken from literature [35].

The Hayden-O'Connell (HOC) equation was used to model the vapor phase and the association parameters for H_2O + EtOH were taken from DAPP. HOC parameters for H_2O + DES, EtOH + DES, DES + DES are not available in the open literature, and they were assumed equal to those existing for interactions with ethyl acetate from the same database.

The parameter fitting was performed with the regression tool in Aspen by minimization of the maximum likelihood objective function (a modified least-squares method of the differences between experimental and estimated data). A list of the UNIQUAC and NRTL parameters is presented in Table 1-5.

For comparison purposes, VLE and LLE data obtained with UNIQUAC parameters from Aspen database using the $q' = q$ default method are also presented in the figures. In this case, DAPP for H_2O-EtOH are available but those for EtOH + DES and H_2O + DES are missing and were predicted using the UNIFAC method.

VLE correlations are presented in Figure 1-2. Both, UNIQUAC and NRTL predictions agree with the experimental data. The DAPP for UNIQUAC equation and those regressed with UNIFAC represent the VLE data very well.

Table 1-5. Binary parameter for UNIQUAC-HOC and NRTL-HOC models. For UNIQUAC, $\tau_{ij} = \exp(a_{ij} + b_{ij}/T)$. For NRTL $G_{ij} = \exp[\alpha_{ij}(a_{ij} + b_{ij}/T)]$.

HOC Association Parameters	H_2O	EtOH	DES
H_2O	1.7	1.55	1.3
EtOH	1.55	1.4	1.3
DES	1.3	1.3	0.53

UNIQUAC	H_2O EtOH	H_2O DES	EtOH DES
a_{ij}	-2.39138	0	0
a_{ji}	1.794768	0	0
b_{ij}	447.8363	25.73932	113.6074
b_{ji}	-573.038	-591.152	-503.063

NRTL	H_2O EtOH	H_2O DES	EtOH DES
a_{ij}	0.514285	4.384591	0
a_{ji}	0.806535	-1.580000	0
b_{ij}	444.8857	184.7326	653.8819
b_{ji}	-266.533	1136.555	-158.856
α_{ij}	0.4	0.36842	0.3

	H_2O	EtOH	DES
r	0.92	2.10547	6.4733
q	1.4	1.972	5.616
q'	1	0.92	5.616

In the case of the LLE showed in Figures 1-3 and 1-4, UNIQUAC and NRTL models agree well with the experimental data at low concentrations of ethanol, but they do not fit the plait point region. Attempts to further improve the fits were unsuccessful because a simultaneous good representation of the plait point, the solubility envelope and the VLE data was not possible. Attempts to fit the plait point better required unrealistic adjustment of the DES + water binary solubilities and thus are not presented. Nonetheless, experimental tie lines are reasonably well predicted with regressed models sufficiently to warn during process design if liquid-liquid immiscibility may occur.

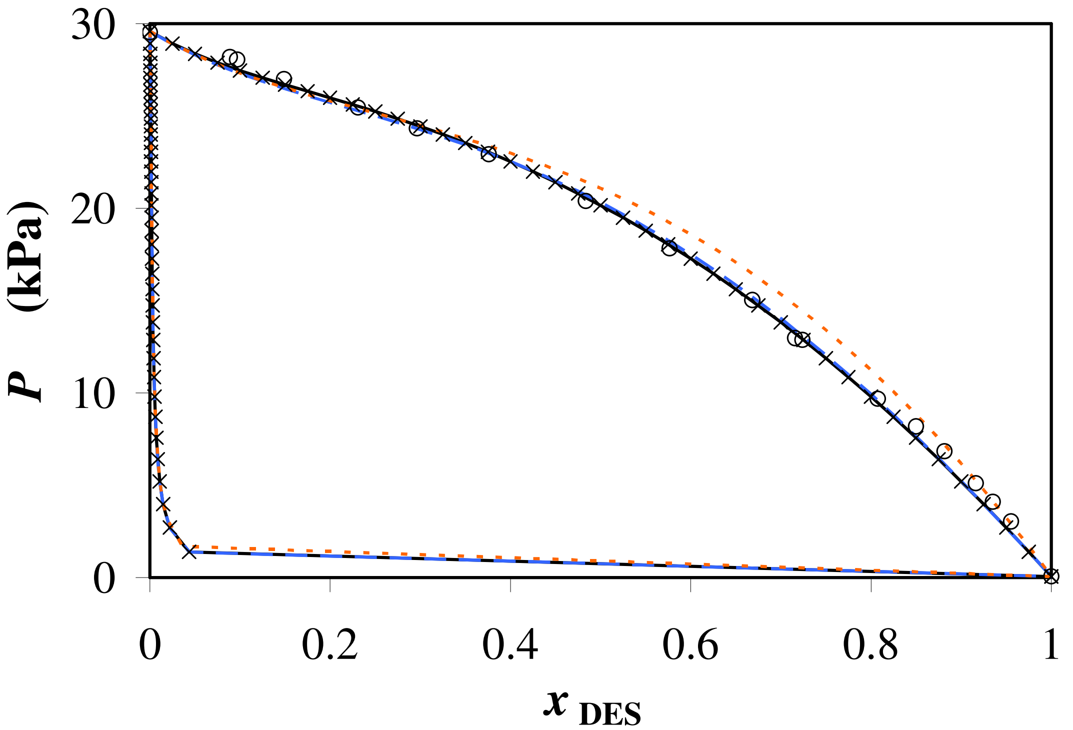

Figure 1-2. Binary *P*-*x* diagram for the binary EtOH + DES at 323.15 K. (○) Experimental data, (–x–) UNIQUAC, (—) NRTL, (-) DAPP, (lines) Fitted models. DAPP are UNIQUAC parameters obtained by regression of UNIFAC predictions in Aspen. (For interpretation of this and all other color images, the reader is referred to the electronic version of this dissertation)

The α_{ij} parameter in the NRTL equation is generally assumed 0.2 for immiscible liquids. For the systems studied here, it was not possible to obtain satisfactory agreement with the experimental data using this parameter value for the binary H_2O + DES, so it was regressed as well. The NRTL model with an additional parameter provides a better agreement with experimental data for higher concentrations of DES (near DES vertex) and so for the mutual solubility of H_2O + DES as shown in Figure 1-5. Regressed UNIQUAC parameters provide an acceptable representation of the LLE and excellent agreement for VLE for the binary EtOH + H_2O presented in Figure 1-6. Predicted azeotropic conditions and boiling points are listed in

Table 1-6, and those are consistent with reported data [36] for the binaries DES + H_2O, and EtOH + H_2O.

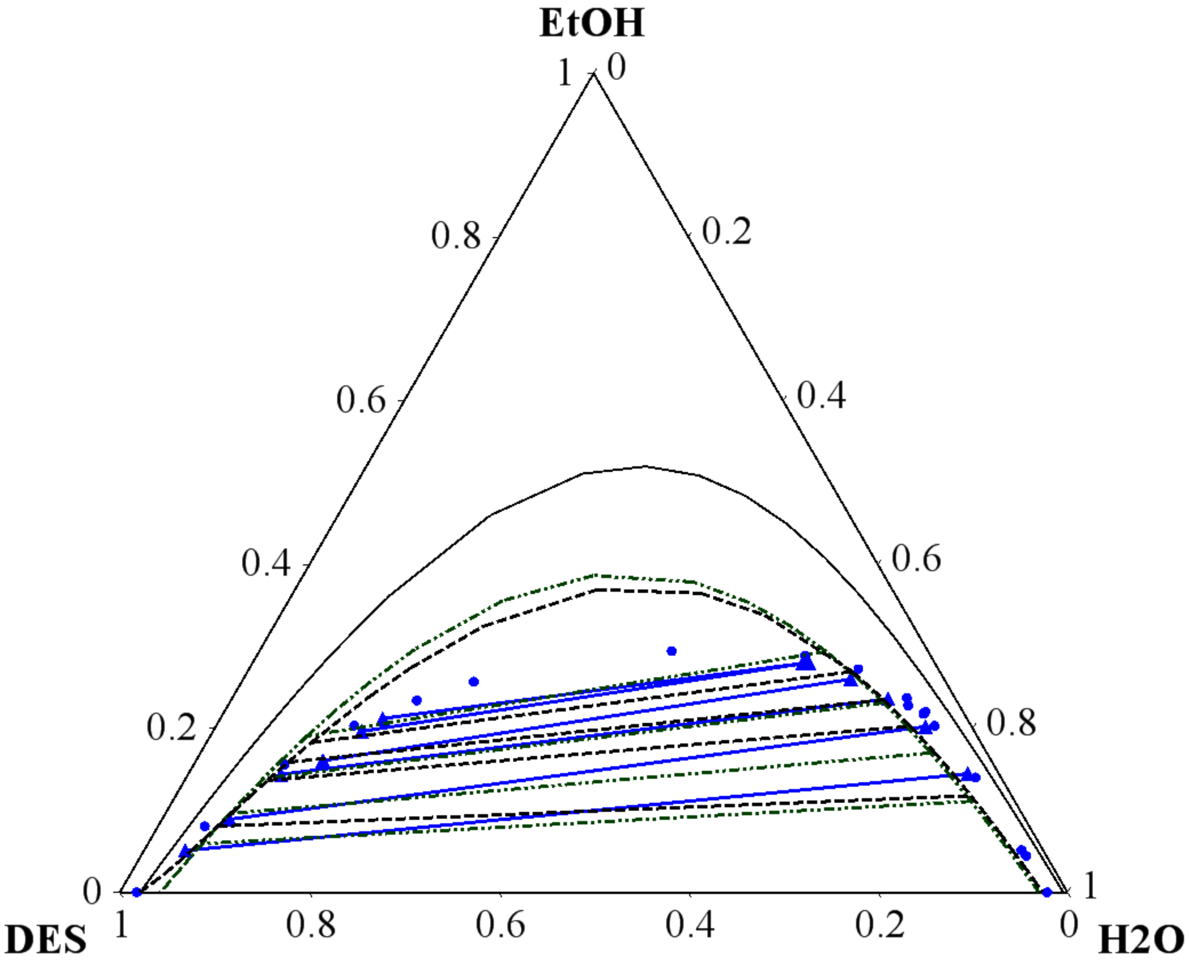

Figure 1-3. LLE data (mass basis) for H_2O + EtOH + DES at 303.15 K. (●) Solubility data. (–▲–) Tie lines. (—) UNIQUAC (DAPP) from Aspen. (– ·· –) UNIQUAC-HOC. (---) NRTL-HOC.

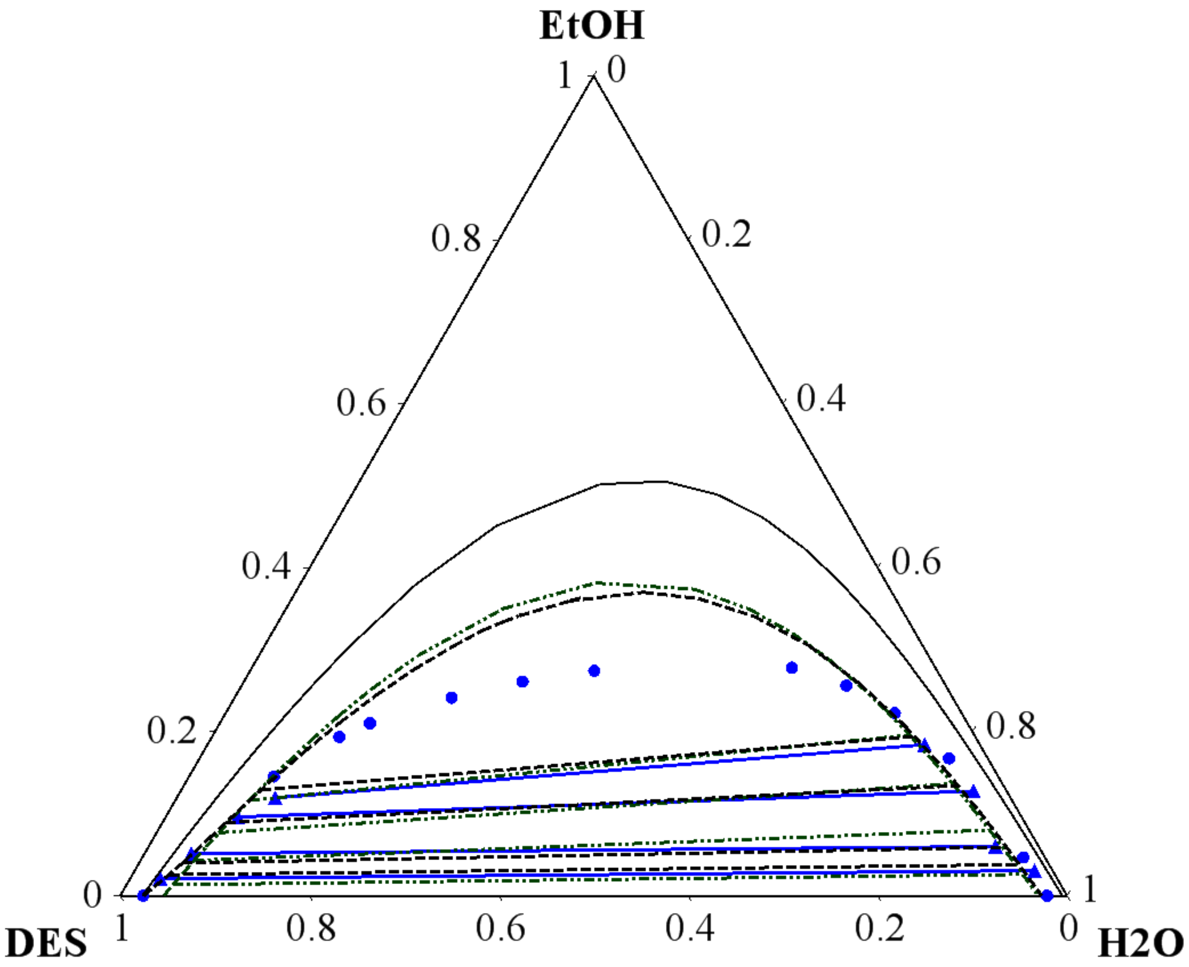

Figure 1-4. LLE data (mass basis) for H_2O + EtOH + DES at 313.15 K. (●) Solubility data. (–▲–) Tie lines. (—) UNIQUAC (DAPP) from Aspen. (- ·· -) UNIQUAC-HOC. (---) NRTL-HOC.

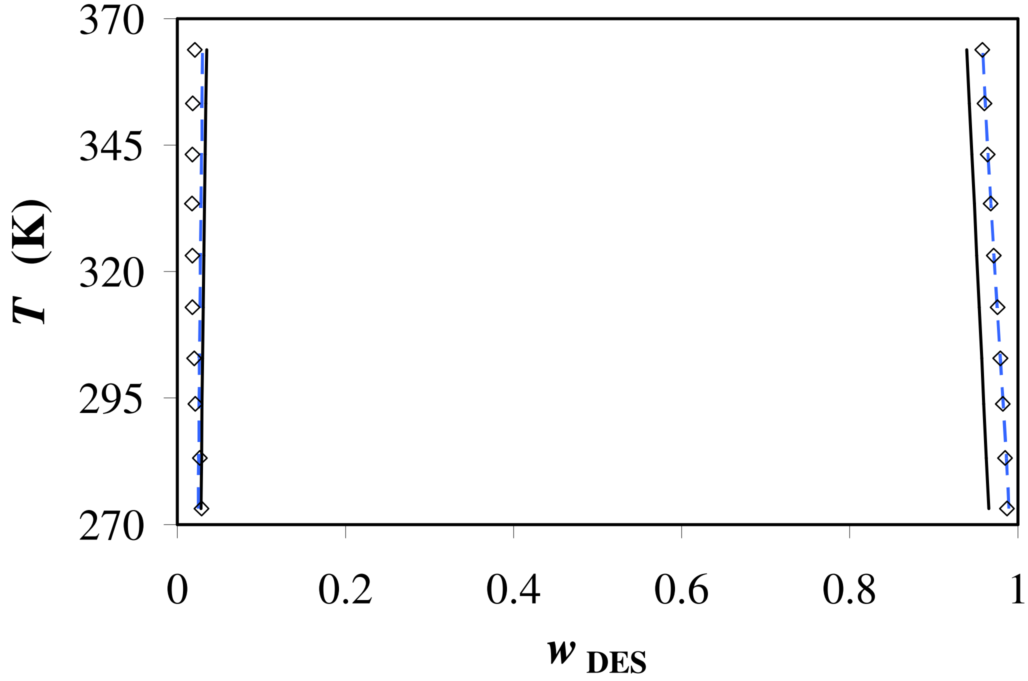

Figure 1-5. Temperature dependence of mutual solubility for H_2O + DES. (◊) Experimental data from Stephenson [28], (─) UNIQUAC, (--) NRTL.

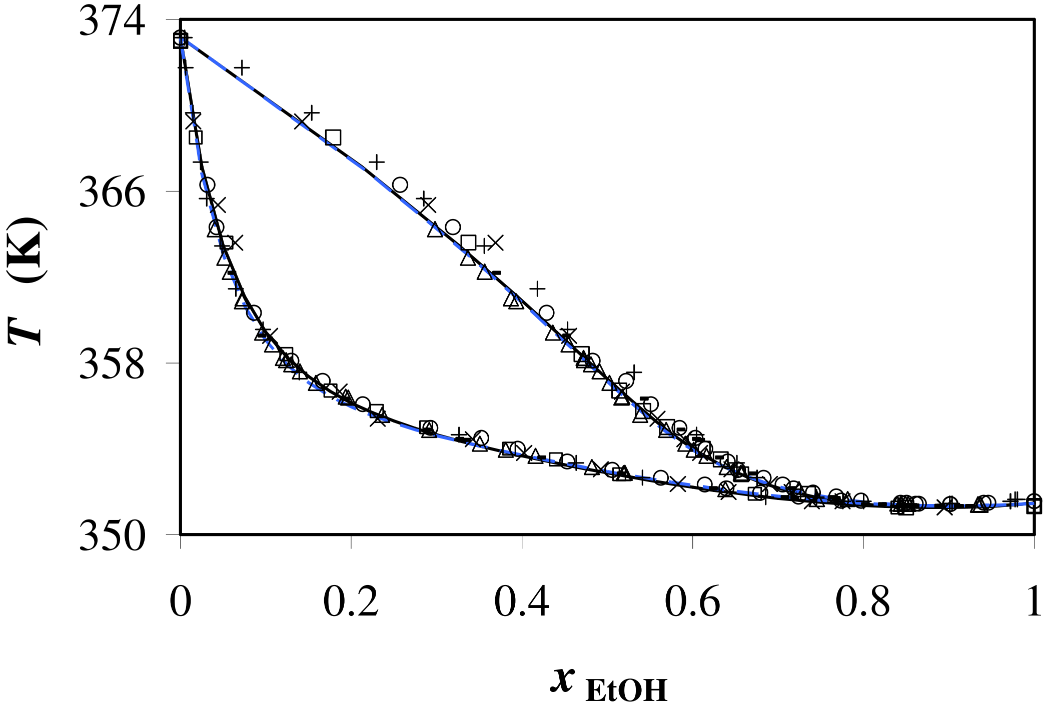

Figure 1-6. VLE for the binary H_2O + EtOH at 101.325 kPa. (□) Jones in [30], (×) Paul [31], (-) Kurihara [32], (○) Arce [33], (Δ) Iwakabe [34], (+) This work, (─) UNIQUAC-HOC, (- -) NRTL-HOC.

Table 1-6. Predicted and reported [36] azeotropes in the system H_2O + EtOH + DES at 101.23 kPa.

	x_{H2O}	x_{EtOH}	x_{DES}	T (K)
Reported Azeotropes	0.0963	0.9037	0	351.32
	0.9899	0	0.0101	373.05
UNIQUAC - HOC	0.1134	0.8866	0	351.26
	0.9895	0	0.0105	372.96
NRTL - HOC	0.0984	0.9016	0	351.33
	0.9873	0	0.0127	372.88

1.7 Conclusions

The LLE data for the ternary system H_2O + EtOH + DES at 303.15 K and 313.15 K are reported. *P-x* data for the binary EtOH + DES at 323.15 K are also presented. Binary parameters for UNIQUAC-HOC and NRTL-HOC equations were obtained by regression. The two models are able to reproduce reasonably well *P-x* data and the azeotropic points for the system. NRTL fits better than UNIQUAC binary and ternary LLE data, but both fail near the plait point. Nevertheless predictions with regressed models are more accurate than those using predicted parameters with UNIFAC. The parameters obtained in this work will represent the VLE reasonably well for reactive distillation design purposes while simultaneously indicating when two liquid phases may exist. Taking into account the limited solubility of succinic acid in EtOH (40-45% by weight at 353 K), a reactive distillation system to produce DES will work best with excess EtOH present. In this condition, the data show that there will be only one liquid phase.

REFERENCES

1.8 REFERENCES

[1] A. Cukalovic, C. V. Stevens. Biofuels, Bioprod. Biorefin. 2 (2008) 505–529.

[2] B. Hermann, M. Patel. Appl. Biochem. Biotechnol. 136 (2007) 361–388.

[3] O. Wolf, M. Crank, M. Patel, F. Marscheider-Weidemann, J. Schleich, B. Hüsing, G. Angerer. Techno-economic feasibility of large-scale production of Bio-based polymers in Europe, European Science and Technology Observatory, EUR 22103 EN. (2005).

[4] T. Werpy, G. Petersen. Top Value Added Chemicals from Biomass. Volume I–Results of Screening for Potential Candidates from Sugars and Synthesis Gas. PNNL-NREL. (2004) [Online]. Available: http://www1.eere.energy.gov/biomass/p dfs/35523.pdf [2008, April 7].

[5] J. Zeikus, M. Jain, P. Elankovan. Appl. Microbiol Biotechnol. 51 (1999) 545–552.

[6] D. Miller, N. Asthana, A. Kolah, D. Vu, C. Lira. Process for reactive esterification distillation. (2006) US Patent 20060252956.

[7] D. Sutton, G. Reed, G. Hiles. Process for the production of esters of mono-, di or polycarboxylic acids. (2007) US Patent 5599976.

[8] A. Kolah, N. Asthana, D. Vu, C. Lira, D. Miller. Ind. Eng. Chem. Res. 47 (2008) 5313–5317.

[9] S. Çehreli, D. Özmen, B. Tatli. J. Chem. Thermodyn. 37 (2005) 1144–115.

[10] S. Hung, H. Lin, C. Yu, H. Huang, M. Lee. Fluid Phase Equilib. 248 (2006) 174–180.

[11] E. Ince. J. Chem. Thermodyn. 38 (2006) 1669–1674.

[12] Ş. Kırbaşlar, E. Ince, S. Şahin, U. Dramur. J. Chem. Thermodyn. 39 (2007) 1493–1499.

[13] Ş. Kırbaşlar, S. Şahin, M. Bilgin. J. Chem. Eng. Data. 52 (2007) 1108–1112.

[14] Ş. Kırbaşlar, S. Şahin, M. Bilgin. J. Chem. Thermodyn. 39 (2007) 1463–1469.

[15] Ş. Kırbaşlar, S. Şahin, M. Bilgin. J. Chem. Thermodyn. 39 (2007) 284–290.

[16] D. Özmen. Fluid Phase Equilib. 269 (2008) 12–18.

[17] D. Özmen, S. Çehreli, U. Dramur. J. Chem. Thermodyn. 37 (2005) 837–842.

[18] T. Anderson, J. Prausnitz. Ind. Eng. Chem. Proc. Des. Dev. 17(4) (1978) 552–561.

[19] T. Anderson, J. Prausnitz. Ind. Eng. Chem. Proc. Des. Dev. 17(4) (1978) 561–567.

[20] T. Magnussen, P. Rasmussen, P. Fredenslund. Ind. Eng. Chem. Proc. Des. Dev. 20 (1981) 331–339.

[21] H. Renon, J. Prausnitz. AIChE J. 14 (1968) 135-144.

[22] U. Weidlich, J. Gmehling. Ind. Eng. Chem. Res. 26 (1987) 1372–1381.

[23] J. Gmehling, J. Li, M. Schiller. Ind. Eng. Chem. Res. 32 (1993) 178–193.

[24] M. Uusi-Penttila, R. Richards, P. Blowers, B. Torgerson, K. Berglund. J. Chem. Eng. Data**,** 41 (1996) 235–238.

[25] D Vu, C. Lira, N. Asthana, A. Kolah, D. Miller.J. Chem. Eng. Data, 51 (2006) 1220–1225.

[26] D. Vu. Properties and separations of plant-derived chemicals. Thesis (Ph. D.) -Michigan State University. Dept. of Chemical Engineering and Materials Science. Michigan, USA. (2007).

[27] D. Othmer, P. Tobias. Ind. Eng. Chem. 34 (1942) 693–696.

[28] R. Stephenson. J. Stuart. J. Chem. Eng. Data 31 (1986) 56–70.

[29] Aspentech, Aspen Physical Property System, physical property models/methods, Burlington, 2007.

[30] J. Gmehling, U. Onken. Vapor Liquid Equilibrium Data Collection. DECHEMA Chemical Data Series, VOL I., Part 1, DECHEMA. Frankfurt, Germany. (1977)

[31] R. N. Paul. J. Chem. Eng. Data. 21 (2) (1976) 165–169.

[32] K. Kurihara, M. Nakamichi, K. Kojima. J. Chem. Eng. Data. 38 (1993) 446–449.

[33] A. Arce, J.M. Ageitos, A. Soto. Fluid Phase Equilib. 122 (1996) 117–129.

[34] K. Iwakabe, H. Kosuge. Fluid Phase Equilib. 192 (2001) 171–186.

[35] Y. T. Tang, H. Huang, I. Chein. J. Chem. Eng. Jpn. 36 (11) (2003) 1352–1363.

[36] L.H. Horsley. Azeotropic Data III. Advances in Chemistry Series 116, American Chemical Society. Washington D.C., USA. (1973).

Included in this section is a copy of the paper: Phase equilibria for reactive distillation of diethyl succinate. Part II. Systems diethyl succinate + ethyl acetate + water and diethyl succinate + acetic acid + water, by A. Orjuela, A. J. Yanez, P. K. Rossman, D. T. Vu, D. Bernard-Brunel, D. J. Miller, C. T. Lira. Published in Fluid Phase Equilibria, 290 (1-2) (2010) 68-74.

The paper is reformatted and figures and tables are enlarged to fulfill edition requirements for the dissertation document.

2. Phase equilibria for reactive distillation of diethyl succinate. Part II. Systems diethyl succinate + ethyl acetate + water and diethyl succinate + acetic acid + water

2.1 Summary

Liquid-Liquid equilibrium data were measured for the ternary systems water + ethyl acetate + diethyl succinate and water + acetic acid + diethyl succinate at 298.15 K and atmospheric pressure. The reliability of the experimental data was confirmed using the Othmer-Tobias correlation. Vapor-Liquid equilibrium data were also measured for the binary systems ethyl acetate + diethyl succinate at 313.15 K, acetic acid + diethyl succinate at 323.15 K and ethyl acetate + ethanol at 101.325 kPa. Binary parameters for the modified UNIQUAC and NRTL equations were obtained by fitting experimental and reported data using the regression tool in Aspen Plus®. The Hayden-O'Connell equation was used to represent interactions in the vapor phase. The models agree reasonably well with the experimental data and can predict reported azeotropic.

2.2 Introduction

Dilute aqueous solutions of organic acids are generated in various processes as a valuable product (fermentation broths), or as a waste stream (acetylation of cellulose, maleic and terephthalic anhydride production, adipic acid processing). Several alternatives have been used to treat those solutions. Among others, reactive distillation (RD) has proved success in the recovery of different acids through esterification with a variety of alcohols. Also, RD provides advantages over traditional processes to upgrade fermentation products as recognized since early 1900s [1]. This method has been successfully applied for esterification of solutions with acetic acid [2-13], lactic acid [14, 15], and citric acid [16, 17].

Succinic acid derivatives have enormous economic potential in the chemical market [18-22]. Derivatives can be produced not only from the acid form but also from the esters [23]. Considering that the fermentation product is a diluted mixture of succinic acid with other acids in lesser concentrations (primarily with acetic acid - AcOH) [22], an esterification process by RD can be used to recover them simultaneously. Using RD, succinates can be separated from other esters and water (H_2O) by distillation, while chemical equilibrium is overcome by product separation [24]. Specifically, esterification with ethanol (EtOH) will produce diethyl succinate (DES), and ethyl acetate (EtOAc), both well known solvents and additives in fragrances formulation.

Reactive distillation provides process intensification by integrating the reactor and the major separation unit, but requires accurate thermodynamic modeling for process design. In the case of a mixed acid esterification, multicomponent phase equilibrium in the reactive mixture must be represented. In particular, for succinic acid or succinic derivatives, there is lack of information on phase equilibria in multicomponent systems. Simulations in ASPEN PLUS® for methyl succinate production by RD [25], showed that only qualitative trends can be obtained using available thermodynamic parameters. In the case of DES, generalized group contribution methods have been used to calculate activity coefficients in mixtures, but predictions did not agree with experimental data [26, 27].

In general, quantitative predictions of phase equilibrium in VLLE multicomponent mixtures based only on binary vapor-liquid equilibrium (VLE) data are not accurate [28-30].

Liquid-liquid equilibrium (LLE) data must be also considered in parameter regression for accurate representation. Therefore, in this work experimental LLE and VLE data were measured for mixtures with DES and other components of the mixed acid esterification. LLE data were obtained for the ternaries H_2O + EtOAc + DES and H_2O + AcOH + DES. VLE data were measured for the binaries EtOAc + DES, AcOH + DES, and EtOAc + EtOH. These data, together with others reported in the open literature were correlated with a modified UNIQUAC equation [28] and the NRTL equation [31] using the regression tool included in Aspen Plus®.

2.3 Material and methods

2.3.1 Materials

Diethyl succinate (DES, 99%, Sigma-Aldrich), ethanol (EtOH, 200 proof, Decon Labs), water (H_2O, HPLC grade, J.T. Baker), ethyl acetate (EtOAc, 99.99%, EMD), acetic acid (AcOH, 99.9%, Aristar), *n*-butanol (99.9%, Mallinckrodt), and acetonitrile (HPLC grade, EMD) were used in the present experiments. Purity was confirmed by gas chromatography and Karl-Fisher analysis (Hydranal-coulomat E solution (Riedel-de Haën)) for water impurities. Traces of water were the only impurities detected. Methyl red (Reagent grade, EM science) was used to reveal liquid-liquid interface for LLE measurements. Phenolphthalein (Sigma) and sodium hydroxide (A.C.S., J.T. Baker) were used during titrations.

DES and EtOAc were purified by vacuum distillation. Only 85-90 % of the pre-distilled volume was used for the experiments, discarding the first overhead fraction (5-10 %) and the reboiler residue (5 %). Ethanol was dried using molecular sieve to a water content less than 800 ppm, and it was stored under dry atmosphere without further purification. Ethyl acetate was dried with $CaCl_2$ prior to VLE experiments.

2.3.2 Experimental procedures

LLE data for ternary mixtures were determined on a mass basis, using glass vials (10 cm^3) stirred with magnetic bar. These vials were placed in an isothermal bath equipped with a circulator pump and temperature control (Isotherm immersion circulator 730, Fisher Scientific). The temperature was measured with an ASTM certified glass thermometer (model 64 C, ± 0.1 K). The total mass for all the experiments was about 10 g.

2.3.3 LLE Tie Lines

Equilibrium lines were obtained by preparing ternary mixtures of known overall composition within the two phase region. Traces of methyl red were added to improve interface visualization. The organic phase preferentially dissolves methyl red causing the ester rich phase to have an orange color and the aqueous phase remained colorless or slightly red. The liquid mixtures were stirred at constant temperature for 12 h. After equilibration the vial was centrifuged for 20 minutes at 4000 rpm and returned to the isothermal bath for 12 more hours. The bottom phase was removed with a syringe and the weight of every phase was recorded. Difference from total initial mass to that of the two phases was checked and it was less than 1% (mass) for all the experiments. A sample of every layer was taken for analysis. H_2O + EtOAc + DES and H_2O + AcOH + DES systems were measured at 298.15 K (± 0.5 K). In the ternary system H_2O + EtOAc + DES at high concentrations of DES, the organic liquid phase was denser than the aqueous phase. For high concentrations of EtOAc the aqueous phase was dense.

2.3.4 LLE Binodal Curve

The solubility envelope was obtained to confirm that obtained from tie lines for the ternary H_2O + EtOAc + DES. Fixed amounts of binary mixtures of H_2O + DES and EtOAc + H_2O were prepared gravimetrically using an analytical balance (Sartorius R 300 S, ± 0.1 mg). Additions of weighted amounts of EtOAc or DES to each binary mixture were done in stages using a syringe (0.1 cm^3). After every addition the mixture was stirred for 10 minutes and checked for single phase region. Experiments were done at 298.15 K (± 0.5 K). In order to enhance visual determination of the two phases, traces of methyl red were added to the mixture. Accuracy of this method around 1% (mass) was reported in a previous work [32]. For the ternary system H_2O + AcOH + DES, solubility data are available at 298.15 K [26], and the binodal curve was not measured.

2.3.5 VLE experiments

P-x experiments were carried out using the apparatus and analytical methods described in detail by Vu *et al* [33] and Vu [34]. Isothermal VLE of the binaries EtOAc + DES and AcOH + DES were measured at 313.15 K and 323.15 (± 0.05 K) respectively. For the AcOH + DES system, the previously described apparatus was improved by using a jacketed vessel with a thermowell. Water from an isothermal bath was circulated in the jacket to maintain constant temperature. The stem between the chamber and the pressure gauge (Baratron® model PDR 2000, MKS Instruments) was traced with heating tape to prevent condensation. The new vessel provided a more direct measurement of liquid temperature and was easier to disassemble. The predetermined mixture composition was stirred with a magnetic bar and the vessel was degassed at under vacuum at the desired temperature. To assure degassing, after the initial pressure stabilized, the pressure was lowered to approximately half the equilibrium pressure and the vacuum valve was closed and the equilibrium pressure restabilized. Following re-equilibration, variations in pressure of ± 0.2 kPa in between repetitions were considered acceptable. Reported pressure is an average of three measurements obtained for every composition.

Using a vapour-liquid equilibrium apparatus VLE 100D (Fischer America, Inc.), *T*-*x*-*y* data at 101.3 kPa for the binary EtOAc + EtOH were obtained. Temperature measurements were within ± 0.05K and pressure control was within ± 0.1 kPa. These data were used to validate reliability of sampling and quantification procedures, and also for parameter regression.

2.3.6 Analysis

Samples from VLE were analyzed as described in [33]. For the binary AcOH + DES, titration with 0.1 M ethanolic solution of sodium hydroxide was used. A weighed aliquot of the original sample from the *P*-*x* apparatus was titrated at 293.15 K until final point with phenolphthalein. It was found that this method was more simple, rapid, and reproducible than gas chromatography for this system. LLE samples were analyzed using a gas chromatograph (HP 5890 series II), equipped with a thermal conductivity detector. *n*-butanol was used as internal standard and acetonitrile as solvent. A 15 m long Alltech EC-WAX column (0.53 mm i.d., 1.20 μm Film thickness) was used with a temperature programmed analysis: The initial column temperature was 313.15 K (3 min), ramped at 30 K/min to a final temperature 523.15 K (and held for 0.5 min). The injection port was maintained at 543.15 K in a splitless mode. The detector temperature was 523.15 K. Helium was used as carrier (0.25 cm^3/s) and injections of 5×10^{-4} cm^3 were used. Samples of known composition in the range of interest were used for calibration, and injected by triplicate to obtain repeatability within 0.5% by mass. Data integration was done using a Peaksimple Chromatography Data System (SRI Model 302) with Peaksimple software version 3.59. Karl-Fisher analysis (Aquacount coulometric titrator AQ-2100) was used to measure and confirm water content in reagents and samples.

2.4 Results and discussion

Experimental tie lines data for the system H_2O + EtOAc + DES and H_2O + AcOH + DES are listed in Table 2-1 where w_i represents mass fraction of each component. The consistency of LLE data was checked with the Othmer-Tobias method [35] as shown in Figure 2-1, and a linear relation was obtained for both systems. Tie lines extremes for the system H_2O + AcOH + DES agree reasonably well with reported immiscible boundaries [26]. Binodal data for the system H_2O + EtOAc + DES are listed in Table 2-2.

Table 2-1. LLE tie line data for H_2O + EtOAc + DES and H_2O + AcOH + DES at 298.15 K. Compositions are in weight fraction.

Aqueous Phase (Aq.)			**Organic Phase (Org.)**		
w **H2O**	w **EtOAc**	w **DES**	w **H2O**	w **EtOAc**	w **DES**
0.960	0.021	0.019	0.037	0.185	0.778
0.950	0.033	0.017	0.033	0.327	0.640
0.944	0.044	0.012	0.044	0.463	0.493
0.937	0.054	0.009	0.050	0.557	0.393
w **H2O**	w **AcOH**	w **DES**	w **H2O**	w **AcOH**	w **DES**
0.893	0.066	0.041	0.073	0.029	0.898
0.824	0.133	0.043	0.084	0.064	0.852
0.690	0.230	0.080	0.141	0.147	0.712
0.442	0.293	0.265	0.275	0.268	0.457

Table 2-2. LLE binodal data for H_2O + EtOAc + DES at 298.15 K. Compositions are in weight fraction.

w_{H2O}	w_{EtOAc}	w_{DES}
0.030	0.817	0.153
0.027	0.678	0.295
0.028	0.536	0.436
0.029	0.385	0.586
0.025	0.243	0.732
0.023	0.100	0.877
0.943	0.048	0.009
0.953	0.033	0.014
0.962	0.021	0.017
0.970	0.012	0.018
0.970	0.008	0.022
0.978	0.000	0.022
0.018	0.000	0.982
0.919	0.0810	0.000
0.040	0.960	0.000

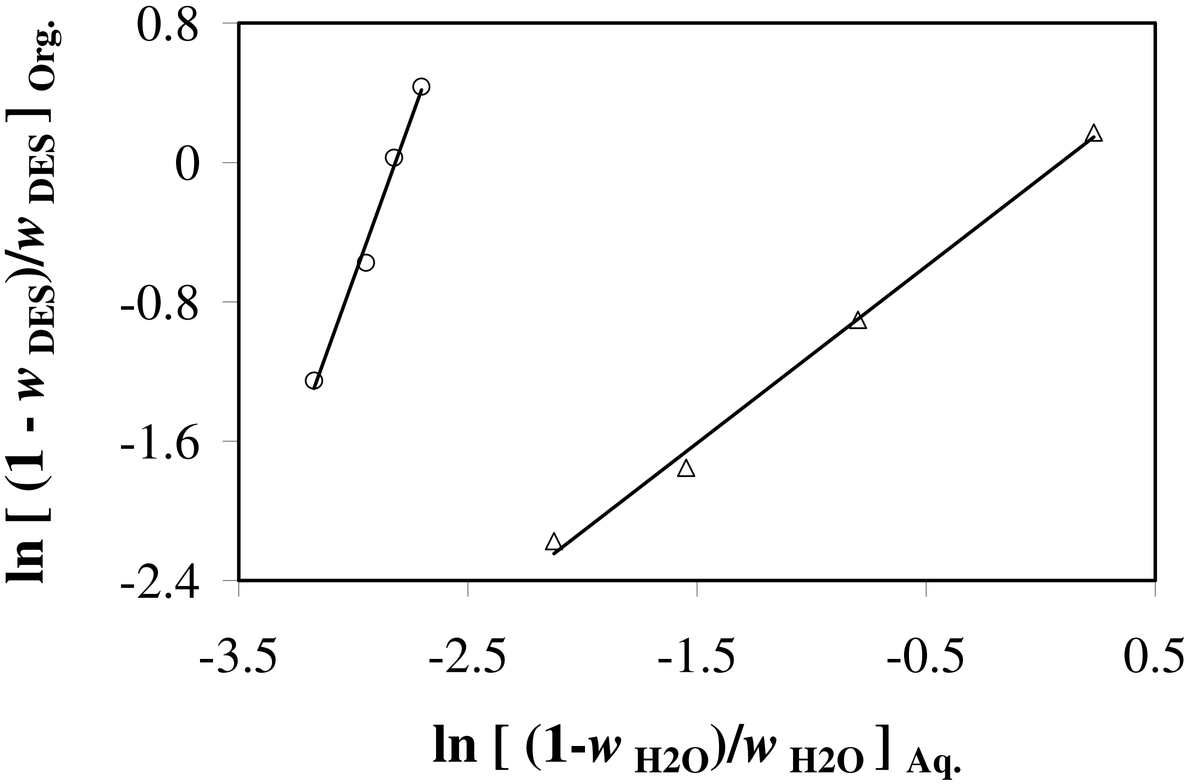

Figure 2-1. Othmer-Tobias plots for the H_2O + EtOAc + DES and H_2O + AcOH + DES ternary systems. (○) ternary with EtOAc, (Δ) ternary with AcOH.

P-x data for the binaries EtOAc + DES and AcOH + DES are listed in Table 2-3. Only few points were taken for EtOAc + DES mixture because the equilibrium data showed minimal deviation from ideal behavior and from UNIFAC predictions. *T-x-y* data for the binary EtOAc + EtOH are presented in Table 2-4.

Table 2-3. ***P-x*** **data for the binary systems EtOAc + DES at 313.15 K and AcOH + DES at 323.15 K.**

P **(kPa)**	x_{EtOAc}
0.4132	0.021
6.825	0.286
12.197	0.483
15.849	0.625
19.275	0.773
24.82	1.000

P **(kPa)**	x_{AcOH}	***P*** **(kPa)**	x_{AcOH}
0.07	0	3.84	0.590
0.31	0.048	4.40	0.658
0.81	0.164	4.40	0.682
1.40	0.235	4.76	0.757
1.97	0.321	5.32	0.807
2.36	0.406	5.89	0.814
2.73	0.439	6.57	0.899
3.11	0.507	7.35	0.980
3.41	0.572	7.52	1.000

Table 2-4. ***T-x-y*** **data for the system EtOAc + EtOH at 101.3 kPa.**

T (K)	x_{EtOAc}	y_{EtOAc}	**T (K)**	x_{EtOAc}	y_{EtOAc}
351.55	0	0	345.35	0.690	0.656
351.35	0.001	0.008	346.75	0.868	0.796
350.85	0.016	0.049	348.25	0.937	0.879
350.35	0.024	0.073	350.25	0.991	-
349.75	0.044	0.120	349.35	0.978	0.959
349.25	0.061	0.164	348.25	0.922	0.883
348.65	0.082	0.206	347.45	0.879	0.836
348.05	0.137	0.260	346.65	0.849	0.799
346.25	0.266	0.398	345.85	0.777	0.731
345.55	0.357	0.460	345.35	0.631	0.629

The UNIQUAC and NRTL equations are implemented as provided in ASPEN PLUS® (Aspen) [36]. To improve the agreement with LLE data using UNIQUAC equation, the modified UNIQUAC equation is used. For the residual activity coefficient contribution, the molecular surface parameter q' for H_2O and EtOH is implemented as suggested by Anderson [28, 29] and the values are taken from that work. For all other components q' was not modified. Values for q and the relative volume r were taken from the Aspen database. Due to the modification of q' for H_2O and EtOH, interaction parameters for the binaries H_2O + AcOH, H_2O + EtOAc, EtOH + AcOH, and EtOH + EtOAc were regressed using VLE and LLE data reported in literature [37-46]. Interaction parameters for the binaries H_2O + EtOH, H_2O + DES, and EtOH + DES were obtained before for the UNIQUAC equation. Specifically, H_2O + DES parameters were used to calculate LLE for H_2O + EtOAc + DES and H_2O + AcOH + DES ternary mixtures, and were fixed during other binary parameter estimation. In the case of the NRTL equation, only binary parameters for AcOH + DES and EtOAc + DES were evaluated. Binary parameters for EtOH + H_2O, H_2O + AcOH, H_2O + EtOAc, EtOH + AcOH, and EtOH + EtOAc were taken from literature [47]. The Hayden-O'Connell (HOC) equation was used to model the vapor phase and the association parameters were taken from Aspen database. HOC association parameters for species with DES are not available in the open literature, and they were assumed equal to those existing interaction parameters for the specie with ethyl acetate.

The parameter fitting was performed with the regression tool in Aspen by minimization of the maximum likelihood objective function (a modified least-squares method of the differences between experimental and estimated data). A list of the UNIQUAC and NRTL parameters is presented in Table 2-5.

VLE correlations for the binaries EtOAc + DES and AcOH + DES are presented in Figures 2-2 and 2-3. Both, UNIQUAC and NRTL predictions agree with the experimental data. LLE data and correlation for the ternary H_2O + AcOH + DES are presented in Figure 2-4. The slope of the experimental tie lines is slightly different from those reported previously [26]. Even though the immiscibility region obtained by regression is consistent with reported data, tie lines produced with NRTL or UNIQUAC do not fit experimental data perfectly. Nonetheless both UNIQUAC and NRTL offer good predictions of LLE together with a good VLE representation.

Table 2-5. Binary parameter for UNIQUAC-HOC and NRTL-HOC models. For UNIQUAC, $\tau_{ij} = \exp(a_{ij} + b_{ij}/T)$. For NRTL, $G_{ij} = \exp[\alpha_{ij}\,(a_{ij} + b_{ij}/T)]$.

HOC Association Parameters					
	H_2O	**EtOH**	**EtOAc**	**AcOH**	**DES**
H_2O	1.7	1.55	1.3	2.5	1.3
EtOH	1.55	1.4	1.3	2.5	1.3
EtOAc	1.3	1.3	0.53	2	0.53
AcOH	2.5	2.5	2	4.5	2
DES	1.3	1.3	0.53	2	0.53

UNIQUAC						
	H_2O EtOAc	**H_2O AcOH**	**EtOH EtOAc**	**EtOH AcOH**	**EtOAc DES**	**AcOH DES**
a_{ij}	-0.5064399	0.0462	0.38212429	0	0	0
a_{ji}	4.0628407	0.59198978	1.8108	0	0	0
b_{ij}	154.99112	148.623424	30.6229951	-258.87313	-334.34066	145.839644
b_{ji}	-2029.8721	-492.96872	-1168.8663	254.278619	212.401927	-354.5179

	H_2O	**EtOH**	**EtOAc**	**AcOH**	**DES**
r	0.92	2.10547	3.47858	2.19512	6.4733
q	1.4	1.972	3.116	2.072	5.616
q'	1	0.92	3.116	2.072	5.616

NRTL		
	EtOAc DES	**AcOH DES**
a_{ij}	0	-3.3257404
a_{ji}	0	18.5048574
b_{ij}	236.073904	1067.92091
b_{ji}	-211.38844	-5736.0599
α_{ij}	0.3	0.3

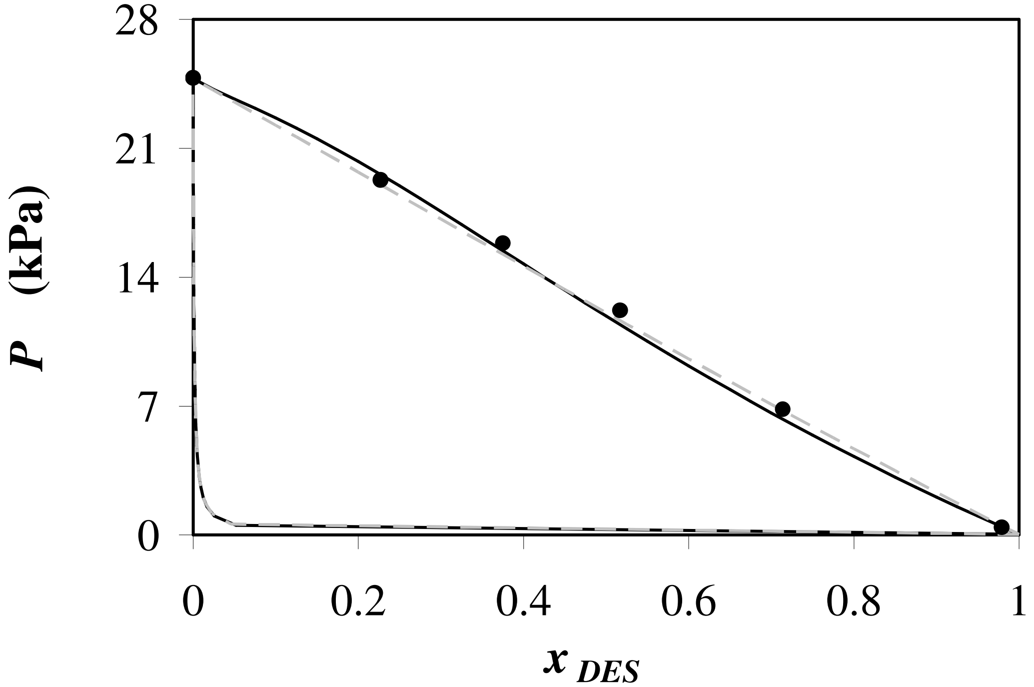

Figure 2-2. *P-x* diagram for the binary EtOAc + DES at 313.15 K. (●) Experimental data, (—) UNIQUAC – HOC, (- -) NRTL – HOC.

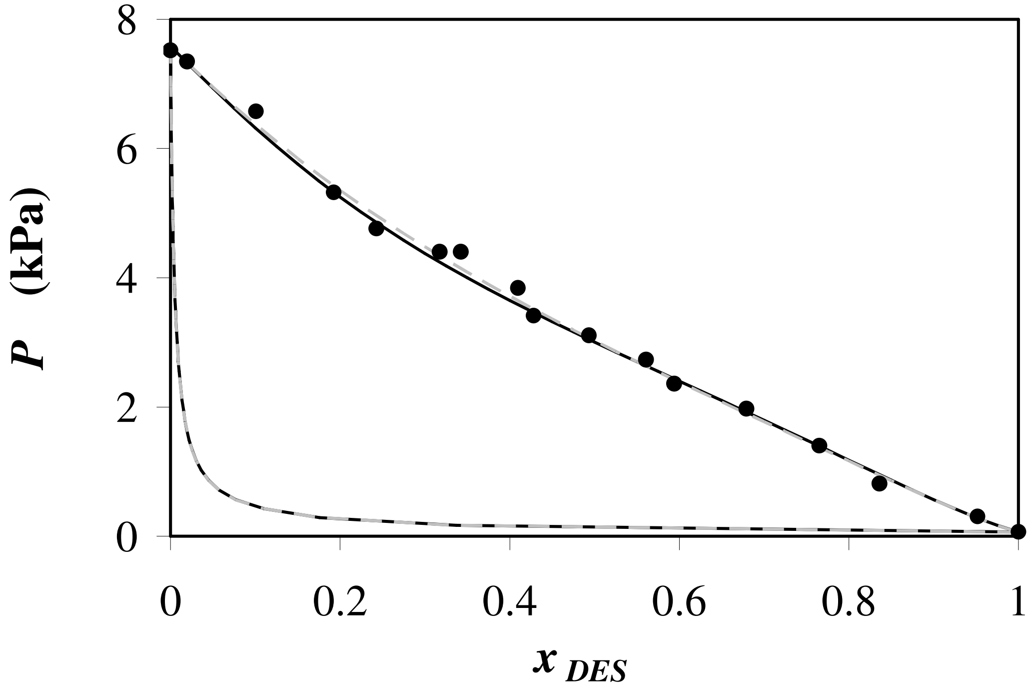

Figure 2-3. *P-x* diagram for the binary AcOH + DES at 323.15 K. (●) Experimental data, (—) UNIQUAC – HOC, (- -) NRTL – HOC.

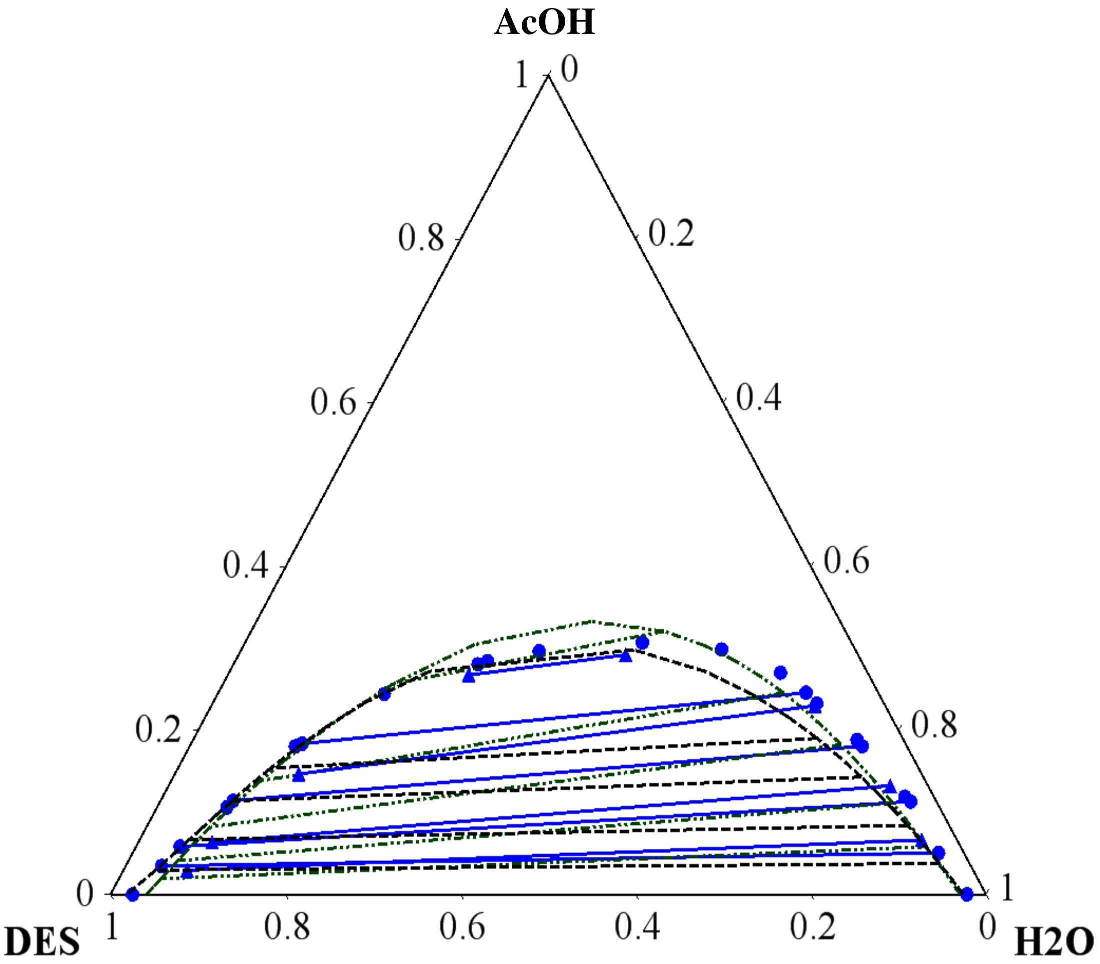

Figure 2-4. LLE data (mass basis) for H_2O + AcOH + DES at 298.15 K. (–Δ–) Experimental tie lines, (●) Solubility data from [26], (–●–) Tie lines from [26], (– ·· –) UNIQUAC-HOC. (- -) NRTL-HOC.

LLE for the system H_2O + EtOAc + DES is presented in Figure 2-5. In this case both UNIQUAC and NRTL give good predictions. It was found that NRTL offers a better representation for the binary H_2O + DES. For that reason NRTL prediction fits better the solubility data near the binary H_2O + DES limit. For the UNIQUAC model, VLE and LLE data reported in literature for the binaries H_2O + EtOAc and H_2O + AcOH were regressed simultaneously. Those provided a reasonably good representation of the ternary systems mentioned before, and also for the binaries as shown in figures 2-6 to 2-8.

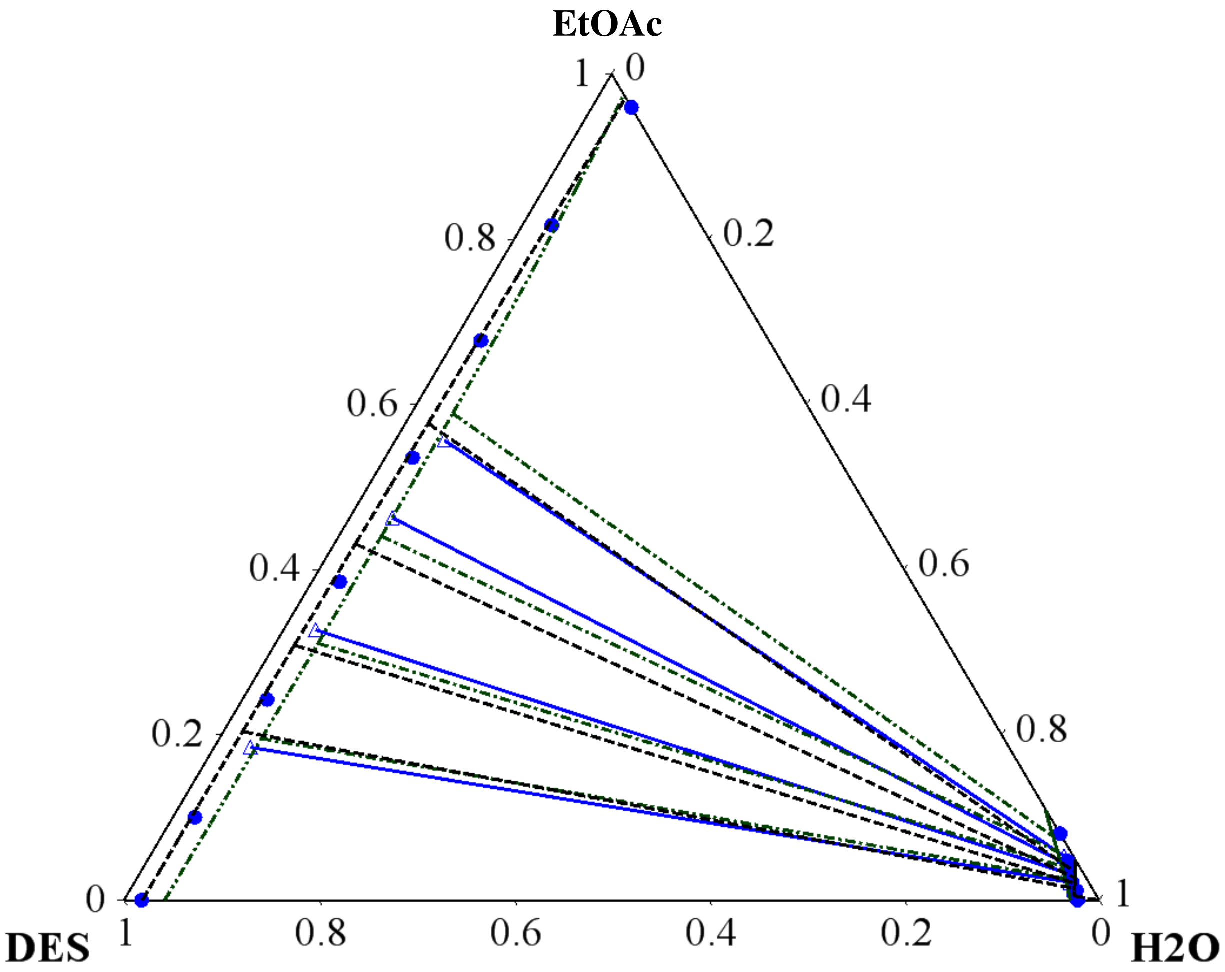

Figure 2-5. LLE data (mass basis) for H_2O + AcOH + DES at 298.15 K. (●) Experimental solubility data, (–Δ–) Experimental tie lines, (– ·· –) UNIQUAC-HOC. (- -) NRTL-HOC.

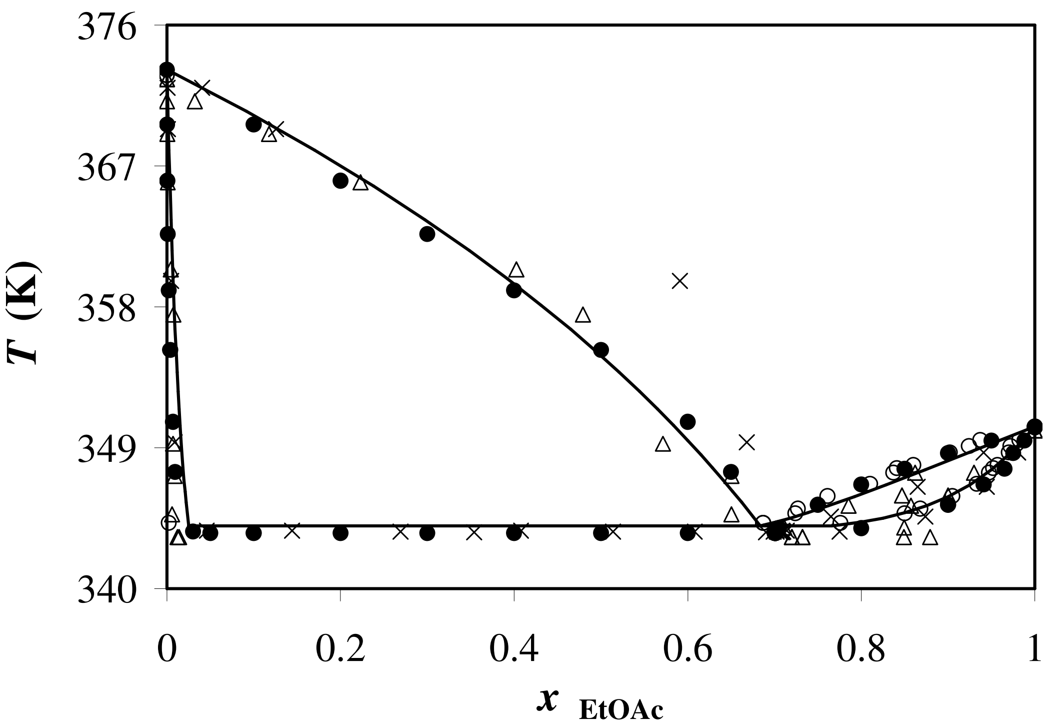

Figure 2-6. VLE for the binary H_2O + EtOAc at 101.325 kPa. (Δ) Reichl [39], (○) Lee [41], (×) Ellis data in [44], (●) Kato [47], (—) UNIQUAC-HOC.

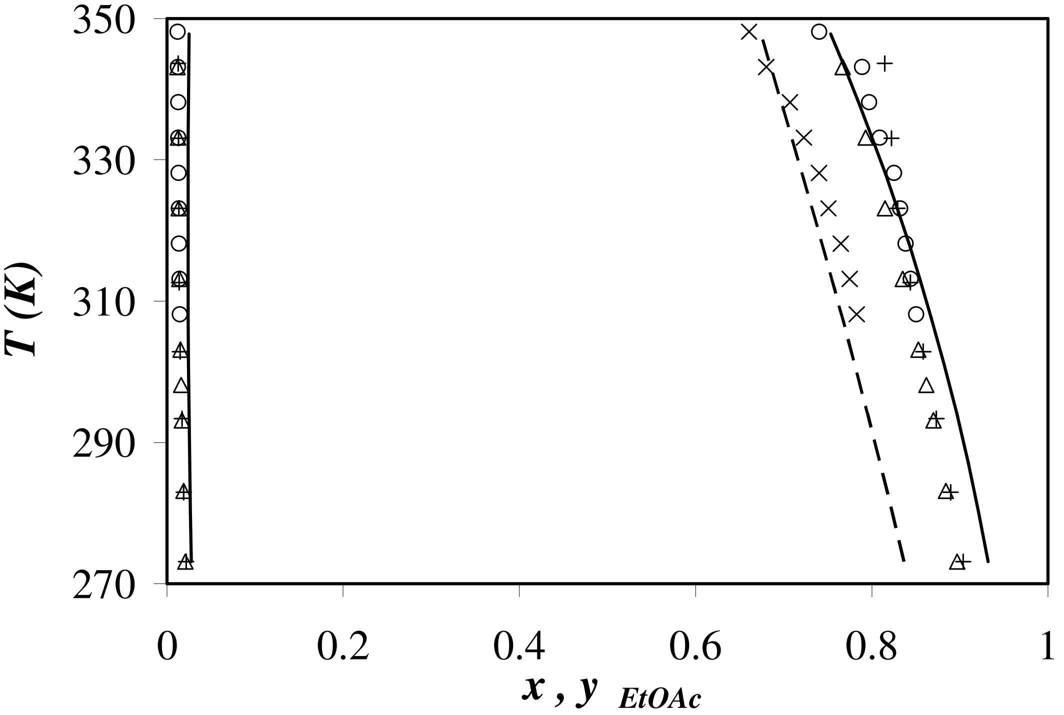

Figure 2-7. VLLE for the binary H_2O + EtOAc at different temperatures. (○) Liquid phase (×) Vapor phase, in Hong [38], (+) Stephenson [42], (Δ) Sørensen [43], (—) Liquid phase (- -) Vapor phase, UNIQUAC-HOC.

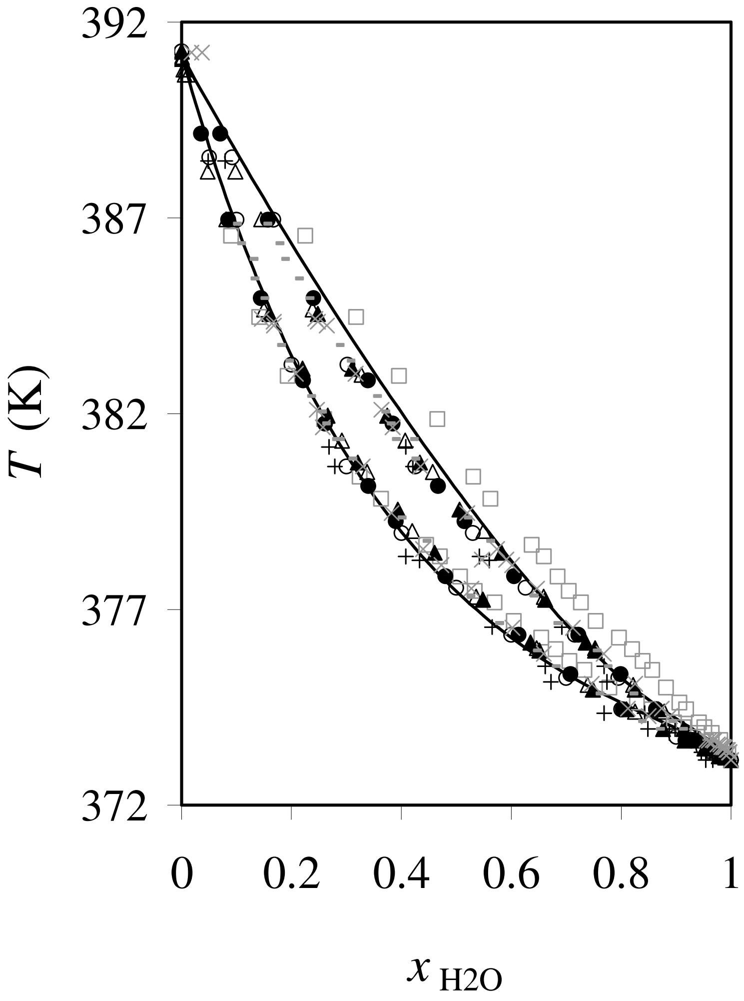

Figure 2-8. VLE for the binary H_2O + AcOH. at 101.32 kPa. Data compiled in [44], (Δ) Brown, (▲) Conti, (○) Chu, (●) Garner, (+) Garwin, (×) Ocon, (-) Sebastiani, (□) Calvar [37]. (—) UNIQUAC – HOC.

VLE Experimental data for the system EtOH + EtOAc agree with those reported before as shown in Figure 2-9. Pursuing a complete set of parameters for the mixed acid process, a regression of VLE reported data for the binary EtOH + AcOH with UNIQUAC equation is presented in Figure 2-10. A good fitting was obtained.

Predicted azeotropic conditions, and those calculated with UNIQUAC and NRTL equations, are listed in Table 2-6. Predictions are consistent with reported data [48].

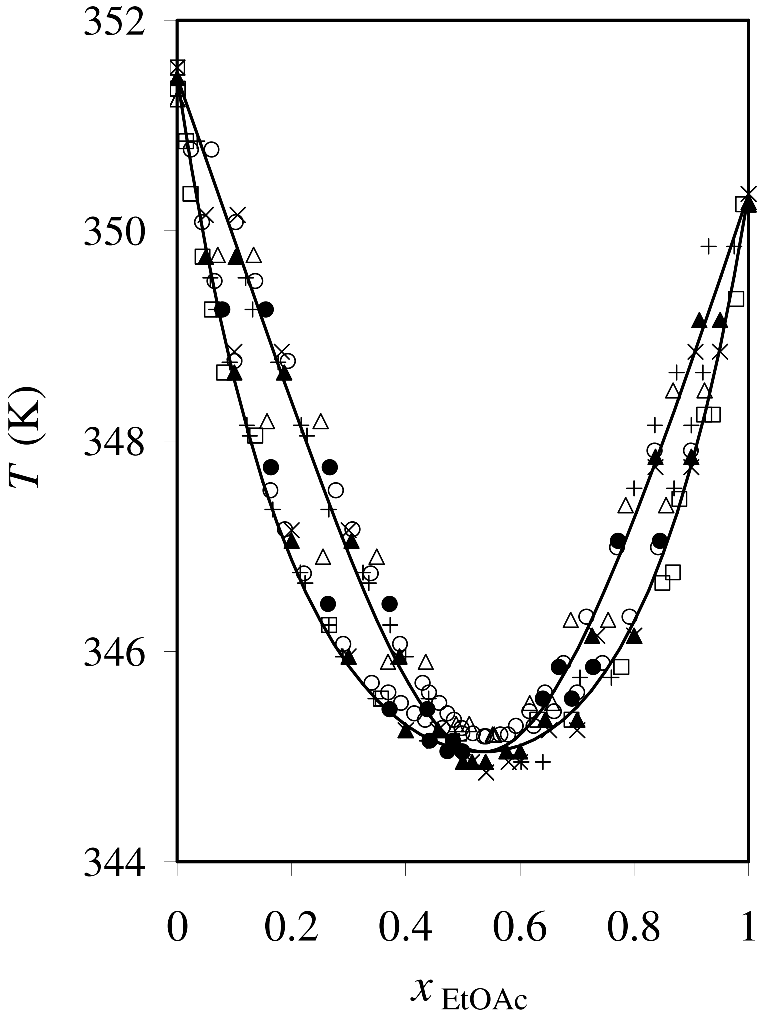

Figure 2-9. VLE for the binary EtOH + EtOAc. (□) Experimental data, (○) Calvar [37], (Δ) Tu [40], (×) Kato [47], Data compiled in [44], (▲) Chu, (●) Griswold, (+) Furnas, (—) UNIQUAC – HOC.

Taking into account the limited solubility of succinic acid in EtOH (40-45% by weight at 353 K), a reactive distillation system to produce DES will work best with excess EtOH present. In this condition, the data show that there will be only one liquid phase. This is also the case for mixtures with AcOH or EtOAc. The parameters obtained in this work will represent the VLE reasonably well for design purposes while simultaneously indicating when two liquid phases may exist.

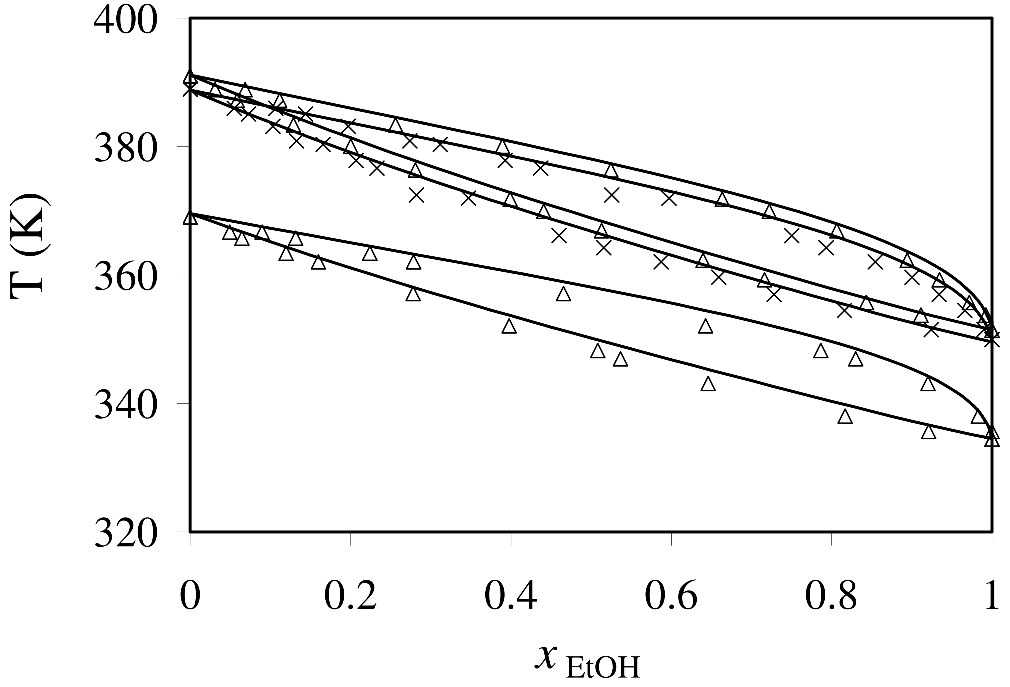

Figure 2-10. VLE for the binary EtOH + AcOH. (Δ) Reichl [39], (×) Ruiz data in [45], (—) UNIQUAC – HOC.

Table 2-6. Predicted and reported [48] azeotropes in the system H_2O + EtOH + DES at 101.23 kPa.

	x_{H2O}	x_{EtOH}	x_{EtOAc}	x_{DES}	T (K)
Reported Azeotropes	0.3085	0.1126	0.5789	0	343.38
	0.3115	0	0.6885	0	343.53
	0	0.4619	0.5381	0	344.96
	0.0963	0.9037	0	0	351.324
	0.9899	0	0	0.0101	373.05
UNIQUAC - HOC	0.2694	0.1709	0.5597	0	343.34
	0.3522	0	0.6478	0	343.77
	0	0.4647	0.5353	0	345.04
	0.1134	0.8866	0	0	351.26
	0.9895	0	0	0.0105	372.96
NRTL - HOC	0.2858	0.1069	0.6073	0	343.24
	0.3131	0	0.6869	0	343.52
	0	0.4572	0.5428	0	344.96
	0.0984	0.9016	0	0	351.33
	0.9873	0	0	0.0127	372.88

2.5 Conclusions

The LLE data for the ternary system H_2O + EtOAc + DES and H_2O + AcOH + DES at 298.15 K are reported. *P-x* data for the binary EtOAc + DES at 313.15 K and AcOH + DES at 323.15 K are also presented. Interaction parameters for the binaries EtOAc + DES, AcOH + DES, were obtained for the models UNIQUAC-HOC and NRTL-HOC. VLE data were also collected for the system EtOAc + EtOH. Together with VLE reported data for different binaries, some interaction parameters for a mixed acid esterification process were obtained by regression with the UNIQUAC-HOC model. The two models are able to reproduce well experimental and reported VLE data and the azeotropic points for the system. The parameters obtained in this work are useful for modeling and design of a RD process.

REFERENCES

2.6 REFERENCES

[1] A. A. Backhaus. Esters from fermented distillery waste. US Patent 1400852. (1921)

[2] R. Neumann, Y. Sasoon. Ind. Eng. Chem. Proc. Des. Dev. 23, 4 (1983) 654–659.

[3] E. M. Jones. Process for the recovery of an organic acid from the manufacture of a cellulose ester. (1997) US Patent 5648529.

[4] M. Scates. Recovery of acetic acid from dilute aqueous streams formed during a carbonylation process. (1997) US Patent 5599976.

[5] Z. Xu, A. Afacan, K. Chuang. Can. J. Chem. Eng. 77 (1999) 676–681.

[6] Z. Xu, A. Afacan, K. Chuang. Can. J. Chem. Eng. 77 (1999) 682-687.

[7] B. Saha, S. P. Chopade, S. M. Mahajani. Catal. Today, 60, 1-2 (2000) 147-157.

[8] C. Bianchi. Appl. Catal., B. 40 (2003) 93-99.

[9] A. Singh, A. A. Tiwari, S. M. Mahajani, R. D. Gudi. Ind. Eng. Chem. Res. 45, 6 (2006) 2017–2025.

[10] W. Hung, I. Lai, Y.W. Chen, S. B. Hung, H. B. Huang, M. J. Lee, C. C. Yu. Ind. Eng. Chem. Res. 45 (2005) 1722-1733.

[11] V. Ragaini, C.L. Bianci, C. Pirola and G. Carvoli. Appl. Catal. B: Environ. 64 (2006) 66-71.

[12] Singh, A. Tiwari, V. Bansal, R. D. Gudi, S. M. Mahajani. Ind. Eng. Chem. Res. 46, 26 (2007) 9196-9204.

[13] A. Arpornwichanop, K. Koomsup, S. Assabumrungrat. J. Ind. Eng. Chem. 14 (2008) 796–803.

[14] R. Kumar, H. Nanavati, S.B. Noronha, S. M. Mahajani. J. Chem. Technol. Biotech. 81, 11 (2006) 1767-1777.

[15] H.G. Joglekar, I. Rahman, S. Babu, B.D. Kulkarni, A. Joshi. Sep. Purif. Technol. 52 (2006) 1–17.

[16] A. Kolah, N. Asthana, D. Vu, C. T. Lira, D. J. Miller. Eng. Chem. Res. 47, 4 (2008) 1017-1025.

[17] D. Miller, N. Asthana, A. Kolah, D. Vu, C. Lira. Process for reactive esterification distillation. (2006) US Patent 20060252956.

[18] C. Delhomme,D. Weuster-Botza, F. E. Kühn. Green Chem. 11 (2009) 13–26.

[19] A. Cukalovic, C. V. Stevens. Biofuels, Bioprod. Biorefin. 2 (2008) 505–529.

[20] B. Hermann, M. Patel. Appl. Biochem. Biotechnol. 136 (2007) 361 – 388.

[21] O. Wolf, M. Crank, M. Patel, F. Marscheider-Weidemann, J. Schleich, B. Hüsing, G. Angerer. Techno-economic feasibility of large-scale production of Bio-based polymers in Europe, European Science and Technology Observatory, EUR 22103 EN. (2005).

[22] J. Zeikus, M. Jain, P. Elankovan. Appl. Microbiol Biotechnol. 51 (1999) 545-552.

[23] S. Varadarajan, D. J. Miller. Biotechnol. Prog. 15 (1999) 845-854.

[24] D. Sutton, G. Reed, G. Hiles. Process for the production of esters of mono-, di or polycarboxylic acids. (2007) US Patent 5599976.

[25] H. Bart, J. Reidetschlager. Sep. Sci. Technol. 30 (1995) 1849-1865.

[26] Ş. Kırbaşlar, S. Şahin, M. Bilgin. J. Chem. Eng. Data. 52 (2007) 1108–1112.

[27] Ş. Kırbaşlar, S. Şahin, M. Bilgin. J. Chem. Thermodyn. 39 (2007) 1463–1469.

[28] T. Anderson, J. Prausnitz. Ind. Eng. Chem. Proc. Des. Dev. 17(4) (1978) 552-561.

[29] T. Anderson, J. Prausnitz. Ind. Eng. Chem. Proc. Des. Dev. 17(4) (1978) 561-567.

[30] T. Magnussen, P. Rasmussen, P. Fredenslund. Ind. Eng. Chem. Proc. Des. Dev. 20 (1981) 331-339.

[31] H. Renon, J. Prausnitz. AIChE J. 14 (1968) 135-144.

[32] M. Uusi-Penttila, R. Richards, P. Blowers, B. Torgerson, K. Berglund. J. Chem. Eng. Data, 41 (1996) 235-238.

[33] D Vu, C. Lira, N. Asthana, A. Kolah, D. Miller.J. Chem. Eng. Data, 51 (2006) 1220-1225.

[34] D. Vu. Properties and separations of plant-derived chemicals. Thesis (Ph. D.) -Michigan State University. Dept. of Chemical Engineering and Materials Science. Michigan, USA. (2007).

[35] D. Othmer, P. Tobias. Ind. Eng. Chem. 34 (1942) 693–696.

[36] Aspentech, Aspen Physical Property System, physical property models/methods, Burlington, 2007.

[37] N. Calvar, A. Domínguez, J. Tojo. Fluid Phase Equilibr. 235 (2005) 215-222.

[38] G. B. Hong, M. J. Lee, H. Lin. Fluid Phase Equilibr. 203 (2002) 227–245.

[39] A. Reichl, U. Daiminger, A. Schmidt, M. Davies, U. Hoffmann, C. Brinkmeier, C. Reder, W. Marquardt. Fluid Phase Equilibr. 153 (1998) 113–134.

[40] C. H. Tu, Y. S. Wu, F. C. Ou. Fluid Phase Equilibr. 130 (1997) 243-252.

[41] L. Lee, W. Chen, J. Huang. J. Chem. Eng. Jpn. 29 (1996) 427-438.

[42] R. Stephenson, J. Stuart. J. Chem. Eng. Data. 31, 1 (1986) 56–70.

[43] J. M. Sørensen, W. Arlt Liquid-Liquid Equilibrium Data Collection. Binary Systems. DECHEMA. Chemistry Data Series, Vol V, Part 1. (1980).

[44] J. Gmenhling, U. Onken, W. Arlt. Vapor-Liquid Equilibrium Data Collection. Aqueous-Organic Systems. DECHEMA. Chemistry Data Series, Vol I, Part 1. (1978).

[45] J. Gmenhling, U. Onken, W. Arlt. Vapor-Liquid Equilibrium Data Collection. Organic Hydroxy Compounds: Alcohols. DECHEMA. Chemistry Data Series, Vol I, Part 2a. (1978).

[46] M. Kato, H. Konishi, M. Hirata. J Chem. Eng. Data 15, 3 (1970) 435-439.

[47] Y. T. Tang, H. Huang, I. Chein. J. Chem. Eng. Jpn. 36 (11) (2003) 1352-1363.

[48] L. H. Horsley. Azeotropic Data III. Advances in Chemistry Series 116, American Chemical Society. Washington D.C., USA. (1973).

3. Phase equilibria in Binary Mixtures with Monoethyl Succinate

3.1 Summary

Monoethyl succinate was produced by partial esterification of succinic anhydride with ethanol using Amberlyst 15 as catalyst. After separation and purification, the purity of monoethyl sucinate was confirmed by nuclear magnetic resonance (NMR). Vapor pressure of monoethyl succinate was measured and correlated with Antoine equation. Vapor-liquid equilibria at constant temperature were measured for the binary systems ethyl acetate + monoethyl succinate, acetic acid + monoethyl succinate, and water + monoethyl succinate at 323.15 K, and ethanol + monoethyl succinate at 313.15 K. Binary parameters for the NRTL equations were obtained by fitting experimental data using the regression tool in Aspen Plus® using the Hayden-O'Connell method for vapor phase fugacities. The model agrees reasonably well with the experimental data.

3.2 Introduction

Esterification of succinic acid (SA) present in diluted solutions is considered a viable recovery and separation alternative from complex mixtures produced during fermentation [1-5]. Owing that extent of esterification is limited by chemical equilibrium, removal of reaction products is necessary to obtain high conversions. As recognized by some researchers [2, 3] this can be accomplished using reactive distillation units in which water (H_2O) and succinate are selectively removed by distillation as top and bottom streams respectively, while SA is completely esterified at intermediate stages. In general the fermentation broth generated during succinic acid production also contains other carboxylic acids, mainly acetic acid (AcOH) [6-8]. Hence esterification of mixed acids occurs providing acetates and succinates are the major products.

In the specific case of esterification with ethanol (EtOH), the reaction proceeds sequentially through a series – parallel reaction scheme (Figure 3-1) with monoethyl succinate (MES) as intermediate product and diethyl succinate (DES) as the final product. Ethyl acetate (EtOAc) is also produce when AcOH is present in the mixture. In addition to the several applications reported for the major product (DES) [1], the intermediate MES can be used in the treatment of diabetes and starvation [9-13]. MES can also be used as raw material for asymmetric succinic esters and other derivatives [14].

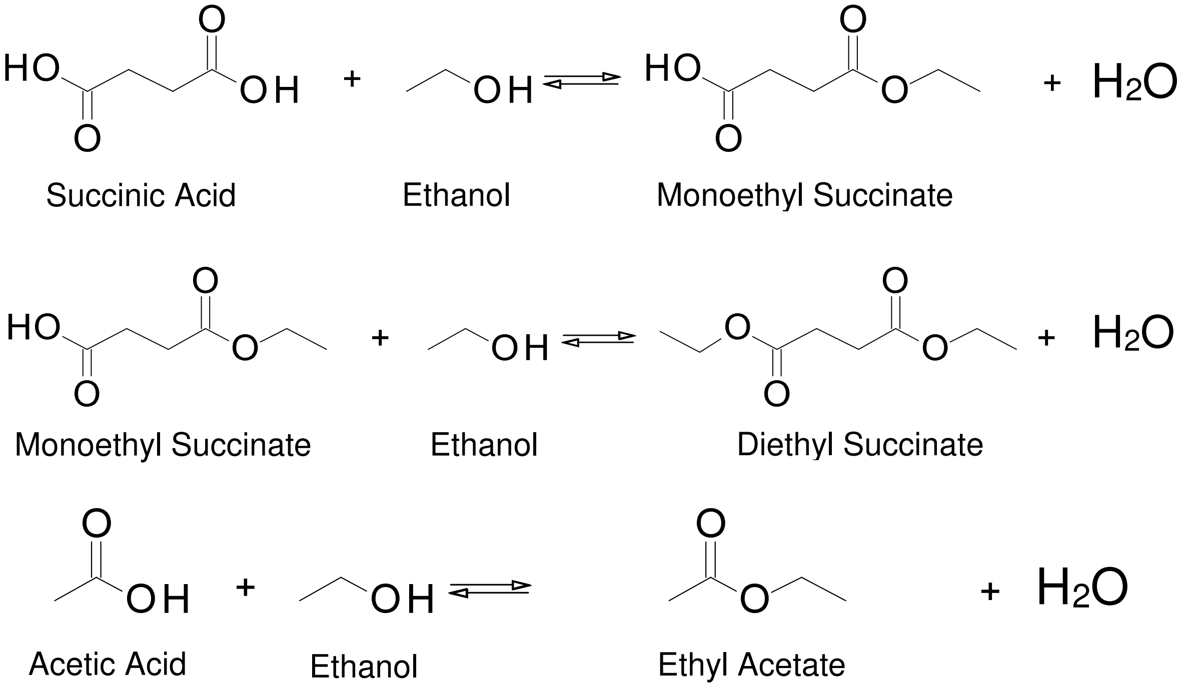

Figure 3-1. Scheme of reactions in a mixed acid esterification process.

In order to exploit a reactive distillation technology to recover SA though esterification with EtOH, computational modeling of the VLE in the reactive column is required including the behavior of the MES. Specifically, for SA or succinic derivatives there is lack of information on phase equilibria in multicomponent systems. Generalized group contribution methods have been used to predict activity coefficients in mixtures with succinic species, but predictions do not agree with experimental data [15, 16]. In previous work from our group, phase equilibria of binary and ternary mixtures with DES where studied [17-18]. Binary interaction parameters for NRTL equation [19] were obtained.

In this study experimental vapor-liquid equilibrium (VLE) data for the systems MES + EtOH, MES + EtOAc, MES + H_2O, and MES + AcOH are presented. These data literature were correlated with the NRTL equation using a regression tool included in Aspen Plus® [20]. We also present a comparison with predictions using a group contribution method (UNIFAC) [21, 22].

3.3 Material and methods

3.3.1 Materials

Succinic anhydride (99.3%, Sigma-Aldrich), succinic acid (100 %, Sigma-Aldrich), monoethyl succinate (89.1%, Sigma-Aldrich), diethyl succinate (99.8%, Sigma-Aldrich), ethanol (200 proof, Decon Labs), water (HPLC grade, J.T. Baker), ethyl acetate (99.99%, EMD), acetic acid (99.9%, Aristar), *n*-butanol (99.9%, Mallinckrodt), and acetonitrile (HPLC grade, EMD) were used for experiments and calibration. Purity of all compounds except MES was confirmed by gas chromatography and Karl-Fisher and the only impurity was water. In the case of MES, the purchased MES contains H_2O, EtOH, SA, and DES, and was used only for calibration purposes. Sodium carbonate (Jade Scientific, 99.5%), hydrochloric acid (EM science, 36.5%) and diethyl ether (EMD chemicals, 99.9%) were used during MES synthesis and purification. Hydranal-coulomat E solution (Riedel-de Haën) was used in Karl-Fisher analysis for water measurement.

3.3.2 Experimental procedures

3.3.2.1 MES synthesis

Among several routes and catalyst to produce succinic acid esters [11, 14, 23-30] and to avoid excessive contamination with other esterification products (water and DES), MES was prepared by partial esterification of succinic anhydride (SAnh) [11, 27] using Amberlyst 15® [31] as catalyst. A mixture of EtOH and SAnh (3:1 molar ratio) was placed in a glass stirred reactor at total reflux during 3 hours. The amount of dry catalyst employed was 2% with respect to SAnh weight, and it was washed with ethanol and dried under vacuum prior use. Once the reaction was completed the catalyst was removed by filtration and the liquid was evaporated at 343.15 K under vacuum in a rotary evaporator. After evaporation, the liquid was cooled down and titrated with a saturated aqueous solution of sodium carbonate until it reached a pH ~ 8 measured with paper test strips. This converted any acid to the sodium salts. To extract DES, the solution was washed twice with equal volumes of diethyl ether in a separatory funnel discarding the organic layer. The aqueous phase was then treated with hydrochloric acid (36.5 % by weight) until pH ~ 2 was reached (as indicated by pH paper). This solution was washed again twice with equal volumes of diethyl ether discarding the aqueous phase. The final organic phase was transferred to a flask and it was placed on a temperature controlled pot containing silicone oil. The pot was located over a magnetic stirring plate to maintain liquid in the flask under agitation.

Then, the organic liquid phase was evaporated under vacuum (~ 0.1 kPa) using an Edwards RV8® high vacuum pump monitoring total pressure by coupling the flash with a pressure control system borrowed from a wiped-film evaporator (Pope Scientific Inc.). Evaporation proceeded by increasing temperature up to 373.15 K until no further vaporization for 8 hours. After cooling at room temperature a cloudy liquid was obtained. Finally a white solid was removed by filtration to obtain a clear viscous liquid.

3.3.2.2 Vapor pressure measurement

Vapor pressure was obtained using the ebulliometer and method described in detail by Hoover *et al* [32]. In brief the ebulliometer consisted of a Thiele-tube-type glass pot with a small tungsten wire passing trough the bottom used as heating element. The pot was located over an asbestos shield and heat was supplied with a gas burner.

MES was added to the bottom of the ebulliometer with a syringe. The system was connected to a vacuum line, and a thermocouple previously calibrated (+/- 0.1 K) was inserted just below the liquid level. The pressure of the system (+/- 1.5 Pa) was measured and regulated using the control system borrowed from a vapor liquid equilibrium apparatus (Fisher VLE 100). The performance of the apparatus was verified measuring vapor pressure for different components (H_2O, EtOH, DES) assuring less than 1 % of difference with reported data.

3.3.2.3 Vapor-liquid experiment

P-x experiments were carried out using the apparatus presented in detail by Vu *et al* [33] and Vu [34] with modification described in a previous study [17]. The initial mixture of predetermined composition was stirred with a magnetic bar and the vessel was degassed under vacuum at the desired temperature. To assure degassing, after the initial pressure stabilized, the pressure was lowered to approximately half the equilibrium pressure and the vacuum valve was closed and the equilibrium pressure re-stabilized. Following re-equilibration, variations in pressure of ± 0.2 kPa in between repetitions were considered acceptable. Reported pressure is an average of three measurements obtained for every composition. A liquid sample was taken for analysis after pressure equilibration.

Subsequent equilibrium points were obtained by successive addition of one component to the binary mixture. In the case of binary mixtures with EtOH or H_2O only one or two successive additions were allowed, and the entire range of compositions was covered in several experiments starting with different initial compositions. This approach was followed because MES + EtOH and MES + H_2O are reactive mixtures, and esterification to DES or hydrolysis to SA might occur at prolonged contact times. In the case of mixtures with AcOH and EtOAc transesterification (acidolysis) did not occur.

Isothermal VLE of the binaries EtOAc + MES, AcOH + MES and H_2O + MES were measured at 323.15 K and the binary EtOH + MES at 313.15 (± 0.05 K). The modest temperatures were used to reduce reactions during experiments. GC and HPLC analysis indicated negligible reaction during the time required for equilibration and measurement.

3.3.3 Analysis

Samples were analyzed using both HPLC and GC. Samples were dissolved in water (~2% w/w) for HPLC analysis. In the case of GC samples were dissolved in acetonitrile (~5 % w/w) using butanol as internal standard (5% w/w).

A HP 5890® GC equipped with a flame ionization detector and a thermal conductivity detector was used. The injection port was maintained at 523.15 K in splitless mode, and detector temperature was 573.15 K. Helium was used as carrier (0.25 cm^3/s) and volume injections of 1×10^{-4} cm^3 were used. Samples were introduced in a single port with a CTC A200 S automatic injector, using *n*-butanol as internal standard and acetonitrile as solvent. A 30 m long Alltech Aquawax-DA column (0.53 mm i.d., 1.0 µm film thickness) coupled to a flow splitter to conduct the sample to both detectors in parallel. The temperature program was: column initial temperature 313.15 K (4 min), ramp rate 20 K/min, final temperature 523.15 K (1 min). Data integration was done using a Peaksimple chromatography data system (SRI Model 302) with Peaksimple software version 3.59.

A HPLC system with a Waters® 717 autosampler, a Waters® 410 refractive index detector and a Perkin Elmer LC90 UV detector was used for succinic species analysis and confirmation. A 100 x 7.6 mm fast acid analysis column (Bio-rad®) was used for the separation. 1 ml/min of 5 mM aqueous solution of H_2SO_4 was used as mobile phase. Because retention time of EtOH and MES was similar, only UV detection was used to evaluate MES.

Samples of known composition in the range of interest were used for calibration of GC and HPLC, and injected by triplicate to obtain repeatability within 0.5% by mass.

Karl-Fisher analysis (Aquacount coulometric titrator AQ-2100) was used to measure water content in reagents and samples.

NMR spectra to confirm structure and purity of the MES was measured with a Varian UnityPlus - 500 spectrometer, using deuterated chloroform ($CDCl_3$) as solvent referenced at 7.24 ppm for ^1H and 77 ppm for ^{13}C.

Tests to confirm reported melting point and to verify thermal stability of MES were conducted using differential scanning calorimetry (DSC) at atmospheric pressure (Mettler-Toledo DSC1). A 10 mg sample of frozen MES (253 K) was weighted (Mettler-Toledo AB265-S, ± 0.01mg) and heated in a hermetically sealed aluminum crucible at 10 K/min under nitrogen flow (20ml/min) over a range of temperature of 223.15 to 523.15 K. An equilibration time at the initial and final temperature of 4 minutes was used.

3.4 Results and discussion

After the synthesis and separation 97.5 % (w/w) MES cloudy liquid was obtained. The only impurities observed by GC and HPLC analysis corresponded to SA (2%) and DES (0.5%). This liquid was filtered and the majority of SA was removed and the clear liquid product obtained (> 99 %) was stored at 278 K. Purity of the product was confirmed several times and it remained constant during the usage period. Low temperature storage turned the liquid cloudy, but at room temperature it became clear again. This behavior is similar to that observed in the standard used for calibration (Sigma-Aldrich, 89.1%).

Because of the difficulties of removing the small amount of SA and DES in the final product, and considering instability of MES in water (the solvent recommended as mobile phase for chromatographic separation of acids), all the experiments were performed with this product without further purification. An NMR spectrum of the product presented in Figure 3-2 agrees with previous reports [35-37]. ^1H NMR (500 MHz, $CDCl_3$) δ 4.13 (q, $J = 7$ Hz, 2 H), 2.66 (m, 2

H), 2.60 (m, 2 H), 1.24 (t, *J* = 7 Hz, 3 H). ^{13}C NMR (126 MHz, $CDCl_3$) δ 178.3, 172.1, 60.8, 28.9 (2 C), 14.1. Despite succinate species have similar structures; MES differentiates clearly because of the shift in peak locations and multiplets observed on CH_2 signals caused by the asymmetry of the molecule around the four carbon block (only one ethyl terminal group). Besides it distinguishes from SA by effect caused by the ester-type bond (CH_2 group signal labeled as B in Figure 3-2) and from DES by the acid functional group (labeled as F in ^{13}C NMR spectrum).

In DSC experiments some challenges were found due to melting of frozen MES while sample weighting or during initial stabilization of the calorimeter. Complete crystallization of MES in the freezer prior experiments took around 3 days, but it readily melted at room temperature.

Calorimetric data presented in Figure 3-3 indicates that below 280 K both exothermic and endothermic events occurred. This behavior might be caused by the slow re-crystallization of fractions of MES melted before the analysis followed by a sudden change of phase at the fusion point of the entire bulk. Even tough melting point was not strictly obtained from DSC data; the minimum signal during melting event peak was located around 281 K, close to reported MES melting point.

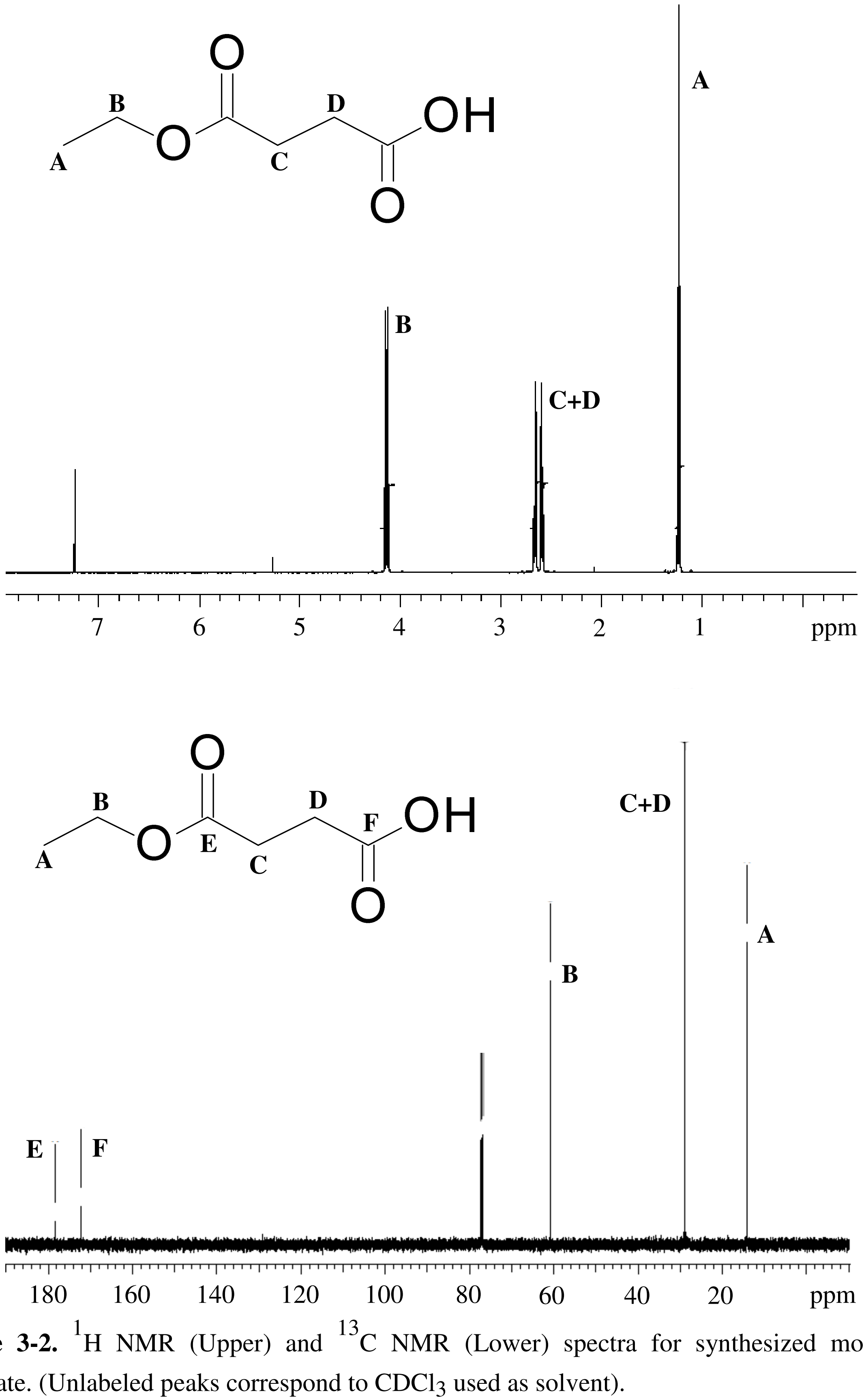

Figure 3-2. ^{1}H NMR (Upper) and ^{13}C NMR (Lower) spectra for synthesized monoethyl succinate. (Unlabeled peaks correspond to $CDCl_3$ used as solvent).

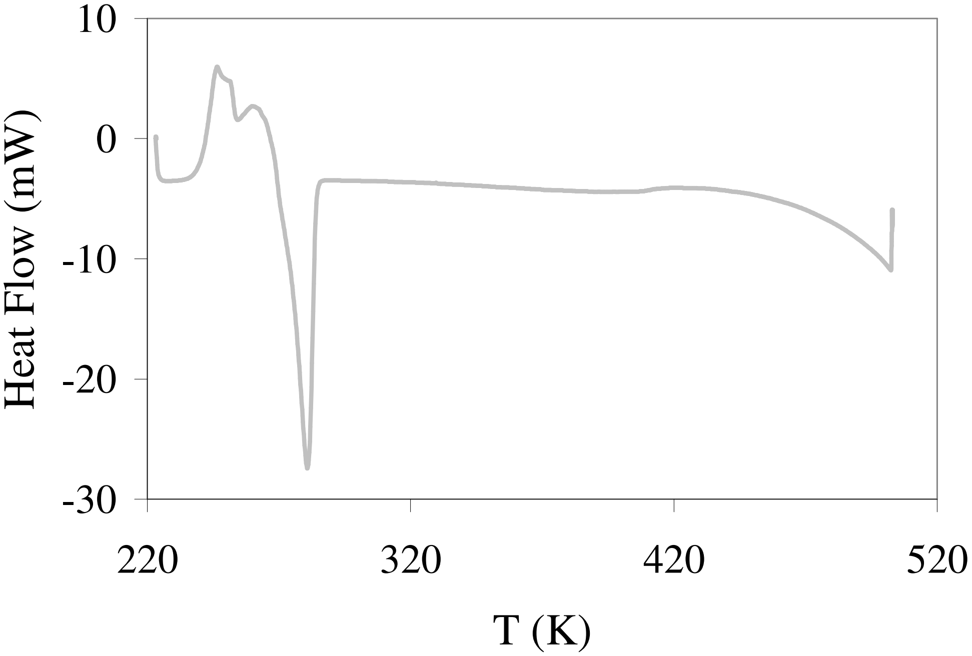

Figure 3-3. Calorimetric curve obtained by DSC of a MES sample measured under N_2 atmosphere at 101.3 kPa.

Another thermal event was observed above 460 K but it was not reproduced in successive heating cycles ran on the same sample. Crucible was weighted after each cycle and changes in weight higher than 10% between runs were observed. This indicates that MES can be affected by thermal decomposition at high temperatures and this can limit maximum working temperatures during phase equilibria experiments.

Taking into account the low volatility and the non-polar character of succinic species compared with other components, it is expected that the low content of SA and DES do not affect vapor pressure measurements or vapor-liquid equilibria significantly. Thus filtrated MES was used without further refining during experiments. Measured vapor pressure data for MES are presented in Table 3-1.

Table 3-1. Experimental vapor pressure data for MES.

T (K)	P (Pa)	T (K)	P (Pa)	T (K)	P (Pa)	T (K)	P (Pa)
417.7	1586.6	449.1	8116.8	460.3	14144.6	468.3	20172.4
421.2	2088.9	450.5	8619.1	461.1	14646.9	468.8	20674.7
425.1	2591.3	452.1	9121.4	462	15149.2	469.5	21177.0
428.5	3093.6	453.2	9623.7	463.3	15651.5	469.7	21679.4
433	3595.9	454.7	10126.0	463.8	16153.9	469.8	22181.7
435.6	4098.2	455.7	10628.4	464.2	16656.2	470.1	22684.0
436.7	4600.5	456.5	11130.7	464.5	17158.5	470.3	23186.3
439.8	5102.8	457.2	11633.0	465.2	17660.8	470.4	23688.6
440.3	5605.2	458.2	12135.3	465.8	18163.1	470.5	24191.0
443	6107.5	458.4	12637.6	466.7	18665.5	471.1	24693.3
444.3	6609.8	459.8	13139.9	467.3	19167.8	471.4	25195.6
445.9	7112.1	460.1	13642.3	467.8	19670.1	471.9	25697.9
447.6	7614.4						

Below 460 K one liquid sample was used to evaluate several different equilibration temperatures. As expected from DSC results, above 460 K a change in color (liquid turned yellowish) and the formation of a solid was observed when MES was heated for several hours during measurement. So for high temperature experiments only 3 or 4 points were evaluated with each sample of MES. Between experiments, the ebulliometer was cleaned and air dried to remove decomposition products of a previous run. Experimental data agree with the trend of literature reports [37-38]. Regression of the Antoine equation parameters was performed in Aspen Plus® obtaining good fitting as observed in Figure 3-4. Final parameters of Antoine model are presented in Equation 3-1.

$$\ln P(Pa) = 20.8887 - \frac{3182.4685}{T(K) - 180.2349} \tag{3-1}$$

VLE experimental data at constant temperature for binary mixtures EtOAc + MES, AcOH + MES, H_2O + MES and EtOH + MES are listed in Table 3-2 and plotted in Figures 3-4 to 3-7. In most cases mixtures were homogeneous but in the case of H_2O a slightly cloudy and stable solution was observed with high MES concentration.

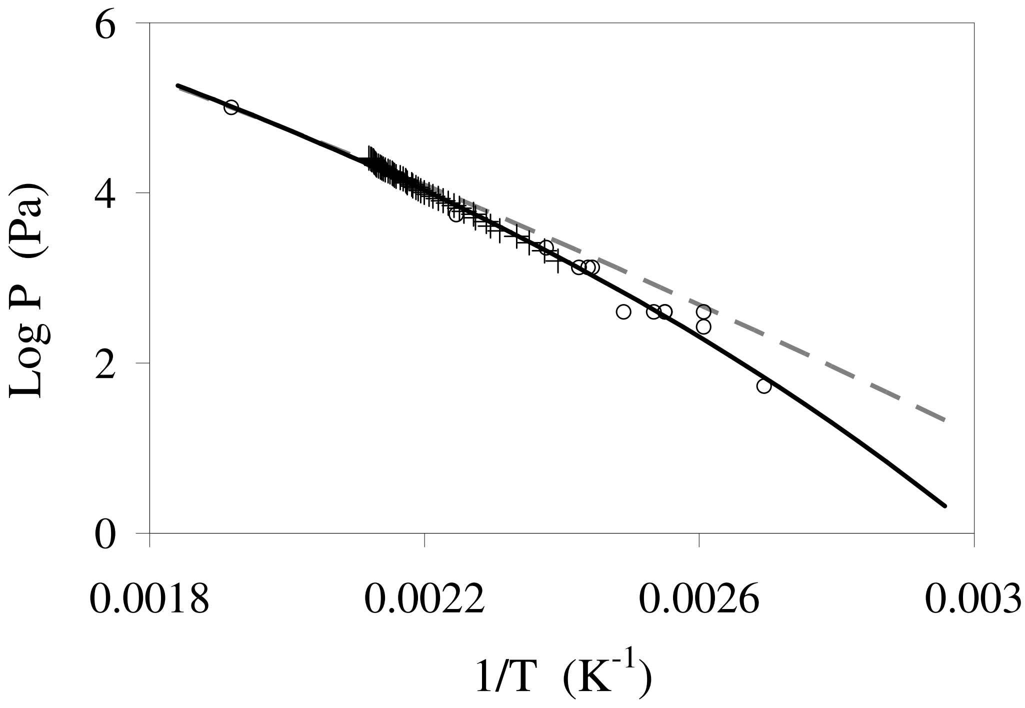

Figure 3-4. Vapor pressure data for MES. (○) Reported data [37, 38], (+) This work, (— —) ASPEN default, (▬) Regression with Antoine equation.

Table 3-2. ***P-x*** **data for binary systems with MES.**

T = 323.15 K						T = 313.15 K	
X_{EtOAc}	P (Pa)	X_{AcOH}	P (Pa)	X_{H2O}	P (Pa)	X_{EtOH}	P (Pa)
0.000	133.3	0.000	133.3	0.000	133.3	0.000	26.7
0.029	1506.5	0.191	706.6	0.109	2639.8	0.015	426.6
0.152	7439.4	0.269	866.6	0.206	4239.7	0.030	813.3
0.232	11065.8	0.284	1079.9	0.265	5146.2	0.032	746.6
0.294	13958.9	0.364	1546.5	0.323	6532.8	0.170	3039.8
0.299	14318.8	0.399	1626.5	0.325	6799.4	0.192	3119.7
0.396	17825.2	0.472	2039.8	0.592	10185.8	0.279	4772.9
0.413	18411.8	0.443	2173.2	0.625	10185.8	0.363	5772.9
0.524	22771.5	0.603	3159.7	0.769	11319.1	0.387	6652.8
0.539	23104.8	0.624	3239.7	0.890	11745.7	0.515	8745.9
0.763	30637.5	0.630	3493.0	1.000	12225.7	0.603	10345.8
0.765	31344.1	0.655	3639.7			0.617	10279.2
0.776	31650.7	0.733	4493.0			0.729	12998.9
0.919	35117.1	0.853	6026.2			0.751	13158.9
1.000	37690.2	1.000	7492.7			0.880	15678.7
						0.971	17265.2
						1.000	17638.6

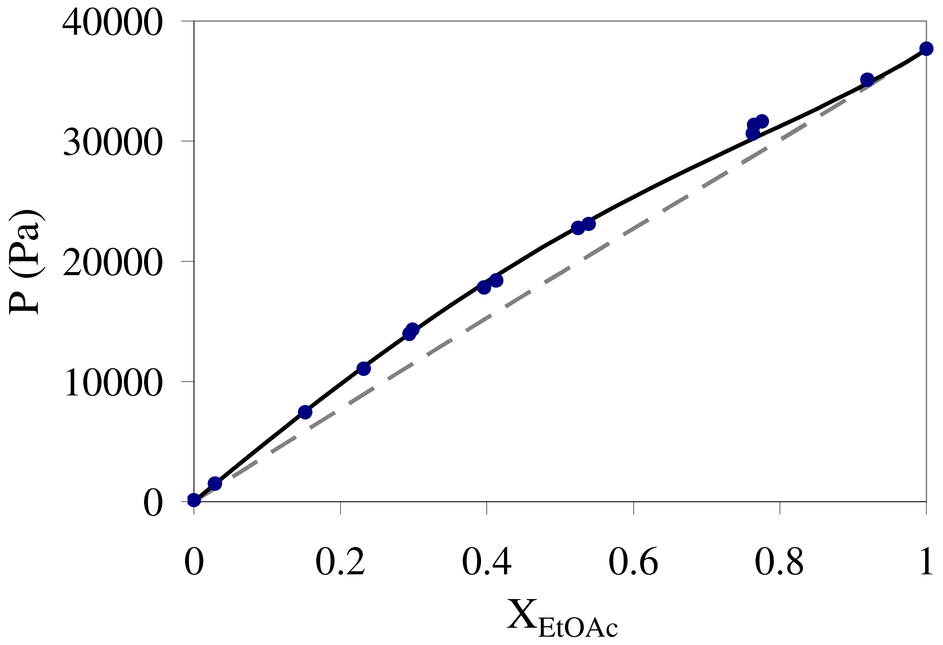

Figure 3-5. Binary *P-x* diagram for the binary EtOAc + MES at 323.15 K. (●) Experimental data, (— —) UNIFAC, (▬) Regressed NRTL - HOC.

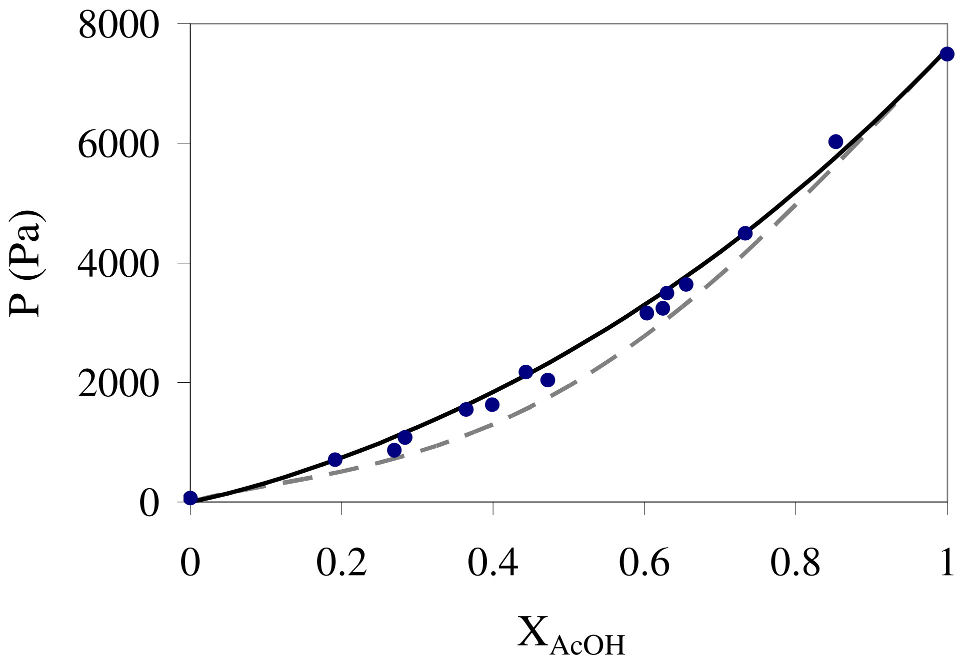

Figure 3-6. Binary *P-x* diagram for the binary AcOH + MES at 323.15 K. (●) Experimental data, (— —) UNIFAC, (▬) Regressed NRTL - HOC.

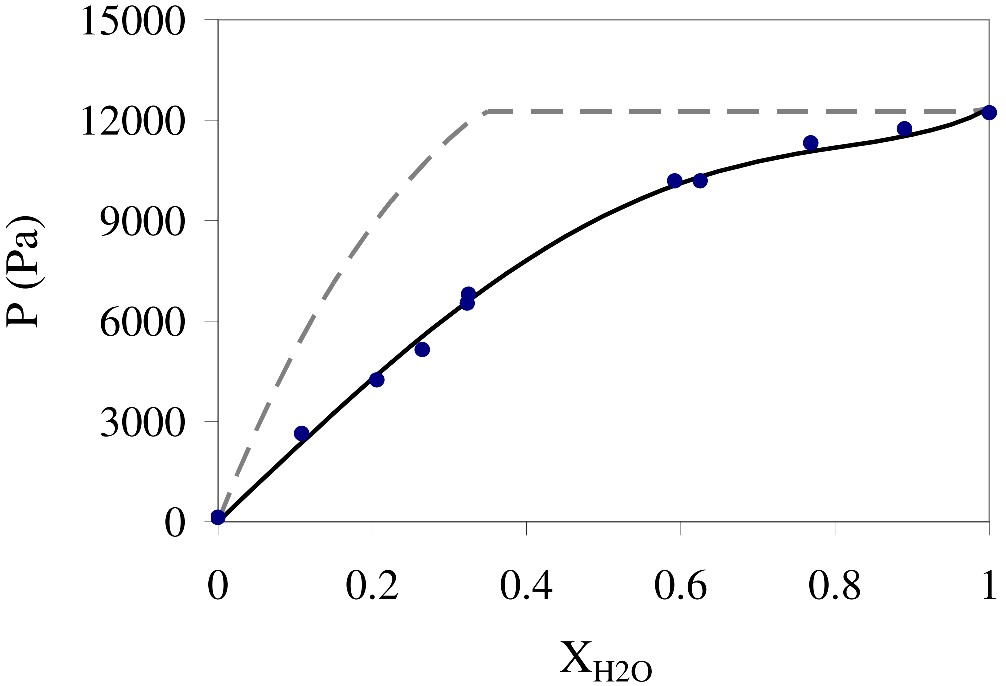

Figure 3-7. Binary *P-x* diagram for the binary H_2O + MES at 323.15 K. (●) Experimental data, (— —) UNIFAC, (▬) Regressed NRTL - HOC.

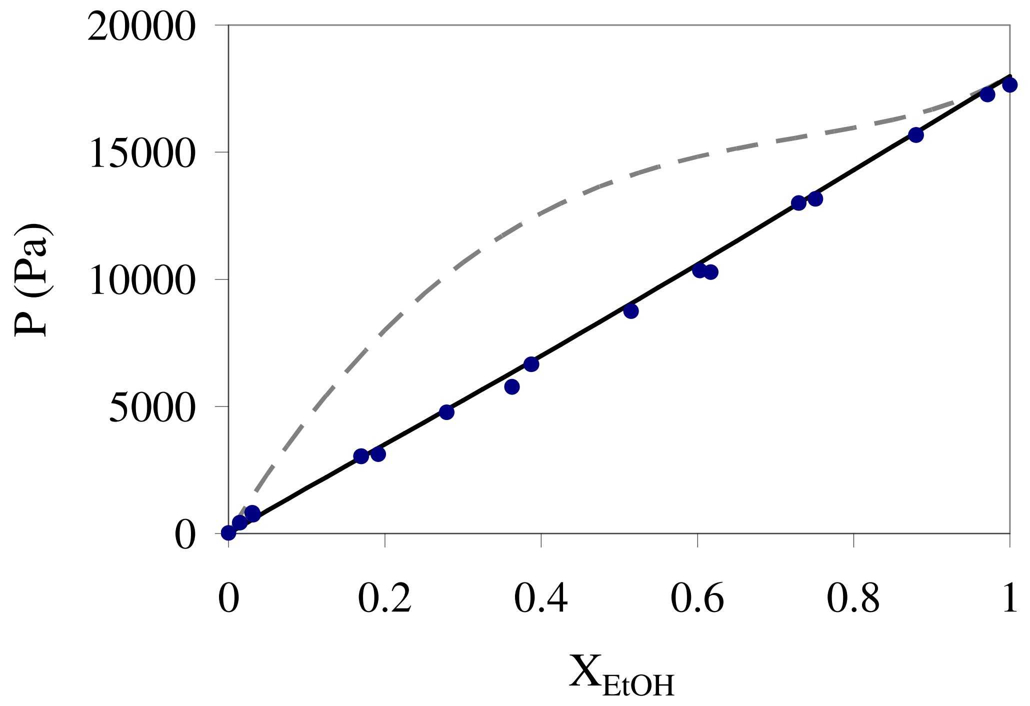

Figure 3-8. Binary *P-x* diagram for the binary EtOH + MES at 313.15 K. (●) Experimental data, (— —) UNIFAC, (▬) Regressed NRTL - HOC.

Binary VLE were fitted to NRTL equation (Equation 2) using Hayden-O'Connell (HOC) equation to model the vapor phase. HOC association parameters were obtained from ASPEN database for H_2O + EtOAc and H_2O + EtOH and EtOH + EtOAc. For the binaries EtOAc + MES, AcOH + MES, H_2O + MES, EtOH + MES, MES + MES the HOC parameters are not available, and they were assumed equal to those existing for interactions with ethyl acetate from the same database summarized in Table 3-3.

$$\ln\gamma_i = \frac{\sum\limits_j x_j\tau_{ji}G_{ji}}{\sum\limits_k x_k G_{ki}} + \sum_j \frac{x_j G_{ij}}{\sum\limits_k x_k G_{kj}}\left(\tau_{ij} - \frac{\sum\limits_m x_m \tau_{mi} G_{mi}}{\sum\limits_k x_k G_{kj}}\right) \tag{3-2}$$

The parameter adjust was performed with the regression tool in ASPEN by minimization of the maximum likelihood objective function. A list of the NRTL parameters is presented in Table 3-3. VLE model fits experimental data and improved predictions obtained by generalized group contribution methods. Figures 3-4 to 3-7 present experimental *P*-*x* data compared with NRTL-HOC and UNIFAC predictions.

Table 3-3. Binary parameter for NRTL-HOC models. $G_{ij} = \exp(-\alpha_{ij}\,\tau_{ij})$, $\tau_{ij} = (b_{ij}/T)$.

HOC Association Parameters					
	H_2O	**EtOH**	**EtOAc**	**AcOH**	**MES**
H_2O	1.7	1.55	1.3	2.5	1.3
EtOH	1.55	1.4	1.3	2.5	1.3
EtOAc	1.3	1.3	0.53	2	0.53
AcOH	2.5	2.5	2	4.5	2
MES	1.3	1.3	0.53	2	0.53

NRTL				
	EtOAc MES	**AcOH MES**	**H_2O MES**	**EtOH MES**
b_{ij}	191.701	-176.711	880.7603	-292.308
b_{ji}	-142.115	302.7477	-200.977	400.6306
α_{ij}	0.3	0.3	0.3	0.3

For the case of H_2O + MES, the experimental data do not exhibit the liquid-liquid phase splitting predicted by UNIFAC. In mixtures with EtOAc and AcOH (less polarity, less hydrogen bonding) UNIFAC predictions are quite good. This behavior has been recognized before in systems with succinic acid derivatives [18]. This indicates that UNIFAC can be used with reasonable confidence to predict phase equilibria in mixtures of MES with low polarity components such as diethyl succinate, diethyl ether. Binary interaction parameters for those mixtures are also required for the complete modeling of the esterification system.

3.5 Conclusions

MES was produced at by partial esterification of SAnh with EtOH using Amberlyst 15 as catalyst. After separation and refining high purity MES (> 99 %) was obtained as confirmed by NMR analysis. MES vapor pressure was measured from 417-471 K and results agreed with previous reports. Parameters for Antoine equation were obtained by fitting using regression in ASPEN. VLE experiments at constant temperature were evaluated in binary mixtures of EtOAc + MES, AcOH + MES and H_2O + MES at 323.15 K and the binary EtOH + MES at 313.15. Finally experimental data were fitted with the NRTL equation to obtain binary interaction parameters for phase equilibria calculation. VLE modeling using NRTL and HOC equation for the vapor phase agrees with experimental observations. Reasonably good predictions of VLE using UNIFAC method were also obtained in binary mixtures of MES with components of low polarity. The parameters obtained in this work will represent the VLE reasonably well for reactive distillation design purposes and can be used to develop activity-based kinetics.

REFERENCES

3.6 REFERENCES

[1] S. Varadarajan, D. J. Miller. Biotechnol. Prog. 15 (1999) 845-854.

[2] D. J. Miller, N. Asthana, A. Kolah, D. Vu, C. T. Lira. Process for reactive esterification distillation. (2006) US Patent application 20060252956.

[3] D. Sutton, G. Reed, G. Hiles. Process for the production of esters of mono-, di or polycarboxylic acids. (2007) US Patent 5599976.

[4] S. V. Budarin, R. Luque, D. Macquarrie, J. Clark. Chem. Eur. J. 13 (2007) 6914-6919.

[5] C. Delhomme, D. Weuster-Botza, F. E. Kühn. Green Chem. 11 (2009) 13–26.

[6] J. Zeikus, M. Jain, P. Elankovan. Appl. Microbiol Biotechnol. 51 (1999) 545-552.

[7] P. Rogers, J. Chen, M. Zidwick. Organic Acid and Solvent Production, Part I: Acetic, Lactic, Gluconic, Succinic and Polyhydroxyalkanoic Acids. Chapter 3.1. Prokaryotes 1 (2006) 511–755.

[8] A. Cukalovic, C. V. Stevens. Biofuels, Bioprod. Biorefin. 2 (2008) 505–529.

[9] M. J. MacDonald, L. A. Fahien, R. J. Mertz, R. S. Rana. Arch. Biochem. Biophys. 269 (1989) 400-6.

[10] L. Ladrière, W. J. Malaisse. Ann. Nutr. Metab. 41, 2 (1997) 118-125.

[11] M. M. Kadiata, W. J. Malaisse. Diabetes Research 33, 6 (1998) 237-243.

[12] L. Pari, R. Saravanan. Chem. Biol. Interact. 169, 1 (2007) 15-24.

[13] R. Saravanan, L. Pari. Mol. Cell. Biochem. 296, 1-2 (2007) 165-76.

[14] G. Sabitha, R. Srividya, J. S. Yadav. Tetrahedron 55, 13 (1999) 4015-4018.

[15] Ş. Kırbaşlar, S. Şahin, M. Bilgin. J. Chem. Eng. Data. 52 (2007) 1108–1112.

[16] Ş. Kırbaşlar, S. Şahin, M. Bilgin. J. Chem. Thermodyn. 39 (2007) 1463–1469.

[17] A. Orjuela, A. Yanez, D. Vu, D. Bernard-Brunel, D. J. Miller, C. T. Lira. Fluid Phase Equilibr. 290, 1-2 (2010) 63-67.

[18] A. Orjuela, A. Yanez, P. Rossman, D. Vu, D. Bernard-Brunel, D. J. Miller, C. T. Lira. Fluid Phase Equilibr. 290, 1-2 (2010) 68-74.

[19] H. Renon, J. M. Prausnitz. AIChE J. 14 (1968) 135-144.

[20] Aspentech, ASPEN Physical Property System, physical property models/methods, Burlington, 2007.

[21] U. Weidlich, J. Gmehling. Ind. Eng. Chem. Res. 26 (1987) 1372-1381.

[22] J. Gmehling, J. Li, M. Schiller. Ind. Eng. Chem. Res. 32 (1993) 178-193.

[23] J. Walker. J. Chem. Soc. Trans. 61 (1892) 696-717.

[24] E. Fourneau, S. Sabetay. Bulletin de la Societe Chimique de France. 43 (1928) 859-61.

[25] M. Dana, M. Campagnole, M. J. Bourgeois, E. Montaudon, S. Laugier. Recent Res. Devel. Org. Chem. 5, 1 (2001) 1-7.

[26] R. Reddy, P. Lyengar, G. Nagendrappa, B. Prakash. Catal. Letters 101, 1–2, (2005) 87-91.

[27] F. H. Wang, P. F. Zou, W. Lei, M. Z. Xia, F. Y. Wang. Jiangsu Huagong. 33, Suppl. (2005) 170-172.

[28] C. R. Reddy, G. Nagendrappa, B.S. Jai Prakash. Catal. Commun. 8 (2007) 241–246.

[29] J. H. Clark, V. Budarin, T. Dugmore, R. Luque, D. J. Macquarrie, V. Strelko. Catal Commun. 9 (2008) 1709–1714.

[30] A. Kolah, N. Asthana, D. Vu, C. T. Lira, D. J. Miller. Ind. Eng. Chem. Res., 2008, 47, 15 (2008) 5313–5317.

[31] Amberlyst 15 dry. Industrial grade strongly acidic catalyst. Technical data sheet. Rohm and Haas, Philadelphia, USA. 2006.

[32] S. R. Hoover, J. Harry, E. F. Mellon. Anal. Chem. 25, 12 (1953) 1940-1941.

[33] D. Vu, C. T. Lira, N. Asthana, A. Kolah, D. J. Miller. Chem. Eng. Data, 51 (2006) 1220-1225.

[34] D. Vu. Properties and separations of plant-derived chemicals. Thesis (Ph. D.) Michigan State University. Dept. of Chemical Engineering and Materials Science. Michigan, USA. (2007).

[35] J. Regourd, A. A. Ali, A. Thompson. J. Med. Chem. 50, 7 (2007) 1528-1536.

[36] L. N. Monsalve, M. Y. Machado, A. A. Ghini, A. Baldessari. Tetrahedron. 64, 8 (2008) 1721-1730.

[37] Scifinder (2010) CAS-1070-34-4, Chemical Abstracts Service: Columbus, OH. [Online]. Available: https://scifinder.cas.org. Accessed May, 2010.

[38] Beilstein Database – Abstracts. Beilstein Institute zur Foerderung der Chemischen Wissenschaften. CAS-1070-34-4. Accessed May, 2010.

4. Solubility and Phase Equilibria for Mixtures with Succinic Acid

4.1 Summary

Solubility of succinic acid in binary mixtures with ethyl acetate, diethyl succinate, diethyl ether, ethanol and water was measured at temperatures from 278 K to 313 K. Using experimental and reported data together with a solid-liquid equilibrium model, activity coefficients for succinic acid in solution were obtained. In order to ensure thermodynamic consistency of the model, thermal properties for succinic acid were reviewed and studied experimentally using differential scanning calorimetry (DSC) at atmospheric pressure and high pressure (ca. 7 MPa). Heat capacities for solid and liquid phases as well as enthalpy of fusion were obtained from calorimetric measurements. Binary parameters for the NRTL equations were obtained by fitting experimental and reported solubility data. The model agrees reasonably well for binary and ternary mixtures.

4.2 Introduction

Succinic acid (SA) obtained by fermentation is considered a major building block for the chemical bio-refinery. It can be used as feedstock and intermediate in production of solvents, surfactants, biodegradable polymers, specialty chemicals and commodities. Commonly, SA produced by fermentation is obtained in diluted aqueous solutions. These solutions might contain other carboxylic acids mainly acetic acid (AcOH), and also small amounts of pyruvic, lactic, and/or formic acid [1, 2], making difficult to isolate SA as pure crystals. Among the different alternatives to retrieve carboxylic acids from fermentation broths, esterification has proven success [3-6]. In the case of SA, a complex mixture of acids and esters are obtained during the recovery process.

When esterification is carried out with EtOH using acid catalysts, diethyl succinate (DES) is produced. This ester is used as solvent, as additive in fragrance formulation, and potentially in the near future as an economical feedstock for butanediol or PBS biodegradable polymers (polybutilene succinate). Together with DES, ethyl acetate (EtOAc) is the major byproduct, and dehydration of EtOH to diethyl ether (DEE) has been observed [7]. A scheme of the process reaction network is presented in Figure 4-1.

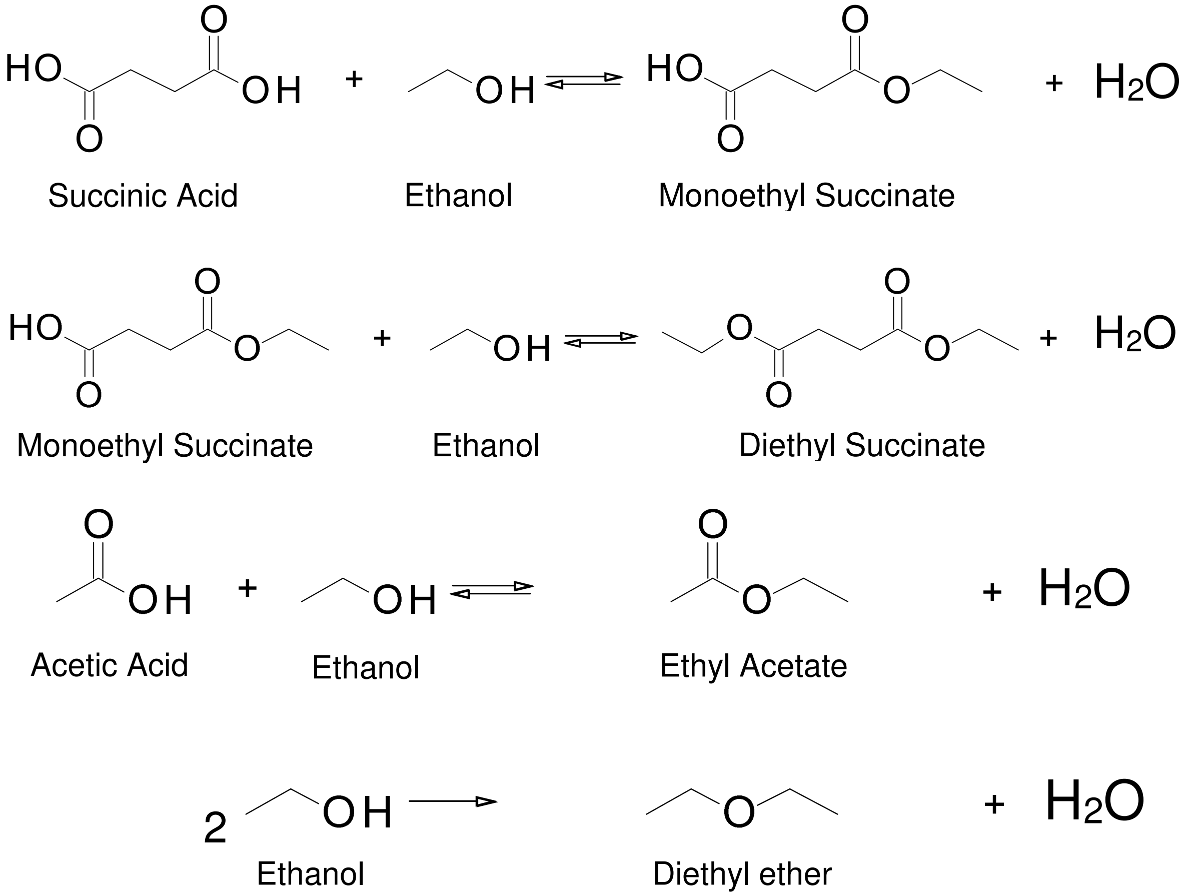

Figure 4-1. Chemical network scheme for mixed acids recovery process by esterification.

In these complex mixtures of polar and non-polar components (generally recognized as highly non-ideal) SA may dissolve, precipitate or react depending on the phase equilibria and kinetic of reactions.

In order to evaluate feasibility of a recovery method by esterification and to compare it with traditional recovery methods, computational modeling based upon reliable phase equilibria and chemical kinetics is required. In the open literature there are many studies describing physicochemical properties of pure solid SA, but only few on SA in mixtures. Equilibrium data in binary mixtures with water (H_2O) have been extensively reported [8-13], but only few in other solvents [13-17]. In previous studies, only the binary SA + H_2O phase equilibria have been modeled and in this case generalized group contribution and local composition methods have been used. In all cases only one of these: solubility data [11, 18], vapor pressure [18], or H_2O activity [19-23], have been used to regress or compare agreement with the models. In some cases predictions do not agree with experimental data or present inconsistency when both solubility of SA and water activity are considered simultaneously [11, 17].

In previous work [24, 25], phase equilibria of DES in binary and ternary mixtures were studied and local composition models were used to predict reasonably well non-idealities for this kind of mixtures. In this work experimental and literature SA solid-liquid equilibria (SLE) data were used to fit binary parameters for the NRTL equation [26]. Solubility data for the binaries SA+DES, SA+DEE, SA+EtOAc, SA+H_2O and SA+EtOH were measured in the range of 283.15K to 313.15 K at 101.325 kPa. Thermal analyses on solid SA and succinic anhydride (SAnh) were performed to confirm reports on physical properties (melting point, lambda transition and heat capacities) used on SLE calculation.

This remainder of the introductory section is used to illustrate thermodynamic inconsistencies noted when literature data are used for calculating activities coefficients. Then the experimental materials, methods and results will be presented. Finally, we revisit the modeling to demonstrate the results incorporating the new experimental measurements, and evaluate the options for thermodynamic modeling.

4.2.1 Model calculations using literature data

The activity coefficient of a solute at the solubility limit at a given temperature is given by the solid-liquid equilibrium equation [27].

$$\ln(a_{SA}) = \ln(x_{SA}\gamma_{SA}) = \frac{\Delta H_{fus}}{R}\left[\frac{1}{T_{fus}} - \frac{1}{T}\right] + \left(\frac{1}{RT}\right)\int_{T}^{T_{fus}}\left(C_{pL} - C_{pS}\right)dT - \left(\frac{1}{R}\right)\int_{T}^{T_{fus}}\frac{\left(C_{pL} - C_{pS}\right)}{T}dT - \lambda_{PT} \tag{4-1}$$

In our application, pure succinic acid is assumed as the solid phase and the temperature of the triple point was assumed equal to the fusion temperature (T_{fus}). a_{SA}, x_{SA}, and γ_{SA} are the activity, mole fraction and the Lewis-Randall activity coefficient of succinic acid in saturated solution respectively. ΔH_{fus} is the enthalpy of fusion, and C_{pL} and C_{pS} are the specific heat per mole of liquid and solid phase. λ_{PT} is the effect of a solid-solid phase transition. In this expression heat capacity of both solid phases is assumed equal.

When a solid-solid phase transition occurs below melting point, it is of the lambda type, and its effect in total Gibb's free energy change is accounted for [27]:

$$\lambda_{PT} = \frac{\Delta H_{PT}}{R}\left[\frac{1}{T} - \frac{1}{T_{PT}}\right] \tag{4-2}$$

where T_{PT} and ΔH_{PT} are the temperature and enthalpy of phase transition. It is known that succinic acid has a lambda transition from a monoclinic crystal (β-form) to a triclinic crystal (α-form). Reported conditions indicate that such transition [28-34] occurs in a broad range of temperatures (up to 50-60 K near the equilibrium temperature). In addition to this there are some challenges to obtain accurate measurements by calorimetric studies due to hygroscopic nature of the acid (melting of the water content may look like a phase transition as mistakenly reported by Parks and Huffman [29, 35], and currently included in NIST reports [36]). Water may also interfere with sublimation [37] and dehydration to form succinic anhydride may interfere near the melting temperature [38]. For these reasons, the solid-solid transition enthalpy for succinic acid has not been reported. For similar aliphatic dicarboxylic acids, reported phase transition enthalpies are all on the same order of magnitude [32, 33] (Oxalic 1.3 kJ/mol, malonic 1.6 kJ/mol, glutaric 2.4 kJ/mol, pimelic 1 kJ/mol), so for succinic acid it is assumed the average between C3 and C5 dicarboxylic acids. Table 4-1 list reported data used for preliminary solid-liquid equilibrium calculation.

Using the solid-liquid equilibrium model (Equation 4-1) together with experimental solubility data in different solvents, binary parameters for NRTL equation are regressed. The format of the equation corresponds to that used in Aspen Plus® [40] and is presented in Equations 4-3 and 4-4.

Table 4-1. Properties of succinic acid.

Property		Value	Reference
T_{fus} (K)		459	[36]
ΔH_{fus} (kJ/mol)		32.945	
T_{PT} (K)		389.7	
ΔH_{PT} (kJ/mol)		2.0	‡
C_{pL} (J/mol K) $C_{pL} = A_L + B_L T(K) + C_L T^2 + D_L T^3$ (471-699 K)	A_L	-152.587	[39]
	B_L	2.2939	
	C_L	-4.35730E-03	
	D_L	3.19590E-06	
C_{pS} (J/mol K) $C_{pS} = A_S + B_S T(K) + C_S T^2$ (90-323 K)	A_S	26.2	
	B_S	0.4252	
	C_S	0	

‡ Assumed as average from reported data for C3-C5 dicarboxylic acids

$$\ln \gamma_i = \frac{\sum_j x_j \tau_{ji} G_{ji}}{\sum_k x_k G_{ki}} + \sum_j \frac{x_j G_{ij}}{\sum_k x_k G_{kj}} \left(\tau_{ij} - \frac{\sum_m x_m \tau_{mi} G_{mi}}{\sum_k x_k G_{kj}} \right) \tag{4-3}$$

$$G_{ij} = \exp\left(-\alpha_{ij}\tau_{ij}\right) \qquad \tau_{ij} = a_{ij} + \frac{b_{ij}}{T} \tag{4-4}$$

Parameters adjustment was performed by minimization of the differences between experimental and estimated activity coefficients over the entire range of compositions and temperatures using a minimum squares method as described in the following objective function:

$$f\left(x_{SA},T\right)=\frac{1}{n}\sum_{k=1}^{n}\left(\gamma_{SA-Exp.}-\gamma_{SA-Calc.}\right)^{2} \tag{4-5}$$

where n is the number of data points, γ_{SA-Exp} is the activity coefficient of succinic acid computed from Equation (4-1) using experimental solubility data, and $\gamma_{SA-Calc.}$ is the activity coefficient of succinic acid computed from NRTL model. For the specific case of the binary SA-H_2O there are also reports on water activity at 298.15 K [12, 19, 20, 41, 42]. In this case the objective function also included differences of the activity coefficient of water.

According to Equation 4-1, the activity of SA in a liquid phase saturated with crystalline SA depends on only temperature, regardless of the solvent, and it can be computed using thermophysical properties from Table 4-1. In general, when temperature is close to the melting point the first term in right hand side of Equation 4-1 is dominant, and integral terms tend to cancel each other [43]. Figure 4-2 shows a comparison of: SA activity calculated using all terms in Equation 4-1; calculated ignoring the integral terms; and calculations also neglecting lambda transition.

Despite activities look similar in Figure 4-2, slight differences observed at temperatures far from the melting point produce significant changes in the activity coefficient of SA in solution when solubility data are used to convert the activities to activity coefficients. For instance, considering solubility data reported for the binary system SA-H_2O [8-11, 14], Figure 4-3 shows the effect on the activity coefficient of SA.

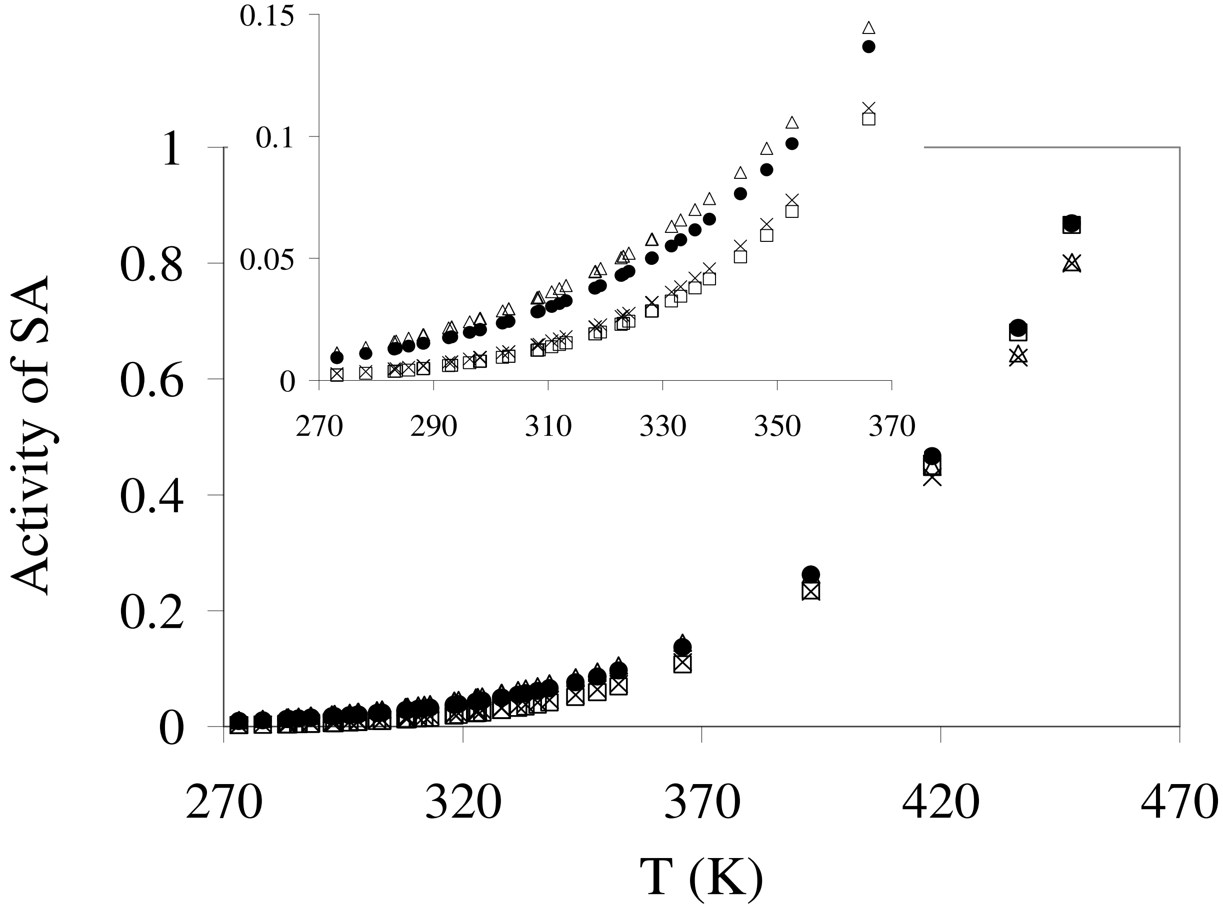

Figure 4-2. Temperature dependence of succinic acid activity in saturated solutions computed from physicochemical properties. (●) - Equation 4-1, (Δ) - Equation 4-1 without λ_{PT} term, (□) - Equation 4-1 without C_P integral terms, (×) - Equation 4-1 without λ_{PT} and C_P integral terms. The inset figure shows the low concentration range.

It is clear that neglecting lambda transition effect does not change activity coefficients significantly. In the other hand, including integral terms associated with the sensible part of the enthalpy change from the solid state to a subcooled liquid phase creates significant difference mainly at low concentrations of SA (low temperature). From the thermodynamic point of view one of these models (including or neglecting integral terms) is not consistent with water activity data because the slopes of the curves in Figure 4-3 have opposite signs.The activity data for water cited above result in a water activity coefficient with a negative slope plotted vs. x_w at low concentrations of SA, thus the succinic acid activity coefficient should have a positive slope plotted vs. x_W in the same concentration range, according to Gibbs-Duhem equation. The calculations including the integrals in equation (4-1) are inconsistent with the activity coefficients of water. Because solubility data from different sources agree, inconsistency found computing SLE might be explained by the physical properties reported for SA. While NIST reports [36] for T_{fus} and ΔH_{fus} are similar to those measured in recent works [37, 44], experimental values for heat capacities are only available for the solid phase. Values obtained with equation for solid heat capacity in Table 4-1 agrees in the lower part of its applicability range with reported data [29, 35] but there is no data available to validate at higher temperatures. In the case of liquid heat capacity there are no experimental data to validate calculations.

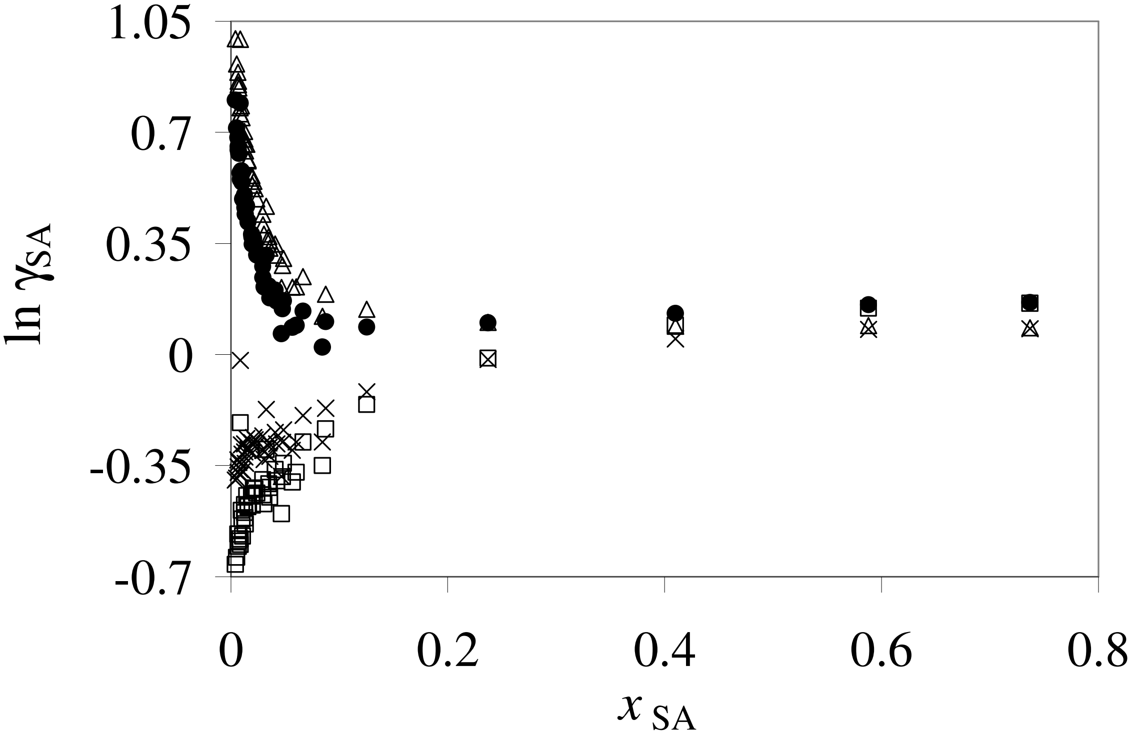

Figure 4-3. Succinic acid activity coefficient in saturated aqueous solutions from reported solubility data [8-11, 14]. (●) - Equation 4-1, (Δ) - Equation 4-1 without λ_{PT} term, (□) - Equation 4-1 without C_P integral terms, (×) - Equation 4-1 without λ_{PT} and C_P integral terms.

Using contribution methods [45-47] to estimate the difference of liquid to solid heat capacities ($\Delta C_p = C_{pL} - C_{pS}$) at 298.15 K, widely varying values of the difference are obtained, 69.6 J/mol K [44] compared to 1.3 J/mol K [47]. Using equations from Table 4-1 results in a value of 75.7 J/mol K. This large variation in heat capacities has been overlooked by several authors leading to contradictory predictions of the activity coefficient for SA as reported for water solubility [11, 17].

4.3 Material and methods

4.3.1 Materials

Succinic acid and succinic anhydride (>99.5 %, Sigma-Aldrich), diethyl succinate (99.92%, Sigma-Aldrich), ethanol (200 proof, Decon Labs), water (HPLC grade, J.T. Baker), ethyl acetate (99.99%, EMD), and diethyl ether (EMD chemicals, 99.9%) were used for experiments and calibration without further purification. Purity was confirmed by gas chromatography and it water was the only appreciable impurity.

4.3.2 Experimental procedures

4.3.2.1 Solubility

Solubility data were determined on a mass basis. Solid SA and the solvent were placed in a closed glass vial (20 cm^3) and stirred with magnetic bar. The amount of SA in every vial was higher than the solubility limit at the experiment temperature to ensure saturation of the liquid phase. These vials were placed in an isothermal bath equipped with a circulator pump and temperature control (Isotemp immersion circulator 730, Fisher Scientific, ± 0.1 K). For low temperature experiments a stainless steel coil connected to a recirculation chiller was submerged in the bath. The temperature was measured with an ASTM certified glass thermometer (model 64 C, ± 0.1 K). After the equilibration period (around 2 h) the stirring was stopped and two liquid samples were removed from the solution on every vial. The samples were centrifuged at 8000 rpm for 2 min to remove suspended crystals. An aliquot (around 1 g) from the supernatant liquid was weighted (Sartorius R 300 S, ± 0.1 mg) and titrated with a NaOH solution prepared in EtOH/H_2O mixture until final point with phenolphthalein. When a low solubility was expected (non-polar solvents) a 0.01 M NaOH solution was used for titration, while for higher solubility the solution was 0.1 M. The procedure was repeated with the second sample obtained from every vial and the average solubility is reported.

4.3.2.2 Calorimetric analysis

Calorimetric measurements were performed using differential scanning calorimetry at atmospheric pressure (Mettler-Toledo DSC1) and at high pressure (Mettler-Toledo HPDSC 827e). Samples around 10 mg were weighed (Mettler-Toledo AB265-S, ± 0.01mg) and heated in hermetically sealed aluminum crucibles at 10 K/min under nitrogen flow (20 cm^3/min) over a range of temperature of 223.15 to 523.15 K. Equilibration time at the initial and final temperature of 4 minutes was used. The procedure was repeated at least twice to observe changes in the sample during calorimetric analysis. To avoid decomposition and sublimation, the liquid phase heat capacity was measured under nitrogen pressure at 6.89 MPa. Calibration using ASTM-1269 standard method [48] was made using a 23.62 mg sapphire standard disc.

4.4 Experimental Results

4.4.1 Calorimetric analysis

Calorimetric scans on succinic acid were performed to evaluate heat capacities for solid and liquid phase in the interval of interest. A typical calorimetric analysis for SA by DSC is presented Figure 4-4.

A small peak repeatedly observed around 410 K is consistent with previous observations of the $\beta \rightarrow \alpha$ lambda phase transition in the solid state [28, 31, 34, 37] and it is in the range of ±30 K around the equilibrium temperature (Table 4-1) reported by Petropablov [30]. An enthalpy change of 0.162 kJ/mol was obtained after analysis of the thermal event, but considering that the broad range of transition increases uncertainty in the integration, assumed value in Table 4-1 is used in calculations, though it makes an insignificant contribution to the resulting models. Scans at atmospheric pressure (Figure 4-4(a)), exhibit a change of weight of the solid sample during each cycle (7% first cycle, 6.86% second cycle) that is consistent with dehydration reaction to SAnh at high temperature [38]. This is confirmed by the appearance of a peak in successive cycles around the melting point of SAnh (392 K) shown by a standard in Figure 4-5.

In the first cycle at atmospheric pressure in Figure 4-4(a) an endothermic event possibly associated with water evaporation (produced by dehydration) is noticed above the SA melting temperature. In subsequent cycles after the major part of water is removed a clear peak around the reported boiling point for SA (508 K) is observed but still accompanied by a large tail. The shift of SA melting temperature on second and third scanning cycles is suggestive of solid (SA) – liquid (SAnh) solutions. The thermal decomposition was mostly suppressed by using high pressure DSC as shown in Figure 4-4(b). Even at higher temperatures, negligible weight change was recorded at the end of the runs. Even though a small peak around SAnh melting temperature was observed, peak area is much smaller than that observed operating under atmospheric pressure.

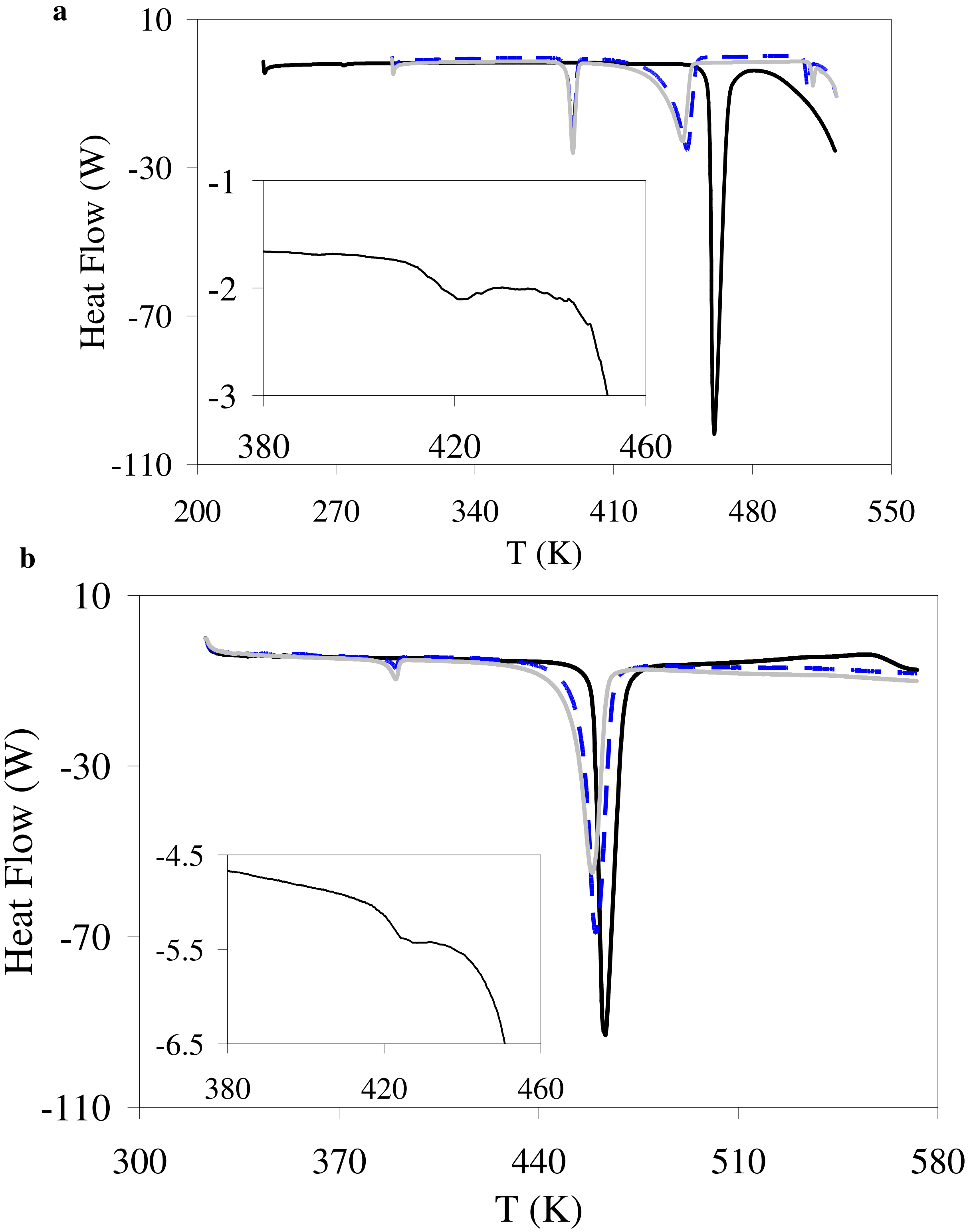

Figure 4-4. Calorimetric curves obtained by DSC at 10 K/min. Successive measurements at (a) 101.325 kPa and (b) 6892.8 kPa. (▬) - Cycle 1, (▬ ▬) - Cycle 2, (▬) - Cycle 3. The insert in figures shows thermal event at reported solid phase transition temperature in cycle 1.

At high pressure it has been proposed that any water released by dehydration remains in the system and reacts back to SA as the system cools [49]. Change in peak shape observed in different curves at high pressure (Figure 4-4b) might be caused by the change of crystalline form of solid SA during heating and cooling cycles. Also the small amount of SAnh observed might shift peak location compared with pure SA.

In order to minimize decomposition of the solid during heat capacity measurements, scanning was carried out up to 493.15 K, and calorimetric curves are presented in Figure 4-5. Due to the characteristics of the machine, calorimetric data from the high pressure DSC presented scatter mainly at low temperatures, so it was only used to calculate liquid phase heat capacity. Figure 4-6 and 4-7 shows heat capacity of SA and SAnh varying with temperature compared with reported equations (Table 4-1) [39].

In the lower range of temperatures, heat capacity for solid SA agree with those previously reported [29] and the correlation from Table 4-1 fits data up to the lambda transition temperature. A change in the solid heat capacity is observed after solid phase transition. However it seems that experimental heat capacity of the liquid is higher (~ 20%) than predicted and the heat capacity measurements indicate an unexpected decrease of liquid Cp with temperature. Due to the scatter on heat capacity for the liquid phase at high temperature data are not correlated or used further in this study. In the case of SAnh neither of liquid or solid phase heat capacity [39] from literature agrees with experiments. In this case predicted solid heat capacity is in average 12 % lower than experimental, while for the liquid phase is ~ 15% higher than measured data.

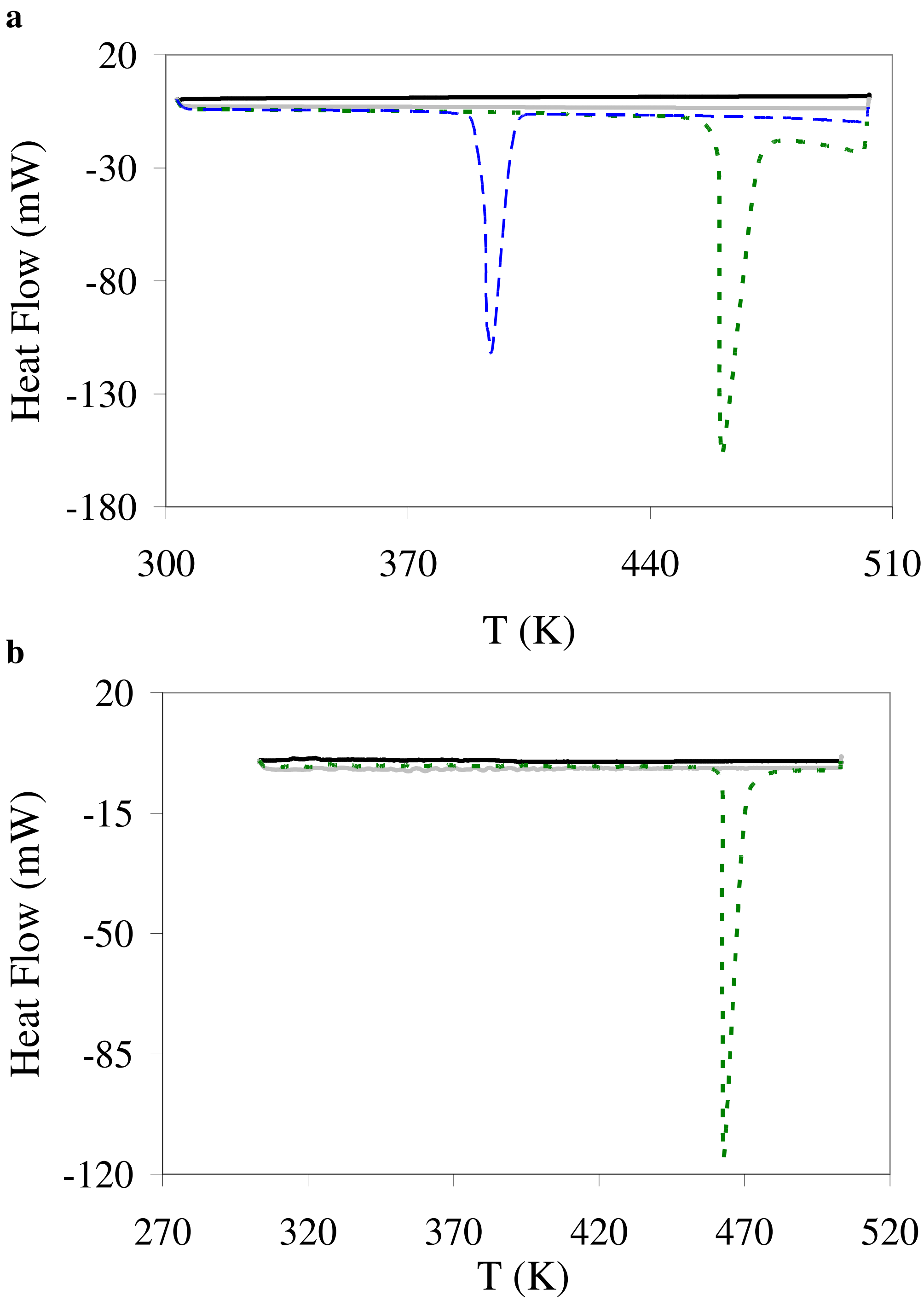

Figure 4-5. Calorimetric curves obtained by DSC during heat capacity measurement under N_2 atmosphere, temperature range 303.15 K – 493.15 K at 10 K/min. (a) 101.325 kPa; (b) 6892.8 kPa. (▬) - Reference aluminum pan, (▬) - Sapphire standard, (▬ ▬) - Succinic anhydride, (- -) - Succinic acid.

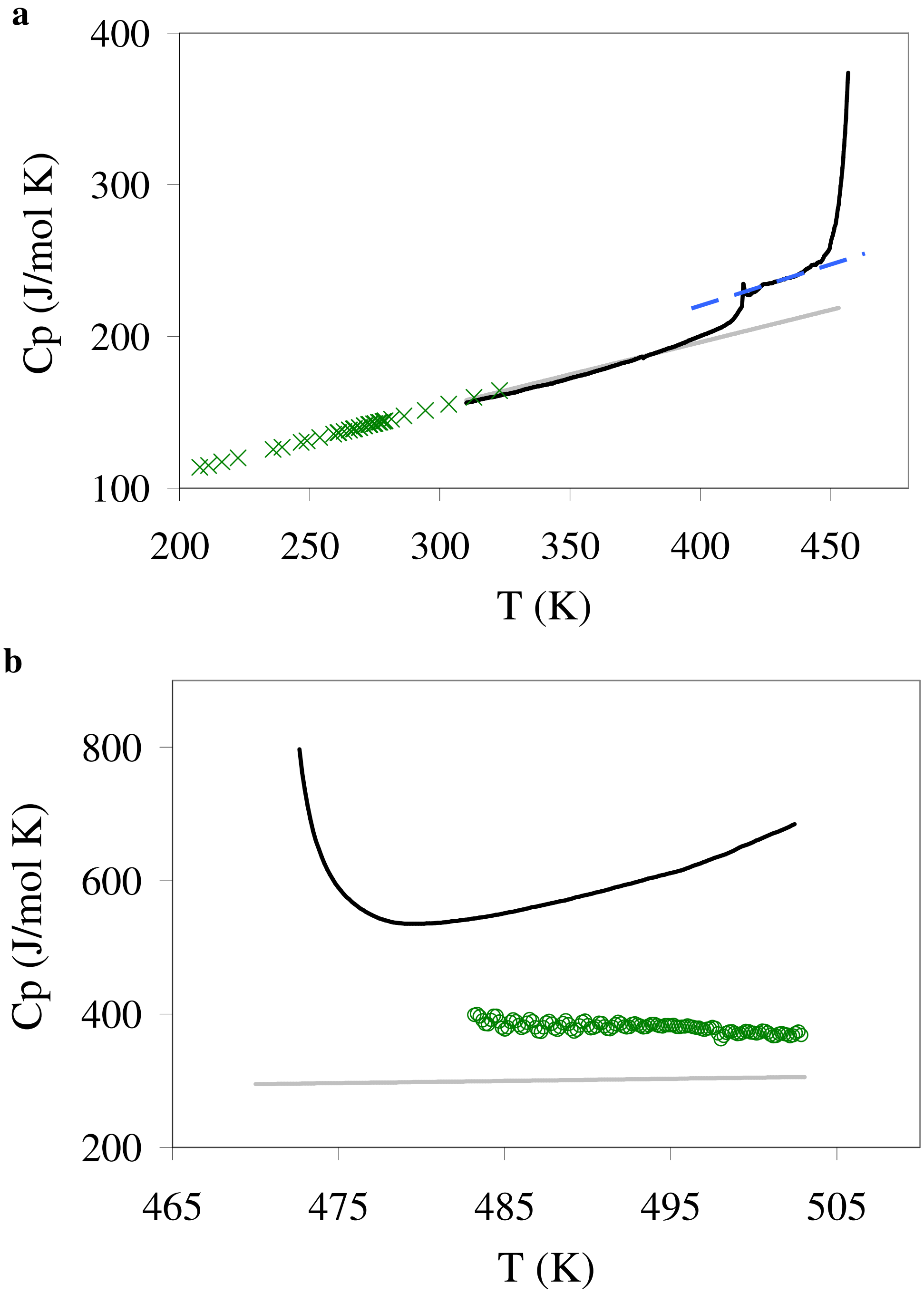

Figure 4-6. Heat capacity of succinic acid. (a) Solid phase, (▬) - This work at 101.325 kPa, (×) - Reported data [29], (▬) - Literature correlation [39], (▬ ▬) - Fitted correlation of experimental data for solid phase after lambda transition. (b) Liquid phase, (▬) - This work at 101.325 kPa, (○) - This work at 6892.8 kPa. (▬) - Literature correlation [39].

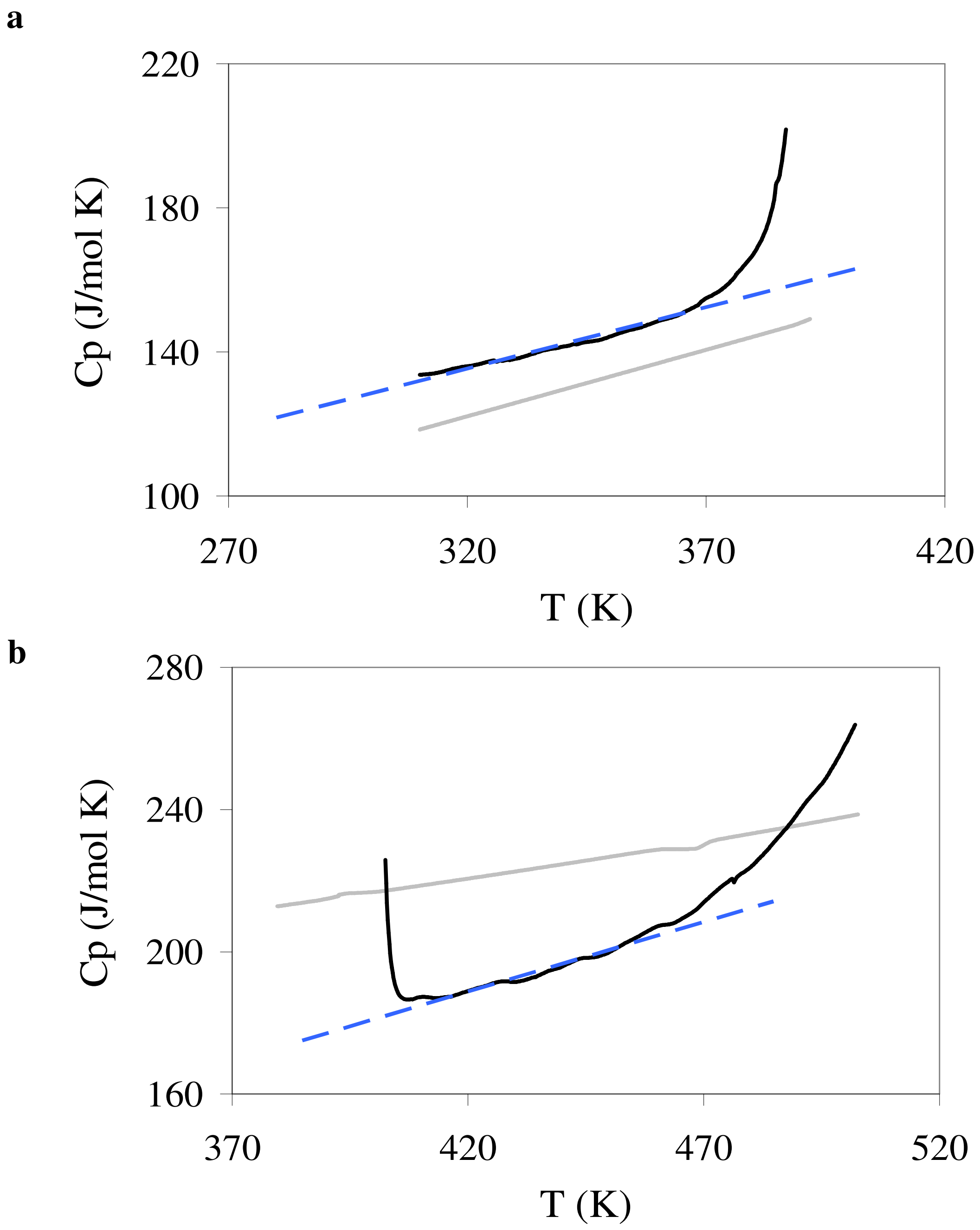

Figure 4-7. Heat capacity of succinic anhydride. (a) Solid phase, (b) Liquid phase. (▬) - This work at 101.325 kPa, (– –) - Fitted correlation of experimental data, (▬) - Literature correlation [39].

A summary of physicochemical data obtained during calorimetric studies for both SA and SAnh is presented in Table 4-2.

Table 4-2. Thermophysical properties of SA and SAnh obtained by DSC.

Property		SA	SAnh
T_{fus} (K)		456.8 ± 1	391.8 ± 1
ΔH_{fus} (kJ/mol)		34.6 ± 1	17.1 ± 0.5
T_{PT} (K)		413 ± 2	-
ΔH_{PT} (kJ/mol)		0.162	-
C_{pS} (J/mol K)	Range (K)	420-445	310-370
$C_{pS} = A_S + B_S T(K)$	A_S	0.5452	26.298
(410-445 K)	B_S	2.1834	0.3408

Considering that the heat capacity of SA solid phases are different, every integral term in Equation 4-1 must be divided into two ranges, one up to T_{PT} and the other up to T_{fus}, including the correspondent expression for the solid heat capacity.

Taking into account scatter in data for SA liquid heat capacity, and even though literature correlation seems to underpredict it by around 20%, these equations were used to correlate SLE when integral terms in Equation 4-1 were evaluated.

4.4.2 Solubility data and SLE modeling

Experimental solubility data obtained in different solvents are listed in Table 4-3 and agree with previous reports indicating the reliability of the experimental method. These data together with literature values were correlated with Equation 4-1 using different heat capacities for the both solid phases and T_{PT} from Table 4-2. Solubility of SA in H_2O was studied to check consistency of experimental data because activity of the solvent was available. NRTL binary parameters were regressed for both, including and neglecting integral terms in SLE equation. Figure 4-8 shows solubility of SA in H_2O and correlation with Equation 4-1.

Table 4-3. Solubility of succinic acid in different solvents (g SA/100 g solution).

T(K)	Solvents EtOAc	 DEE	 DES	 EtOH	 H_2O
		(± 0.01)		(± 0.05)	
278.15	0.27	0.28	0.15	5.46	3.50
283.15	0.33	0.32	0.16	6.18	4.27
288.15	0.37	0.37	0.17	7.17	5.29
293.15	0.43	0.41	0.18	8.07	6.33
298.15	0.50	0.48	0.22	9.15	7.93
303.15	0.59	0.54	0.26	10.28	9.32
308.15	0.73		0.33	11.59	11.24
313.15	0.83		0.38	12.78	12.28

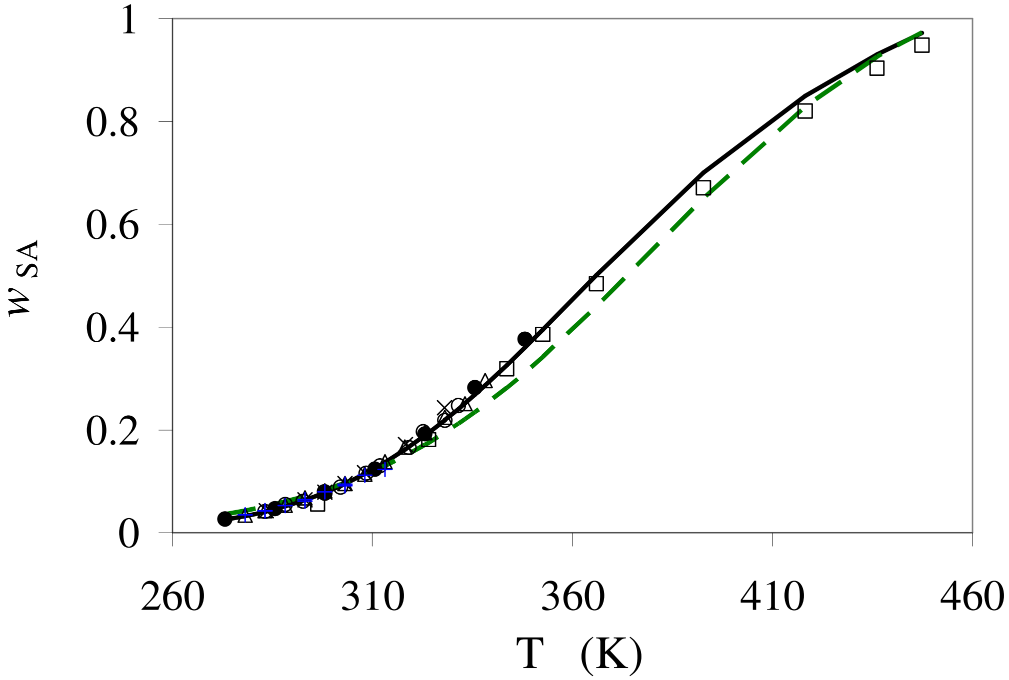

Figure 4-8. Succinic acid solubility in H_2O. (●) - Marshal [8],(×) - Davis [9], (Δ) - Apelblat [10], (□) - Lin [11], (○) - Yu [14], (+) - This work, (▬) - NRTL model without integral terms, (▬ ▬) - NRTL model with integral terms.

Despite agreement with solubility data is similar with both models, when activity and activity coefficient of H_2O are considered (Figure 4-9), the model without integral terms predicts the succinic acid activity coefficient trend consistent with the water activity coefficient data reported in literature.

Activities calculated by group contribution methods (UNIFAC), an electrolyte model [21] and Equation 4-1 using NRTL including integral terms, are all over-predicting the activity coefficient of water. Besides in these models the slope of the curve of activity coefficient has the opposite sing compared with experimental data. This has also been reported by using other equations like COSMO-RS [17].

Results of our study indicate that literature reports on activity of H_2O are consistent with a model without integral terms in equation (4-1). This observation may indicate that either reported activities of water in solution are wrong; integral terms on Equation 4-1 are not correct; or some other thermodynamic factor not considered in the model is important such as dissociation. Considering that our measurements confirmed literature data for all properties except for the liquid heat capacity of SA, further regression of experimental solubility are carried out using Equation 4-1 without integral terms as previously reported [11]. In addition to this, although not presented here, regression results using all terms in Equation 4-1 were not able to model accurately solubility data in other solvents or in ternary mixtures.Figures 4-10 and 4-11 show the correlation obtained for solubility data in EtOH and H_2O + EtOH mixtures when heat capacity integrals are neglected. Experimental and reported SA solubility in AcOH, EtOAc, DES, and DEE are presented in Figures 4-12 and 4-13. Good agreement with experimental data is observed and parameters of NRTL equation are listed in Table 4-4.

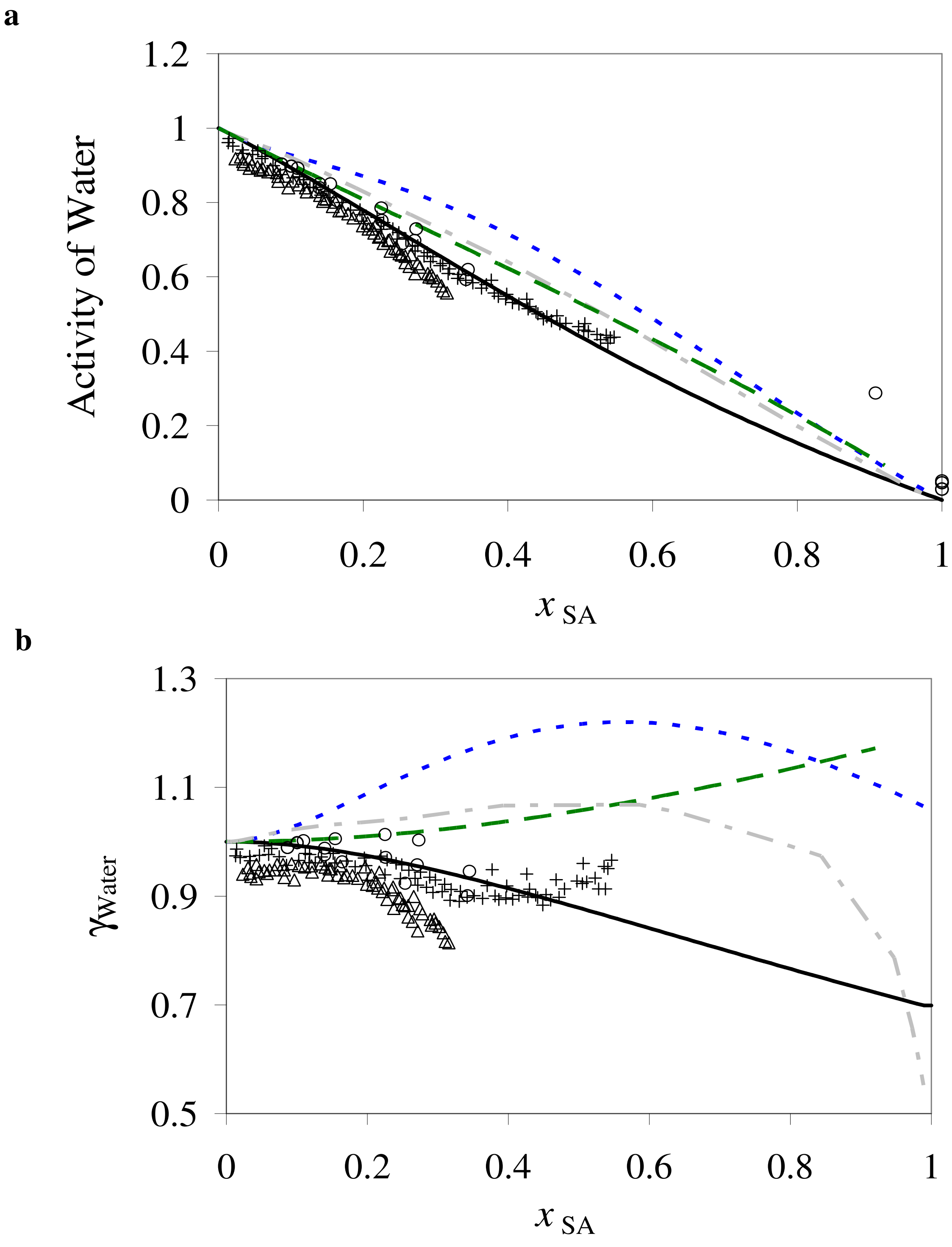

Figure 4-9. Water activity (upper) and activity coefficient (lower) in succinic acid solutions at 298.15 K. (Δ) - Na [42], (+) - Mohan [13], (○) - Peng [19], (▬ · ▬) - Electrolyte model [23], (- - -) - UNIFAC, (▬) - NRTL model without integral terms, (▬ ▬) - NRTL model with integral terms.

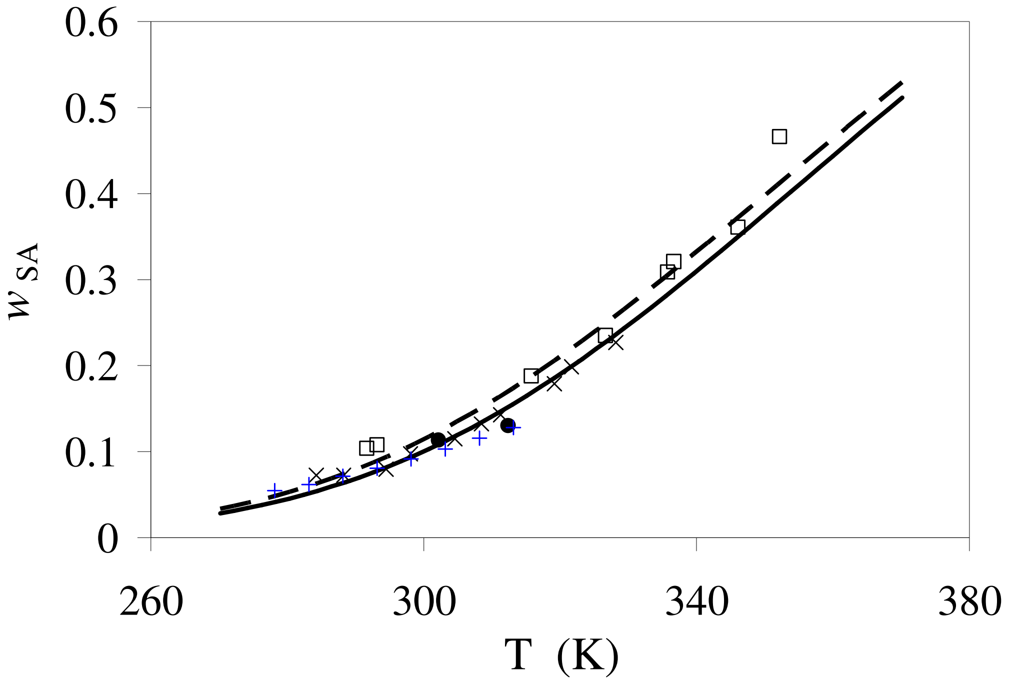

Figure 4-10. Succinic acid solubility in EtOH: (●) - Mohan [13], (×) - Yu [14], (+) - This work, (▬) - NRTL model. Solubility in azeotropic EtOH: (□) - Benedict [15], (▬ ▬) - NRTL model.

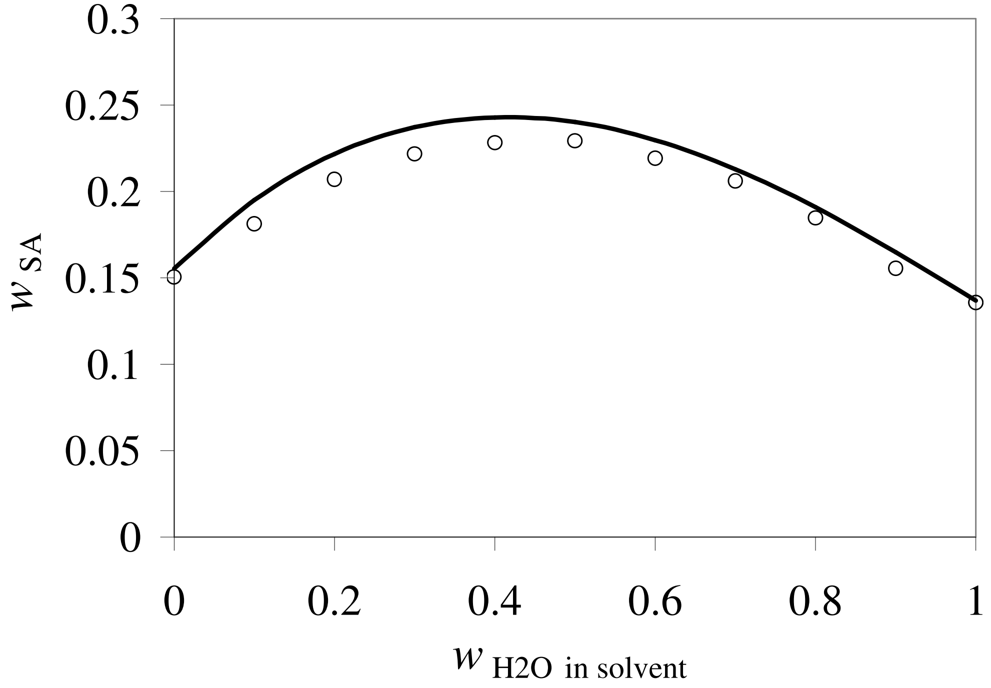

Figure 4-11. Succinic acid solubility in H_2O – EtOH solutions at 213.15 K (○) - Bancroft [12]. (▬) - NRTL model.

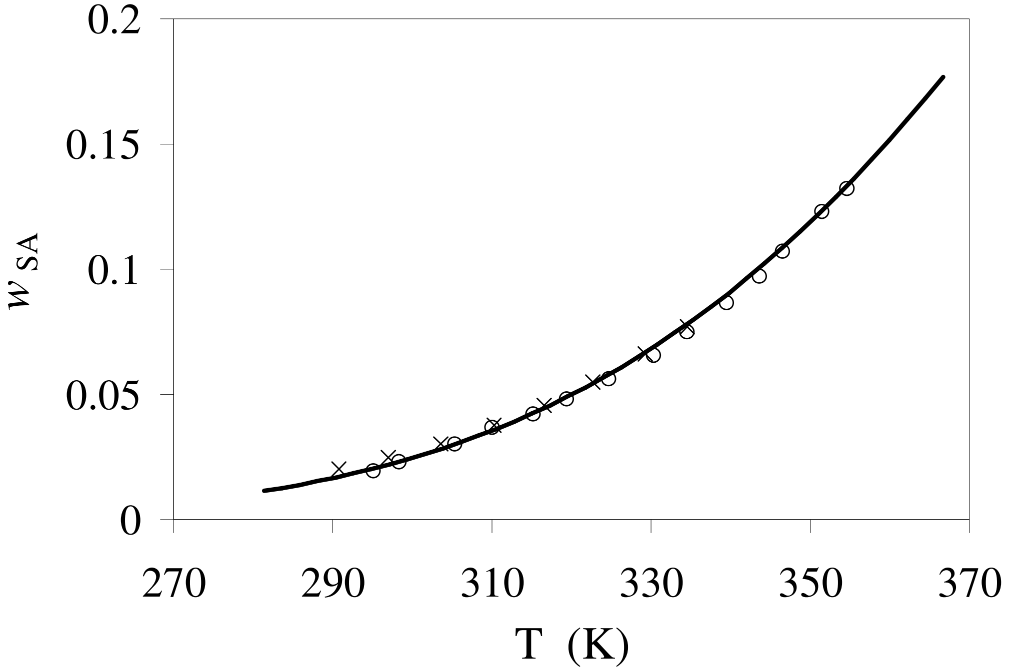

Figure 4-12. Succinic acid solubility in AcOH (×) - Yu [14]. (○) - Song [50], (▬) - NRTL model.

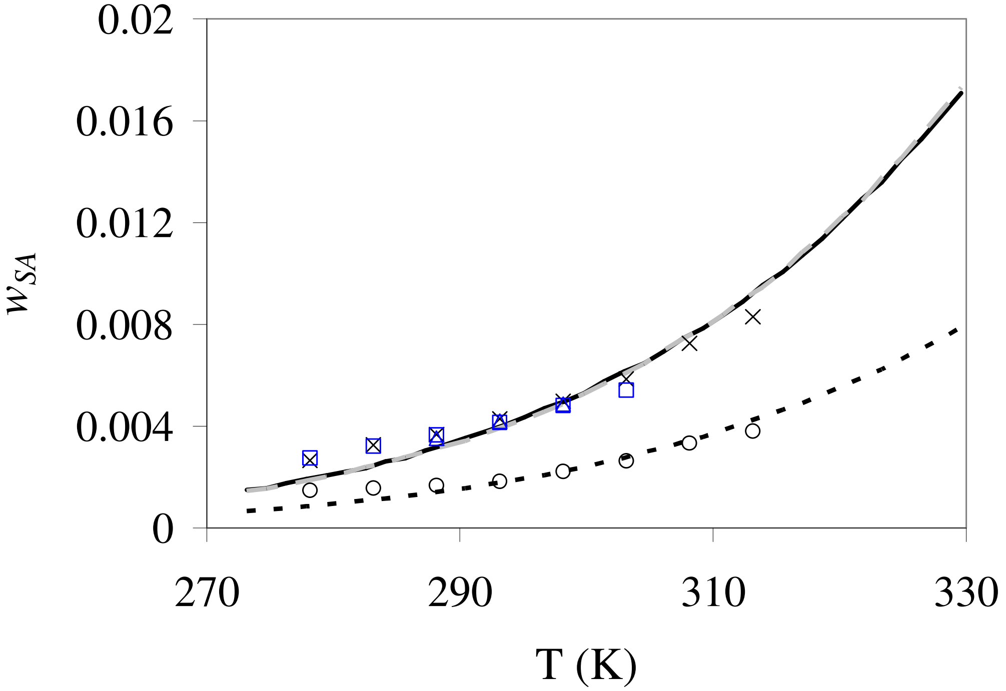

Figure 4-13. Succinic acid solubility in DEE (Δ Washburn [16], □ This work), EtOAc (×) and DES (○). Lines calculated with NRTL model.

Table 4-4. Binary parameters for the NRTL model.

	NRTL					
	DEE **SA**	**EtOAc** **SA**	**AcOH** **SA**	**H_2O** **SA**	**EtOH** **SA**	**DES** **SA**
a_{ij}	0	0	0	0	0	0
a_{ji}	0	0	0	0	0	0
b_{ij}	248.411	191.987	-386.393	296.722	-605.634	218.224
b_{ji}	1947.928	1976.63	2132.132	-328.506	113.448	1946.876
α_{ij}	0.3	0.3	0.3	0.3	0.3	0.3

4.4.3 Final remarks

Difficulties in measuring the high temperature liquid heat capacity of SA are not completely understood. The decrease of SA liquid heat capacity observed in experiments is consistent with a decomposition of the SA to SAnh, but our experiments give no direct evidence that this occurred. Another interesting finding is that the remaining measurements generally confirm the existing literature values and do not resolve the thermodynamic inconsistencies in the activity coefficients of SA and water when the heat capacity integrals are included in solubility calculations. Despite these uncertainties, thermodynamic models that completely disregard the heat capacity integrals provide the best representation of the solubility data in both pure and mixed systems.

4.5 Conclusions

Experimental and reported data on solubility of SA in binary and ternary mixtures were correlated using a SLE model and NRTL equation to account for the non-ideality of the mixtures. Calorimetric studies on SA and SAnh were carried out to obtain and validate thermophysical properties required in the model, and results agreed with literature reports. A correlation for the solid heat capacity for both SA and SAnh were obtained. Measurements of the liquid heat capacity of SA were not considered reliable. Accurate thermodynamic modeling that ignores the heat capacity integrals in the SLE equation gives the best results in this study. Because the main goal of the study is to obtain a reliable model to calculate activities in esterification mixtures with SA, the simplified model was acceptable. The model is able to reproduce solubility data in binary and ternary mixtures as well as activity of the solvent in aqueous solutions.

REFERENCES

4.6 REFERENCES

[1] J. Zeikus, M. Jain, P. Elankovan. Appl. Microbiol Biotechnol. 51 (1999) 545-552.

[2] A. Cukalovic, C. V. Stevens. Biofuels, Bioprod. Biorefin. 2 (2008) 505–529.

[3] R. Datta, S. P. Tsai. Esterification of fermentation derived acids via pervaporation. US Patent 5723639. (1998).

[4] M. C. Cockrem. Process for the production of organic acids and esters thereof. US Patent 6291708 B1. (2001).

[5] D. Dunuwila Process for the direct production of esters of carboxylic acids from fermentation broths. Canadian patent application 02657666. (2009).

[6] C. Bauduin, W. Fischer, R. Pinkos, E. Scholten. Method of producing a carboxylic alkyl ester. US patent application 0137825 A1. (2009).

[7] P. K. Kiviranta-Pääkkönen, L. K. Struckmann, J. A. Linnekoski, A. O. Krause. Ind. Eng. Chem. Res. 37 (1998) 18-24.

[8] H. Marshall, D. Bain. Sodium Succinates. J. Chem. Soc, Trans. 97(1910) 1074-1085.

[9] M. Davies, D. M. Griffiths. Trans. Faraday Soc. 49 (1953) 1405-1410.

[10] A. Apelblat, E. Manzurola. J. Chem. Thermodyn. 19, 3 (1987) 317-320.

[11] H. M. Lin, H. Y. Tien Y. T. Hone, M. J. Lee. Fluid Phase Equilibr. 253, 2 (2007) 130-136.

[12] W. D. Bancroft, F. J. C. Butler. J. Phys. Chem. 36, 9 (1932) 2515-2520.

[13] R. Mohan, A. S. Myerson. J. Crystal Growth 206 (1999) 99-108.

[14] Q. Yu, S. Black, H. Wei. J. Chem. Eng. Data. 54 (2009) 2123-2125.

[15] D. J. Benedict, S. J. Parulekar, S. Tsai. J. Membr. Sci., 281, 1-2 (2006) 435-445.

[16] E. W. Washburn. International Critical Tables of Numerical Data, Physics, Chemistry and Technology (1st Electronic Edition). (pp: 148, 327, 413). Knovel. (1926 - 1930; 2003).

[17] B. Schröeder, L. Santos, I. M. Marrucho, J. A. P. Coutinho. Fluid Phase Equilibr. 289, 2 (2010) 140-147.

[18] I. K. Koponen, I. Riipinen, A. Hienola, M. Kulmala, M. Bilde. Environ. Sci. Technol. 41 (2007) 3926-3933.

[19] C. Peng, M. M. Chan, C. K. Chan. Environ. Sci. Technol. 35 (2001) 4495-4501.

[20] M. C. Maffia, A. Meirelles. J. Chem. Eng. Data. 46 (2001) 582-587.

[21] T. Raatikainen, A. Laaksonen. Atmos. Chem. Phys. 5 (2005) 2475-2495.

[22] A. I. Gaman, M. Kulmala, H. Vehkamäki, I. Napari. J. Chem. Phys. 120, 1 (2004) 282-291.

[23] S. L. Clegg, J. H. Seinfeld. J. Phys. Chem. A. 110 (2006) 5692-5717.

[24] A. Orjuela, A. Yanez, D. Vu, D. Bernard-Brunel, D. J. Miller, C. T. Lira. Fluid Phase Equilibr. 290, 1-2 (2010) 63-67.

[25] A. Orjuela, A. Yanez, P. Rossman, D. Vu, D. Bernard-Brunel, D. J. Miller, C. T. Lira. Fluid Phase Equilibr. 290, 1-2 (2010) 68-74.

[26] H. Renon, J. Prausnitz. AIChE J. 14 (1968) 135-144.

[27] P. B. Choi, E. McLaughlin. AIChE J. 29, 1 (1983) 150-153.

[28] M. F. Dupré la Tour. Ann. de Phys. 10e série, t. XVIII. (1932) 199-284.

[29] C. E. Vanderzee, E. F. Westrum. Succinic acid. J. Chem. Thermodynam. 2 (1970) 681-687.

[30] N. N. Petropavlov, S. B. Yarantsev. Sov. Phys. Crystallogr. 28, 6 (1983) 666-670.

[31] R. Wilhoit, J. Chao, H. Hall. J. Phys. Chem. Ref. data, 14, 1 (1985) 137.

[32] A. Cingolani, G. Berchiesi. J. Thermal Analysis. 6 (1974) 87-90.

[33] N. N. Petropavlov, I. G. Tsygankova, L. A. Teslenko. Sov. Phys. Crystallogr. 33, 6 (1989) 853-855.

[34] S. Ponomarenko, Y. Y. Borovikov, T. E. Sivacheck, D. N. Vovk. Russian J. General Chem. 73, 11 (2003) 1769-1773.

[35] G. S. Parks, H. M. Huffman. J. Am. Chem. Soc. 52 (1930) 4381-4391.

[36] NIST Chemistry WebBook, NIST Standard Reference Database Number 69, Eds. P.J. Linstrom and W.G. Mallard, National Institute of Standards and Technology, Gaithersburg MD, 20899, (2010) [Online]. Available: http://webbook.nist.gov/cgi/ cbook.cgi?Name= succinic+acid&Units=SI, [2010, March 22].

[37] V. Chikhalia, R. T. Forbes, R. A. Storey, M. Ticehurst. Eur. J. Pharm. Sci. 27 (2006) 19-26.

[38] C. Pan, F. Liu, P. Sutton, R. Vivilecchia. Thermochimica Acta 435 (2005) 11-17.

[39] C. L. Yaws. Yaws' Handbook of Thermodynamic and Physical Properties of Chemical Compounds. Knovel. 2003.

[40] Aspentech, Aspen Physical Property System, physical property models/methods, Burlington, 2007.

[41] M. Davies, D. K. Thomas. J. Phys. Chem., 60, 1 (1956) 41–44.

[42] H. Na, S. Arnold, A. S. Myerson. J. crystal growth. 149, 3-4 (1995) 229-235.

[43] J. M. Prausnitz, R. N. Lichtenthaler, E. Gomes de Azevedo. Molecular Thermodynamics of Fluid-Phase Equilibria (3rd Edition). Prentice Hall. 1998, p 635-367.

[44] M. V. Roux, M. Temprado, J. S. Chickos. J. Chem. Thermodyn. 37, 9 (2005) 941-953.

[45] J. S. Chickos, D. G. Hesse, J. F. Liebman. Struct. Chem. 4, 4 (1993) 261-269.

[46] J. S. Chickos, S. Hosseini, D. G. Hesse, J. F. Liebman. Struct. Chem. 4, 4 (1993) 271-278.

[47] E. S. Domalski, E. D. Hearing. J. phys. Chem. Ref. data, 22, 4 (1993) 805-1159.

[48] ASTM Standard E1269-05, (2005) Standard test method for determining specific heat capacity by differential scanning calorimetry, ASTM International, West Conshohocken, PA, 2005,DOI: 10.1520/E1269-05.

[49] C. Fumagalli, L. Spa. Succinic acid and succinic anhydride, In: Kirk–Othmer Encyclopedia of Chemical Technology, Vol. 23, John Wiley & Sons, New York, pp. 416-435. 2010.

[50] W. W. Song, P. S. Ma, Z. L. Xiang. J. Chem. Eng. of Chinese Universities 21, 2 (2007) 341-344.

5. Kinetics of mixed succinic acid/acetic acid esterification with Amberlyst 70 ion exchange resin as catalyst

5.1 Summary

Liquid phase esterification of succinic acid, acetic acid and succinic/acetic mixtures with ethanol was studied using Amberlyst 70 strong cation exchange resin as catalyst. Batch isothermal reactions were performed at different ethanol:acid molar ratios (1:1 – 27:1), temperatures (343 – 393 °K) and catalyst loadings (1 – 9.3 wt% of solution). Esterification kinetics are described using both pseudo-homogeneous mole fraction and NRTL-based activity based models that take ethanol dehydration to diethyl ether into account. The models accurately predict the esterification of individual acids, and a simple additive combination of independent kinetic models provides a good description of mixed acid esterification. The kinetic models can be used in simulation of reactive distillation processes for mixed acid esterification.

5.2 Introduction

Among several carboxylic acids obtained by fermentation, succinic acid (1,4-butanedioic acid, herein SA) has been recognized as a renewable building platform for many chemical derivatives of industrial interest [1-6]. Its potential use as feedstock for 1,4-butanediol, tetrahydrofuran and γ-butyrolactone production opens the opportunity for a growing and sustainable market of renewable polymers [7, 8]. Because SA is a common metabolite in many anaerobic and facultative microorganisms, a number of promising fermentation processes have been developed using bacteria isolated from gastrointestinal systems in animals, including

Anaerobiospirillum succiniciproducens (~50 kg/m^3), Actinobacillus succinogenes (94-106 kg/m^3), Mannheimia succiniciproducens (~52 kg/m^3), and Escherichia coli (~99 kg/m^3) [9-12].

Because of the complex reaction catabolism, the two major challenges in succinic acid fermentation are low SA titer (g/liter) and loss of selectivity via byproduct formation. In addition to cell growth and incomplete conversion, sugar substrate is lost via formation of significant quantities of acetic, formic, pyruvic, and lactic acids depending on the organism. Typical acid concentrations found in SA fermentation broths are listed in Table 5-1.

Table 5-1. Typical product concentrations in SA fermentation [12].

Component	Concentration (kg/m^3)
Succinic acid	40 – 110
Acetic acid	5 – 40
Pyruvic acid	0 – 20
Lactic acid	0 – 14
Formic acid	0 – 5

According to recent studies, recovery of succinic acid from these mixtures can be accomplished by esterification with ethanol (EtOH) [13]. Esterification of SA proceeds sequentially through a series reaction scheme in the presence of an acid catalyst, with monoethyl succinate (MES) as intermediate and diethyl succinate (DES) as final product (Figure 5-1). Because of chemical equilibrium limitations in esterification and the low solubility of SA in ethanol (~10% by weight at 298 K), excess EtOH is required in reaction. Further, achieving high rates and driving the reaction to completion requires continuous water (H_2O) removal, thus making esterification an attractive reaction system for reactive distillation (RD). For esterification of carboxylic acids, a single continuous RD column can selectively separate either product water or ester from the acid reactant as it is formed. The approach is powerful enough to directly esterify acids in dilute solutions produced via fermentation [14-16], both enhancing the overall recovery of acids as esters and making possible novel process approaches to obtain high purity products.

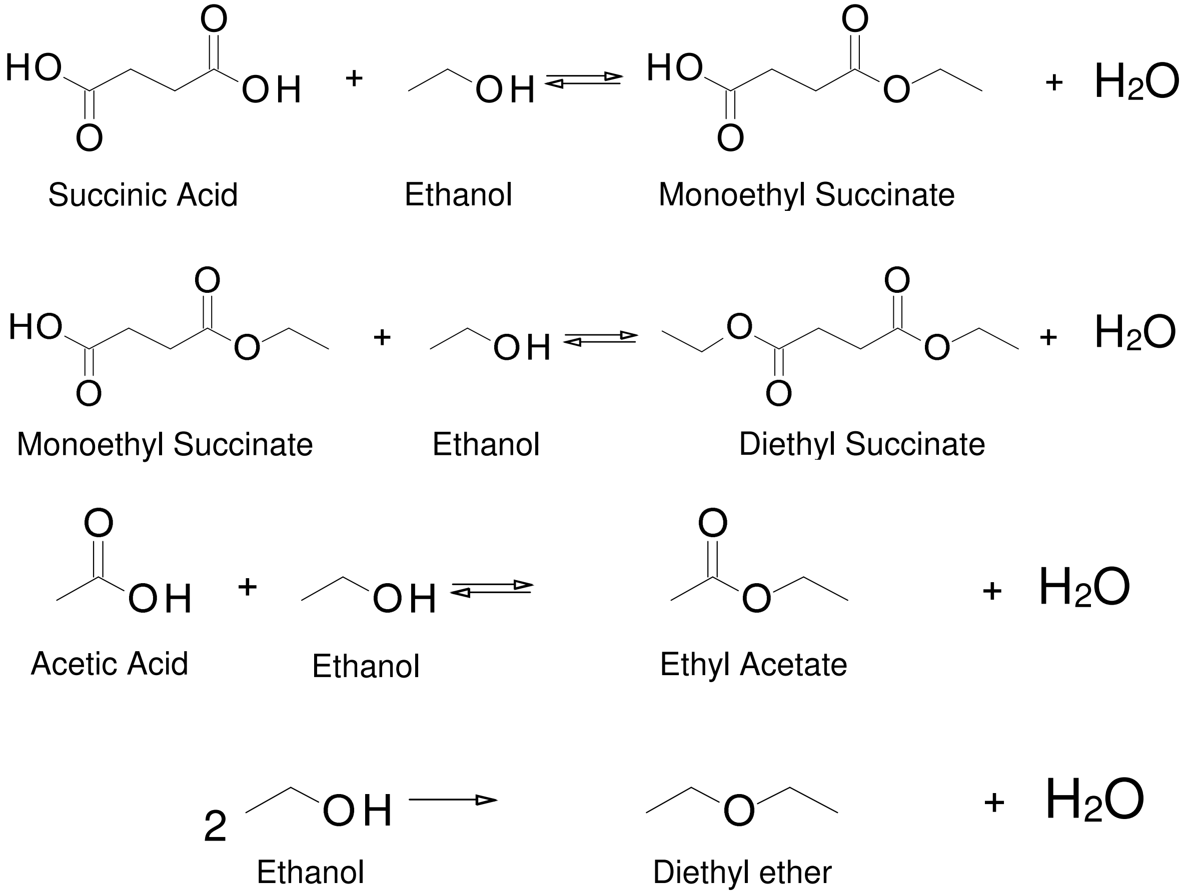

Figure 5-1. Reactions: esterification of succinic acid (SA) to monoethyl succinate (MES) and diethyl succinate (DES); esterification of acetic acid (AcOH) to ethyl acetate (EtOAc); dehydration of EtOH to diethyl ether (DEE).

In SA esterification, it is not known whether the presence of byproduct acids (Table 5-1) accelerates or inhibits SA conversion either kinetically or thermodynamically, or whether formation and recovery of byproduct acid esters overcomplicates the recovery process. As part of our efforts to develop RD strategies for succinic acid esterification, we thus have carried out this study of esterifying mixtures of SA and acetic acid (AcOH), the byproduct in greatest concentration in SA fermentation (Table 5-1), with ethanol (EtOH) for the purpose of understanding how AcOH affects SA esterification under process-relevant conditions.

In recent papers [17-19] it has been demonstrated that the strong cation exchange resin Amberlyst 70®, a low crosslinked styrene-divinylbenzene resin, showed superior performance (e.g. higher turnover frequency) as an acid catalyst for etherification relative to the more commonly used macroreticular ion exchange resins (e.g. Amberlyst 15). The high temperature stability of Amberlyst 70, up to 463 K in some environments [19, 20], also makes it more attractive from a process standpoint.

While there are reports of SA [21] and AcOH [22-29] esterification with EtOH using ion exchange resins, none have used Amberlyst 70 as catalyst. We thus have measured and report here the kinetics of AcOH and SA esterification, both individually and in mixtures, over Amberlyst 70. In addition to ester formation, dehydration of EtOH to diethyl ether (DEE) occurs at the elevated temperatures accessible with Amberlyst 70, so we include it as an integral part of the kinetic model. The kinetics of mixed acid esterification, along with associated physical property and phase equilibrium data, are useful in designing reactive distillation systems for fermentation-derived SA esterification.

5.3 Material and methods

5.3.1 Materials

Succinic acid (>99.5 %, Sigma-Aldrich), acetic acid (99.9%, Aristar), diethyl succinate (99.92%, Sigma-Aldrich), monoethyl succinate (89.3%, Sigma-Aldrich), ethyl acetate (HPLC grade, J. T. Baker), ethanol (200 proof, Decon Labs), water (HPLC grade, J.T. Baker), diethyl ether (EMD chemicals, 99.9%) *n*-butanol (99.9%, Mallinckrodt), and acetonitrile (HPLC grade, EMD) were used without further purification for experiments and calibrations. Species purity was confirmed by gas chromatography; no impurities, other than small amounts of water, were detected in appreciable concentrations. Hydranal-coulomat E solution (Riedel-de Haën) was used in Karl-Fisher analysis for water measurement. Amberlyst 70® resin was purchased from Dow Chemical Company; its physical and chemical properties are listed in Table 5-2.

Table 5-2. Physicochemical properties of Amberlyst 70® [17-20].

Physical form	Dark spherical beads
Ionic form	H^+
Acid equivalents (eq/kg)	≥ 2.55
Surface area (N_2 - BET) (m^2/g)	31-36
Average pore diameter (Å)	195-220
Effective size – dry solid (mm)	0.5
Pore volume (m^3/kg)	$1.5\text{-}3.3 \times 10^{-4}$
Particle porosity	0.19
Uniformity coefficient	≤ 1.5
Skeletal density (kg/m^3)	1520
Swollen surface area (water) (m^2/g)	176
Swollen particle porosity (water) (ε)	0.57
Maximum operating temperature (K)	463

5.3.2 Experimental procedures

5.3.2.1 Catalyst conditioning

As-received Amberlyst 70 resin was sieved and the -45+60 mesh fraction (0.25-0.35 mm diameter) was used in experiments. The resin was rinsed initially with water, followed by several washing cycles with ethanol. After filtration and removal of excess liquid, the catalyst was dried at 353 K under vacuum (1 kPa) and then stored in a sealed container in a vacuum oven prior to use.

The ion exchange capacity of dry Amberlyst 70 was measured by titration with a 0.1 M solution of NaOH in water using phenolphthalein as the indicator. The acid site density, obtained as the average of three measurements, was 2.35 ± 0.1 eq/kg, a value consistent with the value of 2.55 eq/kg reported by the manufacturer [20].

5.3.2.2 Batch kinetic experiments

Isothermal batch kinetic experiments were performed in a Parr 5000 Multireactor® system (Parr Instrument Co., Moline, Illinois) that includes six 75 cm^3 stainless steel reactors equipped with magnetic stirrer, temperature control, and sampling system with a stainless steel frit on the sampling tube to avoid withdrawal of catalyst. Ethanol, AcOH, and SA were placed into each reactor at room temperature in predetermined molar ratios along with the specified quantity of catalyst; the total mass of reactants added was typically 0.050 kg. After sealing each reactor, the stirring rate was set at 900 rpm and heating was initiated. It typically took 15 minutes to reach the desired reaction temperature; this moment was taken as time zero (t = 0) of reaction. During reaction, samples were withdrawn at specified time intervals starting at t=0, with a higher frequency of sampling in the first 2-3 hr. Samples were transferred into hermetically sealed vials and stored in a refrigerator before analysis.

5.3.3 Analysis

Reaction samples were analyzed both by gas and liquid chromatography. For HPLC, samples were diluted 50-fold in water and analyzed in a system containing a Waters® 717 autosampler, a Waters® 410 refractive index detector, and a Perkin-Elmer LC90 UV detector. A 100 mm x 7.6 mm Fast Acid analysis column (BioRad®) at 298 K along with a mobile phase of 5 mM H_2SO_4 in water flowing at 1.0 ml/min was used for the separation. Because the retention times of EtOH and MES were similar, only UV detection was used to evaluate MES concentration.

To evaluate concentration of volatile components, samples were diluted 20-fold into acetonitrile containing 5.0 wt% *n*-butanol as an internal standard and analyzed on a gas chromatograph (HP 5890 series II) equipped with thermal conductivity and flame ionization detectors. A 30 m long Alltech Aqua WAX-DA column (0.53 mm i.d., 1.20 μm film thickness) was used with the following temperature program: initial temperature 313 K for 3 min; ramp at 20 K/min to 523 K, and hold at 523 K for 0.5 min. The GC injection port was maintained at 543 K in a splitless mode, and detector temperature was 523 K. Helium was used as carrier gas (0.25 cm^3/s) and liquid injection volumes of 0.5 μL were used.

For both analyses, standard samples of known composition in the range of interest were injected in triplicate to obtain calibration curves repeatable to within ±0.5% by mass.

Karl-Fisher analysis (Aquacount coulometric titrator AQ-2100) was used to measure water content in reagents and samples.

5.4 Results and discussion

The complete set of batch experiments carried out to characterize the reactions involved in this study is given in Table 5-3.

Table 5-3. Experimental conditions of batch reactions.

RUN	T (K)	Mole Ratio EtOH/SA	Mole Ratio EtOH/AcOH	Catalyst loading (g/g)	Time (h)
1	363	-	-	0.080	48
2	373	-	-	0.088	24
3	388	-	-	0.081	48
4	403	-	-	0.080	48
5	363	-	-	0.160	48
6	373	-	-	0.175	24
7	388	-	-	0.160	48
8	403	-	-	0.160	48
9	373	-	-	0.022	24
10	373	-	-	0.044	24
11	373	-	-	0.131	24
12	393	4.99	-	0.089	24
13	393	7.55	-	0.089	24
14	393	9.98	-	0.089	24
15	393	12.49	-	0.089	24
16	353	5.07	-	0.088	24
17	353	7.59	-	0.088	24
18	353	10.03	-	0.089	23.5
19	353	12.60	-	0.088	24
20	365	5.04	-	0.088	24
21	365	7.54	-	0.089	24
22	365	10.33	-	0.087	24
23	365	12.35	-	0.089	24
24	379	5.03	-	0.088	24
25	379	7.48	-	0.088	24
26	379	9.79	-	0.088	24
27	379	12.50	-	0.087	24
28	353	7.51	-	0.045	24
29	353	7.49	-	0.044	24
30	353	7.55	-	0.044	24
31	365	3.00	-	0.022	24
32	365	5.00	-	0.022	24
33	365	7.49	-	0.022	24
34	365	5.03	-	0.044	24
35	365	7.47	-	0.044	24
36	343	22.80	-	0.011	5
37	353	22.80	-	0.011	5
38	365	22.80	-	0.011	5
39	379	22.80	-	0.011	5
40	353	22.80	-	0.021	5
41	353	22.80	-	0.022	5
42	365	22.80	-	0.019	5
43	379	22.80	-	0.020	5
44	353	23.07	-	0.046	5

Table 5-3 (Continuation).

RUN	T (K)	Mole Ratio EtOH/SA	Mole Ratio EtOH/AcOH	Catalyst loading (g/g)	Time (h)
45	373	23.07	-	0.045	5
46	363	23.07	-	0.046	5
47	383	23.07	-	0.044	5
48	353	23.07	-	0.089	5
49	363	23.07	-	0.087	5
50	373	23.07	-	0.093	5
51	383	23.07	-	0.092	5
52	353	-	1.01	0.020	24
53	353	-	2.02	0.021	24
54	353	-	3.85	0.020	24
55	353	-	7.67	0.020	24
56	353	-	10.46	0.020	24
57	353	-	14.62	0.020	24
58	353	-	21.08	0.020	24
59	353	-	26.83	0.021	24
60	363	-	0.97	0.021	23
61	363	-	1.98	0.021	23
62	363	-	4.44	0.019	23
63	363	-	7.88	0.021	23
64	363	-	0.94	0.020	23
65	373	-	1.97	0.020	23
66	373	-	3.96	0.020	23
67	373	-	7.94	0.020	23
68	353	-	1.02	0.040	12
69	353	-	1.94	0.041	12
70	353	-	3.94	0.041	12
71	353	-	7.75	0.041	12
72	363	-	1.03	0.081	12
73	363	-	2.00	0.080	12
74	363	-	3.92	0.083	12
75	363	-	7.83	0.082	12
76	383	-	1.04	0.010	27
77	383	-	1.98	0.010	27
78	383	-	4.29	0.011	27
79	383	-	7.54	0.010	27
80	343	-	1.06	0.009	27
81	343	-	2.04	0.010	27
82	343	-	3.51	0.010	27
83	343	-	7.48	0.010	27
84	363	11.07	2.23	0.0109	12
85	353	11.67	8.28	0.0096	12
86	373	17.34	0.62	0.0125	12
87	363	11.02	8.58	0.0094	12
88	363	21.12	5.26	0.0216	12

Ethanol dehydration to diethyl ether (DEE) was studied in Runs 1 to 11; SA esterification was examined in Runs 11 to 51; AcOH esterification was evaluated in Runs 52 to 83; and finally mixed SA/AcOH esterification experiments were carried out in Runs 84 to 88. In these experiments, the catalyst loadings used (0.5 to 9.3 wt% Amberlyst 70) correspond to the equivalent acidity of 0.1 to 2.0 wt% H_2SO_4 in solution.

5.4.1 Mass transfer considerations

Preliminary SA esterification experiments in which agitation speed was varied showed nearly identical conversion rates at all speeds above 500 rpm, indicating that no external liquid-solid mass transfer resistances are present. Evaluation of intra-particle mass transfer effects is carried out using the observable modulus (Φ_W) and the Weisz-Prater criterion. For a spherical particle

$$\Phi_W = \frac{\left(r^{\dagger}_{Obs}\right)\rho_{CAT}\left(\frac{d_P}{6}\right)^2}{D_{eff}C_{SA}} \tag{5-1}$$

Here, $r^{\dagger}_{Obs.}$ is the observed rate of reaction per mass of catalyst, ρ_{CAT} and d_P are the particle density and particle diameter of the catalyst, respectively, under reaction conditions (e.g. the particle swelled state in EtOH), D_{eff} is the effective diffusivity of SA inside the catalyst pores, and C_{SA} is the concentration of SA in the bulk phase. Reaction rate $r^{\dagger}$ can be calculated as:

$$r^{\dagger} = \frac{r}{w_{CAT}\rho_{Sol}} \tag{5-2}$$

where r is the rate of reaction per unit volume of reacting (liquid) phase determined as the slope of the SA concentration vs. time curve, w_{CAT} is the mass of catalyst per mass of reacting phase, and ρ_{Sol} is density of the reacting phase.

A simple measurement showed that the swelling ratio (swelled volume $V_{Pswollen}$ divided by dry volume V_{Pdry}) of Amberlyst 70 catalyst was 2.0 in EtOH. Assuming homogeneous swelling of the spherical particles, the actual particle diameter is calculated as

$$d_P = d_{Pdry} \times \sqrt[3]{\frac{V_{Pswollen}}{V_{Pdry}}} \tag{5-3}$$

Taking the average particle diameter of dry solids used in experiments as 0.30 mm, a swelled particle diameter of 0.37 mm is obtained. Because of liquid absorption that gives Amberlyst 70 a porosity similar to macroreticular resins [17- 19], the swelled particle density is 1000 kg/m^3 as reported previously [30]. The effective diffusivity (D_{eff}) is estimated from the liquid-phase diffusion coefficient (D_{SA}) computed from the Wilke-Chang equation and by assuming pore tortuosity (τ) is the inverse of particle porosity (ε) [30]. The effective diffusivity of SA is thus given by

$$D_{eff} = D_{SA}\left(\frac{\varepsilon}{\tau}\right) = D_{SA}\varepsilon^2 \tag{5-4}$$

The Thiele modulus (ϕ) and effectiveness factor (η) for SA esterification can be calculated from the observable modulus if it is assumed the reaction is pseudo-first order in SA because of the large excess of EtOH present.

$$\Phi_w = \eta \phi^2 \tag{5-5}$$

where

$$\eta = \frac{\tanh \phi}{\phi} \tag{5-6}$$

Values for Φ_w calculated for an initial EtOH:SA molar ratio of 7.5:1 and at three different temperatures are presented in Table 5-4.

Table 5-4. Evaluation of mass transfer resistances using the Weisz-Prater criterion.

x_{SA}	0.115		
w_{CAT} (kg$_{CAT}$/kg$_{sol}$)	0.088		
ρ_{Sol} (kg/m^3)	830		
C_{SA} (kmol/m^3)	1.77		
$d_{P\,swollen}$ (mm)	0.37		
ρ_{CAT} (kg/m^3)	1012		
EtOH Association Factor for Wilke-Chang model	1.5		
SA molar volume at T_B (cm^3/mol)	83.58		
T (K)	353.15	379.15	393.15
μ_{liquid} (cP)	0.755	0.507	0.397
D_{SA} (m^2/s)	$2.02\text{x}10^{-9}$	$3.23\ \text{x}10^{-9}$	$4.28\ \text{x}10^{-9}$
D_{eff} (m^2/s)	$6.57\ \text{x}10^{-10}$	$1.05\ \text{x}10^{-9}$	$1.39\ \text{x}10^{-9}$
r_m (kmol / m^3) (1/s)	$8.05\ \text{x}10^{-4}$	$9.92\ \text{x}10^{-4}$	$8.86\ \text{x}10^{-4}$
$r_m^{\dagger}$ (kmol / kg$_{CAT}$) (1/s)	$1.1\ \text{x}10^{-5}$	$1.35\ \text{x}10^{-5}$	$1.20\ \text{x}10^{-5}$
ϕ	0.196	0.171	0.140
η	0.987	0.994	0.993
Φ_w	0.038	0.028	0.019

The effectiveness factor for each of these experiments is greater than $\eta > 0.95$, indicating that internal mass transfer resistances can be neglected in SA esterification [31].

Similar calculations likewise indicated the absence of diffusion limitations in AcOH esterification and dehydration of EtOH to DEE. To validate the above analysis of intraparticle mass transfer, the resin catalyst was separated in a series of US-standard sieves (Dual Manufacturing Co.). First, particles larger than 35 mesh (> 500 μm) were collected in the sieve tray. Smaller particles were ground and collected in two additional fractions: the -35+60 mesh fraction (250-500 μm) and <100 mesh fraction (<< 150 μm). Ion exchange capacity was measured in each fraction; no change in acidity was observed as a result of the grinding process.

Experiments were run at identical conditions with the three different Amberlyst 70 catalyst particle sizes. Results are presented in Figure 5-2; no difference in the rate of reaction was observed for the different catalyst particle sizes, verifying that internal mass transfer resistances can be neglected in this system.

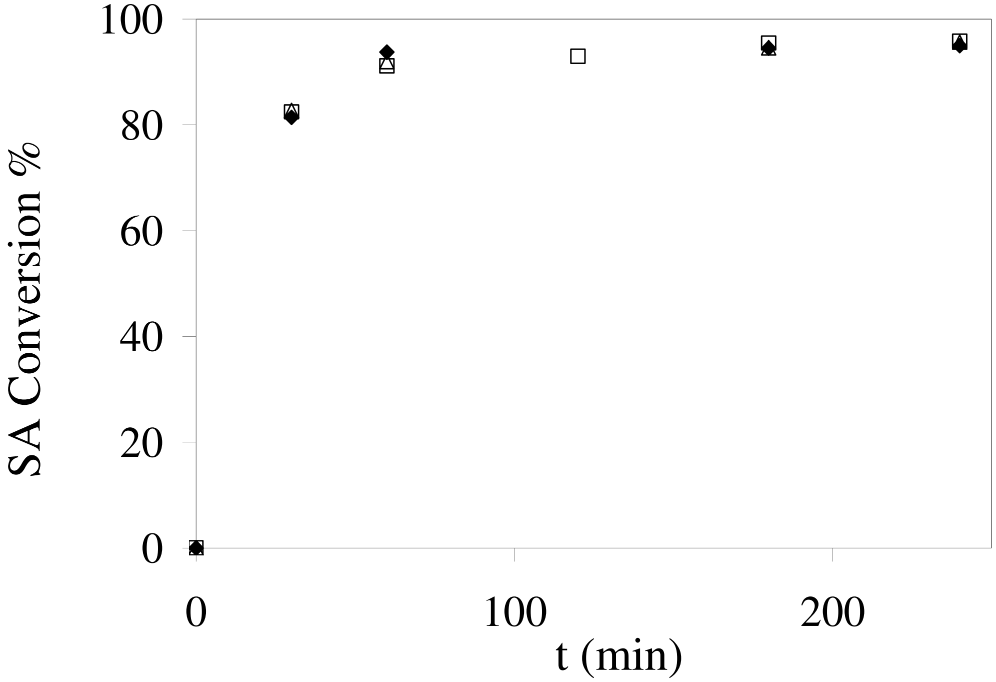

Figure 5-2. Esterification of SA with EtOH over different particle sizes of Amberlyst 70: (●) - $d_P < 150$ μm; (□) - 250 μm $< d_P <$ 590 μm; (Δ) - $d_P >$ 590 μm. Catalyst loading = 0.1 eq/kg solution; mole ratio EtOH:SA = 7.5:1; T = 353 K.

5.4.2 Reaction equilibrium constants

Equilibrium constants for the esterification reactions were measured by running experiments long times (> 23 hr). By taking the average composition of the last two samples, the equilibrium constant (K_{EQ}^{m}) for each reaction was calculated using mole fractions and activity coefficients of each of the N_C components of the reaction:

$$K_{EQ}^{m} = K_x^m K_\gamma^m = \prod_{i=1}^{N_C} \left(x_i \gamma_i \right)_{EQ}^{v_i} \tag{5-7}$$

Here x_i, γ_i, and v_i are the mole fraction, activity coefficient, and stoichiometric coefficient of component *i* in the reactive mixture, respectively. The ratio of activity coefficients K_γ^m accounts for deviations from ideal behavior of the mixture. At 383 K, the irreversible formation rate of diethyl ether (DEE) was significant and thus it was difficult to approach an equilibrium composition, so experiments at this temperature were not included in equilibrium constant calculations.

The NRTL equation was used to evaluate activity coefficients of components in the reaction mixture [32, 33]. Some binary interaction parameters were obtained from literature or from the Aspen Plus (Version 7.1, AspenTech, Inc.) database [33, 34]; others were determined by vapor-liquid equilibrium and liquid-liquid equilibrium measurements in our laboratory [35-38]. Parameters for H_2O-DEE, EtOH-DEE, AcOH-DEE and EtOAc-DEE were regressed from reported vapor-liquid and liquid-liquid phase equilibria data using the regression tool in Aspen Plus [33]. Plots of binary and ternary phase equilibrium data along with fitted predictions are presented in Figure 5-9 to 5-11 of the Supplementary Material. The list of binary parameters used in calculation of activity coefficients is presented in Table 5-6 of the Supplementary Material.

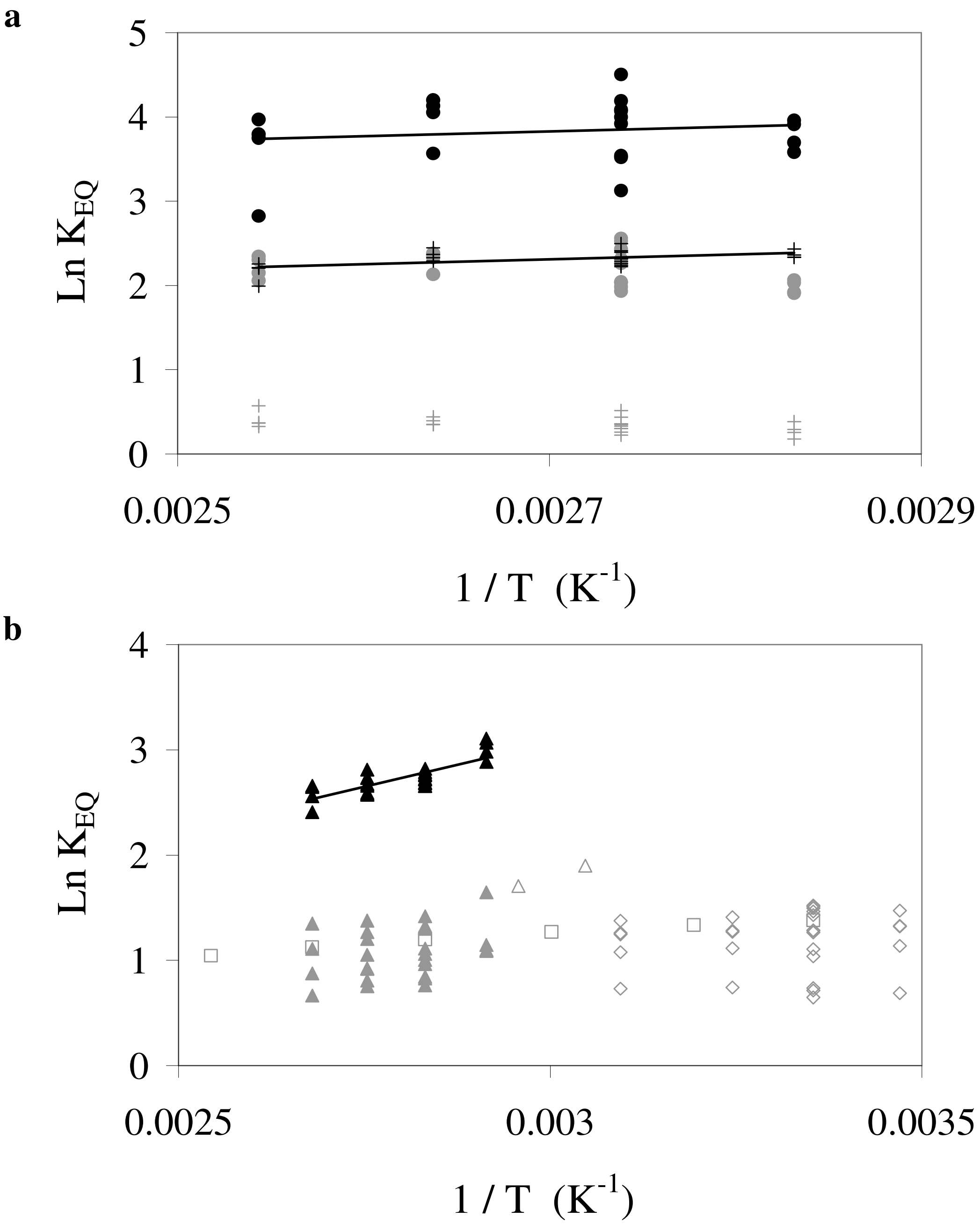

Figure 5-3. Mole fraction (gray) and activity (black) based esterification equilibrium constants from experimental data. a.) Succinic acid esterification: (●,●) - K_{EQ}^{1}: (+,+) - K_{EQ}^{2} (Reported values for mole fraction are $\ln K_{EQ}^{1} = 1.66$ and $\ln K_{EQ}^{2} = 0.182$ [21]) b.) Acetic acid esterification: (▲, ▲) -this work; (◊) - Darlington [22]; (Δ) - Hangx [26]; (□) - Tang [34].

The calculated mole fraction- and activity-based equilibrium constants for SA and AcOH esterification are presented in a Van't Hoff plot in Figure 5-3. These values agree with those reported in the literature under similar conditions [21, 22, 27, 34] as noted on the plot. The difference between activity- and mole fraction-based equilibrium constants reflects the significant non-ideality of the system (K_γ ~ 4).

The scatter in the equilibrium constants (±15%) is attributed to experimental and analytical uncertainties, and was noted to be worse with large excess of EtOH where nearly complete SA or AcOH conversion was obtained. Given that calculation of the equilibrium constant requires values for all species concentrations, some by different means, the uncertainty is reasonable. Further, a prior study of esterification equilibrium over ion exchange resin catalysts [22] reports that selective absorption of reacting components inside the catalyst particles changes the bulk liquid concentration and thus the value of the calculated equilibrium constant. This would affect the mole fraction-based calculation but not the activity-based equilibrium constant, as activity at equilibrium will be the same inside and outside of the catalyst particles.

As observed in Figure 5-3a, the slope of the trend line of SA esterification equilibrium constant is nearly zero, so the heat of reaction can be taken as zero and the equilibrium constant can be considered temperature independent. The averaged mole fraction based values of K_{EQ}^1 = 9.1 and K_{EQ}^2 = 1.4 agree reasonably well with those reported in the literature [21], and are used as initial estimates in regression of the kinetic model that follows.

Figure 5-3b indicates that the equilibrium constant for ethyl acetate formation decreases with increasing temperature. From the slope of this plot, the estimated heat of reaction for ethyl acetate formation is -13.8 kJ/mol, a value consistent with that obtained for similar catalysts [26, 28]. It should be noted, however, that for the kinetic modeling of acetic acid esterification, we have assumed the equilibrium constant is independent of temperature over the range of experimental conditions examined.

5.4.3 Kinetic model

In a batch reactor, the change in number of moles N_i of component *i* participating in *m* reactions can be expressed as

$$\frac{dN_i}{dt} = N_T \frac{dx_i}{dt} = \left(\sum_{m=1}^{m} \theta_{i,m} r_m \right) V \tag{5-8}$$

Here N_T is the total number of moles in the reactor, *V* is the reaction volume, r_m is the rate of reaction *m* per unit volume, and x_i is the mole fraction of component *i* in the liquid mixture. The parameter $\theta_{i,m}$ is the ratio of stoichiometric coefficients of component *i* with respect to the reference component in reaction *m*.

Equation 5-8 can be expressed in terms of total molar concentration in the liquid phase C_T ($V/N_T = 1/C_T$) calculated from average molecular weight (MW_{Avg}) and the density of the solution.

$$\frac{dx_i}{dt} = \frac{1}{C_T} \left(\sum_{m=1}^{m} \theta_{i,m} r_m \right) = \frac{MW_{Avg}}{\rho_{Sol}} \left(\sum_{m=1}^{m} \theta_{i,m} r_m \right) \tag{5-9}$$

Preliminary experiments confirmed that rates of reaction are linearly dependent on the catalyst loading (w_{CAT}) (Figure 5-4); this is further evidence of the intrinsic nature of the reaction rate data collected.

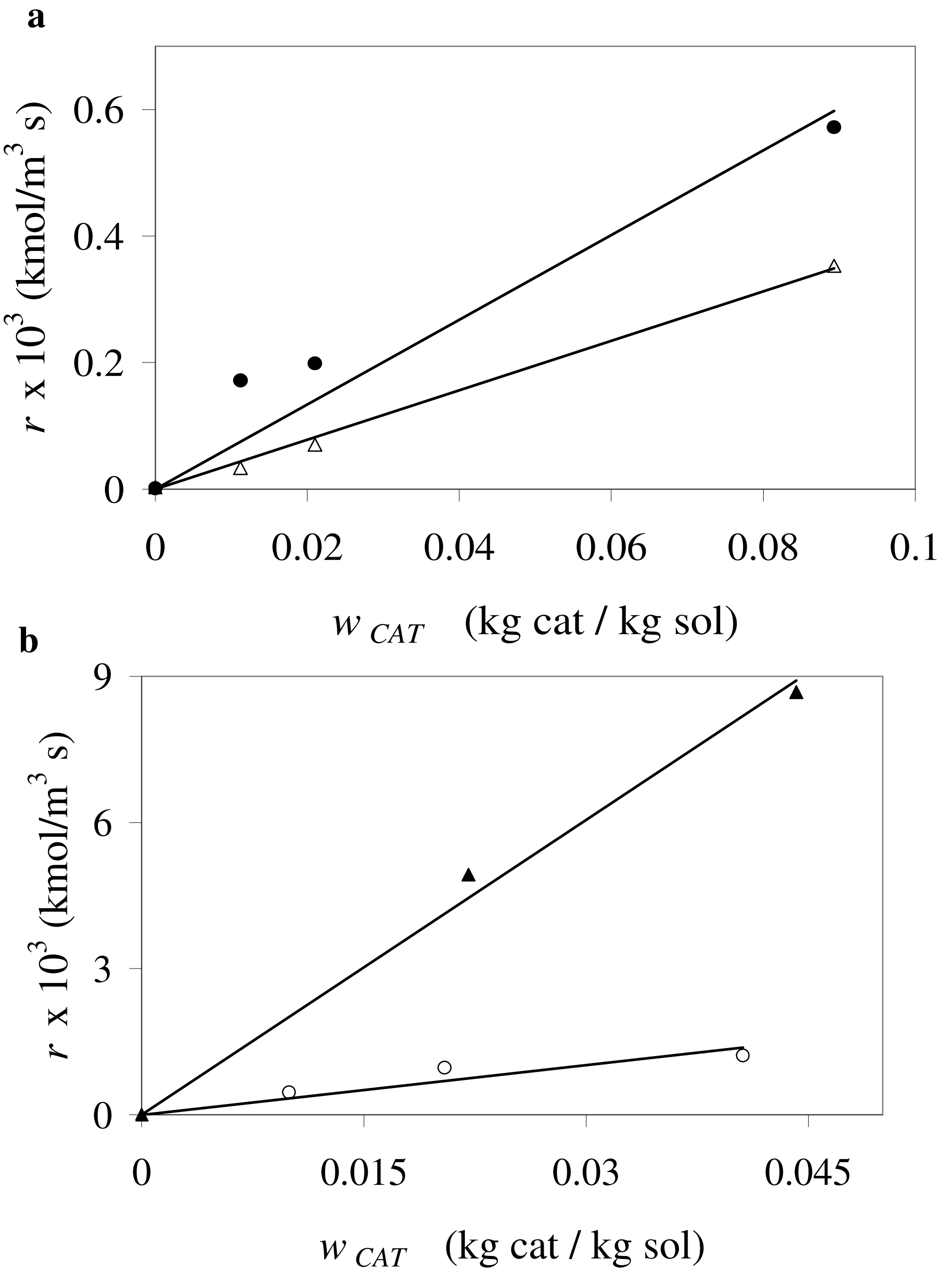

Figure 5-4. Rates of reaction under different catalyst loadings. a) SA esterification at $T = 353$ K, EtOH:SA = 23:1. (●) - r_1; (Δ) - r_2. b) (○) - AcOH esterification (r_3) at $T = 353$ K, EtOH:AcOH = 7.5:1; (▲) - EtOH etherification (r_4) at $T = 393$ K.

Using a pseudo-homogeneous model for the reversible esterification reactions, the rate of reaction of SA with EtOH can be expressed as

$$r_1 = w_{CAT}\rho_{Sol}k_0^1 \exp\left(\frac{-E_a^1}{RT}\right)\left[\left(x_{SA}\gamma_{SA}\right)\left(x_{EtOH}\gamma_{EtOH}\right)-\frac{\left(x_{MES}\gamma_{MES}\right)\left(x_{H2O}\gamma_{H2O}\right)}{K_{EQ}^1}\right] \tag{5-10}$$

Using the same approach for the second step of SA esterification (Figure 5-1), the rate of formation of DES is described by

$$r_2 = w_{CAT}\rho_{Sol}k_0^2 \exp\left(\frac{-E_a^2}{RT}\right)\left[\left(x_{MES}\gamma_{MES}\right)\left(x_{EtOH}\gamma_{EtOH}\right)-\frac{\left(x_{DES}\gamma_{DES}\right)\left(x_{H2O}\gamma_{H2O}\right)}{K_{EQ}^2}\right] \tag{5-11}$$

Here k_0^m and E_a^m represent the pre-exponential factor and the energy of activation of the forward reaction *m*, respectively. The equilibrium constant of reaction *m*, K_{EQ}^m, is the ratio of forward and reverse rate constants. Similarly, the rate of AcOH esterification with EtOH can be expressed as

$$r_3 = w_{CAT}\rho_{Sol}k_0^3 \exp\left(\frac{-E_a^3}{RT}\right)\left[\left(x_{AcAc}\gamma_{AcAc}\right)\left(x_{EtOH}\gamma_{EtOH}\right)-\frac{\left(x_{EtAc}\gamma_{EtAc}\right)\left(x_{H2O}\gamma_{H2O}\right)}{K_{EQ}^3}\right] \tag{5-12}$$

Considering that EtOH dehydration is irreversible, the rate of DEE formation can be expressed as

$$r_4 = w_{CAT}\rho_{Sol}k_0^4 \exp\left(\frac{-E_a^4}{RT}\right)\left[\left(x_{EtOH}\gamma_{EtOH}\right)^2\right] \tag{5-13}$$

Substituting Eq. (5-10) to (5-13) into Eq. (5-9) for each component gives a set of ordinary differential equations to be solved simultaneously in a mixed acid esterification model. Two forms of this model were fit to the experimental data: the first being activity-based with activity coefficients in all rate expressions, and the second a simplified mole fraction form generated by setting all activity coefficients in Eq. (5-10 to 5-13) equal to 1.0.

In the complete mixed acid esterification model, there are 11 adjustable parameters: 4 pre-exponential factors, 4 energies of activation and 3 equilibrium constants. In order to simplify the parameter fitting and ultimately investigate interdependence of the reactions, the kinetics of EtOH dehydration, SA esterification, and AcOH esterification were measured independently and the kinetic parameters for each reaction were obtained.

To determine kinetic parameters, Eq. (5-9) was numerically integrated for each component via a fourth order Runge-Kutta method using differential equation solver ode23 in Matlab 7.0. Optimization of kinetic parameters was performed by minimizing the sum of squared differences between experimental (x_{i-Exp}) and calculated (x_{i-Calc}) species mole fractions using the following objective function in Matlab 7.0.

$$F_{\min}^2 = \frac{1}{n}\sum_{samples}\sum_{i=1}^{N_C}\left(x_{i-Exp} - x_{i-Calc}\right)^2 \tag{5-14}$$

where *n* is the number of experimental samples withdrawn from batch reactors in all experiments fitted and N_C is the number of components considered in each sample. For EtOH etherification and AcOH esterification, all components present were considered in Eq. (5-14); for SA esterification only the succinate species (SA, MES, DES) were considered.

Once optimized constants were obtained, the average absolute error f_{ABS} and average relative percent error f_{REL} for each model were used to evaluate mean relative deviation on an absolute and on a percentage basis as shown in Eq. (5-15) and (5-16).

$$f_{ABS} = \frac{1}{n} \sum_{samples} \sum_{i=1}^{N_C} \left| x_{i-Exp} - x_{i-Calc} \right| \tag{5-15}$$

$$f_{REL} = 100 \times \frac{1}{n} \sum_{samples} \sum_{i=1}^{N_C} \frac{\left| x_{i-Exp} - x_{i-Calc} \right|}{x_{i-Exp}} \tag{5-16}$$

5.4.4 Kinetic constants

For EtOH dehydration, both mole fraction and activity-based models predict DEE formation reasonably well (Figure 5-5). Only one activity-based predicted profile is presented because all others overlap those of the mole fraction model. Experiments at high temperatures (>393 K), high loadings of catalyst ($w_{CAT} > 0.04$) and long reaction time (>500 min) showed significant formation of DEE. At these conditions, flashing of liquid during sampling was observed; this flashing and the resulting change in liquid composition may explain deviation of the model from experiment at the most extreme conditions.

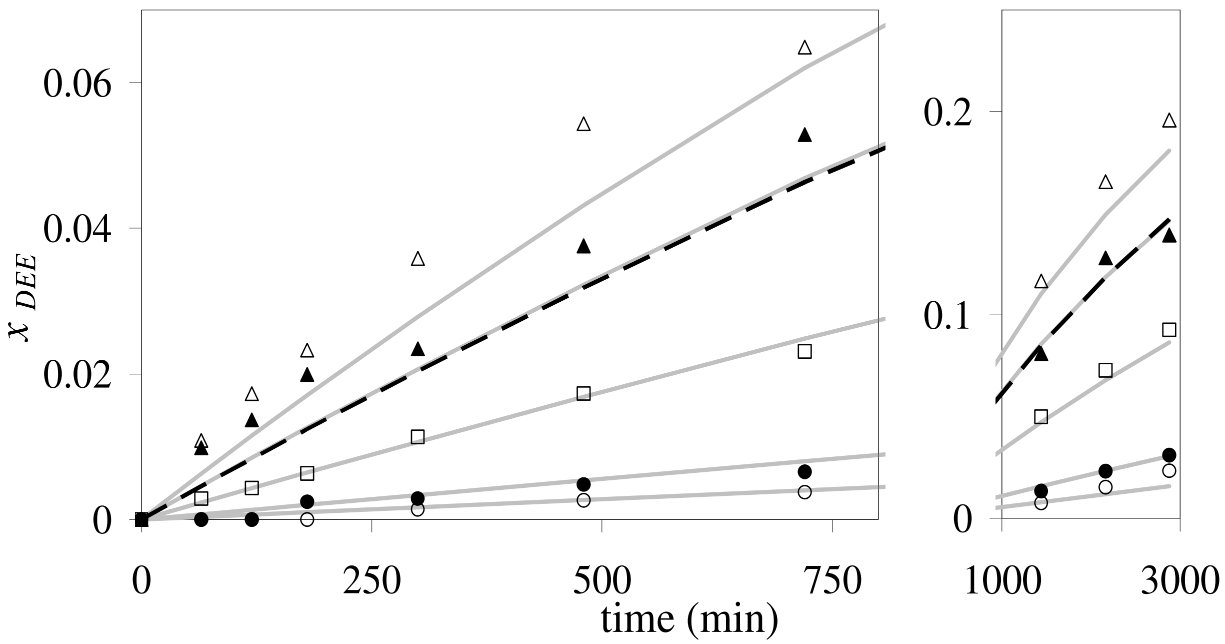

Figure 5-5. Experimental and predicted mole fraction profiles of DEE formation. (○) - Run 1: T = 363 K, w_{CAT} = 0.08; (□) - Run 3: T = 388 K, w_{CAT} = 0.081; (Δ) - Run 4: T = 403 K, w_{CAT} = 0.08; (●) - Run 5: T = 363 K, w_{CAT} = 0.16; (▲) - Run 7: T = 388 K, w_{CAT} = 0.16. (— —) Activity based model; (—) Mole fraction model.

EtOH dehydration kinetics are included in the kinetic analysis of SA esterification (Runs 12-51) and AcOH esterification (Runs 52-83). In these regression analyses, the equilibrium constants determined in experiment (Figure 5-3) were used as initial estimates for predicting reverse reaction rate constants in the model. Although these equilibrium constants were allowed to vary in the optimization, their final values differ negligibly from those reported in Figure 5-3. Final optimized kinetic parameters for Eq. (5-10) to (5-13) are listed in Table 5-5. Experimental results from Runs 33 and 37 for succinic acid, and Runs 61 and 78 for acetic acid are presented and compared with predictions from the kinetic models in Figures 5-6 and 5-7, respectively. Additional kinetic profiles are presented in the Supplementary Material.

Again, the activity-based kinetic model predictions overlap the profiles obtained from the mole fraction model, so only one set is shown. Good agreement between model and experimental data is observed at different conditions for simultaneous esterification and etherification reactions. In general, it is seen that with excess EtOH and high loadings of catalyst ($w_{CAT} > 0.01$), almost complete conversion of SA is obtained after 2 h of reaction. This time is even shorter when temperatures above 373 K are used; however, significant quantities of DEE are produced at the high temperature. This DEE formation limits the maximum temperature that can be used for ethanol esterification reactions.

Table 5-5. Parameters for pseudo-homogeneous kinetic models.

Parameter	Mole Fraction	Activity
SA Esterification		
k_0^1 (kmol / kg $_{CAT}$ / s)	$1.53\text{x}10^3$	$1.04\text{x}10^4$
E_a^1 (kJ/kmol)	44400	46200
K_{EQ}^1	8.83	48.9
k_0^2 (kmol / kg $_{CAT}$) (1/s)	$2.78\text{x}10^4$	$2.11\text{x}10^3$
E_a^2 (kJ/kmol)	54700	46600
K_{EQ}^2	1.35	10.14
AcOH Esterification		
k_0^3 (kmol / kg $_{CAT}$) (1/s)	$1.50\text{x}10^4$	$1.03\text{x}10^4$
E_a^3 (kJ/kmol)	49400	47600
K_{EQ}^3	2.84	12.11
EtOH Dehydration		
k_0^4 (kmol / kg $_{CAT}$) (1/s)	$8.06\text{ x}10^4$	$4.99\text{ x}10^4$
E_a^4 (kJ/kmol)	86900	85400

The kinetic parameters presented in Table 5-5 agree well with those reported for similar catalysts in the literature [21, 26-28, 34]. For the optimized parameters, the average absolute and relative errors for both mole fraction- and activity-based kinetics were computed and are listed in Table 5-7 in the Supplementary Information.

a

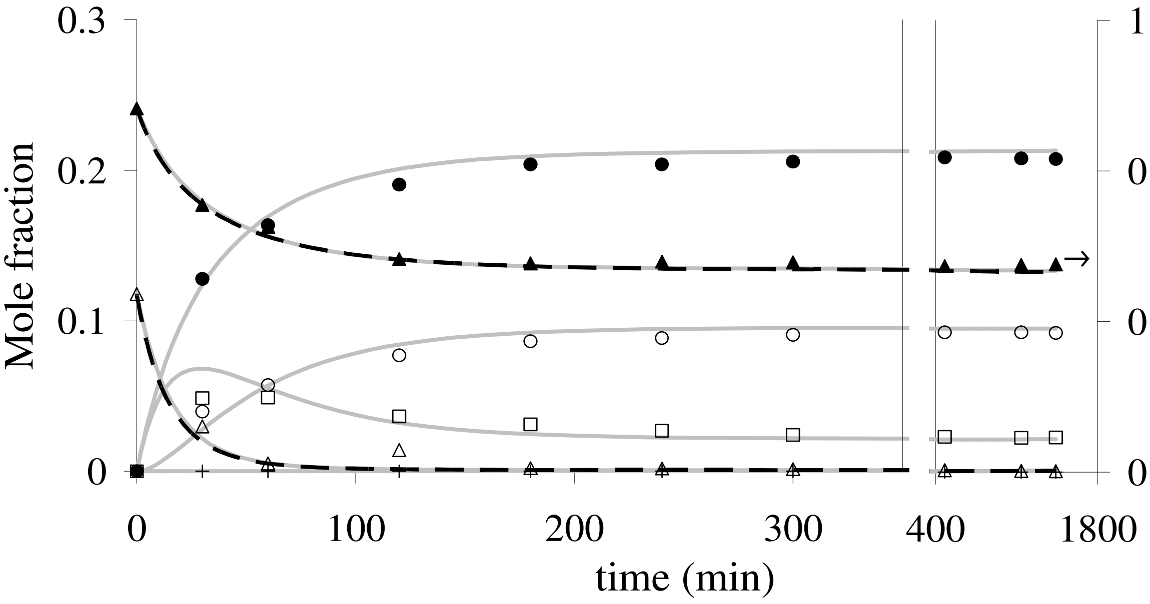

b

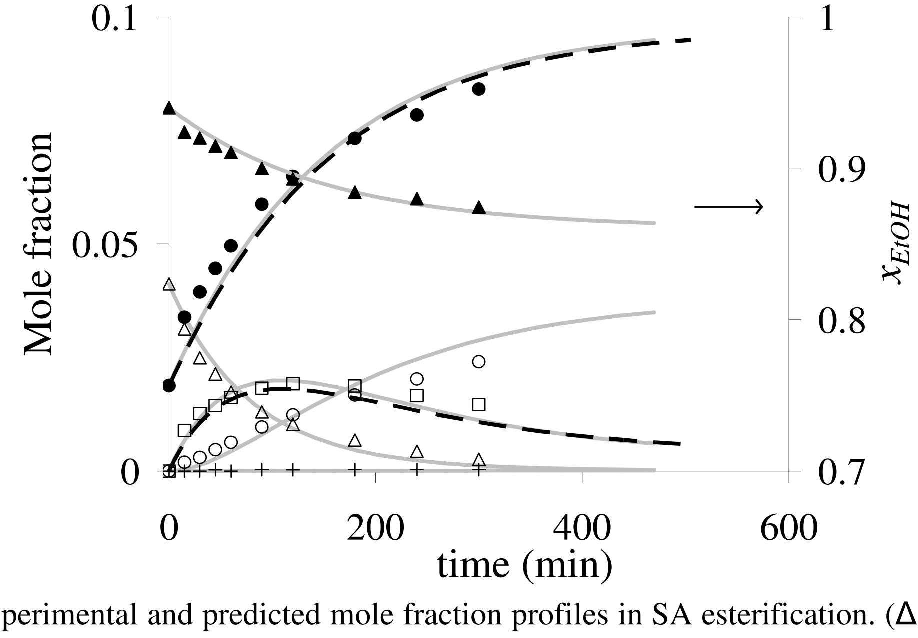

Figure 5-6. Experimental and predicted mole fraction profiles in SA esterification. (Δ) - SA; (○) - DES; (□) - MES; (▲) - EtOH; (●) - H_2O; (+) - DEE; (▬ ▬) - activity based model; (▬) - mole fraction model. a) Run 33: T = 365 K, w_{CAT} = 0.022, EtOH:SA = 7.49. b) Run 37: T = 343 K, w_{CAT} = 0.011, EtOH:SA = 22.8.

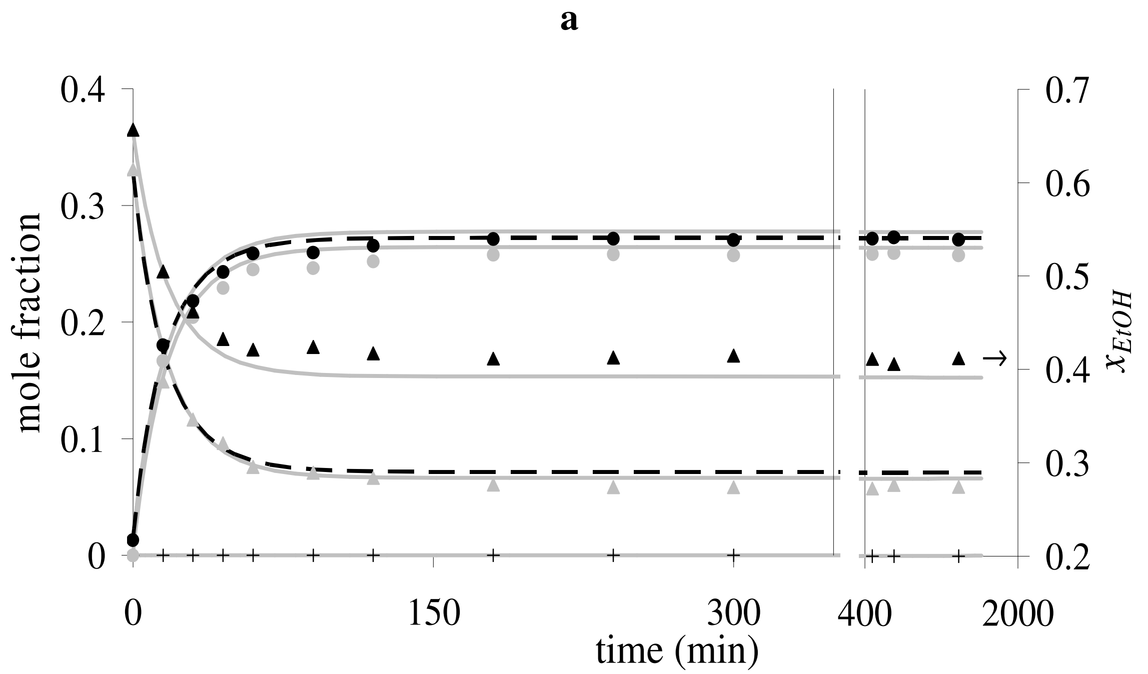

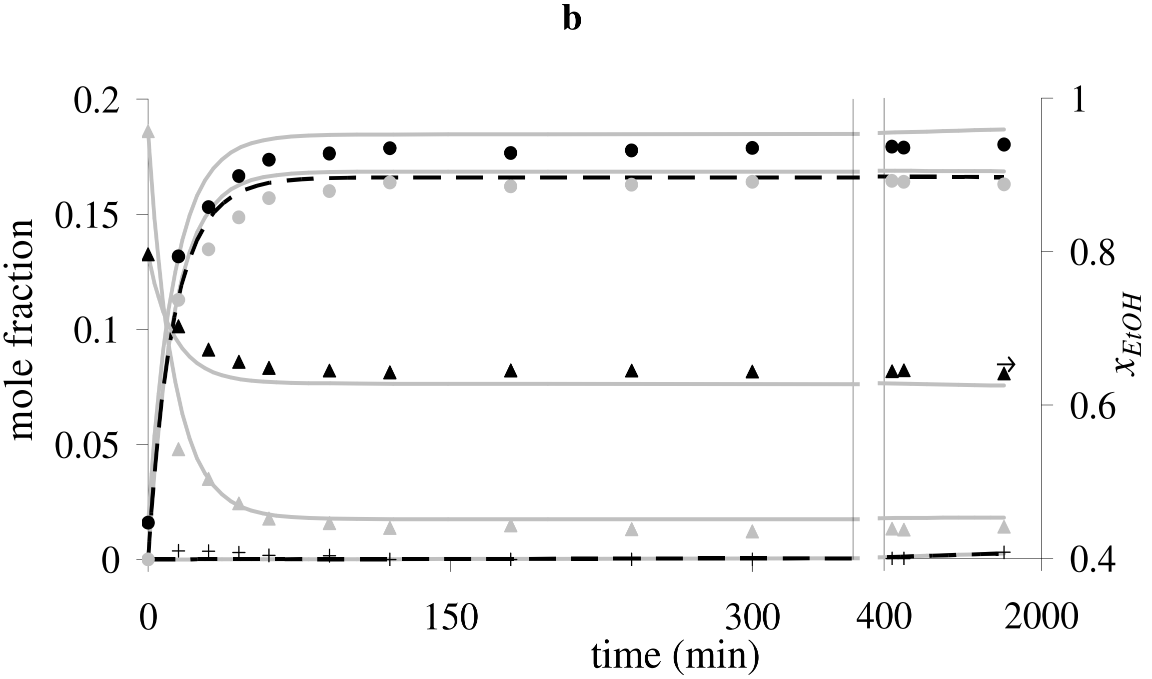

Figure 5-7. Experimental and predicted mole fraction profiles in AcOH esterification. (▲) - AcOH; (●) - EtOAc; (▲) - EtOH; (●) - H_2O; (+) - DEE; (▬ ▬) - activity based model; (▬) - mole fraction model. a) Run 61: T = 363 K, w_{CAT} = 0.0208, Mole ratio EtOH:AcOH = 1.98. b) Run 78: T = 383 K, w_{CAT} = 0.0108, Mole ratio EtOH:AcOH = 4.29.

Relative deviations for both models are similar to those previously reported from our laboratory [21]. The large average relative errors (average values are ~ 16 % for SA esterification, ~ 9% for AcOH esterification and ~ 13% for EtOH etherification) are mainly attributed to components that are present at low concentrations. This was the case for SA, AcOH, and DEE, for which mole fractions were less than 0.005 in the majority of samples, and for MES (mole fraction between 0.01 - 0.04) mainly at long reaction times. For all other components, relative error values were less than 5%.

The large excess of ethanol used in most experiments, and the large deviations arising from analytical uncertainty at the low values of mole fraction for some species, is a consequence of the low solubility of SA (~10 wt% or 23:1 EtOH:SA at 298 K) in the alcohol. We ran experiments at higher SA initial concentrations, but the slow dissolution rate and solubility limits of SA at low temperature resulted in undissolved SA in the reactor after reaction started. This led to error in the mass balance and in the fit of the kinetic data at short reaction times. Thus, experiments with higher SA concentrations were limited to taking samples at least 30 minutes after reaching reaction temperature; no attempt was made to capture the early kinetic behavior of these esterification reactions. Characterizing such early reaction behavior would require handling a predissolved, heated feed solution under pressure, a scenario that we were not prepared to undertake. Based on a catalyst acid site density of 2.35 meq/g, the initial turnover number for SA esterification over Amberlyst 70 at 353 K and 7.5:1 EtOH:SA molar ratio is 69 h^{-1}. At the same conditions, we have found that more commonly used Amberlyst 15 macroreticular resin has a turnover frequency of 48 h^{-1}. These results agree with the higher acid strength and higher turnover numbers reported for sulfonic groups in chlorinated resins such as Amberlyst 70 [19, 39] , and are consistent with higher accessibility (e.g. higher effective diffusivity of reactants) to actives sites in a swelled gel-type structure compared with a macroreticular resin [19].

5.4.5 Mixed acid esterification

Using the kinetic parameters determined in individual SA and AcOH esterification reactions (Table 5-5), the modeling of mixed SA and AcOH esterification was performed by integrating Eq. (5-9) for each species in the mixture. Absolute and relative errors of mixed acid model predictions with respect to experimental observations were calculated from Equations 5-15 and 5-16 and are presented in Table 5-7 of the supplementary material. Larger relative errors (~ 20%) in the mixed acid esterification relative to those in AcOH esterification alone can again be attributed to the large excess of EtOH used in these experiments: mole fractions of acids are initially low and decline rapidly as near-complete conversion of both SA and AcOH is achieved, thus increasing error because of uncertainties in analytical measurements at low concentrations. Nevertheless, the model predicts mixed acid esterification reasonably well, as shown in the kinetic profiles presented in Figure 5-8.

Because the combination of individual esterification reactions reasonably predicts the mixed acid results, it is apparent that the esterification reactions proceed without competition for catalyst active sites among the acid species. In some other esterification studies, a Langmuir-Hinshelwood type expression has been invoked to describe rate [40,41]; it is clear here that the active sites are not occupied to a significant degree by either SA or AcOH, and that the simple second-order rate expressions suffice to describe rate behavior of mixed acid esterification.

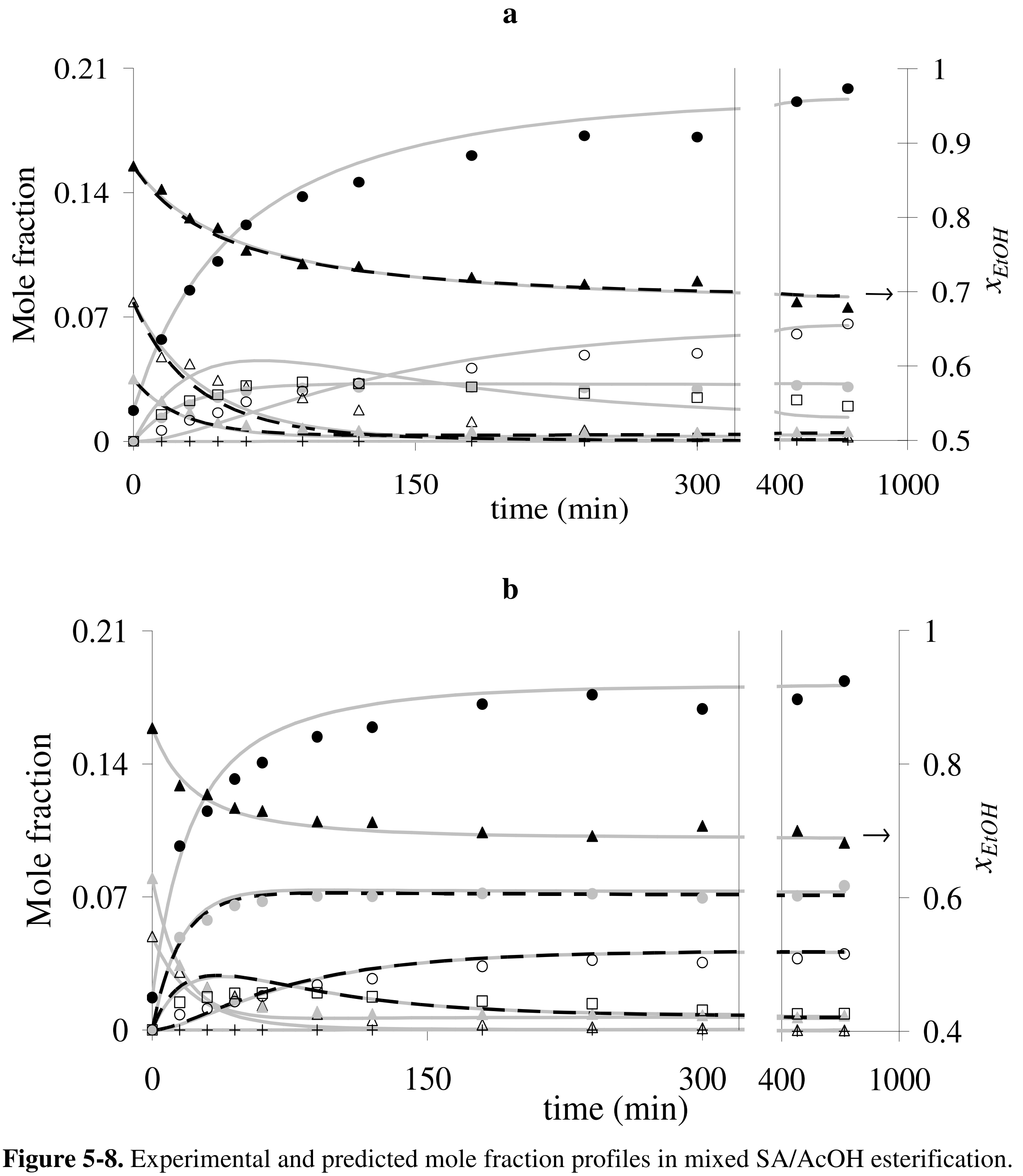

Figure 5-8. Experimental and predicted mole fraction profiles in mixed SA/AcOH esterification. (▲) - AcOH; (●) - EtOAc; (Δ) - SA; (○) - DES; (□) - MES; (▲) - EtOH; (●) - H_2O; (+) - DEE. (━ ━) - activity based model; (━) - mole fraction model. a) Run 84: T = 363 K, w_{CAT} = 0.011, mole ratio EtOH:SA = 11.1 and SA:AcOH = 2.2. b) Run 86: T = 373 K, w_{CAT} = 0.0125, Mole ratio EtOH:SA = 17.3 and SA:AcOH = 0.62.

5.5 Supplementary material

Table 5-6. Binary parameters for NRTL model. $G_{ij} = \exp(-\alpha_{ij}\ \tau_{ij})$, $\tau_{ij} = (a_{ij} + b_{ij}/T)$.

i	j	a_{ij}	a_{ji}	b_{ij}	b_{ji}	α_{ij}
H_2O	EtOH	0.514285	0.806535	444.8857	-266.533	0.4
H_2O	SA	0	0	296.7226	-328.506	0.3
H_2O	DES	4.384591	-1.58	184.7326	1136.555	0.36842
H_2O	MES	0	0	880.7603	-200.977	0.3
H_2O	DEE	8.412378	0.617494	-1496.24	547.9293	0.348988
H_2O	AcOH	3.3293	-1.9763	-723.888	609.8886	0.3
H_2O	EtOAc	3.853826	-2.34561	-4.42868	1290.464	0.364313
EtOH	SA	0	0	-605.634	113.4481	0.3
EtOH	DES	0	0	653.8819	-158.856	0.3
EtOH	MES	0	0	-292.308	400.6306	0.3
EtOH	DEE	4.3596	-3.5877	-1209.49	1381.066	0.3
EtOH	AcOH	0	0	225.4756	-252.482	0.3
EtOH	EtOAc	1.817306	-4.41293	-421.289	1614.287	0.1
AcOH	EtOAc	0	0	-235.279	515.8212	0.3
AcOH	SA	0	0	-386.393	2132.132	0.3
AcOH	MES	0	0	-176.711	302.7477	0.3
AcOH	DES	-3.32574	18.50486	1067.921	-5736.06	0.3
AcOH	DEE	-2.36704	20.157	479.0254	-5769.5	0.2
EtOAc	SA	0	0	191.9869	1976.63	0.3
EtOAc	MES	0	0	191.701	-142.115	0.3
EtOAc	DES	0	0	236.0739	-211.388	0.3
EtOAc	DEE	0	0	144.9525	-113.666	0.3
SA	DES	0	0	1946.876	218.2243	0.3
SA	MES	0	0	-368.762	1039.777	0.3
SA	DEE	0	0	1947.928	248.4113	0.3
DES	MES	0	0	-44.2052	137.2218	0.3
DES	DEE	0	0	595.5747	-404.406	0.3
MES	DEE	0	0	100.6717	88.62851	0.3

Table 5-7. Evaluation of intraparticle mass transport under experimental conditions and relative deviations of compositions calculated form regressed models and experimental data. Mole fraction (MF) and Activity (Act.) based kinetics.

RUN	Experimental diffusion criteria		Average Error			
			Absolute		Relative	
	Φ_w	η	MF	Act.	MF	Act.
1	-	-	0.0019	0.0018	10.29	10.69
2	-	-	0.0026	0.0026	43.17	42.99
3	-	-	0.0021	0.0025	4.05	4.20
4	-	-	0.0097	0.0110	13.26	14.75
5	-	-	0.0011	0.0012	8.84	9.45
6	-	-	0.0024	0.0024	13.41	15.70
7	-	-	0.0072	0.0075	13.98	14.58
8	-	-	0.0225	0.0237	14.30	14.50
9	-	-	0.0004	0.0004	5.09	5.05
10	-	-	0.0006	0.0006	8.53	8.49
11	-	-	0.0022	0.0022	15.26	15.26
12	0.024	0.992	0.0471	0.0469	32.05	36.98
13	0.020	0.993	0.0087	0.0081	12.04	15.68
14	0.020	0.993	0.0076	0.0073	12.74	14.44
15	0.019	0.994	0.0102	0.0102	16.20	16.54
16	0.048	0.984	0.0098	0.0089	15.11	17.65
17	0.038	0.987	0.0066	0.0067	22.16	22.51
18	0.040	0.987	0.0034	0.0033	14.06	11.95
19	0.041	0.986	0.0033	0.0034	19.03	17.47
20	0.042	0.986	0.0075	0.0059	11.28	14.08
21	0.036	0.988	0.0037	0.0033	7.90	8.35
22	0.034	0.989	0.0017	0.0017	9.34	8.22
23	0.033	0.989	0.0016	0.0016	7.16	8.37
24	0.031	0.990	0.0069	0.0054	9.75	14.69
25	0.029	0.990	0.0040	0.0033	6.68	8.64
26	0.027	0.991	0.0040	0.0037	12.15	12.56
27	0.026	0.991	0.0032	0.0031	8.38	7.51
28	0.168	0.945	0.0065	0.0063	20.88	20.94
29	0.172	0.943	0.0056	0.0054	19.49	19.67
30	0.168	0.945	0.0063	0.0060	20.78	21.00
31	0.165	0.946	0.0122	0.0121	14.20	17.08
32	0.128	0.958	0.0042	0.0062	10.84	14.95
33	0.114	0.962	0.0039	0.0042	12.10	12.67
34	0.076	0.975	0.0032	0.0048	9.85	13.72
35	0.056	0.982	0.0035	0.0040	9.93	11.34
36	0.128	0.958	0.0018	0.0018	14.95	16.06
37	0.138	0.954	0.0024	0.0025	19.01	19.60
38	0.238	0.922	0.0052	0.0051	21.63	19.60
39	0.166	0.945	0.0026	0.0025	23.57	22.15
40	0.086	0.972	0.0088	0.0089	46.08	46.45
41	0.125	0.959	0.0027	0.0025	21.03	20.48
42	0.109	0.964	0.0073	0.0073	39.52	39.14
43	0.126	0.958	0.0024	0.0024	23.29	23.79
44	0.075	0.975	0.0056	0.0056	29.67	28.27

Table 5-7. (Continuation).

RUN	Experimental diffusion criteria		Average Error			
			Absolute		Relative	
	Φ_w	η	MF	Act.	MF	Act.
45	0.078	0.974	0.0037	0.0037	22.81	20.79
46	0.080	0.973	0.0031	0.0030	21.72	19.31
47	0.072	0.976	0.0025	0.0025	20.72	18.73
48	0.059	0.981	0.0028	0.0026	20.43	21.97
49	0.049	0.984	0.0024	0.0023	21.44	19.08
50	0.039	0.987	0.0022	0.0022	18.75	24.52
51	0.036	0.988	0.0016	0.0016	16.94	21.90
52	0.080	0.973	0.020	0.014	8.955	6.355
53	0.099	0.967	0.008	0.008	4.161	5.610
54	0.132	0.956	0.009	0.008	6.001	9.458
55	0.117	0.961	0.008	0.006	9.071	6.860
56	0.126	0.958	0.006	0.005	7.446	7.815
57	0.127	0.958	0.006	0.005	15.393	15.506
58	0.131	0.957	0.004	0.003	18.224	28.747
59	0.132	0.956	0.004	0.003	13.980	21.184
60	0.094	0.969	0.021	0.015	9.248	6.647
61	0.100	0.967	0.010	0.008	4.848	5.043
62	0.126	0.958	0.010	0.007	6.567	5.922
63	0.108	0.964	0.009	0.007	9.485	8.062
64	0.076	0.975	0.016	0.018	7.378	8.003
65	0.094	0.969	0.009	0.008	4.459	4.758
66	0.106	0.965	0.012	0.009	6.925	5.968
67	0.098	0.968	0.009	0.008	10.207	7.084
68	0.059	0.981	0.017	0.013	8.182	6.591
69	0.063	0.979	0.009	0.008	4.855	6.028
70	0.077	0.974	0.009	0.006	4.784	7.787
71	0.075	0.975	0.009	0.007	9.558	8.883
72	0.028	0.991	0.017	0.013	8.035	6.557
73	0.033	0.989	0.009	0.009	5.892	7.211
74	0.039	0.987	0.009	0.006	5.247	6.805
75	0.043	0.986	0.006	0.005	6.562	7.435
76	0.156	0.949	0.028	0.022	14.684	12.013
77	0.163	0.946	0.010	0.011	10.287	10.855
78	0.172	0.943	0.009	0.008	8.656	11.363
79	0.175	0.942	0.009	0.008	12.240	15.366
80	0.111	0.963	0.033	0.029	17.261	14.744
81	0.071	0.977	0.037	0.036	18.698	19.067
82	0.089	0.970	0.023	0.021	15.171	15.681
83	0.128	0.958	0.009	0.008	10.258	11.756
84	-	-	0.004	0.004	18.63	16.53
85	-	-	0.005	0.005	22.98	20.87
86	-	-	0.003	0.003	14.82	13.55
87	-	-	0.005	0.005	28.40	26.82
88	-	-	0.003	0.003	23.44	20.76

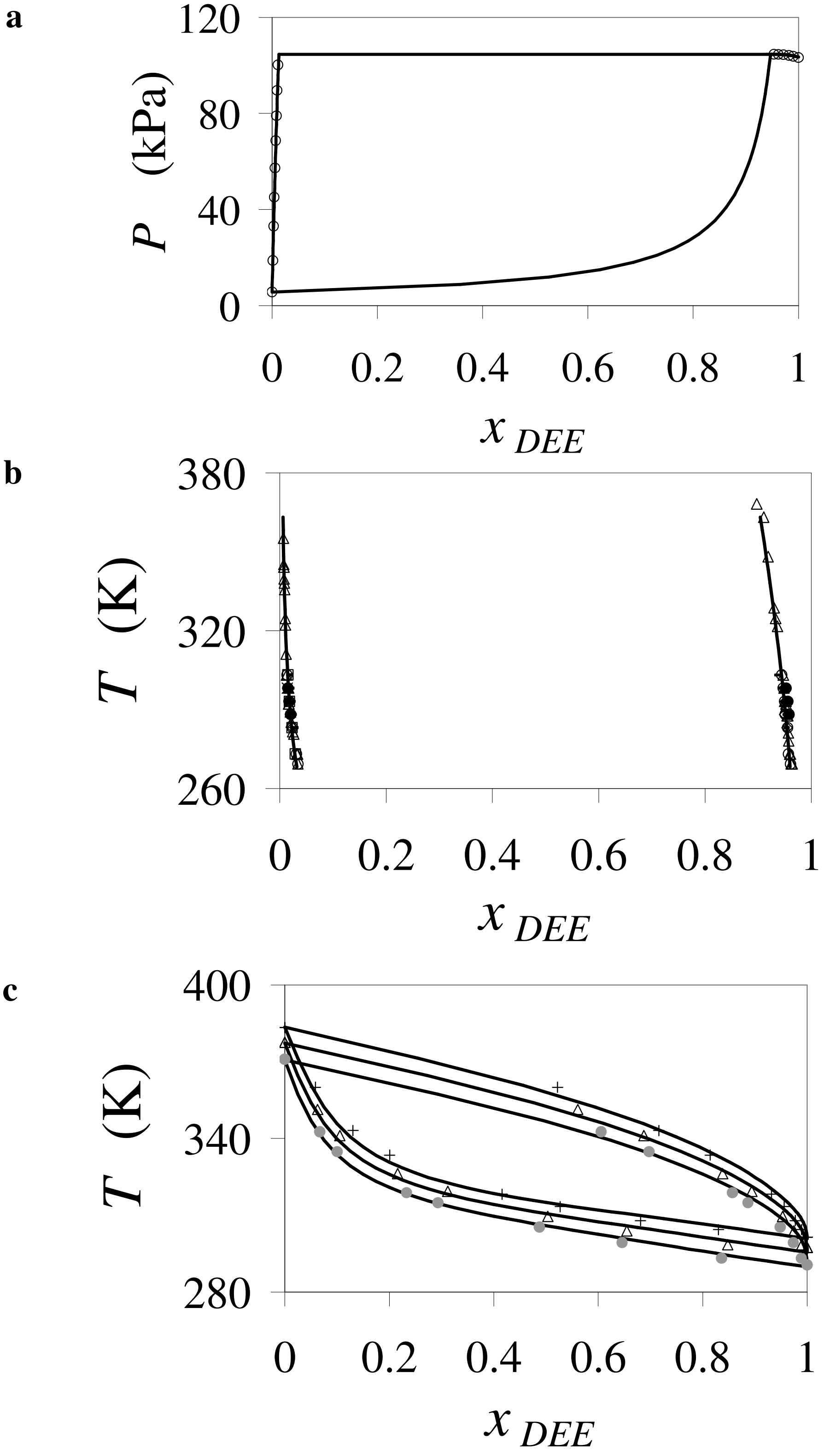

Figure 5-9. Reported phase equilibria in mixtures with DEE and modeling using NRTL-HOC (solid lines). a) vapor-liquid DEE-H_2O at T = 308 K [42]. b) liquid-liquid DEE-H_2O [43]. c) vapor-liquid DEE-AcOH at P = 51.9, P = 65 and P = 79.5 kPa [44].

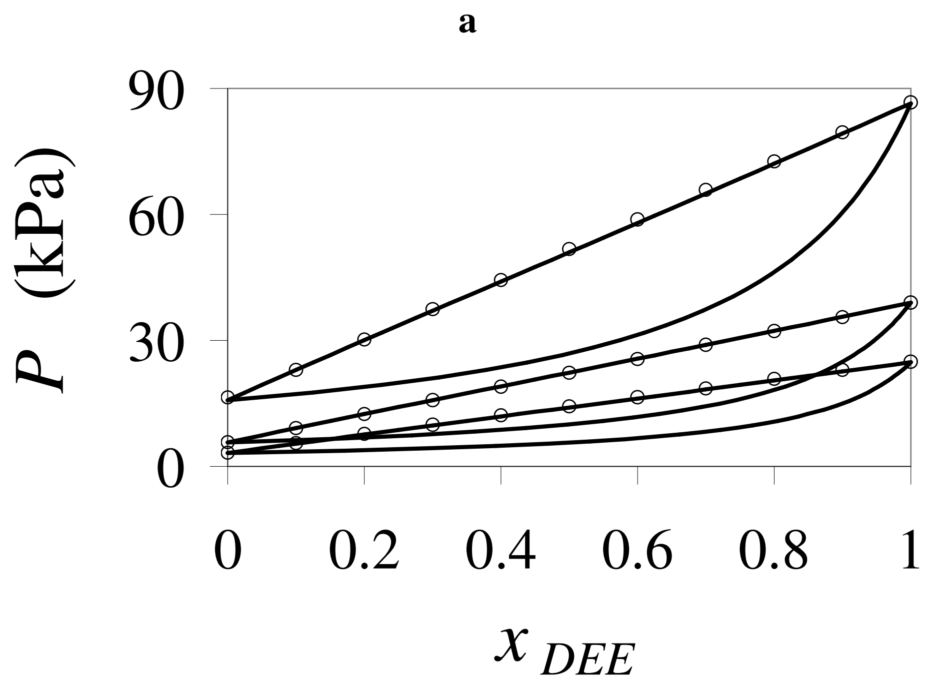

Figure 5-10. a) vapor-liquid DEE-EtOAc at T = 273, T = 283 and T = 303 K [44]. b) vapor-liquid DEE-EtOH at T = 273, T = 283, T = 293, T = 298, T = 303, T = 313 and T = 323 K [45].

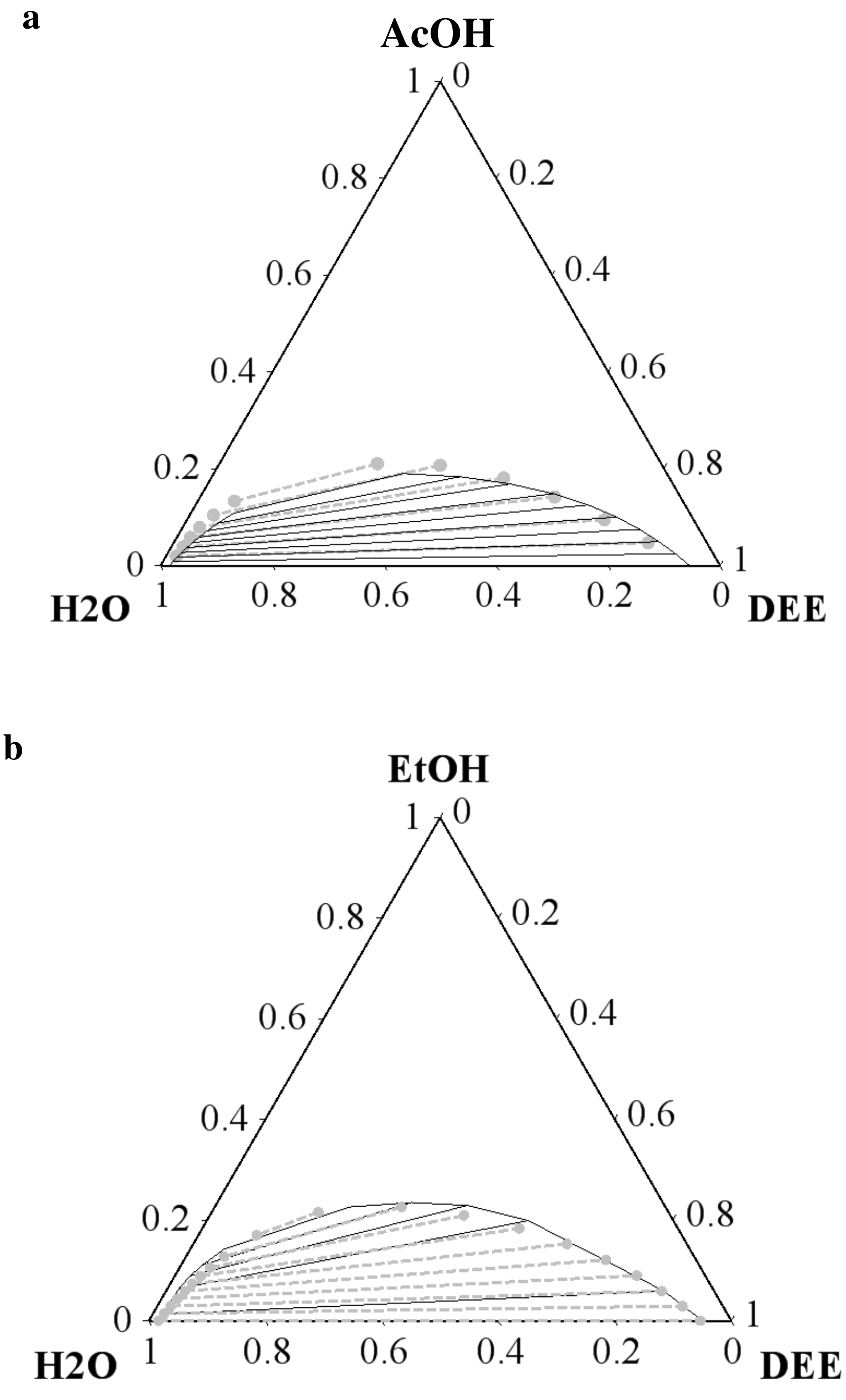

Figure 5-11. a) ternary diagram H_2O-AcOH-DEE at T = 298 K (mole fraction basis) [42]. b) ternary diagram H_2O-EtOH-DEE at T = 298 K (mole fraction basis) [46].

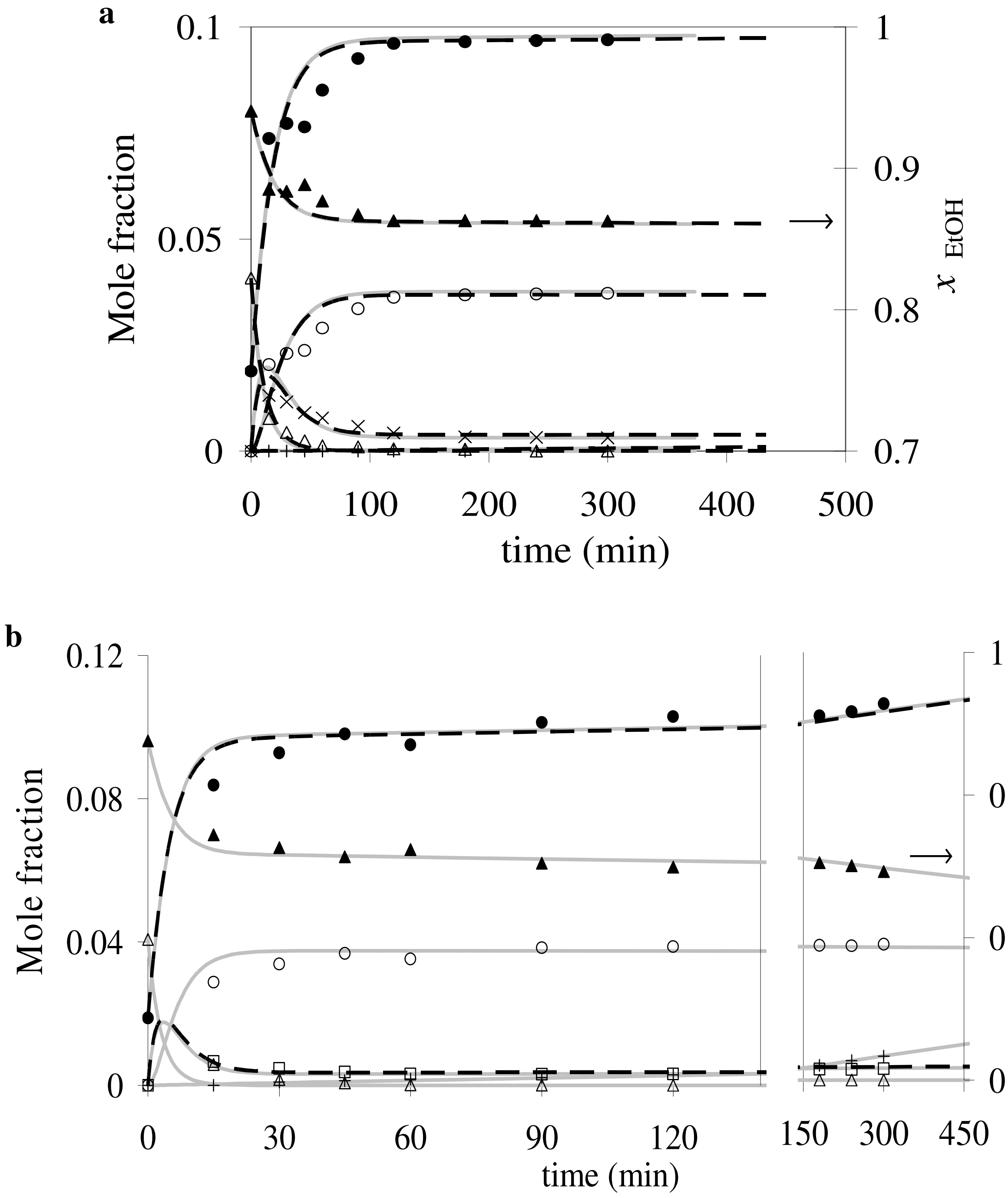

Figure 5-12. Experimental and predicted mole fraction profiles in SA esterification. (Δ) - SA; (○) - DES; (□) - MES; (▲) - EtOH; (●) - H_2O; (+) - DEE; (▬ ▬) - activity based model; (▬) - mole fraction model. a) Run 48: T = 353K, w_{CAT} = 0.093, mole ratio EtOH/SA = 23.07:1. b) Run 51: T = 383 K, w_{CAT} = 0.092, mole ratio EtOH:SA = 23.07:1.

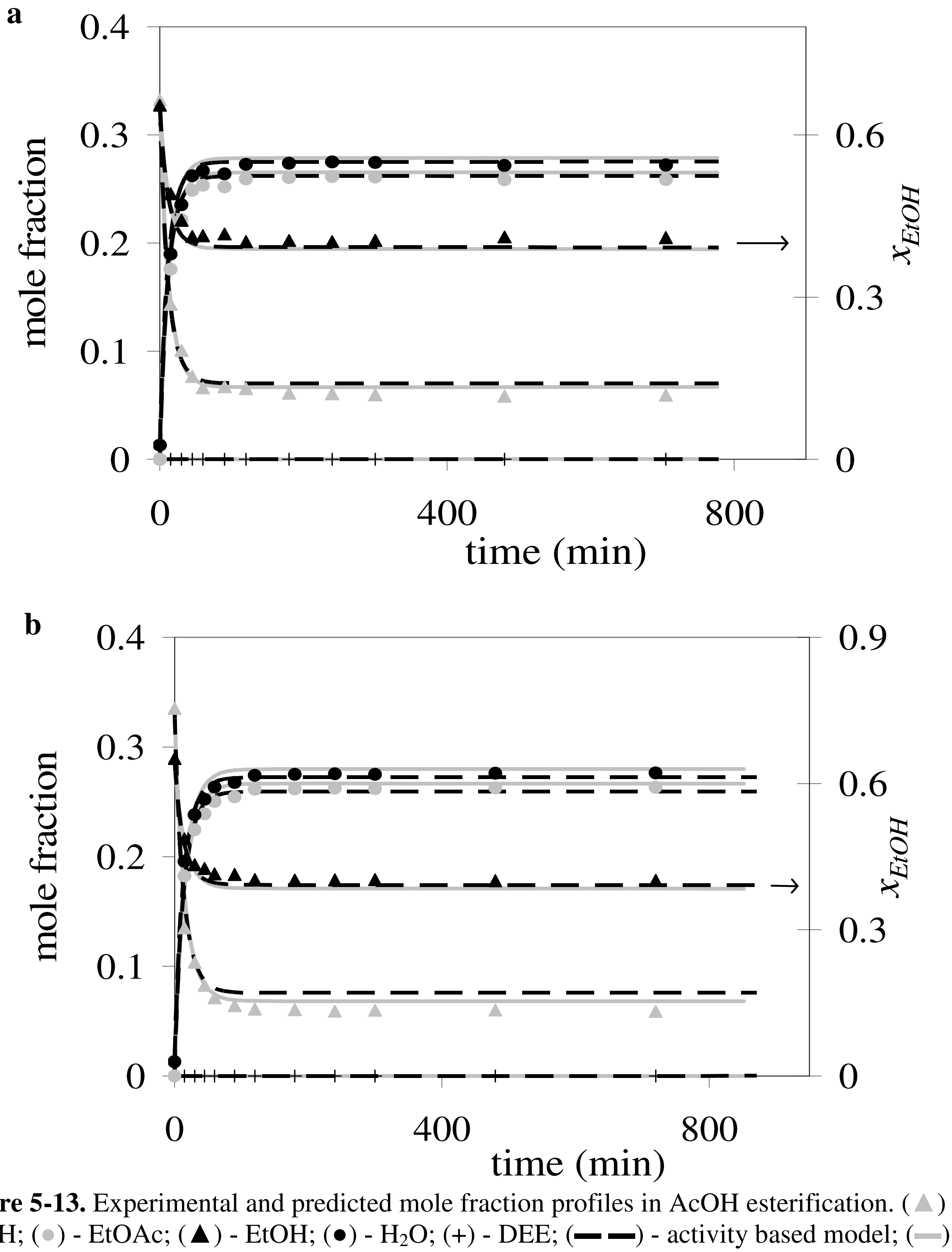

Figure 5-13. Experimental and predicted mole fraction profiles in AcOH esterification. (▲) - AcOH; (●) - EtOAc; (▲) - EtOH; (●) - H_2O; (+) - DEE; (— —) - activity based model; (—) - mole fraction model. a) Run 65: T = 373 K, w_{CAT} = 0.0199, mole ratio EtOH:AcOH = 1.97:1. b) Run 69: T = 353 K, w_{CAT} = 0.0408, mole ratio EtOH:AcOH = 1.94:1.

REFERENCES

5.6 REFERENCES

[1] C. Potera. Environ. Health Persp. 113, 12 (2005) A832-A835.

[2] M. Patel, M. Crank, V. Dornburg, B. Hermann, L. Roes, B. Hüsing, L. Overbeek, F. Terragni, E. Recchia. Medium and long-term opportunities and risks of the biotechnological production of bulk chemicals from renewable resources - The potential of white biotechnology. (The BREW project). Utrecht, Netherlands. 2006. [Online] Available: http://www.bio-economy.net/applications/files/Brew_project_ report.pdf [June, 2010].

[3] B. Hermann, M. Patel. Appl. Biochem. Biotechnol. 136 (2007) 361-388.

[4] J. B. McKinlay, C. Vieille, J. G. Zeikus. Appl. Microbiol. Biotechnol. 76 (2007) 727-740.

[5] A. Cukalovic, C. V. Stevens. Biofuels, Bioprod. Biorefin. 2, 6 (2008) 505-529.

[6] C. Delhomme, D. Weuster-Botz, F. E. Kühn. Green Chem. 11 (2009) 13-26.

[7] O. Wolf, M. Crank, M. Patel, F. Marscheider-Weidemann, J. Schleich, B. Hüsing, G. Angerer. Techno-economic feasibility of large-scale production of Bio-based polymers in Europe, European Science and Technology Observatory, EUR 22103 EN. (2005). [Online] Available: http://ftp.jrc.es/EURdoc/eur22103en.pdf [June, 2010].

[8] I. Bechthold, K. Bretz, S. Kabasci, R. Kopitzky, A. Springer. Chem. Eng. Technol. 31(2008) 647-654.

[9] J. G. Zeikus, M. K. Jain, P. Elankovan. Appl. Microbiol Biotechnol 51(1999) 545-552.

[10] L. Agarwal, J. Isar, R. Saxena. J. Biochem. Biophys. Methods 63 (2005) 24-32.

[11] P. Rogers, J. Chen, M. Zidwick. The prokaryotes. Chapter 3.1. Organic Acid and Solvent Production, Part I: Acetic, Lactic, Gluconic, Succinic and Polyhydroxyalkanoic Acids. (2006) 511-755.

[12] H. Song, S. Y. Lee. Enzime Microb. Tech. 39 (2006) 352-361.

[13] A. Orjuela, A. J. Yanez, Lira, C. T., Miller, D. J. (2009). Carboxylic Acid Recovery from Fermentation Solutions. US Patent Application filed Dec. 2009.

[14] C. Bianchi, Appl. Catal. B. 40, 2 (2003) 93-99.

[15] D. Sutton, G., Reed, G., Hiles. Process for the production of esters of mono-, di or polycarboxylic acids. WO patent 051885 A1, US patent application 0129565 A1. (2005, 2007).

[16] W. Zhao, X. Sun, Q. Wang, H. Ma, Y. Teng. Biomass. Bioenerg. 33, 1 (2009) 21-25.

[17] R. Bringué, M. Iborra, J. Tejero, J. F. Izquierdo, F. Cunill, C. Fité, V. J. Cruz. J. Catal. 244 (2006) 33–42.

[18] R. Bringué, J. Tejero, M. Iborra, J. F. Izquierdo, C. Fité, F. Cunill. Topics in Catal. 45, 1-4 (2007) 181-186.

[19] P. F. Siril, H. E. Cross, D. R. Brown. J. Mol. Catal. A. Chem. 279 (2008) 63-68.

[20] Rohm and Haas. Amberlyst 70 product data sheet. Philadelphia, USA. 2005.

[21] A. Kolah, N. Asthana, D. Vu, C. T. Lira, D. J. Miller. Ind. Eng. Chem. Res. 47, 15 (2008) 5313–5317.

[22] A. Darlington, W. Guenther. J. Chem. Eng. Data. 12, 4 (1967) 605-607.

[23] J. Gimenez, S. Cervera-March. Appl. Catal. 48, 2 (1989) 307-32.

[24] M. Mazzotti, B. Neri, D. Gelosa, A. Kruglov, M. Morbidelli. Ind. Eng. Chem. Res. 36, 1 (1997) 3–10.

[25] J. Helminen, M. Leppämäki, E. Paatero, P. Minkkinen. Chemometr. Intell. Lab. 44, 1-2 (1998) 341-352.

[26] G. Hangx, G. Kwant, H. Maessen, P. Markusse, I. Urseanu. Reaction Kinetics of the Esterification of Ethanol and Acetic Acid Towards Ethyl Acetate. Deliverable 22, Intelligent Column Internals for Reactive Separations (INTINT). Technical Report to the European Commission. (2001). [Online] Available: http://www.cpi.umist.ac.uk/intint/NonConf _Del/22.pdf. [June, 2010].

[27] Ş. Kirbaşlar, Z. Baykal, U. Dramur. Turk. J. Engin. Environ. Sci. 25 (2001) 569-577.

[28] N. Calvar, B. Gonzalez, A. Dominguez. Chem. Eng. Process. 46 (2007) 1317-1323.

[29] I. Lai, Y. Liu, C. Yu, M. Lee, H. Huang. Chem. Eng. Process. 47 (2008) 1831-1843.

[30] T. Dogu, E. Aydiny, N. Bozz, K. Murtezaoglu, G. Doguyy. Int. J. Chem. Reac. Eng. 1 A6 (2003) 1-10.

[31] P. B. Weisz, C. D. Prater. Advan. Catal. 6 (1954) 143-196.

[32] Renon, H., Prausnitz, J. M. AIChE J. 14 (1968) 135-144.

[33] Aspentech, Aspen Physical Property System, physical property models/methods, Burlington, 2007.

[34] Tang, Y., Huang, H., Chien, I. J. Chem. Eng. Japan. 36, 11 (2003) 1352-1366.

[35] A. Orjuela, A. J. Yanez, D. Vu, D. Bernard-Brunel, D. J. Miller, C. T. Lira. Fluid Phase Equilibr. 290, 1-2 (2010) 63-67.

[36] A. Orjuela, A. J. Yanez, P., Rossman, D. Vu, D. Bernard-Brunel, D. J. Miller, C. T. Lira. Fluid Phase Equilibr. 290, 1-2 (2010) 68-74.

[37] A. Orjuela, A. J. Yanez, J. Evans, D. J. Miller, C. T. Lira. Phase Equilibria in Binary Mixtures with Monoethyl Succinate. (2010) Manuscript in revision.

[38] A. Orjuela, A. J. Yanez, A. Lee, D. J. Miller, C. T. Lira. Solubility and Phase Equilibria for Mixtures with Succinic Acid. (2010) Manuscript in revision.

[39] J. R. Collin, D. Ramprasad. Methods, systems and catalysts for the hydration of olefins. European patent application EP 1479665 A1.

[40] T. Pöpken, L. Götze, and J. Gmehling. Ind. Eng. Chem. Res. 39, 7 (2000) 2601-2611.

[41] H.T.R. Teo, B. Saha. J. Catal. 228 (2004) 174-182.

[42] M. Villamañan, A. Allawl, H. Van Ness. J. Chem. Eng. Data 29 (1984) 431-435.

[43] J. M. Sørensen, W. Arlt. Liquid-Liquid Equilibrium Data Collection. Binary Systems. Ternary Systems. DECHEMA. Chemistry Data Series, Vol V, Part 1 and Part 2. 1980.

[44] J. Gmenhling, U. Onken, W. Arlt. Vapor-liquid Equilibrium Data Collection. Aldehydes and kethone ethers. DECHEMA. Chemistry Data Series, Vol I, Part 3+4. 1979.

[45] J. Gmenhling, U. Onken, W. Arlt. Vapor-liquid Equilibrium Data Collection. Organic Hydroxy Compounds: Alcohols. DECHEMA. Chemistry Data Series, Vol I, Part 2a. 1979.

[46] T. Letcher, J. Sewry, D. Naran. Fluid Phase Equilibr. 49 (1989) 187-193

PART 2: RECOVERY OF SUCCINIC ACID FROM FERMENATION BROTHS

6. A novel process for recovery of fermentation-derived succinic acid

6.1 Summary

A novel approach to recovering succinic acid from fermentation broth via acidification and esterification in ethanol is presented, based on solubility of sulfate and succinate salts in ethanol-water mixtures. Acid salts from fermentation are placed in ethanol along with a slight stoichiometric excess of sulfuric acid. Simultaneous acidification and esterification take place, with the inorganic sulfate salt formed precipitating out of the ethanol solution. The succinate recovered in present as a mixture of free succinic acid, monoethyl succinate, and diethyl succinate in ethanol, can be used as a suitable feedstock for further esterification via reactive distillation. Results are reported here for both model succinate salts and for actual fermentation broth mixtures. Recovery of succinate species in excess of 95% is obtained for both model and actual broths.

6.2 Introduction

Succinic acid (SA) produced by fermentation has been recognized as an attractive building block for many chemicals derivatives including monomers and solvents [1]. Prospective studies have estimated the potential market for SA as 270,000 metric tons per year, ten times higher than current manufactured, with a potential production price (0.55 – 1.10 US$/kg) that competes with maleic anhydride ($1.05 to 1.29 US/kg) [2-14]. Demonstration plants are currently under construction [15-16] to produce SA; life cycle assessment indicates a net fossil energy consumption of 30-40% less than the current petroleum-based route [17].

In producing organic acids by fermentation, 50% to 80% of processing costs are typically attributed to recovery and purification of the desired product. The primary challenges in organic acid recovery are low titer (g/liter) of the acid, the presence of byproducts including other carboxylic acids, and the requirement for pH control during fermentation that leads to the carboxylic acids being present in the salt form.

Table 6-1. Summary on patented processes for succinic acid recovery.

PROCESS	REMARKS	RECOVERY	Ref.
Acidification – crystallization	Selective crystallization by pH change	-	[19]
	pH controlled precipitation	-	[20]
	Selective precipitation from sodium sulfate	74 %	[21]
Salt precipitation – acidification	As calcium salt. Ion exchange, re-crystallization	-	[22, 23]
	Crystallization in methanol. Cracking of ammonium salt	78 %	[24]
	Salt is selectively precipitated adding ethanol	-	[25]
Solvent extraction	“wettable” organic solvents (ketones)	84 %	[26]
	Octanol in several cycles	80 %	[27]
	Olefinic co-solvents	-	[28]
Amine extraction with/without solvent	Under CO_2 atmosphere with alcohol as solvent	80 %	[29, 30]
	Tertiary amines with alcohol al solvent	-	[31]
	Water is removed with secondary amine	-	[32]
	Alcohol as solvent. Esters are formed	-	[33]
	Electrolytic membranes required	94 %	[34]
Ion exchange	Back extract with amine removed by stripping	87 %	[35]
	Anionic resin	-	[36]
	Strongly acidic cationic resin	-	[37]
	Anionic resin	-	[38]
	Cationic resins	-	[39]
Nanofiltration	Initial ion exchange of calcium required	-	[40]
	Electrodialysis required	-	[41]
	Initial crystallization under pH control required	-	[42]
Electro-dialysis, Membranes	Salt-splitting, Low recovery per pass	78 %	[43]
	Polishing with ion exchange. Non selective	79 %	[44]
Esterification with/without Reactive distillation	Esterification assisted with pervaporation	-	[45]
	Ammonium salt with ethanol. Amides formation	-	[46]
	Ammonium salt with ethanol. CO_2 as catalyst	-	[47]
	Ammonium salt with butanol. *P*-TSA as catalyst	96.5 %	[48]

In the early 1980's, a comprehensive review covered the major technologies and principles governing recovery of carboxylic acids from fermentative media using solvents, amines, phosphates, or their mixtures [18]. Since then, in addition to reports in the open literature, several patented processes for SA recovery have been developed (Table 6-1).

These methods can be classified as those that use direct precipitation (as salt or acid), extraction (solvents, amines), ion exchange, membranes, or esterification of the free acid followed by hydrolysis. In all cases, acidification of the salts is a key step in the recovery. From a chemical production viewpoint, succinate esters are more desirable than the free acid for derivatives such as tetrahydrofuran and 1-4 butanediol [49] as the maleic anhydride route already goes through the ester. Thus, succinate recovery as esters directly from the fermentation broth would be of economic interest.

6.3 Description of Process

The process concept to recover SA from fermentation broth involves direct esterification of the succinate salts in ethanol (EtOH). To carry out the process, the fermentation broth must be treated as usual by centrifugation to remove cell biomass and by activated carbon addition to remove impurities and color. Water is then removed from the clean broth until the succinate salts are present as wet solids. Then the wet salts are placed in ethanol along with sulfuric acid.

The chemistry of the recovery process is presented for sodium salts (sodium succinate – Na_2Succ) in Eq. (6-1)–(6-5). The solid succinic salts react with H_2SO_4 to form free succinic acid and the corresponding sulfate salt. Unreacted or excess H_2SO_4 acts as a catalyst for esterification of the dissolved free acid with EtOH, forming a mixture of mono- and di-ethyl succinates (MES and DES) along with the free acid. The sodium sulfate formed is insoluble in ethanol and thus precipitates, binding water as available because of its propensity to form hydrates. These reactions occur simultaneously during acidification at rates and extents that depend on temperature, H_2SO_4 concentration, and time. Once acidification is complete, the succinate species dissolved in ethanol are subject to further esterification via reactive distillation to form the desired product, diethyl succinate.

$$\mathrm{Na_2Succ}\ (s) + \mathrm{H_2SO_4}\ (l) \rightarrow \mathrm{SA}\ (sol) + \mathrm{Na_2SO_4}\ (s) \tag{6-1}$$

$$\mathrm{SA}\ (sol) + \mathrm{EtOH}\ (l) \leftrightarrow \mathrm{MES}\ (l) + \mathrm{H_2O}\ (l) \tag{6-2}$$

$$\mathrm{MES}\ (l) + \mathrm{EtOH}\ (l) \leftrightarrow \mathrm{DES}\ (l) + \mathrm{H_2O}\ (l) \tag{6-3}$$

$$\mathrm{Na_2SO_4}\ (s) + 10\ \mathrm{H_2O}\ (l) \rightarrow \mathrm{Na_2SO_4}{\bullet}10\ \mathrm{H_2O}\ (s) \tag{6-4}$$

$$\mathrm{Na_2SO_4}\ (s) + \mathrm{H_2SO_4}\ (l) \leftrightarrow \mathrm{NaHSO_4}\ (s) + \mathrm{H_2O}\ (l) \tag{6-5}$$

A more detailed description of this process with different salts has been presented by the authors in a parallel work [50].

6.4 Material and methods

6.4.1 Materials

Succinic acid (>99.5 %, Sigma-Aldrich), acetic acid (AcOH, 99.9%, Aristar), diethyl succinate (DES, 99.92%, Sigma-Aldrich), monoethyl succinate (MES, 89.3%, Sigma-Aldrich), ethyl acetate (EtOAc, HPLC grade, J. T. Baker), ethanol (200 proof, Decon Labs), water (HPLC grade, J.T. Baker), anhydrous sodium succinate (Na_2Succ, ≥ 98 %, SAFC), sodium succinate hexahydrate ($Na_2Succ•6H_2O$ ≥ 99 %, Fluka), calcium succinate monohydrate ($CaSucc•H_2O$ ≥ 99 %, GFS), sodium acetate (NaOAc, ≥ 99.6 %, J.T. Baker), sulfuric acid (H_2SO_4, 98%, EMD), *n*-butanol (99.9%, Mallinckrodt), and acetonitrile (HPLC grade, EMD) were used without further purification for experiments and calibrations. Species purity was confirmed by gas chromatography; no impurities other than small amounts of water were detected in appreciable concentrations. Hydranal-coulomat E solution (Riedel-de Haën) was used in Karl-Fisher analysis for water measurement.

6.4.2 Experimental procedures

6.4.2.1 Solubility measurements

The solubility of sodium succinate and sodium acetate in EtOH-H_2O mixtures was determined by placing measured quantities of the salt into solution within glass vials (10 cm^3) stirred with a magnetic stir bar. The total mass placed in each vial was about 10g. These vials were placed in an isothermal bath equipped with a circulator pump and temperature control (Isotemp immersion circulator 730, Fisher Scientific, ± 0.1 K). Temperature was measured with an ASTM certified glass thermometer (model 64 C, ± 0.1 K).

To first obtain the coarse range of solubility (+/- 5 w %) for a specific EtOH- H_2O solution composition, 10 vials containing the same amount of solution were charged with different amounts of Na_2Succ near the expected solubility limit. After equilibration at the desired temperature under agitation for 12 h, the solubility range was obtained by visual observation of remaining solids and total dissolution in two consecutive (by salt concentration) vials. After this, the experiment was repeated as above using 10 vials but with initial masses of salt in between upper and lower solubility limits as determined in the coarse measurement. After equilibration for 12 h, the solubility value was obtained as before by visual inspection with an uncertainty of ± 0.5 % w/w. This experimental approach avoids ethanol or water vaporization if the vials are opened for sequential addition of solids. It also avoids crystallization of solids during sampling. This methodology was repeated for different EtOH-H_2O compositions, and was also used to evaluate the solubility of sodium acetate (NaOAc).

Because of experimental uncertainty, sodium salt content in solutions containing >90 wt% EtOH was measured by sodium detection using ICP-AES (Simultaneous sequential inductively coupled plasma - atomic emission spectrometer, Thermo-Jarrel-Ash-Polyscan-61E) with vacuum spectrometers and Ar-purged optical paths. Yttrium was used as an internal standard in 2% HNO_3.

6.4.2.2 Conditioning of fermentation products

Two fermentation products, consisting of dilute succinate salt solutions, were obtained from independent sources; the two fermentation processes involved different microorganisms, nutrient blends, and operating conditions in the fermenter. One broth was contained succinic acid in the form of the sodium salt, the other as magnesium succinate. The raw broth was filtered to remove biomass and treated with activated carbon to remove nutrients and color bodies. The liquid solution was then concentrated in a rotary evaporator, followed by drying under vacuum at 343 K to a constant weight. The dried solids were scraped out of the evaporator, ground and stored in sealed containers at 278 K. A sample of each dry solid was dissolved in water for analysis.

6.4.2.3 Succinate recovery experiments

Simultaneous acidification and esterification of Na_2Succ, $Na_2Succ{\bullet}6H_2O$, $CaSucc{\bullet}H_2O$ and NaOAc was conducted in EtOH using different molar ratios of H_2SO_4 to the corresponding salt. Tracking the reaction using aliquot samples does not provide the degree of conversion because of the interchange of species between liquid and solid phases. Further, the mass of each phase changes during the reaction, and the degree of hydration of the solid phase may change during conversion. To overcome these challenges, analysis was performed using the entire contents of reaction vials. A set of stirred test tubes were identically loaded with reagents and placed in an isothermal bath. Tubes were removed from the bath at specified times and their entire contents analyzed, thus mimicking the operation of a multiphase batch reactor over time.

To prepare each tube, a solution of H_2SO_4 in EtOH was stored in a flask maintained in an ice bath to avoid heating and evaporation of the alcohol during mixing. Fifty-ml test tubes were charged with a measured amount of this solution (~ 30 cm^3), and succinate salt was added to each tube at a measured ratio with respect to H_2SO_4. The quantity of succinate salt was set such that the amount of SA produced was able to dissolve in EtOH at the reaction temperature. Each tube was taken out of the bath at a specified time and quenched; after centrifugation at 7000 rpm for 5 minutes, the supernatant liquid was removed, weighed and collected for analysis. The solids remaining were washed in the same tube with anhydrous ethanol to remove remaining soluble succinic species, and were then centrifuged again to collect, weigh, and analyze the supernatant liquid. Finally, the remaining solids were dissolved in water for further analysis. In the case of calcium succinate, because of its limited solubility in water, the solids were mixed with an aqueous solution of H_2SO_4 to dissolve any succinate salt remaining, and the liquid phase was analyzed. Total recovery is calculated on a molar basis, taking into account initial salt loading.

6.4.3 Analysis

Samples were analyzed by both by gas and liquid chromatography. Reaction samples were diluted 50-fold in water and analyzed via HPLC with a system containing a Waters® 717 autosampler, a Waters® 410 refractive index detector, and a Perkin-Elmer LC90 UV detector. A 100 mm x 7.6 mm fast acid analysis column (BioRad®) at 298 K along with a mobile phase of 5 mM H_2SO_4 in water flowing at 1.0 cm^3/min was used for the separation.

Volatile component concentrations were measured in a gas chromatograph (HP 5890 series II) equipped with thermal conductivity and flame ionization detectors. Reaction samples were diluted 20-fold into acetonitrile containing 5.0 wt% *n*-butanol as an internal standard. A 30 m Alltech Aqua WAX-DA column (0.53 mm i.d., 1.20 μm film thickness) was used with the following temperature program: initial temperature 313 K for 3 min; ramp at 20 K/min to 523 K, and hold at 523 K for 0.5 min. The GC injection port was maintained at 543 K in a splitless mode, and detector temperatures were 523 K. Helium was used as carrier gas (15 cm^3/min) and liquid injection volumes of 0.5 μL were used.

For both HPLC and GC analyses, standard samples of known composition in the range of interest were injected in triplicate to obtain calibration curves repeatable to within ±0.5% by mass. Karl-Fisher analysis (Aquacount coulometric titrator AQ-2100) was used to measure water content in reagents and samples.

6.5 Results and discussion

6.5.1 Salts solubility

Experimental solubility data of Na_2Succ in EtOH-H_2O mixtures obtained at different temperatures are shown in Figure 6-1. The solubility of Na_2SO_4 in EtOH-H_2O from the literature [51] is also presented. For Na_2Succ at 60 °C, phase splitting was observed in solutions containing 20 to 60 wt% EtOH. This effect is characteristic of the salting out observed in similar water – organic mixtures, and was previously reported for potassium succinate [52].

Data in Figure 6-1 indicate that solubility of salts in EtOH is negligible up to water concentrations of 20 wt%. This is advantageous for the recovery process described herein, because EtOH containing some water (e.g. azeotropic EtOH) may be used and fermentation solids do not have to be completely dried. In fact, recovery can be enhanced in the presence of small quantities of water, because solubility of SA is higher in mixtures of EtOH-H_2O than in EtOH or water alone [53, 54]. Sodium acetate is more soluble than sodium succinate, suggesting that acidification of NaOAc in EtOH can be enhanced by dissolution of solids in the reacting media, mainly at high temperatures.

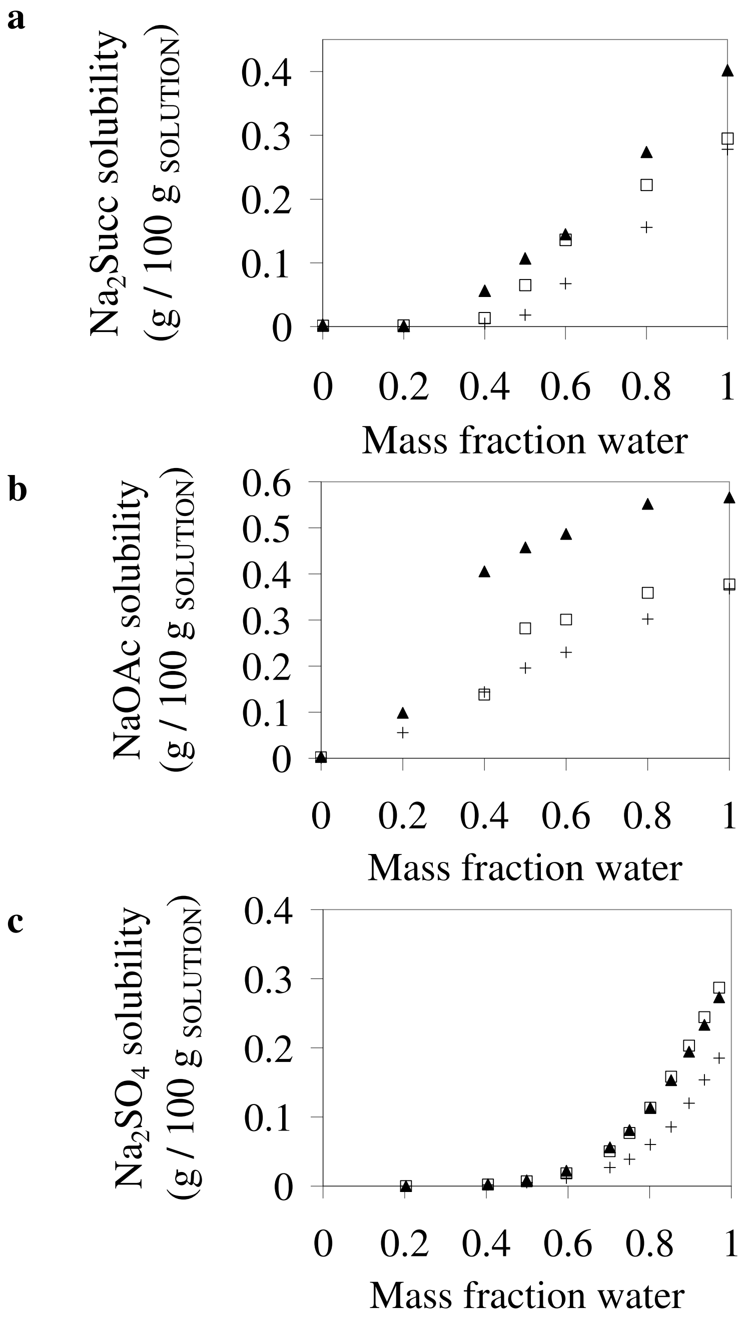

Solubility (g/100g solution) at 298 K

	EtOH	**H_2O**
Na_2SO_4	< 0.095	21.5
Na_2Succ	< 0.08	27.8
NaOAc	< 0.008	36.8

Figure 6-1. Experimental and reported solubilities of sodium salts in ethanol/water mixtures at different temperatures. (+) - 298 K, (□) - 313 K, (▲) - 333 K. a) Na_2Succ, this work; b) NaOAc, this work; c) Na_2SO_4, reported by Vener [51].

6.5.2 Demonstration of recovery method

Early exploratory tests gave succinate recoveries greater than 80% [50]. The proof-of-concept recovery experiments described here were performed with pure sodium and calcium succinate salts and with mixtures of sodium succinate and sodium acetate. The conditions and material quantities used for these experiments are presented in Table 6-2. Because it is more stable, the hydrated form of Na_2Succ ($Na_2Succ \cdot 6H_2O$) was used instead of the anhydrous salt because it is expected to be the species resulting from precipitation from the fermentation broth. The quantities of H_2SO_4 added were equal to or in excess of the amount required to acidify the organic acid salts.

Table 6-2. Experimental conditions for acidification tests.

Run	Time (h)	Salt	Succinate salt (g)	Acetate salt (g)	EtOH (g)	H_2SO_4 (g)	$H^+:Na^+$ ($2H^+:Ca^{+2}$) Ratio	T (K)
1	6	$Na_2Succ \cdot 6H_2O$	4.13	-	23.7	1.50	Stoich.	303
2	6	$Na_2Succ \cdot 6H_2O$	4.13	-	23.73	1.8	1.2	303
3	6	$Na_2Succ \cdot 6H_2O$	4.13	-	23.74	2.1	1.4	303
4	6	$CaSucc \cdot H_2O$	2.66	-	23.77	1.49	Stoich.	303
5	24	$Na_2Succ \cdot 6H_2O$ + NaOAc	2.42	0.15	20.42	1.16	1.2	323
6	2	$Na_2Succ \cdot 6H_2O$	2.43	-	20.21‡	1.03	1.16	323
7	2	$Na_2Succ \cdot 6H_2O$	2.42	-	20.60	1.44	1.63	323
8	24	$CaSucc \cdot H_2O$	2.66	-	23.73	1.81	1.21	303

‡ Ethanol 95% w/w

Results of proof-of-concept experiments are presented in Table 6-3; succinate species profiles over time are shown in Figures 6-2 and 6-3. Results in Table 6-3 illustrate that recovery of SA by direct esterification of sodium salts with EtOH is possible even at ambient temperatures. Recoveries are good in most experiments, and in some runs more than 95% of the initial succinate salts are extracted into ethanol after 3 hr. Even with the uncertainty in the mass balances, these recoveries are higher than those reported using other methods in the patent or open literature, indicating the attractiveness of the recovery approach.

Table 6-3. Product yields during acidification reactions.

Run	Molar recovery in liquid phase mol %						Succinate remaining in solid phase mol %	Total succinate recovery mol %
	Acetate		Succinate					
	AcOH	EtOAc	SA	MES	DES	TOTAL		
1	-	-	78.09	12.31	0.91	91.3	13.67	105.0
2	-	-	31.43	50.68	14.23	96.4	1.36	97.7
3	-	-	4.79	40.93	47.26	93.0	0.43	93.4
4	-	-	29.70	39.64	23.37	92.7	7.62	100.3
5	38.35.	52.83	3.62	27.91	58.45	90.0	-	90.0
6	-	-	74.82	9.47	0.20	84.5	21.85	106.4
7	-	-	48.28	31.27	18.50	98.1	7.82	105.9
8	-	-	0.60	11.92	88.86	101.4	1.29	102.7

Because multiple phases are present in recovery experiments and because quantities of succinate species were measured by three independent methods (GC, HPLC, Karl-Fischer) as described in Section 3.2.4, some scatter in species profiles and uncertainty (±5%) in closure of the overall mass balances is observed. Differences in agitation patterns were noticed in every set of reactors studied under identical conditions, contributing to the scatter in species profiles with time. Overall, however, the quality of the results is reasonable and clearly demonstrates the viability of the recovery method.

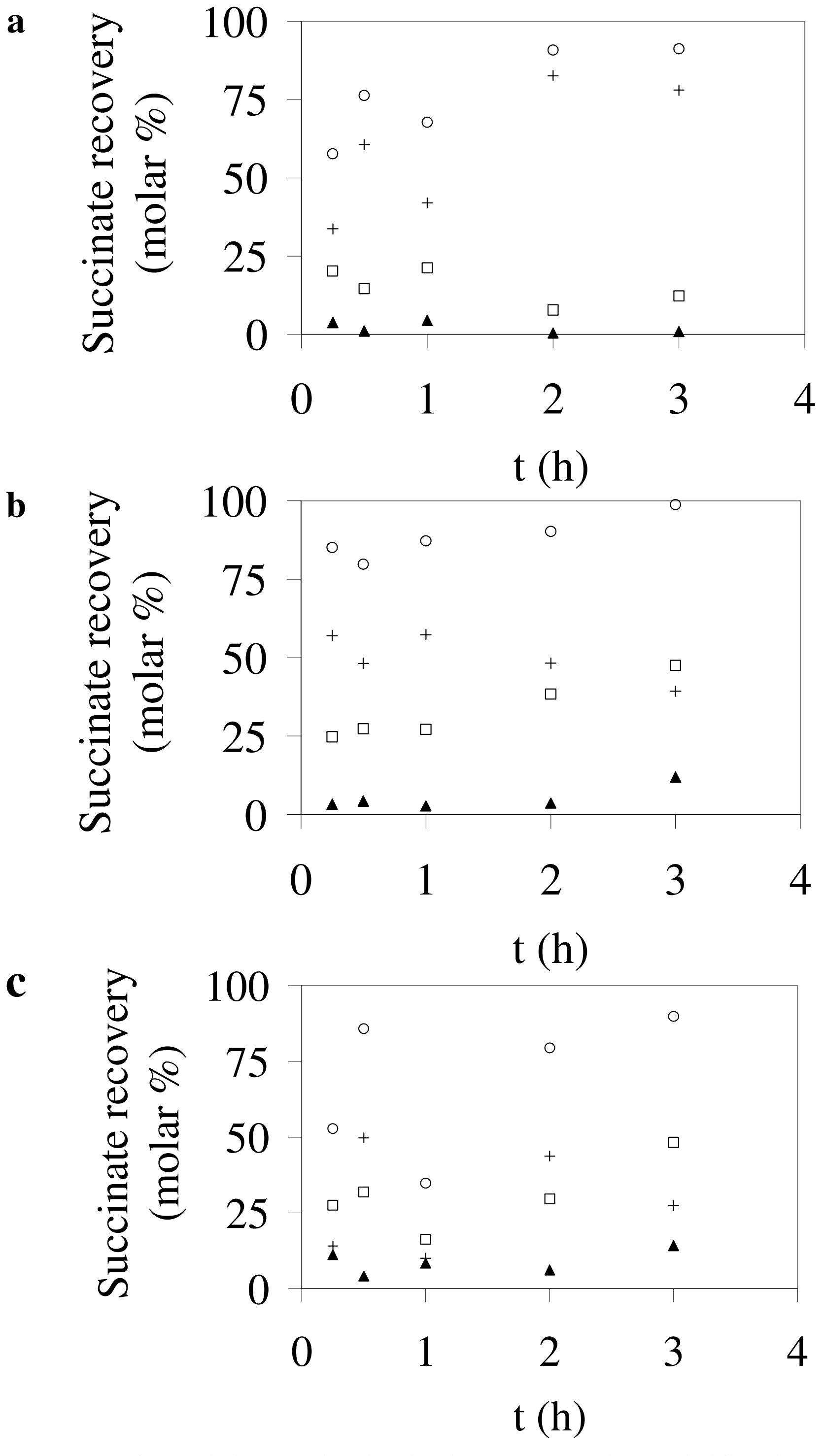

Figure 6-2. Recovery of succinic species in liquid phase during acidification of $Na_2Succ \bullet 6H_2O$ in EtOH at 303 K. (+) - SA, (□) - MES, (▲) - DES, (○) - Total succinate species. a) Stoichiometric H_2SO_4 (Run 1); b) 20 % molar excess of H_2SO_4 (Run 2); c) 40 % molar excess of H_2SO_4 (Run 3).

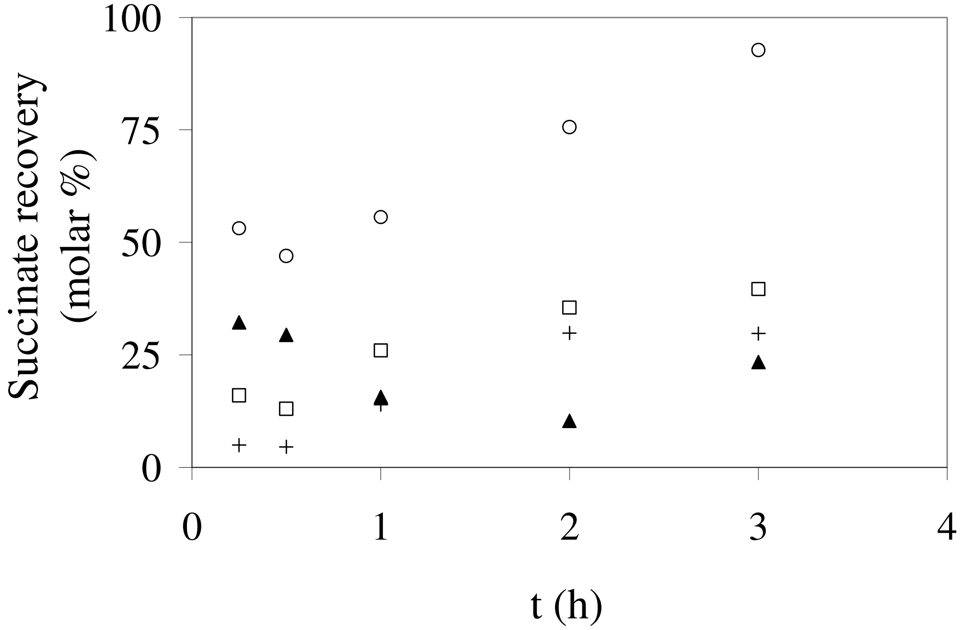

Figure 6-3. Recovery of succinic species in liquid phase during acidification of CaSucc•H_2O in EtOH at 303 K C in Run 4. Stoichiometric H_2SO_4. (+) - SA, (□) - MES, (▲) - DES, (○) - Total succinate species.

The distribution of succinate species changes with the quantity of H_2SO_4 used; at higher excesses of sulfuric acid, MES and DES predominate over free SA. This result is observed for both sodium and calcium salts. In Run 5, the simultaneous recovery of acetate species along with succinates is achieved, indicating that the process can produce a mixture of esters that can be more easily separated (i.e. by distillation) than the original acids mixture.

A qualitative indicator of the extent of recovery is the observed change in the nature of the solid phase during reaction. Initially, crystalline succinate salts were suspended in the EtOH solution; after a few minutes of reaction, a white-powdery slurry started to form. After centrifugation two clearly different solid layers were observed.

Because the reaction occurs between a solid and a liquid phase, good mass transfer is important for a rapid recovery process. This is perhaps evidenced by the initial rapid increase of succinate species in the ethanol solution during the first 15 minutes of reaction, during which succinate salt is quickly acidified and Na_2SO_4 forms. The solid sulfate salt formed must separate from the succinate salt surface to some extent (in accordance with the observation of a second solid type), but at some point it is likely that the sulfate salt layer encases the succinate crystals and slows acidification. This results in the need for 3 hr of reaction time to achieve the highest yields of succinate in ethanol (Figure 6-2).

6.5.3 Succinate recovery from fermentation products

After demonstration of the process concept using pure succinate salts, a set of solids obtained from fermentation were subjected to the acidification/esterification process in EtOH. Characteristics of these solids are listed in Table 6-4. Concentration of salts in the broth is reported as the equivalent SA or AcOH mass fractions in aqueous solution.

Because of the high glucose content in batch A, a viscous, sticky solid was obtained after drying. The hygroscopic nature of glucose made water removal difficult by evaporation. For this reason, dispersion and dissolution of particles within the reactive media was poor. Other batches in Table 6-4 were dried without difficulties and particle size reduction was conducted until fine brownish dusts were obtained.

Solids from batch E corresponded to crude SA obtained in the acid form because acidification was carried out in the aqueous broth before evaporation. In this case the amount of H_2SO_4 added was the required to catalyze esterification reaction (1 wt % of total solution). Acidification conditions for fermentation solids are listed in Table 6-5 and results are summarized in Table 6-6.

Table 6-4. Characterization of culture broth solids.

	Batch code				
	A	B	C	D	E
Salt form	Na^+	Mg^{+2}	Mg^{+2}	Mg^{+2}	H^+
	Concentration wt %				
SA	24.8	38	39.6	38.4	52.6
AcOH	2.5	-	-	-	-
Lactic acid	-	5.2	5.5	5.8	0.87
Other acids	-	~ 3.0	~ 3.8	~ 3.8	~ 1
Glucose	29	0.4	0.36	0.42	-

Table 6-5. Experimental conditions for acidification-esterification experiments on solids obtained from fermentation.

Run	Time (h)	Batch code	Solids (g)	EtOH (g)	H_2SO_4 (g)	Mole ratio H_2SO_4 : SA	T (K)
9	24	A	5	19.8	1.3	1.1	303
10	6	A	3	19.5	1.8	1.3	303
11	2	A	3	19.7	0.9	1.3	323
12	8	B	2.04	6.7	0.7	1.04	303
13	5	B	2.01	7.4	0.9	1.43	303
14	5	B	2.01	7.4	0.9	1.44	333
15	8	C	2.04	6.7	0.7	0.98	303
16	5	C	2.03	7.8	1.0	1.4	303
17	5	C	2.02	7.7	1.0	1.41	333
18	8	D	2.03	6.8	0.8	0.98	303
19	5	D	1.99	8.3	1.0	1.57	303
20	5	D	2.01	8.3	1.0	1.57	333
21	24	D	399.8	1580	205	1.5	353
22	24	E	199.96	946.8	12.0	0.13	353

Table 6-6. Results of acidification-esterification of solids obtained from fermentation.

Run	Molar recovery in liquid phase (mol %)						
	Acetate			Succinate			
	AcOH	EtOAc	TOTAL	SA	MES	DES	TOTAL
9	53.1	38.1	91.2	61.7	15.1	0	76.8
10	15	31.6	46.6	7.3	14.6	12.6	34.5
11	20.6	36.7	57.3	20.0	22.8	9.4	52.2
12	-	-	-	43.2	10.2	6.2	59.8
13	-	-	-	58.4	8.6	1.3	68.3
14	-	-	-	73.4	5.2	3.9	82.6
15	-	-	-	46	2.9	3.7	52.6
16	-	-	-	57.1	18.6	3.4	79
17	-	-	-	61.2	2.4	3.2	66.8
18	-	-	-	51.8	6.1	4.4	62.4
19	-	-	-	57.3	9.3	1.3	67.9
20	-	-	-	78.8	6.1	5.2	90.1
21	-	-	-	13.6	54.1	33.3	101
22	-	-	-	1.3	12.1	73.4	86.9

Experiments 21 and 22 were carried out in 2L batch reactors to evaluate the process in bench scale. In these runs reaction was performed under total reflux to avoid EtOH losses.

Even with excess of H_2SO_4, recovery of succinate and acetate species during acidification of solid in Batch A was lower than that obtained with pure salts. After 2 h, around 40% recovery of succinate species was achieved compared with 80% in pure salts. However, after 24 h, comparable results with those obtained for pure solids are observed. This indicates that transport limitations are playing an important role in the process due to difficulties observed in dissolution of solids in batch A. In Figure 6-4 evolution of the recovery process in run 9 is presented. Recovery on Runs 12 to 22 was generally lower compared with pure salts. In these experiments sulfuric acid loading was calculated only with respect to SA, therefore when stoichiometric ratio was used molar loading was about 86 % of the required to acidify all the acid species.

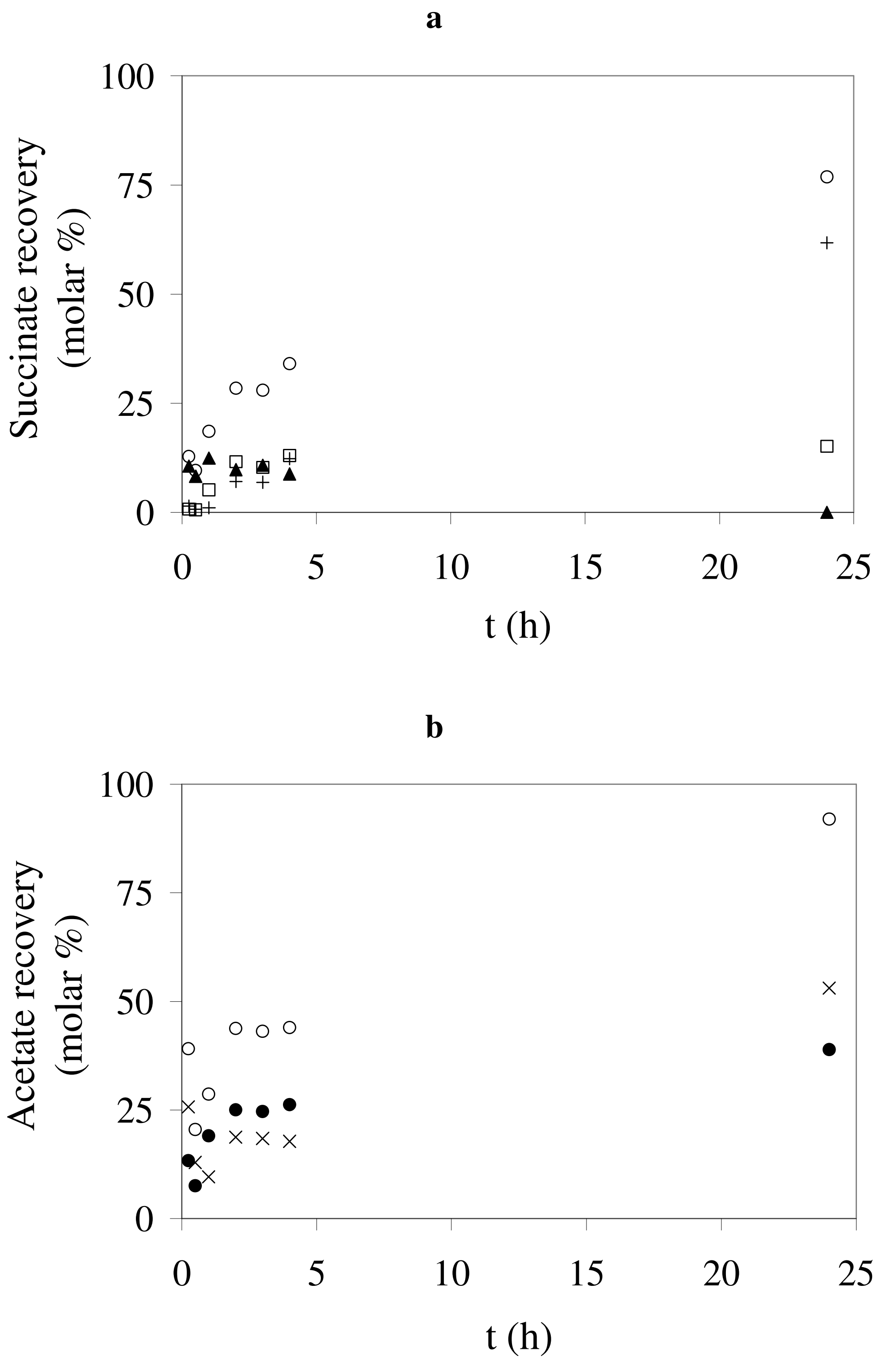

Figure 6-4. Recovery of succinate and acetate species in liquid phase during acidification of solids from fermentation broth W-1 in EtOH at 303.15 K C and Stoichiometric H_2SO_4 (run 9). (+) - SA, (□) - MES, (▲) - DES, (X) - AcOH, (●) – EtOAc, (○) - Total species. a) Succinate species; b) acetate species.

This might explain the low recovery in experiments 12, 15 and 18. Remarkably, succinate esters were also produced during the process, confirming that H_2SO_4 acts as a catalyst before being consumed in salt acidification. Increasing H_2SO_4 loading enhances recovery as observed in experiments 13, 16 and 19 but temperature is still low to promote esterification. Operating at higher temperatures (333 and 383 K) similar recoveries to those obtained with pure salts were achieved as demonstrated in runs 20 and 21.

In bench scale experiments with succinate salts and with crude SA (runs 21 y 22) high recovery and high conversion to MES and DES were obtained verifying feasibility of the process in a large scale. Evolution of recovery in bench scale experiments is presented Figure 6-5.

6.5.4 Process for succinate ester production direct from fermentation

As observed, acidification in ethanol is a feasible alternative to recover succinic acid as its ester from fermentative broths, thus by-passing the need for purification of the free acid. Figure 6-6 describes a process concept for a complete recovery and separation process to produce diethyl succinate from fermentation product.

Conventional conditioning of fermentation broth to remove biomass and impurities is followed by evaporation and solids drying using available technologies. After acidification in ethanol, esterification of the succinate species in ethanol to diethyl succinate may be driven to completion using reactive distillation [55]. If the fermentation process is engineered in such a way that succinate salt precipitate along the process (for example as calcium salt), then solid salts can be removed by filtration out of the broth and only drying is required before acidification; therefore evaporation costs might be reduced.

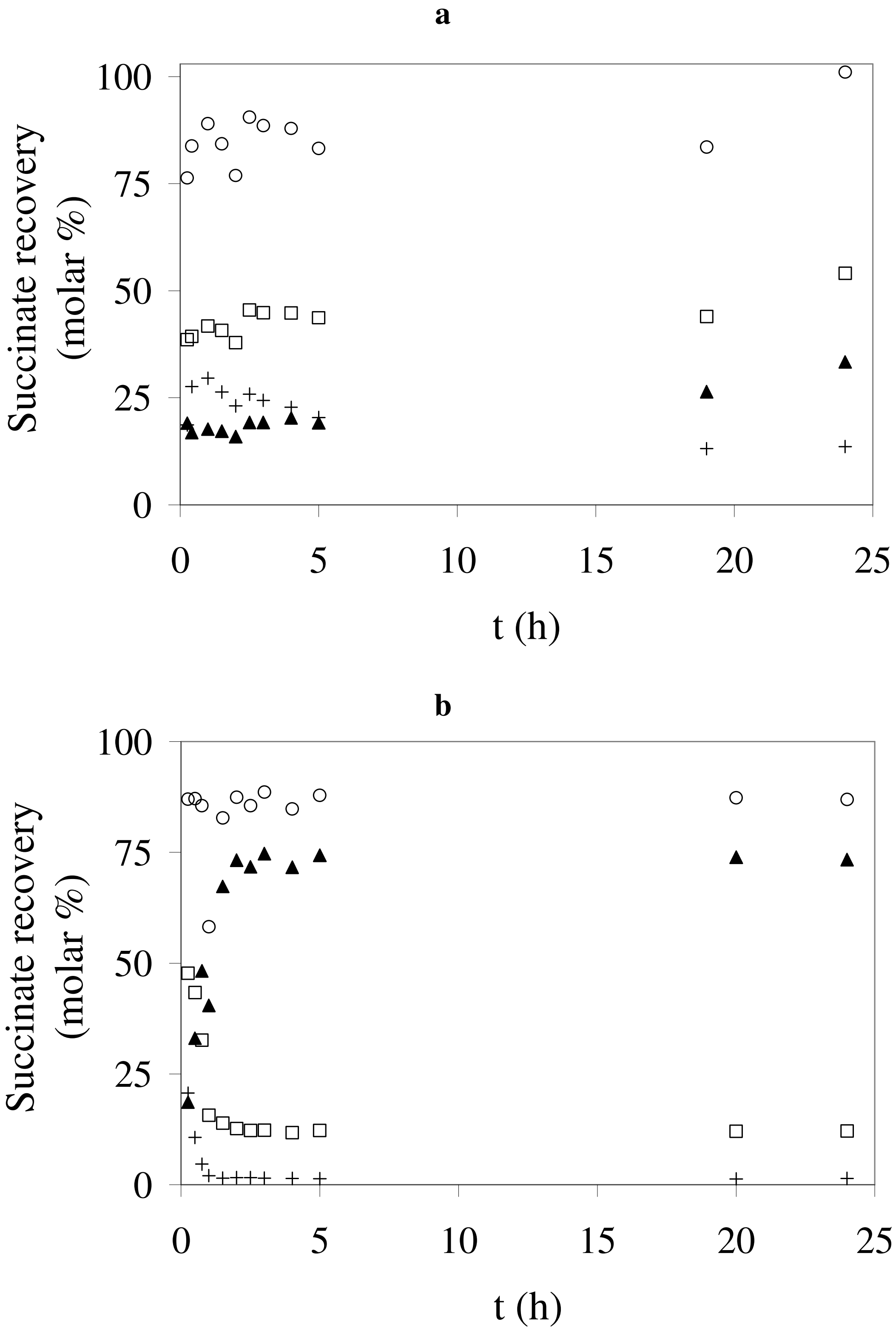

Figure 6-5. Recovery of succinate species in liquid phase during acidification of solids from fermentation at bench scale. (+) - SA, (□) - MES, (▲) - DES, (○) - Total succinate species. a) run 21; b) run 22.

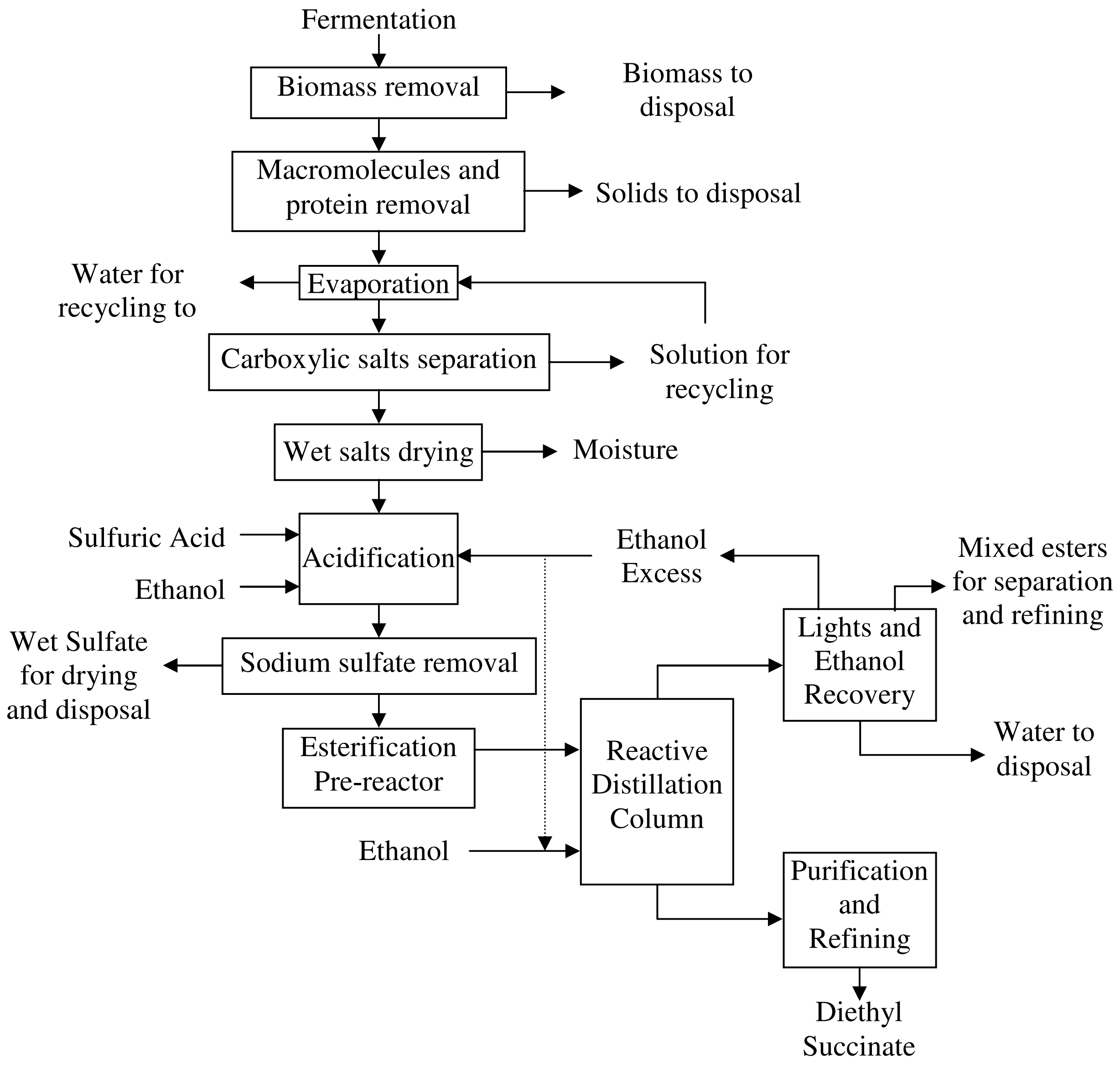

Figure 6-6. Proposed recovery process for succinic acid form fermentation broth by esterification with ethanol.

In the processing approach developed here, sulfate salts are generated as byproducts. Some sulfates have extensive use as fertilizers or intermediates in the chemical industry (i. e. magnesium, ammonium), so an appropriate choice of base for neutralization during fermentation can lead to a valuable byproduct.

6.6 Conclusions

The limited solubility of succinate and sulfate salts in ethanol solutions containing less than 20% water forms the basis for the recovery of succinate esters from the salts formed in fermentation. Solid succinate salts were acidified in ethanol using H_2SO_4 under different conditions, and recoveries exceeding 95% were obtained using pure salts as model fermentation products. Solid sulfates formed were easily removed by filtration or centrifugation. The succinate species formed in ethanol included both esters and free acid, and other acids present in the fermentation product were recovered as well. Using solids obtained from actual fermentation media, recovery around 80% was obtained under different conditions. Recovery in ethanol is easily integrated into an overall process to recover succinic acid as its diethyl ester directly from the succinate salts formed in fermentation.

REFERENCES

6.7 REFERENCES

[1] R. Landucci, B. Goodman, C. Wyman. Appl. Biochem. Biotech. 45/46 (1994) 677-698.

[2] J. Zeikus, M. Jain, P. Elankovan. Appl. Microbiol Biotechnol. 51(1999) 545-552.

[3] T. Werpy, G. Petersen. Top Value Added Chemicals from Biomass. Volume I—Results of Screening for Potential Candidates from Sugars and Synthesis Gas. PNNL-NREL. (2004). [Online]. Available: http://www1.eere.energy.gov/biomass/pdfs /35523.pdf [2009, Oct 21].

[4] Th. Willke, K. Vorlop. Appl. Microbiol. Biotechnol. 66 (2004) 131-142.

[5] L. R. Lynd, C. Wyman, M. Laser, D. Johnson, R. Landucci. Strategic biorefinary analysis: analysis of biorefinaries. NREL/SR-510-35578. (2005) [Online]. Available: http://www.nrel.gov/docs/fy06osti/35578.pdf [Oct, 2009].

[6] C. Potera. Environ. Health Persp. 113, 12 (2005) A832-A835.

[7] O. Wolf, M. Crank, M. Patel, F Marscheider-Weidemann, J. Schleich, B. Hüsing, G. Angerer. Techno-economic feasibility of large-scale production of Bio-based polymers in Europe, European Science and Technology Observatory, EUR 22103 EN. (2005).

[8] B. Hermann, M. Patel. Appl. Biochem. Biotechnol. 136 (2007) 361-388.

[9] B. Kamm, M. Kamm. Advances in biochemical engineering and biotechnology. White biotechnology, ed. R. Ulber and D. Sell, Springer, Heildelberg, vol 105, ch. 4, 175-203. (2007).

[10] J. B. McKinlay, C. Vieille, J. G. Zeikus. Appl. Microbiol Biotechnol. 76 (2007) 727-740.

[11] I. Bechthold, K. Bretz, S. Kabasci, R. Kopitzky, A. Springer. Chem. Eng. Technol. 31, 5 (2008) 647-654.

[12] A. Cukalovic, C. V. Stevens. Biofuels, Bioprod. Bioref. 2 (2008) 505-529.

[13] C. Delhomme, D. Weuster-Botz, F. E. Kühn. Green Chem. 11 (2009) 13-26.

[14] M. Sauer D.Porro, D. Mattanovich, P. Branduardi. 26, 2 (2008) 100-108.

[15] J. Elbert. The quest to commercialize biobased succinic acid. Biomass magazine. (2007). [Online]. Available: http://www.biomassmagazine.com/article.jsp? article_id=1228 [Sept, 2010].

[16] D. Ruth. Bio-based succinic acid bring 'green' chemicals closer to the market. Medical news today. (2008) [Online]. Available: http://www.medicalnewstoday.com /articles/133890.php [Sept, 2010].

[17] H. Kidwell. Bio-succinic acid to go commercial. In-pharma technologist. (2008). [Online]. Available: http://www.in-pharmatechnologist.com/Materials-Formulation/Bio-succinic-acid-to-go-commercial [Sept, 2010].

[18] A. S. Kertes, C. J. King. Biotechnol Bioeng. 28 (1986) 269-282.

[19] N. A. Collins, M. R. Shelton, G. W. Tindall, S. T. Perri R. S. O'Meadhra, C. W. Sink, B. K. Arumugam, J. C. Hubbs. Process for the recovery of organic acids from aqueous solutions. US Patent 6670505 B1. (2003).

[20] W. H. Hong, S. Y. Lee, Y. G. Hong, H. J. Won, S. Yue, H. H. Song, E. J. Lee, Crystallization of succinic acid from filtered fermentation broth. Korean patent application KR2007-134710. (2007).

[21] I. Fujita, K. Wada. A process for producing succinic acid. World patent application. WO 2008/010373 A1. (2008).

[22] R. Datta, Process for the production of succinic acid by anaerobic fermentation. US Patent 5143833. (1992).

[23] R. Datta, D. Glassner, M. Jain, J. Vick, Fermentation and purification process for succinic acid. US Patent 5168055. (1992).

[24] S. Yedur, K. Berglund, D. Dunuwila. Succinic acid production and purification. US Patent 6265190 B1. (2001).

[25] S. Yoshito, W. Minato, H. C. Moon, S. Praneetrattananon. Method for producing succinic acid form raw garbage and method for separating and purifying the same. Japanese patent. JP2006296306. (2006).

[26] C. J. King, J. Starr. Recovery of carboxylic acids from water by precipitation from organic solutions. US Patent 5104492. (1992).

[27] G. Vice, M. Staley, L. Rebrovic, W. Kozak. Process for recovering carboxylic acids from fermentation broth. Patent WO/00/20620. (2000).

[28] M. Staley. Isolation of carboxylic acids from fermentation broth. US patent 6.777.213 B2. (2004).

[29] A. Baniel. A process for the recovery of dicarboxylic acid. European patent WO98/01413. (1998).

[30] A. Baniel. Recover of carboxylic acid from organic solution that contains an amine and an extraction enhancer. US Patent 5773653. (1998).

[31] A. Eyal. Process and extractant composition for extracting acids. US Patent 5831122. (1998).

[32] M. Holtzapple, R. Davison, T. Luettich. Recovery of fermentation salts from dilute aqueous solutions. US Patent 6478965. (2002).

[33] D. W. Verser, T. J. Eggeman. Recovery of organic acids. US Patent Application 0256337 A1. (2005).

[34] J. Van Erkel, E. L. V. Goetheer. Process for the recovery of acids. European patent EP1659197A1. (2006).

[35] C. J. King, L. Tung. Sorption of carboxylic acid from carboxylic salt solution at pHs close to or above the pKa of the acid, with regeneration with an aqueous solution of ammonia or low-molecular-weight alkylamine. US patent 5132456. (1992).

[36] M. Cockrem, I. Kovacs, I. Mohamednur, D. Heidel. Process for purifying an organic acid. US patent 6641734 B2. (2003).

[37] T. Kushiku, K. Fujiwara, T. Satou, C. Sano. Method for purifying succinic acid from fermentation broth. US Patent Application 0276674 A1. (2006).

[38] Z. Sun, P. Zheng, Y. Ni, J. Dong. Method for extracting succinic acid from fermentation broth by anionic resin adsorption. Chinese patent application CN2008-10195851. (2008).

[39] Z. Sun, P. Zheng, Y. Ni, J. Dong. Cationic resin exchange method for separating succinic acid from fermentation broth. Chinese patent application CN2008-10195852. (2008).

[40] M. A. Theoleyre, Y. Bathany. Procede de purification d'acides organiques. French patent application 2910823. (2008).

[41] Y. Wan, J. Lu, S. Gu, W. Hua, X. Rui. Method for extracting succinic acid from ferment broth. Chinese patent application CN2009-10067834. (2009).

[42] C. Wu, M. Jiang, P. Wei, D. Lei, Z. Yao, P. Zuo. Nanofiltration method for separation of succinic acid from its fermented broth. Chinese patent application CN2009-10025531. (2009).

[43] K. Berglund. Carboxylic acid purification and crystallization process. US patent 5034105. (1991).

[44] D. Glassner, R. Datta. Process for the production and purification of succinic acid. US Patent 5143834. (1992).

[45] R. Datta, S. P. Tsai. Esterification of fermentation derived acids via pervaporation. US Patent 5723639. (1998).

[46] M. C. Cockrem. Process for the production of organic acids and esters thereof. US Patent 6291708 B1. (2001).

[47] D. Dunuwila. Process for the direct production of esters of carboxylic acids from fermentation broths. Canadian patent application 02657666. (2009).

[48] C. Bauduin, W. Fischer, R. Pinkos, E. Scholten. Method of producing a carboxylic alkyl ester. US patent application 0137825 A1. (2009).

[49] S. Varadarajan, D. J. Miller. Biotechnol. Prog. 15, 5 (1999) 845-854.

[50] A. Orjuela, A. J. Yanez, C. T. Lira, D. J. Miller. Carboxylic Acid Recovery from Fermentation Solutions. US Patent Application filed Dec. 2009.

[51] R. E. Vener, A. R. Thompson. Ind. Eng. Chem. 42, 1 (1950) 171-174.

[52] H. Marshall, A. T. Cameron. J. Chem. Soc., Trans. 91 (1907) 1519-1537.

[53] W. D. Bancroft, F. J. C. Butler. J. Phys. Chem. 36, 9 (1932) 2515-2520.

[54] A. Orjuela, A. J. Yanez, A. Lee, D. J. Miller, C. T. Lira. Solubility and Phase Equilibria for Mixtures with Succinic Acid. (2010) In revision.

[55] A. Orjuela, A. J. Yanez, C. T. Lira, D. J. Miller. Recovery of succinic acid from fermentative broth through esterification with ethanol. World Congress on Industrial Biotechnology & Bioprocessing. Jun. 27-30, Washington DC, USA, (2010).

PART 3: REACTIVE DISTILLATION EXPERIMENTS AND SIMULATION

7. Diethyl Succinate Synthesis by Reactive Distillation

7.1 Summary

Diethyl succinate is continuously produced from succinic acid and ethanol in a six-meter, elevated pressure reactive distillation column. Esterification is carried out in excess ethanol such that water and ethanol are produced in the distillate and diethyl succinate is produced in the bottoms stream. The reaction is catalyzed by Amberlyst 70 cation exchange resin contained in KATAPAK SP-11® structured packing within the stainless steel column. Succinic acid conversions approaching 100%, and diethyl succinate yields of up to 98% have been experimentally achieved in the lab scale column. The esterification process has been simulated using the RADFRAC module in Aspen Plus®. Simulations used reaction kinetic and phase equilibrium data collected in our laboratory to predict the steady state stream compositions from the column. Good agreement between experimental and simulation results was observed, thus facilitating the use of the model for design and scale up of the reactive distillation process.

7.2 Introduction

Among the large variety of “green” chemicals of industrial importance, succinic acid (SA) has been highlighted as a renewable platform for production of major commodities. SA can replace petrochemical derived maleic anhydride as a feedstock for 1,4-butanediol, tetrahydrofuran, γ-butyrolactone, 3-hydroxypropionic acid, polymers and a large variety of value-added products. This corresponds to a current addressable market of about 1.6 million tonnes per year [1]. Despite technical improvements in SA fermentation processes, recovery and purification of the free acid still constitutes 50 to 80 percent of processing costs, because high purity SA is required for downstream conversions.

To reduce these recovery costs, the authors have recently demonstrated a novel recovery approach in which products obtained from SA fermentation are acidified and esterified in ethanol [2]. At the end of this process, partially esterified succinic acid remains dissolved in ethanol, from where it can be further converted to the pure ester. These pure esters can be catalytically transformed into commercial SA derivatives [3-10].

Esterification with ethanol (EtOH) proceeds though a series reaction scheme as shown in Figure 7-1, with monoethyl succinate (MES) as intermediate and diethyl succinate (DES) as final product. Depending on reaction temperature, dehydration of EtOH to form diethyl ether (DEE) also occurs.

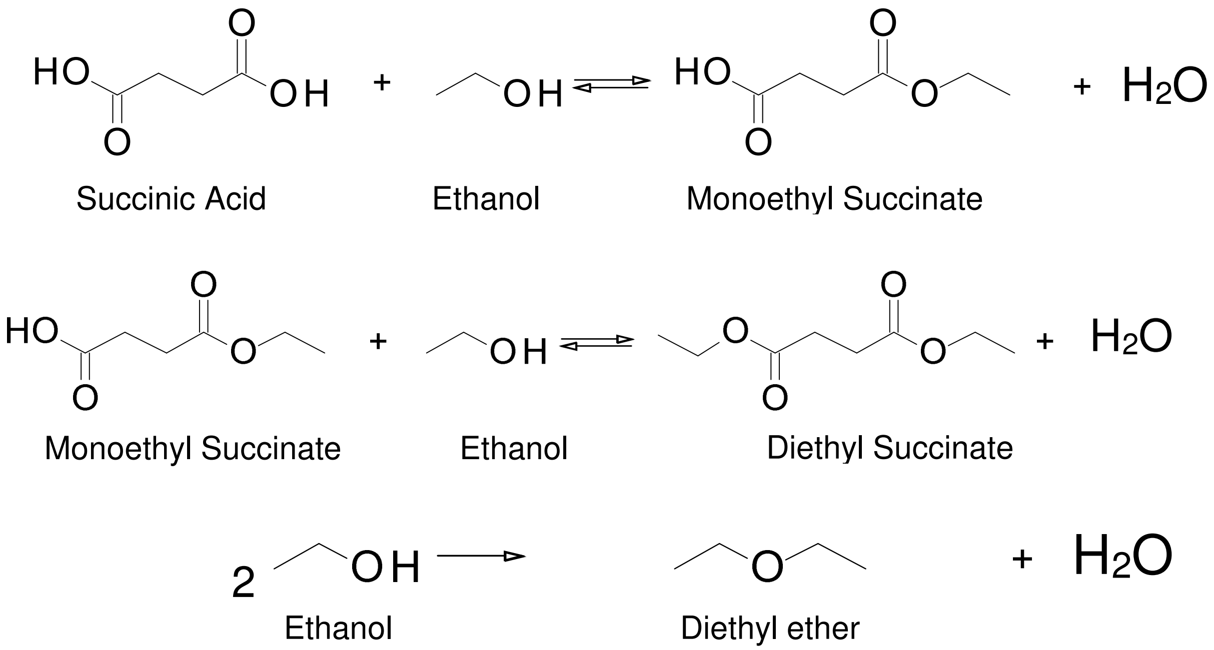

Figure 7-1. Esterification of succinic acid with ethanol.

Because the extent of esterification is thermodynamically limited, removal of reaction products is required to achieve complete conversion. To overcome such thermodynamic limitations, reactive distillation (RD) can be implemented as a scalable industrial process [11-16] to continuously remove either water or ester from the reactive media as it is formed.

Esterification of fermentation-derived acids by RD has been practiced since the 1920's when acids and alcohols from distillery waste were recovered using this method [17]. Recent studies have used RD for esterification of dilute solutions of acetic, lactic, citric, and succinic acids [18-28]. For example, dimethyl succinate was produced in a semi-batch RD process by esterification of succinic anhydride with methanol excess using H_2SO_4 as catalyst [24]. Similarly, dibutyl succinate was obtained in high yields (96%) by reacting ammonium succinate with butanol using *p*-toluene sulfonic acid as catalyst in a batch RD column [25].

Preliminary experiments in a glass reactive distillation column showed that achieving high reaction rates is the primary challenge in succinic acid esterification. To raise the temperature and obtain the highest possible rates, we examine here the esterification of succinic acid with EtOH in a stainless steel, elevated pressure distillation column. Industrial-scale systems a process simulations are developed using the RADFRAC module in ASPEN Plus® (Version 7.1, ASPENTech) based on: (1) models of thermodynamic and kinetic batch experiments; (2) verification of experimental observations of the lab-scale column performance. The effect of major processing variables on SA conversion and DES purity are presented, along with a proposed column design for commercial production.

7.3 Material and methods

7.3.1 Materials

Succinic acid (>99.5 %, Sigma-Aldrich), diethyl succinate (99.92%, Sigma-Aldrich), monoethyl succinate (89.3%, Sigma-Aldrich), ethanol (200 proof, Decon Labs), water (HPLC grade, J.T. Baker), diethyl ether (EMD chemicals, 99.9%), *n*-butanol (99.9%, Mallinckrodt), and acetonitrile (HPLC grade, EMD) were used for experiments and analysis. Hydranal-coulomat E solution (Riedel-de Haën) was used in Karl-Fisher analysis. Amberlyst 70® and Amberlyst 15® ion exchange resins, used as the catalysts in the reactive distillation packing, were purchased from Dow Chemical Co.

7.3.2 Analysis

Analysis was performed using gas chromatography (GC), liquid chromatography (HPLC) and Karl Fisher titration. Samples were dissolved in water (~2 wt %) for HPLC analysis. When samples contained high amount of DES, EtOH was also added (~2 wt %) to ensure a homogeneous solution. A HPLC system with a Waters® 717 autosampler, and Waters® 410 refractive index and Perkin Elmer LC90 UV detectors was used for characterization of succinate species. A 100 mm x 7.6 mm fast acid analysis column (BioRad®) was used for the separation. A 5 mM aqueous solution of H_2SO_4 flowing at 1.0 ml/min was used as the mobile phase.

For GC analysis, samples were diluted 20-fold in acetonitrile containing 5 wt% n-butanol as an internal standard. A Shimadzu® 2010 GC equipped with a flame ionization detector and AOC-5000 autoinjector was used with a 15 m Alltech® EC-WAX column capillary column (0.53 mm i.d., 1.20 μm film thickness). The column temperature program consisted of an initial hold at 313 K for 1.37 min, ramping at 30 K/min to 353 K, ramping at 40 K/min to 523 K, and holding at 523 K for 4 min. The injection port was maintained at 553 K with a split ratio 5:1, and the detector temperature was 573 K. Hydrogen was used as carrier gas (50 cm/min), with volume injections of 1 μL.

Samples of known composition in the range of interest were used for calibration and injected by triplicate to obtain repeatability within 0.5% by mass.

Karl-Fisher analysis (Aquacount coulometric titrator AQ-2100) was used to measure water content in reagents and samples.

7.3.3 Reactive distillation column description

Continuous RD experiments were carried out in a 5.1 cm ID x 4.9 m tall pilot-scale stainless steel reactive distillation column (Figure 2). The column is constructed of six removable sections joined by flanges and separated by liquid redistributors that allowed sample collection. The reactive zone (3.6 m) consists of sections of Katapak-SP-11® (Sulzer Chemtech Ltd.) structured packing containing approximately 76 kg/m^3 of 0.5 mm diameter Amberlyst 70® cation exchange resin beads (Dow Chemical Co.). The non-reactive stripping (0.74 m) and rectifying (0.42 m) sections contain BX® structured gauze packing (Sulzer Chemtech Ltd.). Stage labels in Figure 7-2 were assigned by applying the number of theoretical stages per meter (NTSM = 2 m^{-1}) reported for structured packing on the literature [29, 30].

The column and the kettle-type reboiler are wrapped with electric heating tapes and glass wood insulation. Internal thermocouples and external surface thermocouples were used to register temperature profiles inside and outside the column.

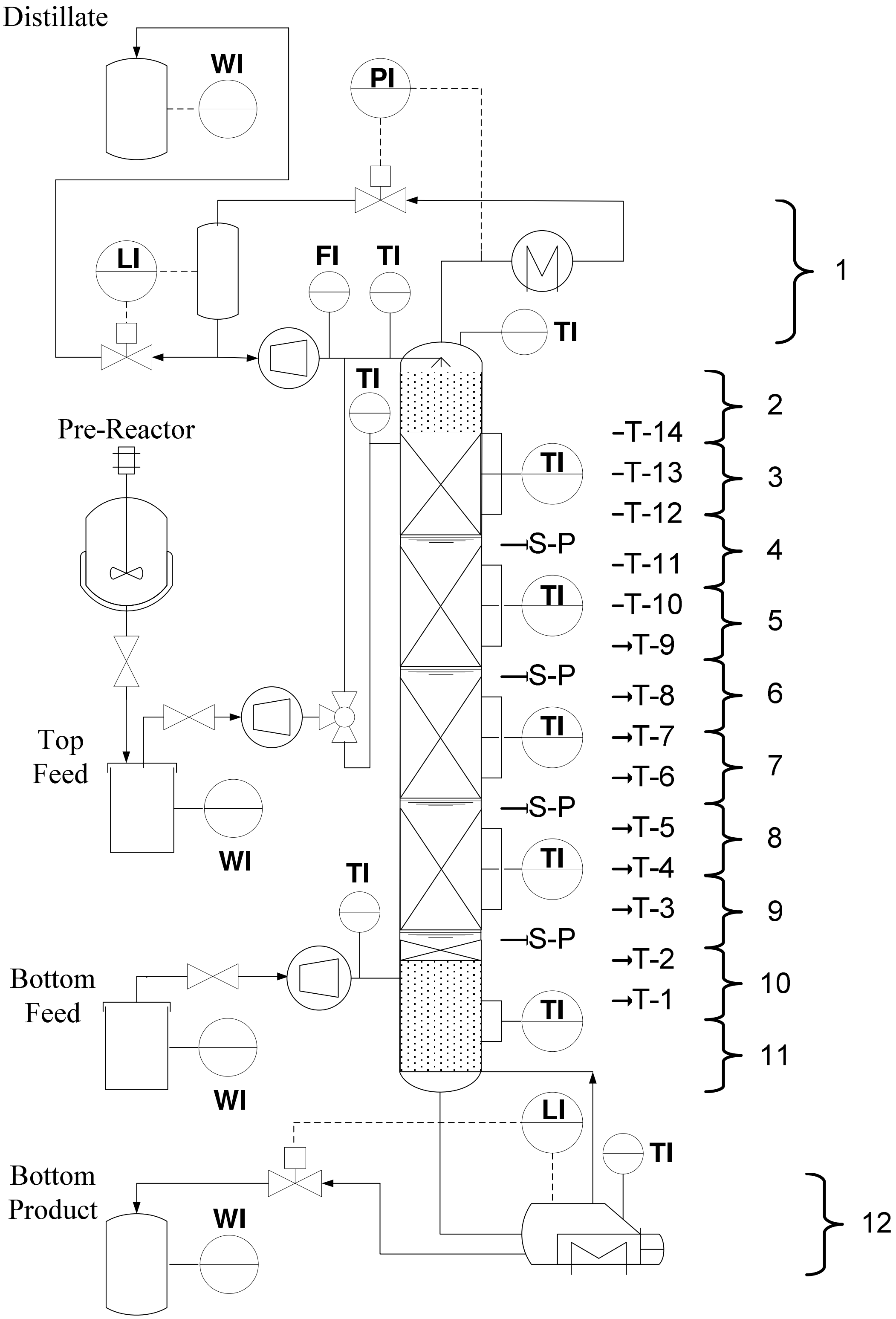

Figure 7-2. Scheme of pilot plant RD column with internal catalytic packing Katapack-SP-11® (middle zone) and BX® structured packing (shaded zones). The brackets on the right indicate the approximate theoretical stages as described in the text. TI – Temperature indicator, S-P – Sampling port, LI – Level indicator, WI – Weight indicator, PI-Pressure indicator.

The tapes along the column exterior were individually controlled at the internal column temperature to minimize heat loss to the surroundings. The operational liquid volume in the reboiler was 1.5 liter with a level controller. Heating power was supplied with a 2.4 kW stainless-steel-coated electric resistance heater submerged in the liquid and connected to an Omega temperature controller.

The column was equipped with a total condenser; coolant was supplied by a chiller capable of providing liquid at 253 K to allow recovery of any diethyl ether (DEE).

The vapor outlet flow at the top of the column was controlled with a solenoid valve, thus maintaining constant pressure in the column. A constant liquid level reservoir was used to collect condensate, with an overflow outlet for distillate withdrawal. Reflux was also dispensed from this reservoir via a controlled flow pump, and the flow rate was measured with a Coriolis flowmeter.

Inlet streams were drawn from tanks positioned on electronic balances using two diaphragm pumps. Pumps were calibrated prior to experiments and flow rates were controlled by adjusting stroke length.

Because succinate species have lower volatilities than EtOH, succinic acid in EtOH was fed above the reactive zone of the column to provide sufficient contact with the catalyst and with EtOH vapors rising through the column. For experiments in which the column was operated without reflux, succinic acid was introduced at the top of the column. Pure EtOH (when required) was introduced to the column below the reactive zone. Inlet streams were fed through heat-traced and insulated pipelines, and inlet temperatures were maintained as close as possible to the correspondent internal temperature of the column at the feed location.

When required, a 0.075 m^3 stirred Pyrex-glass vessel was used as a batch pre-reactor for succinic acid in EtOH, thus providing a partially converted feed solution to the column. For the prereactor, dry Amberlyst 15® cation exchange resin (Dow Chemical Co.) was used as catalyst (2% by total mass) and reaction was allowed to take place for 24 hr prior to feeding. Partial conversions were determined prior to feeding the column.

7.3.4 Reactive distillation column operation

Because the solubility of SA in ethanol is approximately 8 wt% at 298 K, a large excess of EtOH was used during experiments. Temperatures in the reactive zone were maintained below 393 K to avoid excessive dehydration of EtOH to DEE and to protect the Amberlyst catalyst. Additionally, in these elevated-pressure experiments some EtOH was allowed to flow into the reboiler to maintain temperature low enough to avoid unsafe conditions or thermal decomposition of succinate species (as was observed in a similar system) [22].

To reduce excessive use of reactants and minimize waste generation during start-up, the liquid hold-up from the column at the end of a run was kept in the reboiler and the lower part of the column. This liquid contained mainly succinate species, which are generally removed in the bottom product during operation. Considering both the large reboiler holdup and the low SA feed concentration, this method provides a large initial inventory of succinate species and thus reduces the time required to reach steady state in subsequent runs.

In typical operation, the column was started by slowly adding power to the reboiler heater and external heating tapes as the vapor reached each zone of the column. After vapors reached the condenser, total reflux was maintained until a stable temperature profile and pressure were reached. Feed pumps were then started at the specified rates for the experiment and products from distillate and bottoms were collected.

Stream flow rates, acid values of the bottom product, column top pressure, and temperature profiles were recorded on time intervals of 15 to 30 minutes throughout the run. Inlet flows were measured by weight change of the feed tanks during operation. Outlet flows from distillate and bottoms were obtained by measuring volume and density of liquid collected in volumetric flasks. The acid value (AV) of the bottom product, reported as mg KOH per gram of sample, was obtained by titration with 0.1M solution of NaOH in EtOH-H_2O until final point with phenolphthalein. This parameter was used to indicate the approach to steady state and was calculated as:

$$AV = \frac{V_{NaOH} \times M_{NaOH} \times 56100 \ \frac{mg\ KOH}{equivalent}}{g\ sample} \tag{7-1}$$

V_{NaOH} and M_{NaOH} are the volume and molarity of NaOH solution used in the titration.

After reaching steady state, liquid samples were collected in sealed vials from sampling ports along the column and from the bottom and top streams every hour until the end of the experiment. These samples were labeled and refrigerated at 277 K before analysis.

The criteria for achieving steady state during column operation included reaching acid values (AV) with less than ~ 5 % variation in consecutive samples, temperature profiles changing less than ± 0.5 K/hr, and pressure remaining constant (± 7 kPa) at the top of the column. Additional criteria were variations of less than 5% in inlet and outlet mass flow rates, and closure of total and component mass balances over the column within ± 5%. This last criterion was evaluated after the run ended, because most analyses were done following the experiment.

7.4 Results and discussion

7.4.1 Reactive distillation experiments

The complete set of conditions and results of the reactive distillation runs carried out in this study are presented in Tables 7-1 and 7-2. Experimental conditions are given in Table 7-1, and outlet flow rates and compositions are given in Table 7-2.

Numbers within square brackets in flow column in Table 7-1 correspond to mass flow rate of EtOH from bottoms. The SA/EtOH feed was converted in the pre-reactor only in Runs 11A, 11B and 11C. All experiments were conducted without reflux (RR) except for experiments, 9B (RR = 0.58) and 9C (RR = 1.88). In all experiments, flow rates and temperatures of feed streams (succinate/EtOH and pure EtOH) were maintained as constant as possible to facilitate comparison among different operating conditions, although some variation in feed rates was observed. Variations in outlet flow rates are caused by foaming, pressure variations, and uneven boiling, all of which affect the level controller in the reboiler and condensate reservoir. Both inlet and outlet flow rates are therefore reported in Tables 7-1 and 7-2 as the average total inlet feed rate ($\dot{W}$) over the course of experiment with the mean absolute deviation (MAD) of flow rate from the average over all measurements ($\dot{W} \pm$ MAD). In almost all experiments, the difference between the sum of average flow rates in and the sum of average flow rates out was less than 5%, although a few experiments (Runs 6A, 7A and 11A) exhibited slightly larger differences and were thus deemed not to have entirely reached steady state.

Table 7-1. Experimental conditions for continuous RD. Corresponding outlet compositions are summarized in Table 7-2

Run Code	Reboiler Power (kW)	Gauge *P* (kPa)	Top Feed (SA in EtOH-H_2O) [Bottom Feed, (100 % EtOH)]			Distillate flow (g/min)	Bottoms		
			wt% SA	wt% H_2O	Flow (g/min)		flow (g/min)	AV (mg KOH / g)	*T* (K)
5A	0.84	310	6.7	-	31.9 ± 0.8	17.1 ± 0.9	13.9 ± 1.0	-	393.1
5B	0.72	310	6.7	-	30.2 ± 0.3	11.1 ± 0.5	18.2 ± 1.1	-	392.4
5C	0.55	310	6.7	-	30.4 ± 0.1	4.0 ± 0.1	26.1 ± 0.4	-	393.1
6A	1.03	310	6.7	-	31.2 ± 0.2	30.8 ± 0.9	3.3 ± 0.6	33	404.7
7A	0.74	138	6.7	-	31.9 ± 1.3	22.7 ± 0.8	11.8 ± 1.3	12.7	378.2
8A	0.98	310	6.7	-	31.1± 0.1 [5.0 ± 0.2]	25.5 ± 0.2	10.1 ± 0.3	13.7	394.4
8B	1.08	310	6.7	-	31.2 ± 0.2 [10.3 ± 0.1]	31.2 ± 0.5	9.7 ± 0.4	8.7	393.9
9A	0.89	310	6.7	-	30.7 ± 0.7	19.9 ± 0.3	10.6 ± 0.5	10	393.9
9B	1.13	310	6.7	-	30.0 ± 1.2	19.1 ± 0.4	10 ± 0.9	12.6	394.6
9C	1.61	310	6.7	-	30.8 ± 0.1	20.7 ± 0.5	9.4 ± 0.4	9.4	393.8
10A	1.08	579	6.7	-	30.6 ± 0.3	21.5 ± 0.5	10.1 ± 0.7	19	411.0
10B	1.34	579	6.7	-	30.4 ± 0.1 [14.8 ± 0.6]	33.7 ± 0.4	11.6 ± 0.9	9.1	410.6
11A	1.15	310	25.0[†]	-	30.0 ± 0.5	20.8 ± 0.2	11.6 ± 1.0	148.4	439.7
11B	1.54	310	25.0[†]	-	31.6 ± 1.3 [16.5 ± 0.3]	35.6 ± 0.3	11.8 ± 0.6	4.7	474.8
11C	1.78	310	25.0[†]	-	31.6 ± 0.1 [27.9 ± 0.8]	47.6 ± 0.5	12.4 ± 0.6	2.3	481.0
15A	0.77	72	6.7	-	32.8 ± 0.5	23.5 ± 1.0	9.2 ± 0.7	12.5	368.1
15B	0.74	41	6.7	-	30.8 ± 0.1	23.1 ± 0.5	8.2 ± 0.6	15.6	362.6
16A	1.25	41	6.7	-	59.3 ± 1.1	51.1 ± 0.9	7 ± 0.7	54	373.2
17A	1.74	34	6.7	-	90.5 ± 0.8	81.2 ± 0.7	9.8 ± 1.0	89.4	380.1
18A	1.28	41	6.7	7.0	59.7 ± 0.6	49.5 ± 0.8	10.3 ± 0.7	80.8	365.7
19A	1.33	41	6.7	7.0	60.2 ± 0.4	49.9 ± 2.0	8 ± 1.2	112.8	372.0

[†] SA concentration in top feed is reported before pre-reaction

Table 7-2. Summary of outlet streams composition obtained in RD experiments. Corresponding flowrates are in Table 7-1.

Run Code	Distillate composition wt%						Bottoms Composition wt%						SA conversion (%)	Selectivity to DES (%)
	H_2O	DEE	EtOH	MES	DES	SA	H_2O	DEE	EtOH	MES	DES	SA		
5A	1.0	1.5	97.5	0.0	0.0	0.0	4.3	0.0	71.3	2.7	21.9	0.1	99.5	87.2
5B	0.4	3.1	96.4	0.0	0.0	0.1	3.7	0.0	77.9	1.6	16.6	0.1	98.1	89.6
5C	0.2	8.3	91.4	0.0	0.0	0.1	3.0	0.0	84.2	0.9	11.7	0.2	97.8	91.4
6A	1.8	0.6	97.6	0.0	0.0	0.0	5.0	0.0	21.0	12.6	61.1	0.8	98.8	80.3
7A	0.9	0.3	98.7	0.0	0.0	0.1	4.0	0.0	70.6	2.4	22.8	0.2	97.8	88.6
8A	1.3	1.1	97.5	0.0	0.0	0.1	3.2	0.0	64.2	3.3	29.2	0.2	98.1	88.1
8B	1.8	1.1	97.1	0.0	0.0	0.1	1.4	0.0	68.4	1.6	28.6	0.0	98.8	93.7
9A	2.5	1.9	95.5	0.0	0.0	0.0	3.6	0.0	63.8	2.9	29.7	0.1	99.7	89.7
9B	3.1	1.7	95.2	0.0	0.0	0.0	2.5	0.0	61.5	3.0	32.9	0.1	99.7	90.2
9C	2.9	2.2	94.9	0.0	0.0	0.0	3.0	0.0	62.4	1.8	32.7	0.1	99.5	93.7
10A	1.1	6.5	92.2	0.0	0.0	0.1	6.6	0.0	62.4	4.4	26.3	0.3	97.1	83.5
10B	2.4	4.3	93.3	0.0	0.0	0.1	1.7	0.0	72.2	1.6	24.5	0.1	98.3	92.8
11A	6.7	1.0	91.9	0.1	0.2	0.2	2.8	0.0	1.8	30.4	63.2	1.8	96.7[§]	86.4[§]
11B	7.1	1.6	90.8	0.1	0.2	0.2	0.1	0.0	2.9	0.5	96.0	0.5	92.2[‡] 98.4[§]	62.7[‡] 99[§]
11C	6.6	1.3	91.7	0.0	0.2	0.2	0.1	0.0	1.8	0.3	97.5	0.2	98.4[§]	99.6[§]
15A	1.9	0.1	98.0	0.0	0.0	0.0	2.4	0.0	63.5	3.5	30.5	0.1	99.7	87.9
15B	2.4	0.0	97.5	0.0	0.0	0.0	2.5	0.0	58.2	4.6	34.6	0.1	99.4	86
16A	2.1	0.0	97.8	0.0	0.0	0.0	2.1	0.0	24.6	12.9	59.3	1.2	95.7	79.5
17A	1.6	0.0	98.4	0.0	0.0	0.0	2.3	0.0	19.0	18.3	57.8	2.5	93.1	72.6
18A	6.8	0.0	93.2	0.0	0.1	0.0	10.6	0.0	28.9	16.1	42.1	2.4	92.1	68.9
19A	6.8	0.0	93.1	0.0	0.1	0.0	14.1	0.0	12.0	22.8	47.3	3.7	90.1	63.7

[‡] Intermediate calculation for pre-reactor contents fed to the column.

[§] Total conversion including pre-reactor and RD column.

Characteristic dynamics of flows and compositions during approach to steady state in a typical experiment (Run 11) are presented in Figures 7-3 and 7-4. As presented in Table 7-1, Run 11 operated with a pre-reacted acid mixture as the top feed. Column performance was evaluated by feeding EtOH to the bottom of the reactive zone at three different flow rates (A, B and C). As seen in Figure 7-3, the total time to initially reach steady state was 18 to 24 h; this value depended on the bottoms flow rate used in the experiment.

Acid value (AV) of the bottoms stream was measured during operation and gave a good indicator of approach to steady state, particularly when compared with product composition profiles reported in Figures 7-3 and 7-4.

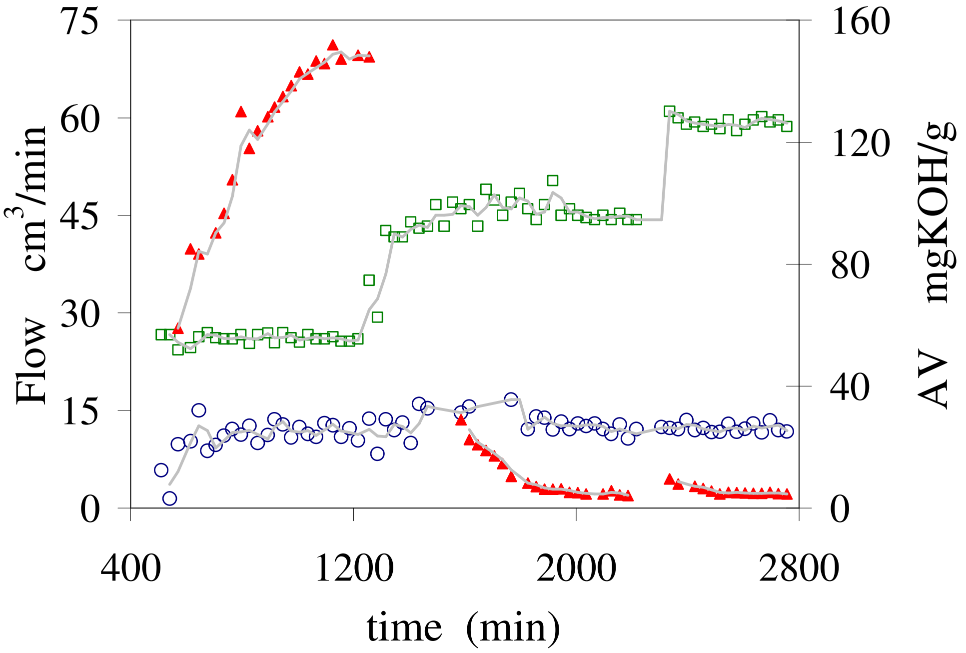

Figure 7-3. Outlet flows and acid value profiles with time during approach to steady state in run 11A (left), 11B (middle) and 11C (right). (□) - Distillate flow, (○) – Bottoms flow, (▲) Acid value at the bottoms.

Chromatographic analyses of product samples were conducted following completion of reactive distillation runs as described in Section 7.3. Concentrations of succinate species reported in Table 7-3 are the average of HPLC and GC measurements; H_2O concentration was obtained by Karl Fischer analysis. Variations in stream compositions with time are mainly attributed to flow instabilities and pressure perturbations during operation.

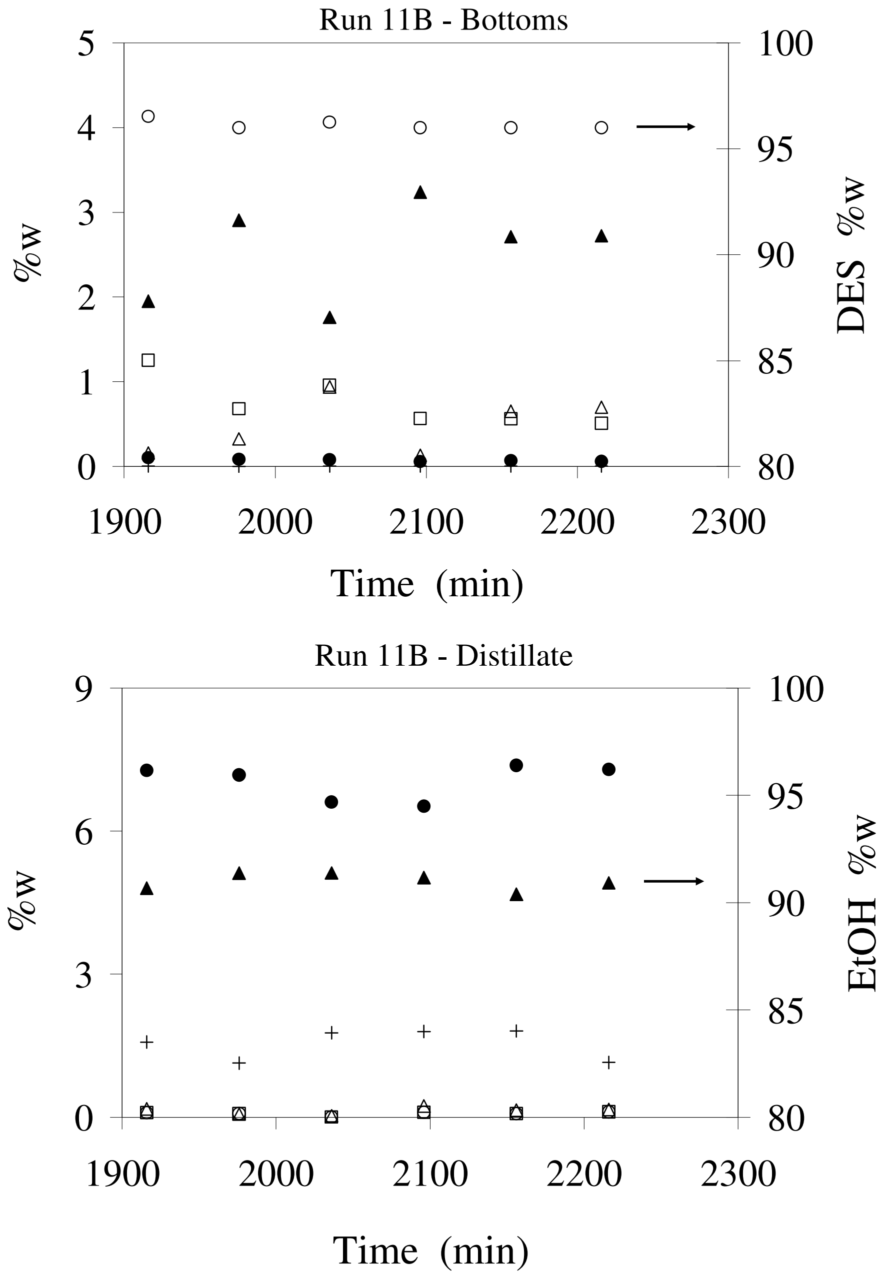

Figure 7-4. Time evolution of composition in distillate and bottom product in run 11B during approach to steady state. (○) - DES, (□) - MES, (Δ) - SA, (●) - H_2O, (▲) - EtOH, (+) - DEE.

In general, high conversions of SA and high selectivity to DES were achieved in all experiments. This was expected, considering the large excess of EtOH fed to the RD column. Also because of this large excess of EtOH, temperatures along the column remained within a few degrees of the boiling point of EtOH at the column pressure, except in the reboiler where EtOH was not the dominant species. As the reboiler temperature is strongly influenced by the presence of light species, slight changes in distillate flow rate removing light components from the system resulted in significant changes in reboiler temperature. This effect was observed in experiments operated at identical pressures (Runs 11A and 11B in Table 7-1).

7.4.1.1 Effect of reboiler power

Runs 5 and 6 illustrate the effect of reboiler power from a high level in 6A to a low level in 5C. When boilup rate increases, SA conversion remains almost constant because of the large excess of EtOH in the system. Meanwhile, there is a slight decrease of selectivity to DES as reboiler power increases. In general, the first step of esterification to produce MES is faster (1.2 – 1.5 times) and more favored thermodynamically ($K_{EQ1} = 6K_{EQ2}$ [31]) than the second step to DES. Thus when higher boilup rates are used, EtOH is stripped out of the liquid phase and less reaction of MES to DES takes place. At low boilup rates, in contrast, DEE formation increases because of increased EtOH content in the lower part of the column and in the reboiler.

As expected water removal at the top was higher by increasing boilup rate because EtOH vaporization also enhances stripping of water from liquid phase.

7.4.1.2 Effect of column pressure

In Runs 5B, 7A, 15A and 15 B reboiler power and inlet flows were maintained constant under different pressures. As pressure is reduced, lower temperatures along the column and higher distillate flow rates were observed. Operating at high pressures high SA conversion and high selectivity to DES were obtained but higher temperatures enhanced undesirable dehydration of EtOH.

7.4.1.3 Effect of EtOH feed

When pure EtOH is fed below the reactive zone (Runs 8A and 8B) and a constant bottoms flow rate is maintained, a higher concentration of DES is achieved in the bottoms along with more extensive removal of H_2O in the distillate. In this case, EtOH acts both as a reactant and as stripping agent to pull H_2O out of the liquid phase via formation of the azeotrope. Operating with EtOH feed to the column at higher pressures (Runs 10A and 10B) improved DES yield, but also increased DEE generation because of higher temperatures and a larger excess of EtOH.

7.4.1.4 Effect of reflux ratio

Increasing reflux ratio (Runs 9A, 9B, 9C) while maintaining constant outlet flow rates gave no appreciable change in SA conversion and a slight increase in DES selectivity.

7.4.1.5 Operation with pre-reactor

In Run 11, a pre-reacted succinate acid-ester mixture in EtOH that was run to nearly an equilibrium composition was used as the feed. This prereacted feed contained a much higher succinate concentration (25 wt% SA equivalent) than the regular feed (7 wt% SA). Higher boiling points were thus observed in the reboiler; however, no decomposition products were detected in the bottoms. With only the prereacted feed stream to the column, high concentrations of MES were found at bottoms. In contrast, when EtOH was fed to the column in a second feed stream below the reactive zone, almost complete conversion of SA was achieved with DES purity in the bottoms of 98%. This demonstrates clearly the attractiveness of reactive distillation for the production of DES.

7.4.1.6 Effect of inlet acid flow rates

In Runs 15B, 16A and 17A, the effect of different flow rates of acid feed was studied at low pressure to evaluate processing capacity of the pilot equipment. As expected, increasing flow rate of the top feed reduces SA conversion and DES purity. Considering that KATAPAK SP-11 is a sandwich-type structured packing with one catalytic layer per non-catalytic layer, excess liquid may bypass the catalyst layer and flow downwards without reacting. In this case, a higher dynamic liquid hold-up on the structured packing may be created by the higher vapor flow rate generated in the reboiler. This condition has been extensively reported in the literature as operation over the catalytic loading point [29, 32-36].

7.4.1.7 Effect of water in the feed

The presence of water in the acid feed was evaluated in Runs 18A and 19A, where the SA solution was prepared with the azeotropic mixture of EtOH and water. A substantial drop in SA conversion and selectivity to DES relative to Run 16A (with pure EtOH fed) was observed, and substantial water was found in the reboiler (up to 14 wt %) that contributes to product hydrolysis.

After analysis of experiments described above, a preferable RD process to obtain high purity DES would include a pre-reactor and an EtOH feed below the reactive zone of the column. Operating pressures must be as high enough to guarantee high conversion but as low as possible to minimize DEE formation. According to experimental results, operating at 140 kPa with EtOH feed near the bottoms may drive reaction to completion with low dehydration to DEE. Despite results indicating that higher reflux ratios benefit conversion, the inlet flow rate of EtOH at the bottom port also affects conversion. It is expected that, above a certain limit, reflux water content starts to have a negative impact on the extent of esterification in the column.

Considering the large amount of work required to evaluate a variety of operating conditions that still remain to be studied more operating conditions by experiment, further analysis of RD column performance is addressed by simulation in next section.

7.4.2 Simulation of RD experiments

Simulation of RD operation was performed using a steady state model (RADFRAC®) in Aspen Plus® process design software (Version 7.1, AspenTech). Modeling of distillation was carried out using an equilibrium stage approach with chemical reactions modeled using pseudo-homogeneous kinetics. Description of the calculation algorithm has been previously described in detail in the literature [37]. Phase equilibria of these non-ideal reactive mixtures were modeled by the NRTL equation to calculate activity in the liquid phase [38], and by the Hayden O-Connell (HOC) equation for fugacity coefficient in the vapor phase [39, 40]. Most binary parameters were obtained by regression of experimental data, as reported in previous work from our group [41-44]. Remaining parameters were obtained or regressed from literature data [31, 45], or used directly from the ASPEN database. A list of parameters used in phase equilibria models are summarized in Table 7-3. In the absence of strong association in the vapor phase listed in table, the HOC parameter is zero.

Table 7-3. Binary parameters for NRTL and HOC equations [38, 39].

HOC binary parameters								
i	*j*		*i*	*j*		*i*	*j*	
H_2O	H_2O	1.7	EtOH	EtOH	1.4	DES	DEE	0.5
H_2O	EtOH	1.55	EtOH	DES	1.3	DEE	DEE	0.5
H_2O	DES	1.3	EtOH	DEE	0.5			
H_2O	DEE	0.5	DES	DES	0.53			

NRTL binary parameters						
i	*j*	a_{ij}	a_{ji}	b_{ij}	b_{ji}	α_{ij}
H_2O	EtOH	0.514285	0.806535	444.8857	-266.533	0.4
H_2O	SA	0	0	296.7226	-328.506	0.3
H_2O	DES	4.384591	-1.58	184.7326	1136.555	0.36842
H_2O	MES	0	0	880.7603	-200.977	0.3
H_2O	DEE	8.412378	0.617494	-1496.24	547.9293	0.348988
EtOH	SA	0	0	-605.634	113.4481	0.3
EtOH	DES	0	0	653.8819	-158.856	0.3
EtOH	MES	0	0	-292.308	400.6306	0.3
EtOH	DEE	4.3596	-3.5877	-1209.49	1381.066	0.3
SA	DES	0	0	1946.876	218.2243	0.3
SA	MES	0	0	-368.762	1039.777	0.3
SA	DEE	0	0	1947.928	248.4113	0.3
DES	MES	0	0	-44.2052	137.2218	0.3
DES	DEE	0	0	595.5747	-404.406	0.3
MES	DEE	0	0	100.6717	88.62851	0.3

Reactions were described by a pseudo-homogeneous activity-based kinetic model previously developed for Amberlyst 70® [31]. Collected data on self-catalytic and Amberlyst 15® catalyzed SA esterification previously fitted with a mole fraction based kinetics [46] were also regressed with the activity model. Volumetric rates of reaction for the first and second steps of esterification and also for DEE formation are presented in Equations 7-2, 7-3 and 7-4 respectively.

$$r_2 = w_{CAT}\rho_{Sol}k_0^2 \exp\left(\frac{-E_a^2}{RT}\right)\left[(x_{MES}\gamma_{MES})(x_{EtOH}\gamma_{EtOH}) - \frac{(x_{DES}\gamma_{DES})(x_{H2O}\gamma_{H2O})}{K_{EQ}^2}\right]$$

(7-2)

$$r_1 = w_{CAT}\rho_{Sol}k_0^1 \exp\left(\frac{-E_a^1}{RT}\right)\left[(x_{SA}\gamma_{SA})(x_{EtOH}\gamma_{EtOH}) - \frac{(x_{MES}\gamma_{MES})(x_{H2O}\gamma_{H2O})}{K_{EQ}^1}\right]$$

(7-3)

$$r_3 = w_{CAT}\rho_{Sol}k_0^3 \exp\left(\frac{-E_a^3}{RT}\right)\left[(x_{EtOH}\gamma_{EtOH})^2\right] \qquad (7\text{-}4)$$

In Eq. (2) – (4), k_0^m and E_a^m are the pre-exponential factor and the energy of activation of the forward reaction *m*, respectively. The equilibrium constant of reaction *m*, K_{EQ}^m, is the ratio of forward and reverse rate constants. x_i, and γ_i, are the mole fraction and activity coefficient of component *i* in the liquid phase. w_{CAT} is the catalyst weight loading per weight of liquid and ρ_{Sol} is density of the reactive solution.

In self-catalyzed reactions, w_{CAT} and ρ_{Sol} are set to one for Eq. 7-2, 7-3 and 7-4. Etherification was only considered when catalysts were present.

The above kinetics for Amberlyst 70® was used to model reactive stages in the column. Self-catalyzed kinetics, evaluated experimentally for homogeneous mixtures of SA and EtOH, were included to model reactions in stripping stages (including the reboiler) below the reactive zone to account for hydrolysis caused by H_2O remaining in the reboiler and bottoms streams.

The pre-reactor was modeled as a continuous stirred tank reactor with 24 hr retention time using the kinetic expression for Amberlyst 15® resin. The complete list of kinetic parameters used in simulations is summarized in Table 7-4. Parameters used for simulation of pilot plant experiments are summarized in Table 7-5.

The catalyst volumetric concentration C_{CAT} (kg $_{\text{Catalyst}}$ / m^3 $_{\text{Liquid}}$) in AspenPlus for each reactive stage was calculated from the volumetric hold-up (h = 0.1 m^3 $_{\text{Liquid}}$ / m^3 $_{\text{Column}}$) and the catalyst loading (or catalyst packing density in the column, ρ_{Cat} = 78 kg $_{\text{CAT}}$ / m^3 $_{\text{Column}}$) using Equation 7-5.

$$C_{CAT} = w_{CAT} \times \rho_{Sol} = \frac{\rho_{Cat}}{h} \tag{7-5}$$

Table 7-4. Parameters for activity-based kinetics used in simulation of RD experiments.

Parameter	Amberlyst 70®	Amberlyst 15®	Self-Catalytic
k_0^1 (kmol/ kg $_{\text{CAT}}$) (1/s)	1.04x10^4	5.17x10^3	1.57 x10^{5} §
E_a^1 (kJ/kmol/K)	46200	46900	57300
K_{EQ}^1		48.9	
k_0^2 (kmol/ kg $_{\text{CAT}}$) (1/s)	2.11x10^3	7.0x10^4	17.8 §
E_a^2 (kJ/kmol/K)	46600	61400	34400
K_{EQ}^2		10.14	
k_0^3 (kmol/ kg $_{\text{CAT}}$) (1/s)	4.99 x10^4	8.06 x10^4 ‡	-
E_a^3 (kJ/kmol/K)	85400	86900 ‡	-

§ Pre-exponential factor has units of (kmol/m^3)(1/s)

‡ Mole fraction model assuming unity activity coefficients in Eq. 7-4.

Table 7-5. Parameters used for simulation of RD system.

Parameter		
Total number of stages (N)		12
HETP – Height equivalent to theoretical plate (m)		0.5
Reactive stages	Catalytic (3-9)	7
	Non-catalytic (10-12)	3
Feed Stages	Acid feed	Above 3
	EtOH feed	On 10
Column pressure drop per stage (kPa)		0.07
Reflux ratio		0.001
Murphree stage efficiency (stages 2 to 11)		0.5
Liquid holdup (cm^3) (stages 2 to N-1) (10 % vol)		98.2
Reboiler holdup (cm^3)		1500
Product removal stage	Top	1
	Bottom	12
Catalyst loading ($kg_{Catalyst} / m^3_{Column}$)		78

Catalyst concentration (C_{CAT}) was multiplied by k_0 in Eq. 7-2 to 7-4 and results were used as pre-exponential factors in Aspen input formats of reactive distillation type-kinetics. For the pre-reactor, k_0 was multiplied by the catalyst loading used in experiments (0.02 kg_{CAT} / kg_{Liq}) and the average liquid density of 900 kg/m^3.

To estimate hydrodynamic conditions attained in the column, the fractional approach to maximum capacity (f_{MC}) was calculated in each simulation using the Aspen pack sizing tool. Hydrodynamics for catalytic packing were evaluated by using a structured packing available in Aspen database (MELLAPAK-250Y®, Sulzer) with similar HETP, holp-up and pressure drop per meter to KATAPAK SP-11. In every simulation, f_{MC} was adjusted until calculated column diameter matched that of the pilot column.

Considering the strong dependence of reboiler temperature on boilup rate observed in column operation, simulations were matched with experiments by equating bottoms temperature and EtOH concentration in the reboiler. For this purpose, distillate flow rates were adjusted in simulations within the range of variation observed in experimental flows (~ 5%) to obtain a reboiler temperature and EtOH mass fraction as close as possible to those obtained in experiments.

Simulation results are summarized in Table 7-6. In general, the results are in good agreement with experimental results reported in Tables 7-1 and 7-2; for example, most simulated column temperature profiles agree with experimental profiles to within a few degrees Centigrade. The average deviation between predicted and experimental concentrations of DES in the bottoms stream and EtOH in the distillate stream is less than 10% in most experiments. As expected, higher relative deviations were observed in components present at low concentrations (<5%) because at low concentrations uncertainty in analytical measurements are more significant.

Table 7-6. Summary of results of simulation of RD experiments.

Run Code	Reboiler			Distillate	Bottoms		SA	Selectivity	Distillate composition wt %						Bottoms Composition wt%					
	T (K)	Power kW	f_{MC}	Flow (g/min)	Flow (g/min)	AV	conversion (%)	to DES (%)	H_2O	DEE	EtOH	MES	DES	SA	H_2O	DEE	EtOH	MES	DES	SA
5A	393.7	0.27	0.04	18.0	13.9	3.8	99.9	94.9	2.9	1.6	95.1	0.0	0.3	0.0	1.8	0.0	76.2	1.0	21.1	0.0
5B	393.0	0.16	0.03	12.0	18.2	2.8	99.9	94.7	2.9	2.4	94.4	0.0	0.3	0.0	2.1	0.0	81.9	0.7	15.3	0.0
5C	392.5	0.06	0.02	4.5	25.9	2.0	100.0	94.8	2.7	5.6	91.4	0.0	0.3	0.0	2.4	0.1	86.1	0.5	10.9	0.0
6A	404.5	0.37	0.05	27.2	4.0	7.2	100.0	97.5	2.5	1.1	96.0	0.0	0.3	0.0	0.3	0.0	25.1	1.9	72.8	0.0
7A	377.6	0.29	0.04	21.5	8.3	7.1	99.9	93.9	3.5	0.4	95.9	0.0	0.2	0.0	1.8	0.0	63.7	1.8	32.7	0.0
8A	377.8	0.31	0.05	26.7	9.3	4.1	100.0	96.2	3.4	1.1	95.2	0.0	0.3	0.0	0.9	0.0	67.4	1.0	30.7	0.0
8B	394.8	0.43	0.05	31.2	10.3	2.4	100.0	97.5	3.1	1.0	95.7	0.0	0.3	0.0	0.5	0.0	70.8	0.6	28.1	0.0
9A	394.7	0.30	0.04	21.5	9.2	6.5	99.9	93.9	3.8	1.3	94.6	0.0	0.3	0.0	1.8	0.0	66.4	1.7	30.2	0.0
9B	394.8	0.46	0.06	21.0	9.0	6.2	99.9	94.2	3.9	1.4	94.6	0.0	0.1	0.0	1.6	0.0	66.1	1.6	30.7	0.0
9C	394.7	0.84	0.10	21.0	9.8	5.8	99.9	94.3	4.0	1.4	94.6	0.0	0.1	0.0	1.5	0.0	67.9	1.5	29.1	0.0
10A	411.8	0.27	0.03	20.5	10.1	7.1	99.9	92.7	4.3	3.9	91.4	0.0	0.4	0.0	2.3	0.0	69.0	1.8	26.9	0.0
10B	412.2	0.44	0.06	34.1	11.1	1.9	100.0	97.9	3.2	2.7	93.7	0.0	0.4	0.0	0.4	0.0	73.9	0.5	25.2	0.0
11A	440.4	0.29	0.04	18.9	11.1	67.4	99.4[§]	80.1	10.8	1.0	87.0	0.0	1.2	0.0	0.5	0.0	5.2	16.6	77.3	0.4
11B	475.2	0.54	0.08	36.8	11.5	7.4	88.6[‡] 99.9[§]	54.1[‡] 97.7	6.7	0.8	91.3	0.0	1.2	0.0	0.0	0.0	2.5	1.9	95.6	0.0
11C	480.1	0.69	0.10	49.0	11.2	2.5	100[§]	99.3	5.0	0.6	93.1	0.0	1.2	0.0	0.0	0.0	2.1	0.6	97.2	0.0
15A	368.4	0.34	0.05	23.5	9.3	7.8	99.9	93.2	3.4	0.2	96.3	0.0	0.2	0.0	2.0	0.0	63.9	2.0	32.1	0.0
15B	362.3	0.34	0.05	23.1	7.7	9.4	99.9	92.7	3.3	0.1	96.4	0.0	0.1	0.0	2.0	0.0	59.7	2.4	35.9	0.0
16A	368.1	0.75	0.12	51.0	8.3	25.3	99.5	89.6	3.2	0.1	96.6	0.0	0.1	0.0	1.0	0.0	30.7	6.1	62.1	0.2
17A	373.9	1.17	0.18	79.8	10.7	50.8	98.5	83.6	3.1	0.0	96.7	0.0	0.1	0.0	0.7	0.0	19.4	11.3	67.8	0.8
18A	365.4	0.82	0.12	50.5	9.2	66.1	97.7	71.4	8.9	0.0	91.0	0.0	0.1	0.0	7.7	0.0	32.3	14.8	44.2	1.0
19A	368.3	0.85	0.12	52.5	7.7	85.8	97.4	69.4	9.1	0.0	90.8	0.0	0.1	0.0	6.1	0.0	21.9	19.0	51.6	1.3

[‡] Data evaluated on pre-reactor.

[§] Data evaluated over non-converted SA still remaining in pre-reacted feed.

At identical conditions, SA conversion and selectivity to DES are slightly higher in simulation than in experiments. Possible explanations for this observation include: 1) actual column operation at a low fraction of flooding ($f_{MC} < 0.2$), which likely results in incomplete liquid distribution and therefore incomplete catalyst wetting within the structured packing; and 2) the particle size of Amberlyst 70 catalyst used in the structured packing ($d_P > 0.5$ mm) was larger than that used in kinetic measurements ($d_P < 0.3$ mm), thus reducing effectiveness factor of the column catalyst [31, 46].

In simulations, HETP is taken as a constant along the column height. In reality, changes in flows (and other parameters such as pressure, reflux ratio, number and location of feed streams, etc. [47, 48]) in different sections of the column result in changes in HETP along the column height. The differing stage-to-stage HETP values will result in a mismatch of temperature and composition profiles between experiment and simulation. Temperature and composition profiles obtained by simulation of experimental Run 11C are presented in Figure 7-5. While simulated outlet flow compositions and temperature profiles match well with experiments, composition profiles within the column differ significantly, mainly in the lower part of the column. Nevertheless, the simulations carried out here using the equilibrium stage model reproduce all major trends seen in experiments, and are able to predict reasonably accurately column performance. We therefore use the model to examine column behavior over a broader range of operating conditions than what was done experimentally.

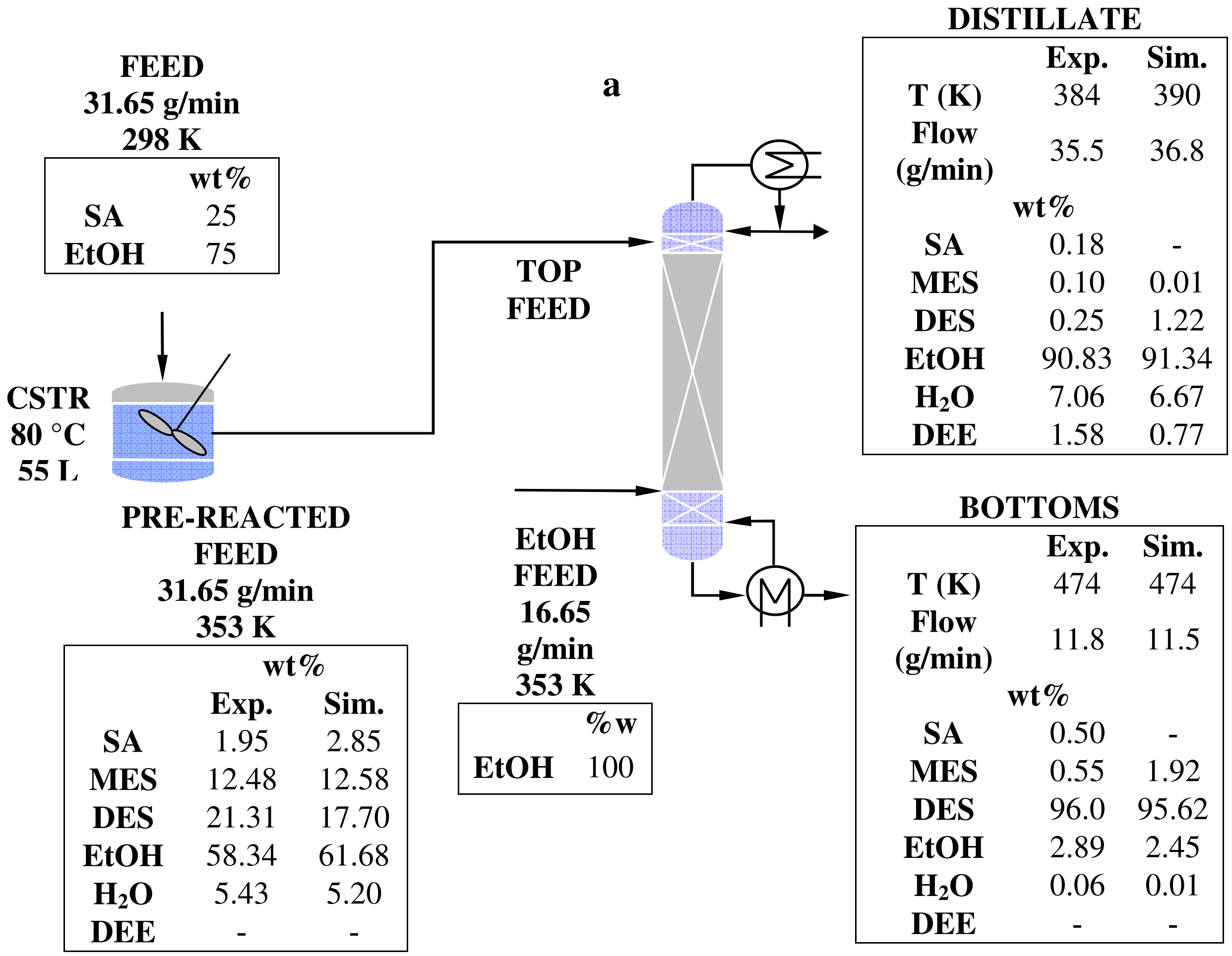

FEED

	wt%
SA	25
EtOH	75

PRE-REACTED FEED

	wt% Exp.	wt% Sim.
SA	1.95	2.85
MES	12.48	12.58
DES	21.31	17.70
EtOH	58.34	61.68
H_2O	5.43	5.20
DEE	-	-

EtOH FEED

	%w
EtOH	100

DISTILLATE

	Exp.	Sim.
T (K)	384	390
Flow (g/min)	35.5	36.8
wt%		
SA	0.18	-
MES	0.10	0.01
DES	0.25	1.22
EtOH	90.83	91.34
H_2O	7.06	6.67
DEE	1.58	0.77

BOTTOMS

	Exp.	Sim.
T (K)	474	474
Flow (g/min)	11.8	11.5
wt%		
SA	0.50	-
MES	0.55	1.92
DES	96.0	95.62
EtOH	2.89	2.45
H_2O	0.06	0.01
DEE	-	-

Figure 7-5. Results obtained by simulation of run 11C. a) Global mass and component balance comparison with experimental data. b) Temperature and concentration profiles. Lines in column profiles represent results obtained by simulation. (○, ▬) - DES, (□, - -) - MES, (Δ, - - ▬ - -) - SA, (●, ▬ ▬) - H_2O, (▲, ▬ ▬) - EtOH, (X, ▬) - DEE.

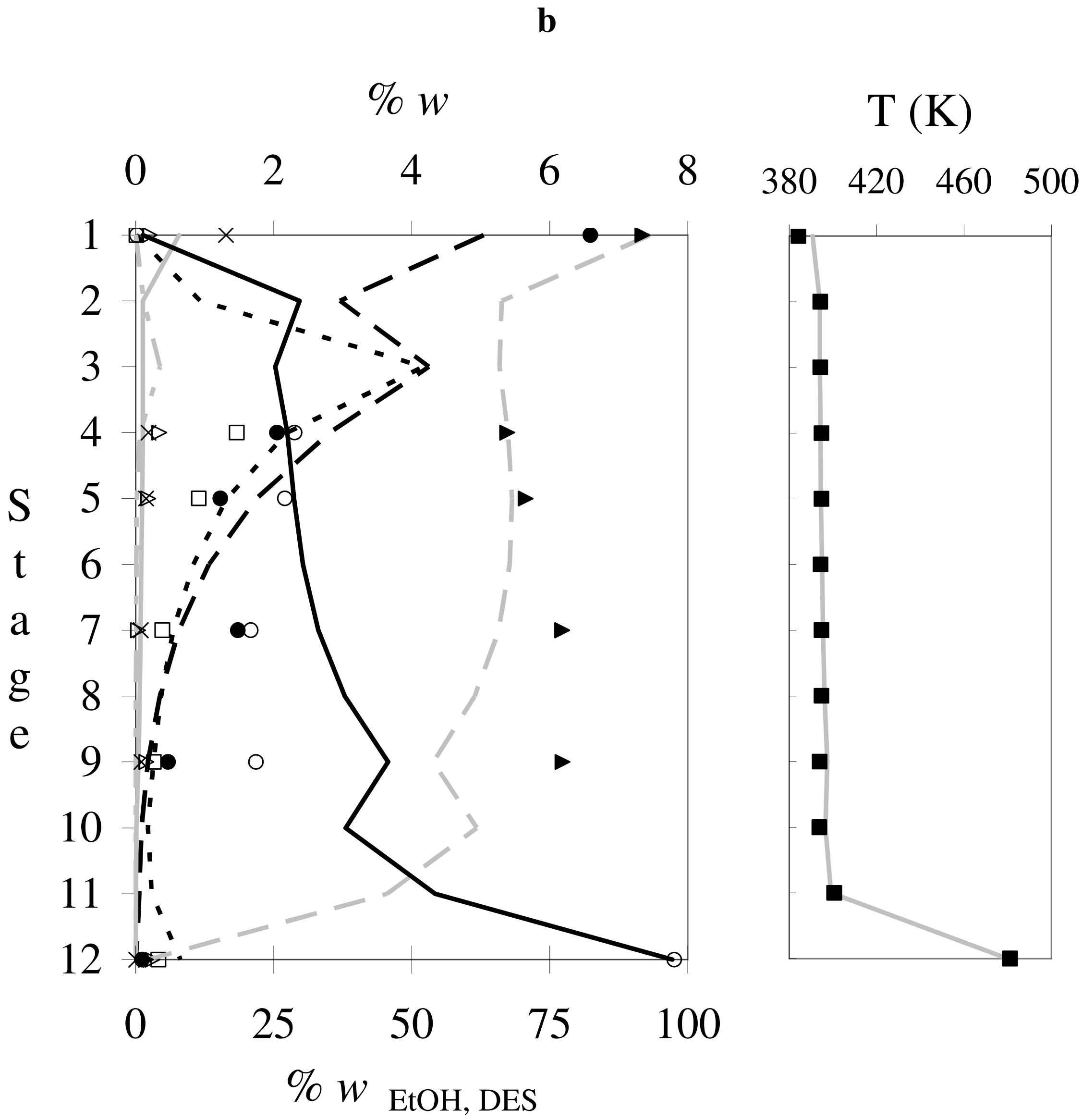

Figure 7-5. Continuation. b) Temperature and concentration profiles. Lines in column profiles represent results obtained by simulation. (○, ▬) - DES, (□, - -) - MES, (Δ, - - ▬ - -) - SA, (●, ▬ ▬) - H_2O, (▲, ▬ ▬) - EtOH, (X, ▬) - DEE.

7.4.2.1 Effect of reflux ratio in operation without pre-reactor

Figure 7-6 describes results obtained by simulation of Run 9 in which reflux ratio was varied. It is seen that SA conversion remains high even up to a reflux ratio of 10, because the large excess of EtOH drives first step of esterification (SA to MES) to completion.

However, in accord with experiment, the selectivity to DES goes through a maximum around a reflux ratio of 2.0 and declines at higher reflux ratios because H_2O recycling limits MES conversion and leads to DES hydrolysis. Low reflux ratios are therefore desirable for optimal column operation.

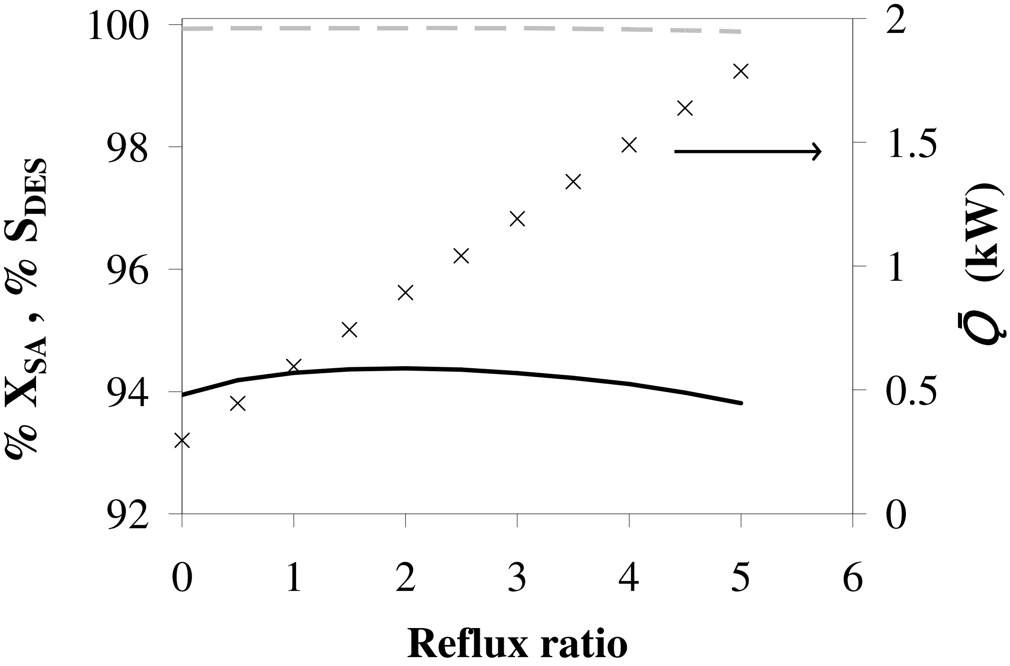

Figure 7-6. Effect of reflux ratio under experimental conditions in run 9. (▬ ▬) - SA conversion, (▬) - Selectivity to DES, (X) - Power at the reboiler.

7.4.2.2 Effect of splitting EtOH inlet flow

As discussed above, the use of the pre-reactor with the RD column requires less EtOH to achieve a homogeneous solution of the SA feed stream. Also, adding EtOH near the bottom of the column enhances overall DES yield (Run 11). Here, simulations were conducted to examine the effect of distributing EtOH between top and bottom feeds at conditions of Run 11A. Split ratio is defined as the ratio of EtOH flow introduced to a bottom feed over EtOH fed with SA.

The effect of varying split ratio from zero (Run 11A) to 0.5 (maximum to achieve a homogeneous SA solution) is presented in Figure 7-7.

Despite a lower SA conversion in the pre-reactor (from 88% to 82%) because of the smaller concentration of EtOH in the acid feed, increasing the EtOH split ratio produces a higher global SA conversion and higher selectivity to DES at the same reboiler power. Even with a higher DES concentration in the reboiler and thus a slightly higher reboiler temperature as split ratio is increased, a negligible increase in DEE formation is observed. This result indicates that using an elevated temperature pre-reactor (i.e. high SA solubility) and redirecting some ethanol to a feed near the bottom of the column results in increased DES yield from the process.

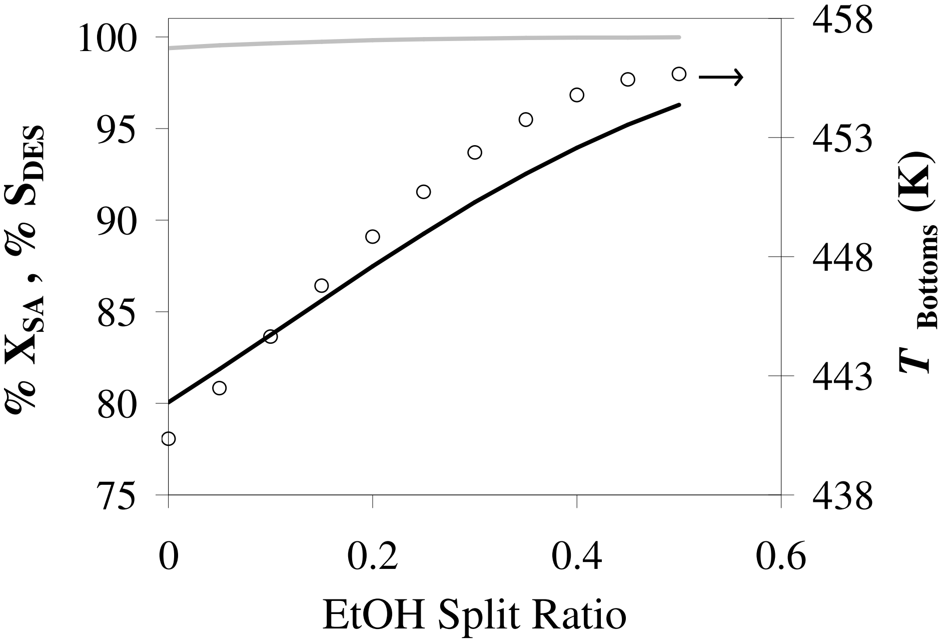

Figure 7-7. Effect of splitting total EtOH inlet flow in run 11A between two inlet streams: pre-reacted acid feed steam at the top and pure EtOH stream at bottom. (▬) - SA conversion, (▬) - Selectivity to DES, (○) – Reboiler temperature.

7.4.2.3 Effect of EtOH inlet flow at bottoms

Taking into account improvements achieved by splitting EtOH at Run 11A conditions, further simulations were carried out to examine the effect of increasing EtOH feed rate to the bottom of the column (Runs 11B, 11C), with the SA feed stream containing minimal EtOH (e.g. with SA at its solubility limit for the elevated temperature pre-reactor). The maximum inlet EtOH flow rate evaluated (25 g/min) corresponded to $f_{MC} = 1$ according to hydrodynamic calculations. Results are presented in Figure 7-8. As expected, SA conversion remains essentially complete while DES selectivity increases from 96% to 99.5%. Unfortunately, nearly twice the reboiler power is required to achieve this increase in selectivity, so such large EtOH use is not likely warranted.

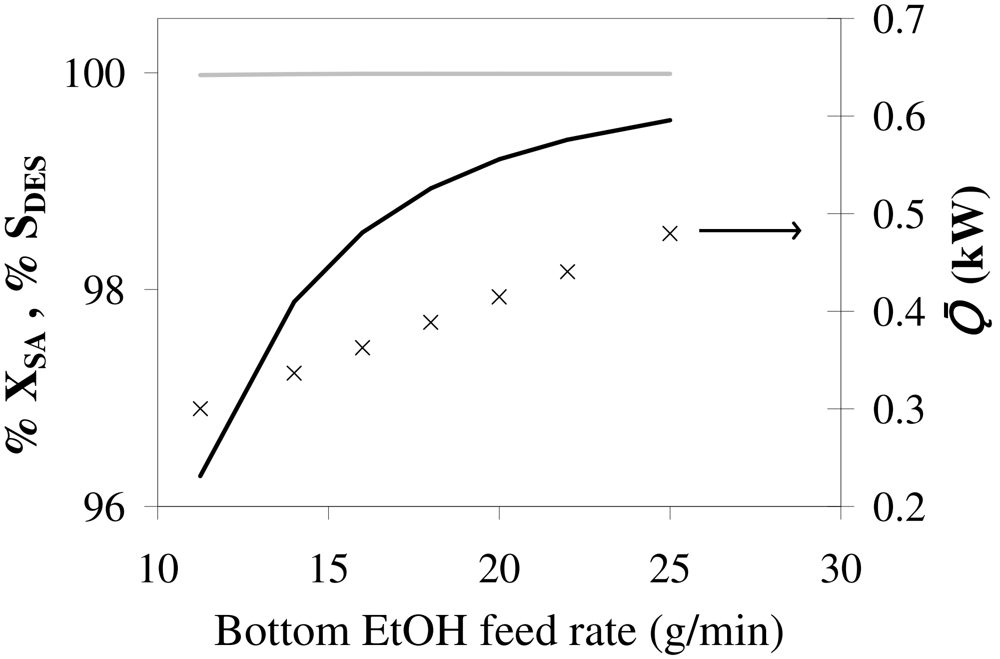

Figure 7-8. Effect of EtOH inlet flow at bottoms operating with pre-reacted acid fed at the solubility limit of SA in EtOH. (—) - SA conversion, (▬) - Selectivity to DES, (X) - Power at the reboiler.

7.4.2.4 Effect of reboiler power and reflux ratio using pre-reactor – column configuration

The effect of increasing boilup rate at improved conditions of Run 11A (with SA at its solubility limit and an EtOH split ratio of 0.5) at several reflux ratios up to the maximum hydrodynamic capacity of the column ($f_{MC} = 1$) is presented in Figure 7-9 and 7-10. In general, both SA conversion and selectivity to DES increase with reboiler power at low reflux ratios. As EtOH is removed in the distillate stream, it entrains water, thus driving esterification to completion. However, as observed in Figure 7-10a, increasing reflux ratio has a negative impact on selectivity to DES mainly due to H_2O recycling. In Figures 7-9b – 7-10, distillate flows were plotted to facilitate comparison between different reflux ratios. As observed in Figure 7-9b, above a certain distillate flow limit (~ 9 g/min) mostly succinic species remain at the bottom of the column and a sudden increase in reboiler temperature is observed. Above this level, any increase in heating power results in removal of MES and DES from the reboiler and the separation efficiency is severely reduced. Selectivity to DES increases above this limit because MES remains in the catalytic zone where it is consumed. However, a significant amount of DES appears at the top of the column, signifying a change in overall column performance. This sudden increase of temperature with a small change of inlet power was experienced experimentally in Run 11C. In Figures 7-10a and 7-10b, it is seen that when operating with distillates flows below ~ 9 g/min both SA conversion and selectivity to DES slightly increase with increased reflux ratio. Below this boilup rate, EtOH fed at the bottom flows downwards to the reboiler and is not used efficiently in the catalytic stages. However, some H_2O is removed in the distillate, shifting the equilibrium toward the product while EtOH is still at a large excess.

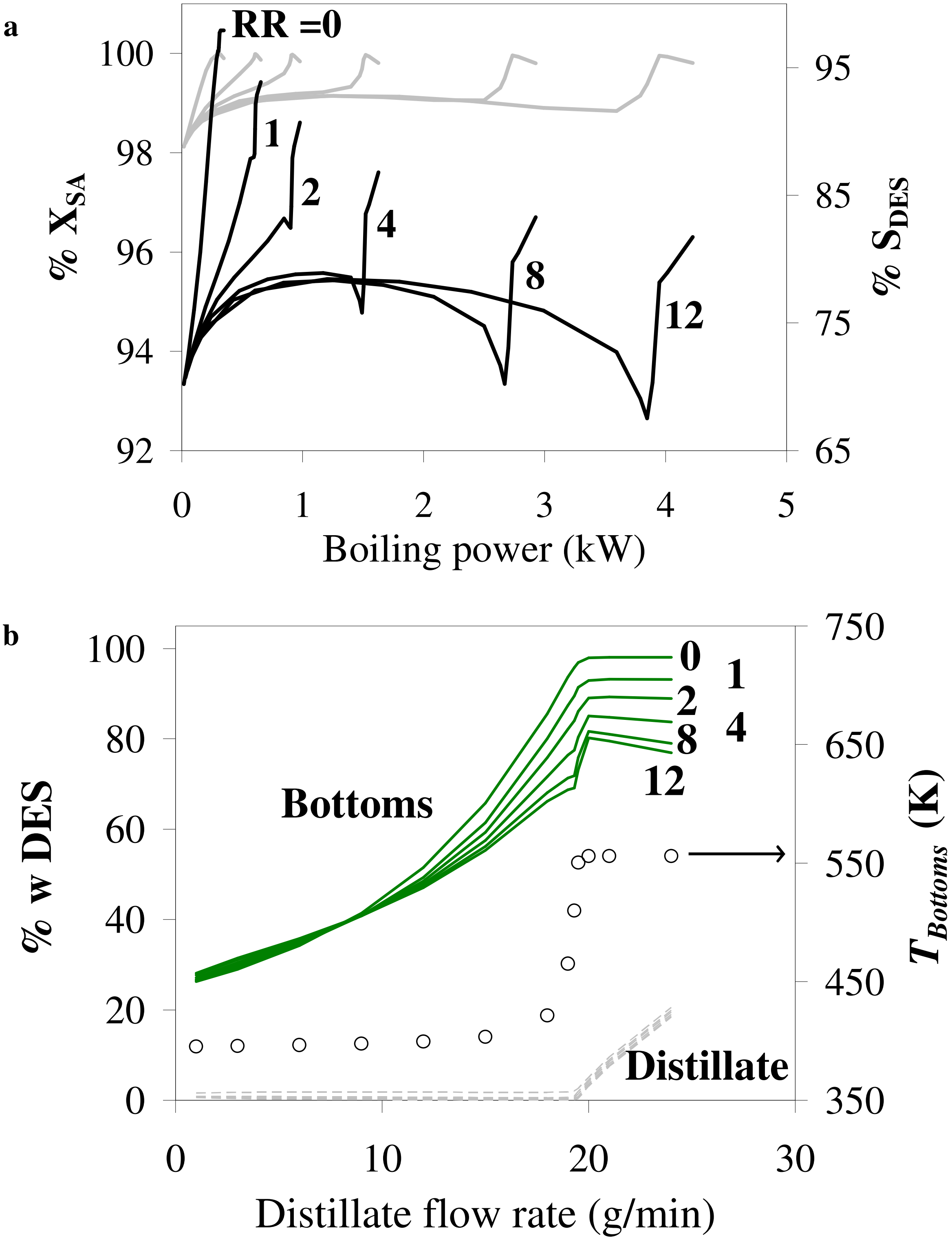

Figure 7-9. Effect of boiling power under different reflux ratios (RR = 0, 1, 2, 4, 8, 12) using pre-reactor and acid feed at the solubility limit of SA in EtOH. a) (▬) - SA conversion, (▬) - Selectivity to DES; b) (▬) - DES composition at bottoms, (- -) - DES composition in distillate, (○) - Reboiler temperature.

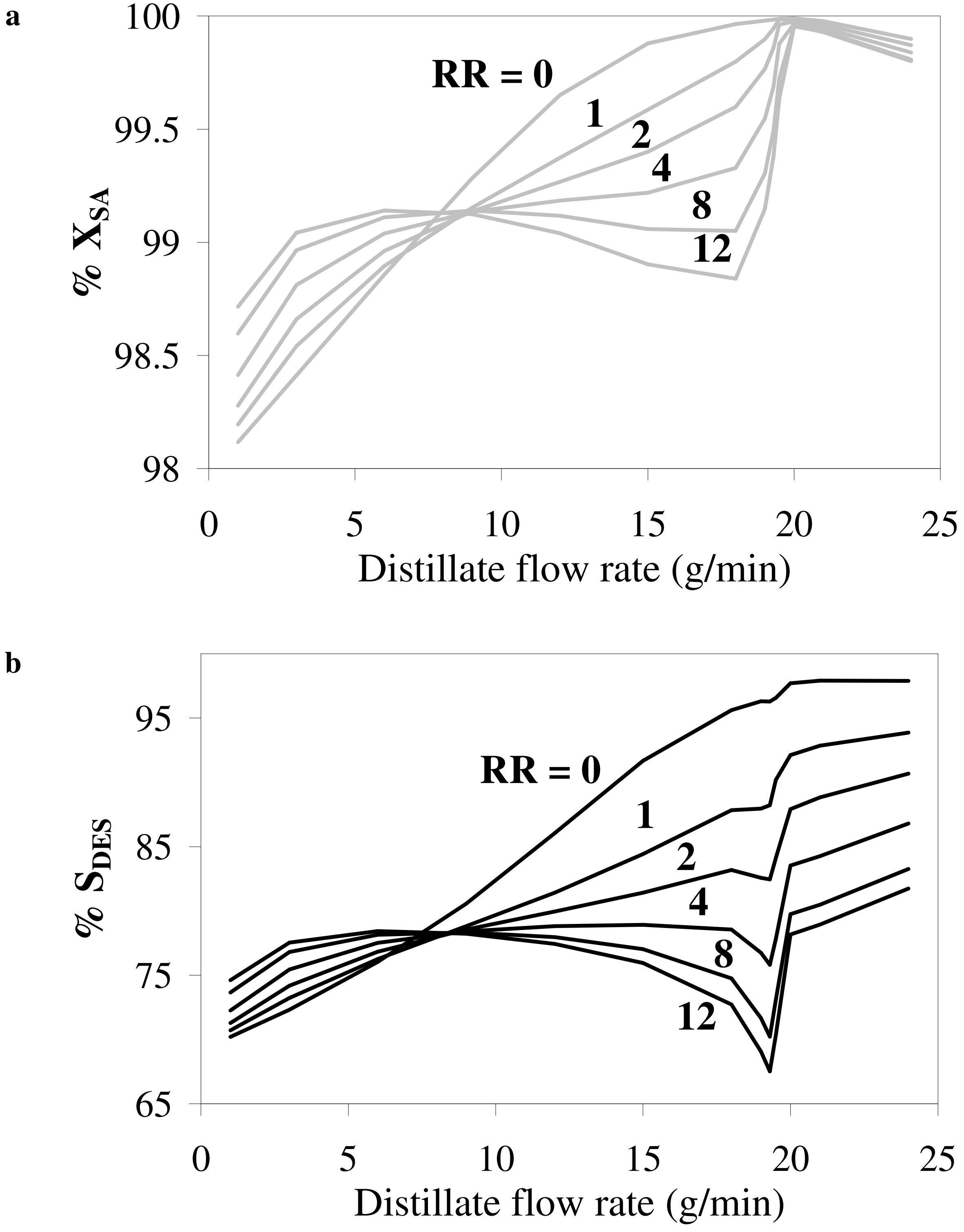

Figure 7-10. Effect of boiling power under different reflux ratios (RR = 0, 1, 2, 4, 8, 12) using pre-reactor and acid feed at the solubility limit of SA in EtOH. a) (▬) - SA conversion; b) (▬) - Selectivity to DES.

Increasing distillate flow above this level causes EtOH fed below the catalytic stages to move upward in the column and participate in reaction, also enhancing H_2O removal. At distillate flows above 9 g/min, any increase in reflux ratio has a negative impact on column performance as expected.

7.5 Conclusions

The synthesis of diethyl succinate by esterification of succinic acid and ethanol was studied using a stainless steel pilot scale reactive distillation system containing KATAPAK SP-11® filled with Amberlyst 70® as catalytic packing and Sulzer BX® in non-reactive stages. A set of experiments were carried out to investigate the performance of the system varying total pressure, reflux ratio, boiling power, feed flows, and use of ethanol feed below the reactive zone. Results indicated that is possible to obtain high conversions and yields of diethyl succinate above 98%. Simulations using a simple equilibrium stage model including phase equilibria and chemical kinetics previously obtained were developed to validate experimental observations using RADFRAC® model in Aspen Plus®. The model also took into account dehydration reaction to produce diethyl ether. Simulation results were compared with experiments showing good agreement and the model has prediction capabilities under different operation conditions.

Detailed analysis of experimental and simulation results indicated that a preferable configuration will require a pre-reactor operating with initial compositions of succinic acid and ethanol close to the solubility limit at reactor temperature. The pre-reacted feed has to be introduced in the column above the reactive zone while an ethanol stream must be located below catalytic stages to enhance both reaction conversion and water entrainment. Power supplied to the reboiler must be sufficient to drive ethanol fed at bottoms to the catalytic stages, and low reflux ratios (<0.5) are required to obtain high yields of diethyl succinate. While operation at higher pressures enhanced esterification rates, it also increased production of undesirable diethyl ether. The model developed here can be used to perform optimization of the process and to evaluate economics under different production configurations and scales.

REFERENCES

7.6 REFERENCES

[1] H. Van der Pol. Biobased innovations @ Purac: from lactic acid and lactide/PLA to succinic acid. The world Congress on Industrial Biotechnology & Bioprocessing. Washington D.C., USA. June. (2010).

[2] A. Orjuela, A. Yanez, C. T. Lira, D. J. Miller. Carboxylic Acid Recovery from Fermentation Solutions. US Patent application. Filed 2009.

[3] D. J. Thomas, D. L. Trimm and M. S. Wainwright, N. W. Cant. Chem. Eng. Process. 31, 4 (1992) 241-245.

[4] T. Turek, D.L. Trimm, D.StC. Black, N.W. Cant. Appl. Catal. A - Gen. 116, 1-2 (1994) 137-150.

[5] S. Varadarajan, D. J. Miller. Biotechnol. Prog. 15 (1999) 845–854.

[6] S.H. Vaidya, C.V. Rode, R.V. Chaudhari. Catal. Commun. 8, 3 (2007) 340-344.

[7] A. Cukalovic, C. V. Stevens. Biofuels, Bioprod. Bioref. 2 (2008) 505-529.

[8] C. Delhomme, D. Weuster-Botz, F. E. Kühn. Green Chem. 11 (2009) 13-26.

[9] G. Ding, Y. Zhu, H. Zheng, W. Zhang, Y. Li. Catal. Commun. 11, 14 (2010) 1120-1124.

[10] G. Ding, Y. Zhu, H. Zheng, H. Chen, Y. Li. J. Chem. Thechnol Biotechnol. 2010. n/a. doi: 10.1002/jctb.2503.

[11] S. Kulprathipanja (Ed.). *Reactive separation processes*. Ed. Taylor & Francis, Philadelphia - USA. 2000.

[12] A. Stankiewicz. Chem. Eng. Proc. 42 (2003) 137-144.

[13] A. Tuchlenski, A. Beckmann, D. Reusch, R. Düssel, U. Weidlich and R. Janowsky. Chem. Eng. Sci. 56 (2001) 387-394.

[14] S. Schoenmakers, B. Bessling. Chem. Eng. Proc. 42 (2003) 145 -155.

[15] R. Hiwale, N. Bhate, Y. Mahajan, S. Mahajani. Recent trends. Int. J. Chem. React. Eng. Review R1. 2 (2004) 1-52.

[16] G. Jam Harmsen. Chem. Eng. Process. 46, 9 (2007) 774-780.

[17] A. A. Backhaus. (1921) Method for the production of esters. US Patent 1400852.

[18] Cockrem, M. C. (2001). Process for the production of organic acids and esters thereof. US Patent 6291708 B1.

[19] C. Bianchi, V. Ragaini, C. Pirola and G. Carvoli. Appl. Catal. B. 40, 2 (2003) 93-99.

[20] N. Asthana, A. Kolah, D. Vu, C. T. Lira, D. J. Miller. J. Org. Process Res. Dev. 9 (2005) 599-607.

[21] D. J. Miller, N. Asthana, A. Kolah, D. Vu, C. T. Lira. (2006). Process for reactive esterification distillation. US Patent 7667068.

[22] A. Kolah, N. Asthana, D. Vu, C. T. Lira, D. J. Miller. Ind. Eng. Chem. Res. 47, 4 (2008) 1017-1025.

[23] D. Dunuwila. (2009). Process for the direct production of esters of carboxylic acids from fermentation broths. Canadian patent application 02657666.

[24] H. Bart, J. Reidetschlager. Sep. Sci. Technol. 30 (1995) 1849-1865.

[25] C. Bauduin, W. Fischer, R. Pinkos, E. Scholten. (2009). Method of producing a carboxylic alkyl ester. US patent application 0137825 A1.

[26] D. Sutton, G. Reed, G. Hiles. (2005, 2007). Process for the production of esters of mono-, di or polycarboxylic acids. WO patent 051885 A1, US patent application 0129565 A1.

[27] A. Orjuela, A. Kolah, X. Hong, C. T. Lira, D. J. Miller. Reactive Distillation in a Mixed Acid Esterification Process for Biobased Chemicals Production. 2009 AIChE Annual Meeting, Nov 8-13, Knoxville, TN, USA, (2009).

[28] A. Kolah, A. Orjuela, N. Hanna, C. T. Lira, D. J. Miller. Reactive distillation for the biorefinary: Pilot plant synthesis of succinic acid esters. 10AIChE - 2010 AIChE Spring Meeting and 6th Global Congress on Process Safety. Mar 21-25, San Antonio, TX, USA (2010).

[29] L. Götze, O. Bailer, P. Moritz, C. von Scala. Catal. Today 69 (2001) 201–208.

[30] J. Sieres, J. Fernández-Seara. Int. J. Refrig. 30 (2007) 58-67.

[31] A. Orjuela, A. J. Yanez, C. T. Lira, D. J. Miller. Kinetics of mixed succinic acid/acetic acid esterification with Amberlyst 70 ion exchange resin as catalyst. Submitted. Appl. Catal. A. (2010).

[32] M. Behrens, Ž. Olujić, P. J. Jansens. Chem. Eng. Technol. 31, 11 (2008) 1630-1637.

[33] S. Ratheesh, A. Kannan. Chem. Eng. J. 104 (2004) 45-54.

[34] A. Hoffmann, C. Noeres, A. Górak. Chem. Eng. Process. 43 (2004) 383-395.

[35] A. Kolodziej, M. Jaroszyński, I. Bylica. Chem. Eng. Process. 43 (2004) 457-464.

[36] Ž. Olujić, M. Behrens. Chem. Eng. Technol. 29, 8 (2006) 979-985.

[37] S. Venkataraman, W.K. Chan, J.F. Boston. Chem. Eng. Prog. 86, 8 (1990) 45-54.

[38] H. Renon, J. M. Prausnitz. AIChE J. 14 (1968) 135-144.

[39] J. G. Hayden, J. P. O'Connell. Ind. Eng. Chem. Process Des. Dev., 14, 3 (1975) 209-216.

[40] Aspentech, Aspen Physical Property System, physical property models/methods, Burlington, 2007.

[41] A. Orjuela, A. Yanez, D. Vu, D. Bernard-Brunel, D. J. Miller, C. T. Lira. Fluid Phase Equilibr. 290 (1-2) (2010) 63-67.

[42] A. Orjuela, A. Yanez, P. Rossman, D. Vu, Bernard-Brunel, D. J. Miller, C. T. Lira. Fluid Phase Equilibr. 290 (1-2) (2010) 68-74.

[43] A. Orjuela, A. Yanez, J. Evans, D., D. J. Miller, C. T. Lira. Phase equilibria in binary mixtures with monoethyl succinate. In revision. (2010).

[44] A. Orjuela, A. Yanez, J. A. Lee, D. J. Miller, C. T. Lira. Solubility and phase equilibria for mixtures with succinic acid. In revision. (2010).

[45] Y. Tang, H. Huang, I. J. Chien. Chem. Eng. Japan. 36, 11 (2003) 1352-1366.

[46] A. Kolah, N. Asthana, D. Vu, C. T. Lira, D. J. Miller. Ind. Eng. Chem. Res. 47 (15) (2008) 5313-5317.

[47] F. Carrillo, A. Martin, A. Rosello. Chem. Eng. Technol. 23 5 (2000) 425-428.

[48] Sulzer Chemtech. (2010) Structured packings for distillation, adsoption, and reactive distillation. [Online]. Available: http://www.sulzerchemtech.com/portaldata/11/ Resources //brochures/mtt/Structured_Packings_April_2010.pdf [2010, Nov 1].

8. Mixed Succinic Acid/Acetic Acid Esterification with Ethanol by Reactive Distillation

8.1 Summary

Simultaneous esterification of succinic acid and acetic acid with ethanol in a continuous reactive distillation unit has been studied. Experiments were carried out in a 6 m tall, 51 mm diameter pilot scale stainless steel column. The reactive zone consisted of structured packing KATAPAK SP-11® containing Amberlyst 70® as catalyst. BX® structured gauze packing was used in stripping and enrichment stages. Steady state experiments were performed under different conditions varying composition and number of inlet streams, column pressure, heating power at the reboiler, and reflux ratio. Conversions of ~ 100 % for both succinic acid and acetic acid were verified experimentally. While succinate esters were obtained as bottom products with purities of diethyl succinate higher than 98 %, acetate species were recovered mostly from distillates. Computer simulations based upon experimental phase equilibria and chemical kinetics were performed in Aspen Plus® using RADFRAC® model to reproduce steady state results. Good agreement between experiments and simulations was observed under different conditions evaluated. Model develop here can be used to scale-up a mixed acid esterification process.

8.2 Introduction

Fermentation of renewable substrates has been used as an alternative method to produce many chemical commodities currently obtained from petrochemical routes. Particularly, synthesis of carboxylic acids has gained major attention because they occur naturally in metabolisms of many microorganisms and can be used as building blocks for many other bio-based chemicals of commercial interest [1-5]. Among these, succinic acid (SA) has been recognized as a potential substitute for maleic anhydride to be used in the synthesis of 1,4 butanediol, γ-butyrolactone and tetrahydrofuran. SA can also be used to produce biodegradable deicing agents, bio-polymers, surfactants, plasticizers, green solvents and a large variety of value-added products [6-9].

Despite the large variety of organisms studied in SA production, major challenges include low titers produced in the broth (50-100 kg/m^3) and contamination with other byproducts. Reports indicate that acetic acid (5-40 kg/m^3), pyruvic acid (0-20 kg/m^3), lactic acid (0-14 kg/m^3), formic acid (0-5 kg/m^3), traces of other acids and even ethanol are also found in final products depending on microorganisms used during fermentation [2, 10-12].

Among many separation alternatives, reactive extraction of fermentation products with ethanol (EtOH) has been successfully applied to isolate SA in the form of esters [13]. In such processes, extraction occurs by esterification of the acid mixture while inorganic salts are removed from the organic solution. Using this approach, different esters can be obtained simultaneously and separation of the complex mixture can be performed by distillation. However esterification extent is limited by chemical equilibrium and removal of reaction products is required to drive reaction to completion.

In order to avoid thermodynamic reaction limitations in the system, reactive distillation (RD) can be used to simultaneously drive the reaction to high conversions and also simultaneously separate acids from various acids. RD also can reduce capital and energy costs by combining reactions and separations in a single unit. These advantages have been recognized at the industrial scale where many RD processes has been implemented [14-17].

Although RD has been successfully applied in esterification of single acids with EtOH, less is known about multiple reactions in a single column. Because SA has low volatility and low solubility in most solvents, fast esterification kinetics is required to avoid accumulation or precipitation at the bottom of the column, where succinate species are withdrawn as product. Fast kinetics is also required for other acids present in the mixture (e. g. lactic acid, pyruvic acid, malic acid). If SA is mixed with light carboxylic acids (e. g. formic acid, acetic acid), boiling rate and reflux ratio can strongly affect the performance of the operation because light acid esters are removed with the distillate stream. To achieve complete esterification of volatile acids they must have enough residence time in the reactive zone of the column and some reflux may be required to drive to high conversions. However water content in the reflux can be detrimental to the goal of high conversions.

Mixed acids esterification was studied even at earliest stages of RD development. Mixtures of acetic, propionic and butyric acids were simultaneously esterified with methanol using sulfuric acid as catalyst in one of the first reports of continuous RD processes [18]. Since then, few applications have been reported. Only recently, a mixed acid esterification by RD has been explored as a recovery method for maleic acid present in mixtures with different carboxylic acids in aqueous solutions [19].

Previous studies developed by our research program indicated that esterification of SA with EtOH can be carried out in a RD unit achieving high conversion and selectivity to diethyl succinate (DES) under continuous operation [20, 21]. Considering that the most common impurity in SA fermentation broths is acetic acid (AcOH), this work explores esterification of mixtures of SA and AcOH with EtOH using a continuous RD system.

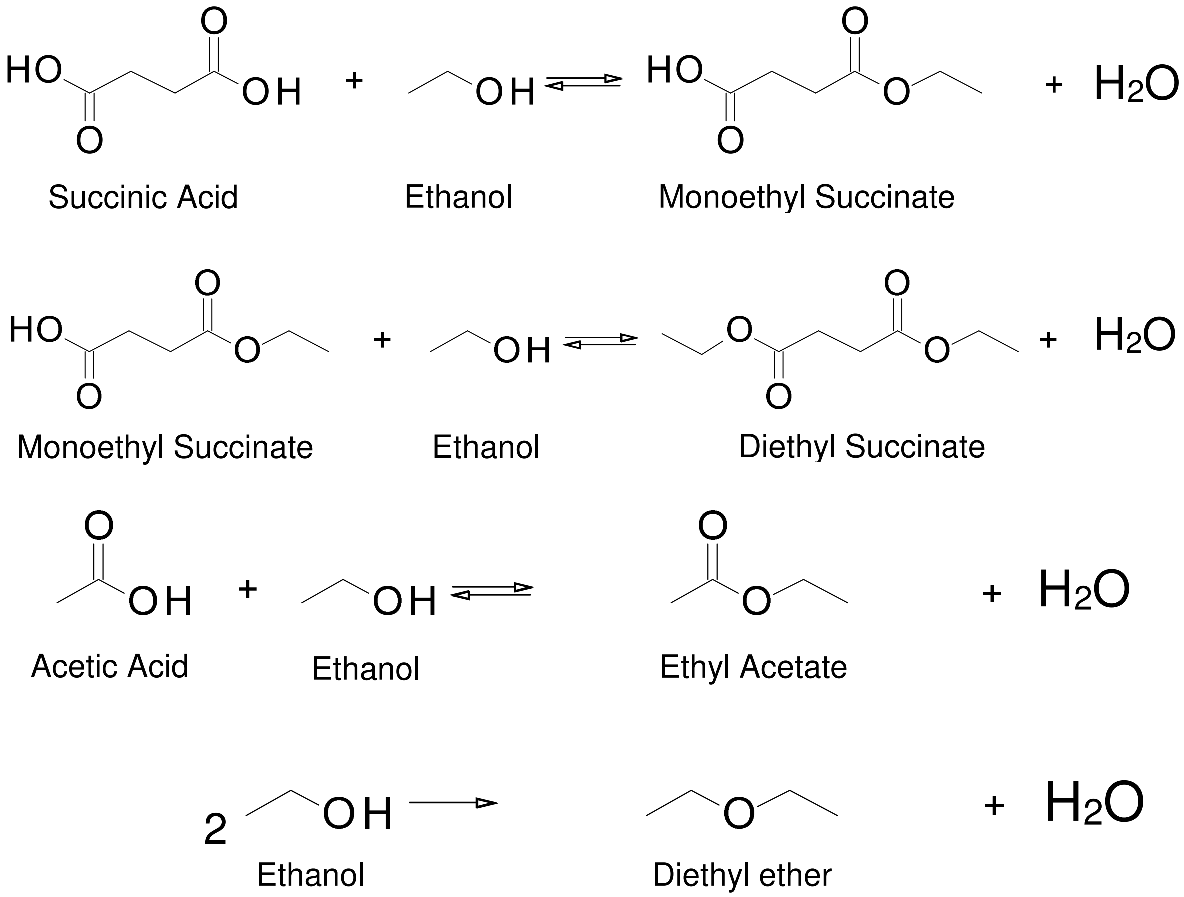

Figure 8-1. Reactions in mixed acids esterification process: esterification of succinic acid (SA) to monoethyl succinate (MES) and diethyl succinate (DES); esterification of acetic acid (AcOH) to ethyl acetate (EtOAc); dehydration of EtOH to diethyl ether (DEE).

Figure 8-1 presents chemical descriptor of the mixed acid esterification including possible dehydration of EtOH to diethyl ether (DEE).

Experiments to evaluate feasibility of the mixed acid esterification were conducted in pilot scale RD column under different conditions. Simulations to verify experimental observations and to explore improvements on the system were performed using process design software (Aspen Plus®, Version 7.1, AspenTech). The effect of major processing variables on

SA and AcOH conversions, separation efficiency, and DES purity were studied. Finally a preferable process configuration obtained by simulation of experimental RD system is presented.

8.3 Material and methods

8.3.1 Materials

Succinic acid (>99.5 %, Sigma-Aldrich), acetic acid (99.9%, Aristar), diethyl succinate (99.92%, Sigma-Aldrich), monoethyl succinate (89.3%, Sigma-Aldrich), ethyl acetate (HPLC grade, J. T. Baker), ethanol (200 proof, Decon Labs), water (HPLC grade, J.T. Baker), diethyl ether (EMD chemicals, 99.9%) *n*-butanol (99.9%, Mallinckrodt), and acetonitrile (HPLC grade, EMD) were used for experiments and analysis. Hydranal-coulomat E solution (Riedel-de Haën) was used in Karl-Fisher analysis. Amberlyst 70® and Amberlyst 15® ion exchange resins used as catalysts were purchased from Dow Chemical Co.

8.3.2 Analysis

Analysis was performed using gas chromatography (GC) for volatile components, liquid chromatography (HPLC) for succinate species, and Karl Fisher titration for water measurement. Samples were diluted 50-fold in water for HPLC analysis. When samples contained high amount of DES, EtOH was also added (~2% w/w) to ensure a homogeneous solution. A HPLC system with a Waters® 717 autosampler, and Waters® 410 refractive index and Perkin Elmer LC90 UV detectors was used for characterization of succinic species. A 100 x 7.6 mm fast acid analysis column (Bio-rad®) was used for the separation. 1 cm^3/min of 5 mM aqueous solution of H_2SO_4 was used as mobile phase.

In GC analysis, samples were dissolved 20 fold in acetonitrile using butanol as internal standard (5 % w/w). A Shimadzu® 2010 GC equipped with a Flame ionization detector and AOC-5000 autoinjector was used. 15 m Alltech® EC-WAX column (0.53 mm i.d., 1.20 μm film thickness) was used with the following temperature program: column initial temperature 313 K (1.37 min), ramp at 30 K/min to 353 K, and ramp at 40 K/min to 523 K (hold 4 min). The injection port was maintained at 553 K with a split ratio 5:1, and detector temperature was 573 K. Hydrogen was used as carrier gas (50 cm/s), with volume injections of 1 μL. Total

Calibration for both GC and HPLC was performed by analysis of samples of known composition in the range of interest. Repeatability within 0.5 % by mass was obtained.

Karl-Fisher analysis was performed using an Aquacount coulometric titrator AQ-2100.

8.3.3 Reactive distillation column description

Continuous RD experiments were carried out in a stainless steel pilot scale column. Table 8-1 describes major characteristics of the experimental equipment and Figure 8-2 shows a scheme of RD system.

High separation efficiency structured packings (Sulzer Chemtech Ltd.) were used in both catalytic and non-catalytic zones. As shown in Figure 8-2, the column was built with six flanged sections, 4 reactive and 2 non reactive. Reactive sections were separated by liquid redistributors that allowed sample collection. The column and the reboiler were wrapped with electric heating tapes and glass wood bands. Internal thermo-probes and external surface thermocouples were used to record temperature profiles inside and outside the column. The tapes along the column were individually controlled to reduce temperature gradients with surroundings.

Heating power in the reboiler was supplied with an electrical resistance submerged in the liquid and it was connected to an Omega controller. Liquid level was maintained with an overflow outlet controlled with a level indicator and a pneumatic valve.

Table 8-1. Characteristics of reactive distillate unit

Material of construction		SS-316
Rated pressure (kPa)		2000
Rated temperature (K)		573
Diameter (cm)		5.1
Stripping zone	Height (cm)	74
	Packing	BX®
Reactive zone	Height (cm)	360
	Packing	Katapak-SP-11®
	Catalyst	Amberlyst 70®
	Catalyst Particle size (mm)	> 0.5
	Catalyst loading (kg/m^3)	76
Enrichment zone	Height (cm)	42
	Packing	BX®
Reboiler	Type	Kettle
	Heating element	Stainless steel coated electrical resistance
	Maximum Power (kW)	2.4
	Hold-up (m^3)	0.0015
Condenser	Type	Total
	Geometry	Coiled concentric tubes
	Inner tube diameter (cm)	0.63
	Outer tube diameter (cm)	1.27
	Cooling fluid	Water-glycol
	Cooling fluid chiller	Julabo FL 2506®
	Operating temperature range (K)	258 – 313
	Cooling power at 263 K (kW)	0.3
Pre-reactor	Construction material	Pyrex glass
	Volume (m^3)	0.075
	Maximum Power (kW)	2
	Stirrer power (kW)	0.25
	Catalyst	Amberlyst 15®
	Catalyst loading (% w/w)	2

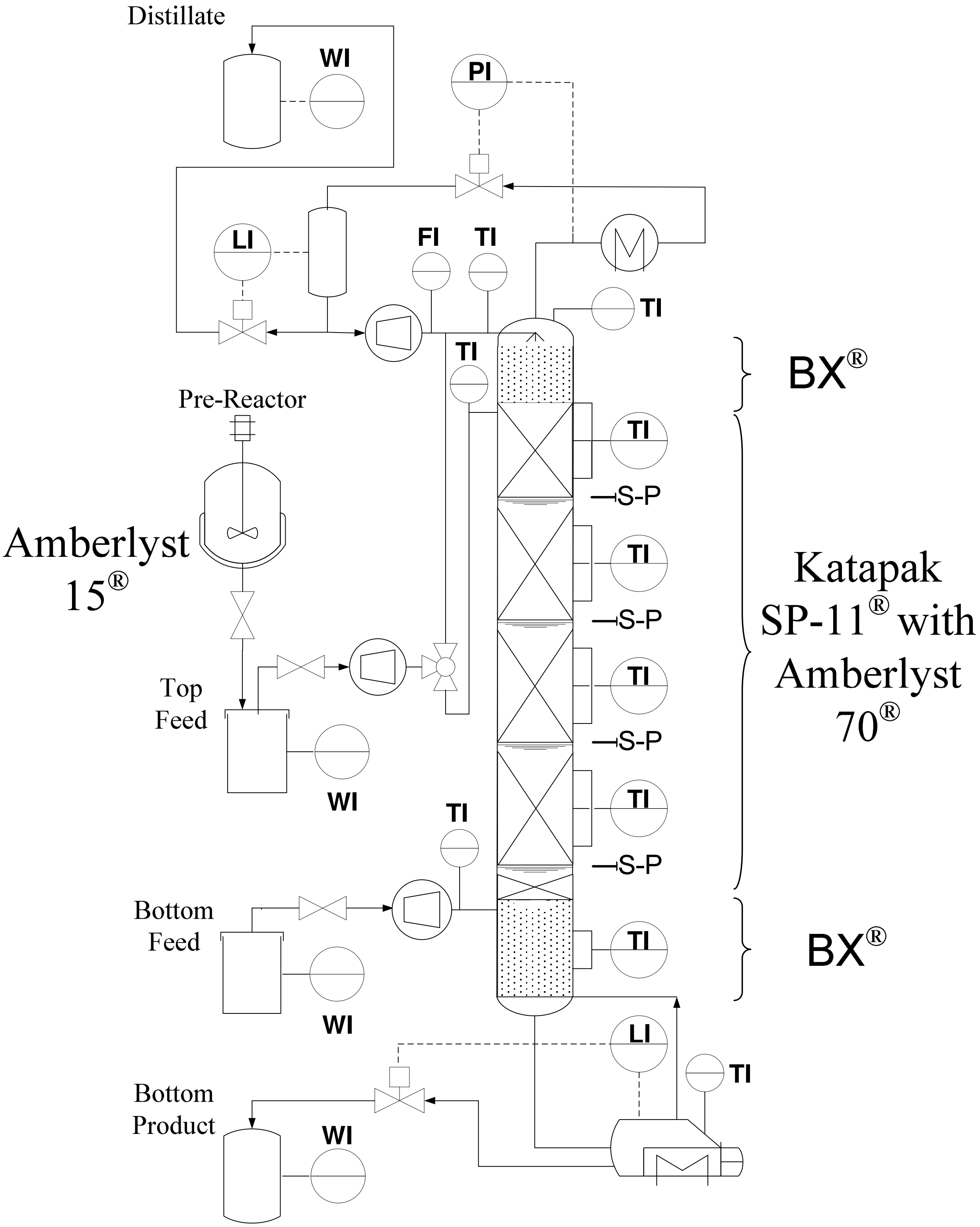

Figure 8-2. Scheme of pilot plant RD column with internal catalytic packing Katapack-SP-11® (middle zone) and BX® structured packing (doted zone).

Column pressure was maintained with a solenoid valve that controlled outlet vapor flow at the top. After the condenser, a liquid reservoir was used to collect distillate. Reflux was dispensed from this reservoir via a controlled flow pump, and the flow rate was registered with a coriolis flowmeter. Because succinate species and acetic acid have lower volatilities than EtOH, acid solution was fed from the upper part of the column. When the column operated without reflux acid stream was fed closer to the top of the column. Using reflux, acid fed was introduced just above the catalytic packing. In some experiments an additional EtOH inlet stream was fed below the catalytic zone.

Inlet streams were fed from tanks positioned on electronic balances using heat-traced and insulated pipelines and diaphragm pumps. Inlet temperatures were maintained as close as possible to the correspondent internal temperature of the column at the feed location.

8.3.4 Reactive distillation column operation

To avoid solids precipitation, the acid stream was introduced at the column close to the solubility limit of SA in EtOH at room temperature (~ 8 wt %). Concentration of AcOH in this stream was 1/3 to 1/10 of SA. This is the usual ratio of concentrations observed in different fermentation broths. In most experiments some EtOH was kept in the reboiler to maintain boiling temperature low enough to avoid unsafe conditions or thermal decomposition of succinate species. When the column was operated with high concentrations SA in acid feed, this stream was pre-reacted in a separate batch reactor under total reflux at atmospheric pressure for 24 h before the experiment. The resulting feed solution was a partially converted mixture (acids, esters, EtOH and H_2O) soluble in EtOH.

To reduce the time required to achieve steady state liquid hold-up drained from a previous run was kept in the reboiler. In typical operation, the column was started by slowly turning on the reboiler heater and the external heating tapes as the vapor reached the different zones of the column. After vapors reached the condenser, total reflux was maintained until a stable temperature profile and pressure were attained. Then feed pumps were started at the specified rates for the experiment and products from distillate and bottoms started to be collected.

Stream flow rates, acid value of bottom product, column top pressure and temperature profiles were recorded on time intervals of 15 to 30 minutes throughout the run. Outlet flows from distillate and bottoms were obtained by measuring volume and density of liquid collected in volumetric flasks. The acid value (AV, mgKOH/g) of the bottom product was obtained by titration with 0.1M solution of NaOH in EtOH-H_2O until final point with phenolphthalein.

After reaching steady conditions, liquid samples from column redistributors, reboiler and distillates reservoir were collected in sealed vials every hour until the end of the experiment. These samples were refrigerated until they were analyzed.

Experimental steady state was assumed after reaching AV within maximum ~ 5 % variation in consecutive samples, temperature profiles change over time of ± 0.5 K, and constant pressure at the top (± 7 kPa). Additional steady state criteria were: maximum variations of inlet and outlet within a ± 5 wt % of the set point, and closed mass and component balance on the column streams (± 5 %).This last criterion was evaluated after run ended because the long time required for sample preparation and analysis.

After final samples were collected, feed pumps were shut down, inlet and outlet valves closed, and reboiler and column heaters were turned off. Evaporation was stopped by pressurizing the column at ~ 700 kPa with nitrogen. Finally refrigeration at the condenser was stopped and the general power supply was shut down.

8.4 Results and discussion

8.4.1 Reactive distillation experiments

Operating conditions during RD experiments are listed in Table 8-2. In most experiments, the inlet feed rate and temperature of the acid stream were maintained as constant as possible to facilitate comparison among different operational conditions.

A typical dynamic behavior of the RD system is presented in Figures 8-3 and 8-4 in run 14A and 14B. In general steady conditions were obtained after ~ 20 h of operation.

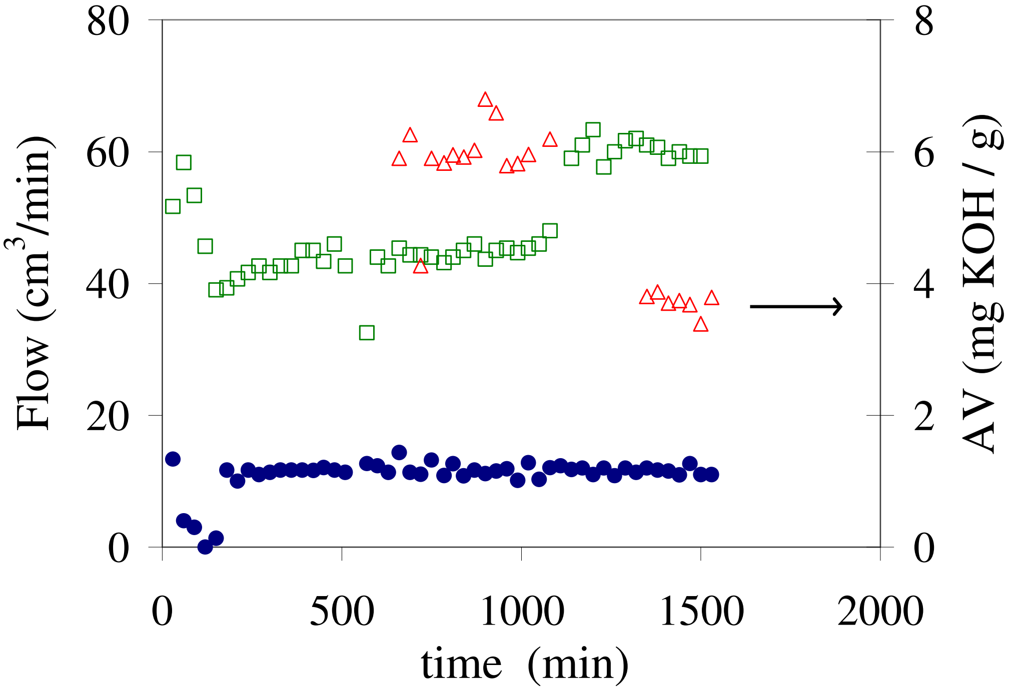

Figure 8-3. Outlet flows and acid value profiles with time during approach to steady state in runs 14A (up to 1100 min) and 14B (after 1100 min). (□) - Distillate flow, (●) - Bottoms flow, (Δ) - Acid value at the bottoms.

Table 8-2. Experimental conditions for continuous RD at pilot plant scale

Run Code	Pre-Reactor	Reboiler Power (kW)	Gauge *P* (kPa)	Reflux Ratio	Top Feed (SA in EtOH-H_2O)				Bottom feed (EtOH)	Distillate Flow (g/min)	Bottoms		
					wt% SA	wt% H_2O	wt% AcOH	Flow (g/min)	Flow (g/min)		Flow (g/min)	AV[‡]	*T* (K)
12A	No	0.96	310.3	0	6.7		2.2	30.3 ± 0.3	0.0	20.6 ± 0.4	10.1 ± 0.2	12.5	394.2
12B	No	1.15	310.3	0.59	6.7		2.2	30.2 ± 0.2	0.0	20.1 ± 0.5	10.6 ± 0.4	11.8	394.2
12C	No	1.41	310.3	0.36	6.7		2.2	30.3 ± 0.2	11.2 ± 0.5	32.2 ± 0.7	9.4 ± 0.7	5.6	394.2
13A	No	1.03	310.3	0	6.7		2.2	30.7 ± 0.5	0.0	25.2 ± 0.7	5.4 ± 0.7	22.3	394.2
13B	No	1.44	310.3	0.97	6.7		2.2	30.3 ± 0.2	0.0	24.9 ± 0.4	5.8 ± 0.5	19.4	394.2
13C	No	1.68	310.3	0.65	6.7		2.2	30.4 ± 0.1	12.5 ± 0.2	36.1 ± 0.4	6.3 ± 0.4	5.8	394.2
14A	Yes	1.63	310.3	0	25.0[†]		2.5[†]	31.2 ± 0.4	16.6 ± 0.6	35.9 ± 0.7	11.7 ± 0.8	5.9	505.3
14B	Yes	1.85	310.3	0	25.0[†]		2.5[†]	30.9 ± 0.1	28.7 ± 0.6	46.5 ± 0.7	11.7 ± 0.5	3.7	515.8
20A	Yes	1.92	34.5	0.35	25.0[†]		2.5[†]	29.6 ± 0.3	30.5 ± 0.9	49.7 ± 1.0	9.6 ± 1.2	7.8	498.2
21A	No	1.49	34.5	0	8.0	5.5	0.8	41.9 ± 2.6	23.2 ± 0.4[§]	57.4 ± 3.6	7.8 ± 2.4	75.8	364.6
22A	Yes	1.50	34.5	0	8.0[†]	5.5[†]	0.8[†]	45.2 ± 0.7	23.5 ± 0.4[§]	58.8 ± 1.2	9.4 ± 1.6	42.9	365.6
22B	Yes	1.94	34.5	0.29	8.0[†]	5.5[†]	0.8[†]	45.0 ± 0.4	23.8 ± 0.4[§]	59.5 ± 0.5	8.5 ± 0.7	47.7	363.3
23A	No	1.92	34.5	0	8.0	91.2	0.8	30.6 ± 0.6	29.8 ± 0.3	44.0 ± 4.1	17.2 ± 6.0	131.2	379.1
24A	No	2.40	34.5	0	6.2	93.0	0.8	30.9 ± 0.4	55.4 ± 0.9	67.9 ± 1.7	17.3 ± 2.0	50.6	362.9
26A	No	2.35	34.5	0.58	6.7	92.7	0.6	29.4 ± 1.1	28.9 ± 1.2	40.9 ± 0.7	14.7 ± 1.0	119.2	381.3

[†] SA concentration is top feed is reported before pre-reaction

[§] 6 wt% H_2O in EtOH

[‡] Acid value, mg KOH / g

Table 8-3. Summary of outlet streams composition obtained in RD experiments

Run Code	Distillate composition wt%								Bottoms Composition wt %								Conversion §		S_{DES} (%) ‡
	H_2O	DEE	EtOAc	EtOH	AcOH	MES	DES	SA	H_2O	DEE	EtOAc	EtOH	AcOH	MES	DES	SA	SA	AcOH	
12A	3.1	2.1	4.2	90.4	0.1	0.1	0.0	0.0	2.9	0.0	0.1	61.6	0.1	2.9	32.3	0.1	99.2	94.9	89.5
12B	3.2	2.0	4.3	90.3	0.1	0.1	0.0	0.0	3.4	0.0	0.0	66.5	0.1	2.7	27.1	0.1	99.2	95.0	88.6
12C	3.3	1.3	2.6	92.5	0.1	0.1	0.0	0.0	0.8	0.0	0.0	66.5	0.1	1.4	31.0	0.1	99.4	94.7	93.2
13A	3.0	1.4	3.6	91.8	0.1	0.1	0.0	0.0	2.1	0.0	0.0	37.3	0.1	5.5	54.5	0.3	98.7	94.4	88.7
13B	3.9	1.2	3.4	82.4	0.1	0.1	0.0	0.1	1.9	0.0	0.0	55.8	0.1	4.3	37.7	0.1	98.2	95.1	86.9
13C	2.9	1.6	2.3	93.0	0.1	0.1	0.0	0.1	0.3	0.0	0.0	48.6	0.1	1.2	49.6	0.2	98.6	94.1	96.3
14A	8.2	1.8	2.7	87.2	0.0	0.1	0.0	0.0	0.1	0.0	0.0	0.5	0.1	1.2	98.0	0.2	95.3† 99.7	82.1† 97.9	98.4
14B	6.1	1.8	2.0	90.0	0.0	0.1	0.0	0.0	0.1	0.0	0.0	0.4	0.1	0.9	98.3	0.2	99.7	97.4	98.7
20A	5.1	0.1	1.7	92.9	0.1	0.0	0.0	0.2	0.0	0.0	0.0	6.5	0.0	2.3	90.4	0.6	96.8† 97.6	86.1† 95.5	97.0
21A	7.6	0.0	0.7	91.6	0.1	0.0	0.0	0.0	6.0	0.0	0.0	35.4	0.1	13.8	42.9	1.8	95.7	85.4	72.2
22A	7.4	0.0	0.5	92.1	0.0	0.0	7.4	0.0	3.7	0.0	0.0	34.4	0.3	9.7	3.7	0.0	96.8† 98.2	78.5† 87.0	81.5
22B	6.9	0.0	0.7	92.3	0.1	0.0	6.9	0.0	6.1	0.0	0.0	35.4	0.4	10.8	6.1	0.0	98.0	78.9	78.2
23A	40.3	0.0	0.3	59.2	0.1	0.0	0.0	0.1	80.5	0.0	0.8	5.4	0.0	4.3	0.1	8.8	28.4	77.7	2.2
24A	34.0	0.0	0.2	65.5	0.1	0.0	0.0	0.1	34.8	0.0	0.0	53.2	0.1	5.3	4.4	2.3	72.6	60.9	41.0
26A	36.1	0.0	0.4	63.3	0.1	0.0	0.0	0.0	85.9	0.0	0.0	0.0	0.1	1.9	0.0	12.0	11.7	70.1	5.3

§ Conversion in mole percentage.

‡ Selectivity to diethyl succinate.

† Pre-reactor final concentration fed to column.

As observed in Figure 8-4, a slight change in a process variable between runs 14A and 14B (different EtOH feed flow as reported in Table 8-2) drove the system to a new steady condition but in less time (~ 6h). In most experiments this programmed study of variables allowed to reduce operating time and also to minimize waste generation.

Scatter observed in flows are due to pulsating behavior obtained by using overflow level control in the reboiler and the condensates reservoir. Level controllers might be affected by excessive foaming and also by uneven evaporation. This might cause displacement of liquid level from operating set point, creating flow fluctuations. During experiments, short flow irregularities in top and bottoms outlet streams were observed even at steady state. However bottoms and distillates concentrations were fairly constant with time in most experiments. Figure 8-4 suggests that on-site AV measurement is a rapid and good indicator to ensure steady state conditions. A summary of results obtained during RD experiments are listed in Table 8-3. Reported concentrations were obtained by reconciliation of different analytical methods. Succinate species are reported as the average of HPLC and GC analysis, while concentrations of other components are obtained by GC. H_2O content was obtained by Karl Fischer analysis.

In general, high conversions of SA and AcOH together with high selectivity to DES were achieved in most experiments. In order to evaluate feasibility of processing acid streams diluted in water (resembling acidified fermentation broth), aqueous acid solutions were used as feed in experiments 23A, 24A and 26A. Only in these experiments low conversions were observed.

Operating at low conversion conditions was challenging because solids would precipitate and obstruct bottom outlet lines as the streams cooled. This affected normal liquid withdrawal at bottoms, and large flow fluctuations were observed during operation. After data reconciliation it was noticed that that experiments 23A, 24A and 26A did not reach steady state.

Run 14A - Bottoms

Run 14A - Distillate

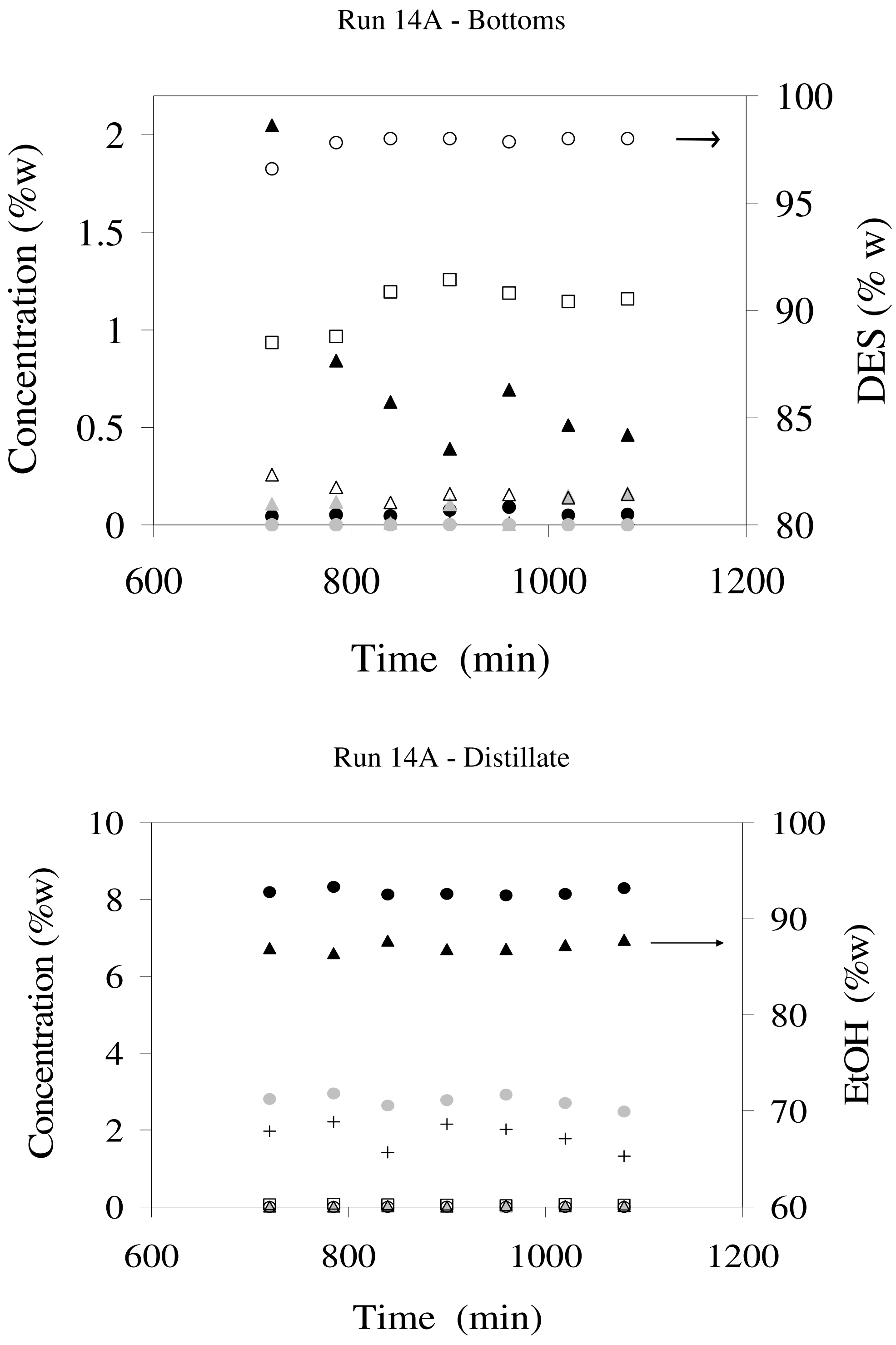

Figure 8-4. Time evolution of composition in bottom and distillate products in run 14A during approach to steady state. (○) - DES, (□) - MES, (Δ) - SA, (▲) – AcOH, (●) – EtOAc, (●) - H_2O, (▲) - EtOH, (+) - DEE.

In experiments 21A, 22A and 22B the acid feeds were prepared in ethanol 190 proof (~ 5 wt % H_2O) and a pre-reactor + column configuration was used. These experiments were performed to evaluate feasibility of operation using recycled ethanol.

Owing to the large excess of EtOH in the system, the column operated within few degrees of EtOH boiling point at working pressure. However, the reboiler temperature was higher due to high concentration of succinate species and it was strongly affected by the EtOH concentration. This was clearly observed in runs 14B and 20A that were operated under the same pressure and similar feeds. An increase of ~ 20 K in reboiler temperature was observed with a slight change in EtOH composition. Even though the reboiler operated at high temperatures in some experiments, no degradation products were observed in chromatographic analysis.

During experiments it was observed that the temperature sensor at the top of the column consistently reported temperatures below the boiling point of the mixture indicating that it could be cooled by inlet streams (top stream or reflux).

8.4.1.1 Effect of reflux ratio

In experiments operated without water in the inlet streams, and due to the large excess of EtOH in the system, conversions of SA and AcOH were not significantly affected by increasing reflux ratio as observed in runs 12A and 12B. However a slight decrease was observed in selectivity to DES. This was confirmed in experiments 13A and 13B that operated at different reflux ratios but with higher distillate flows than experiment 12. The negative effect of increasing reflux ratio was clearer in experiments 22A and 22B (introducing water in feed streams). In this case conversion of AcOH dropped significantly as well as selectivity to DES due to water recycling into the system.

8.4.1.2 Effect of column pressure

As column pressure increased, higher temperatures were observed along the column and in the reboiler. Despite the higher temperatures esterification conversions were not particularly enhanced. However higher dehydration of EtOH to DEE was observed. This behavior is explained considering the large excess of EtOH in the system and also strong acidity of Amberlyst 70®.

8.4.1.3 Effect of EtOH feed

Higher conversions and high selectivity to DES were obtained by feeding EtOH below the catalytic zone of the column. This can be observed by comparing results obtained in runs 12B and 12C, and also in experiments 13B and 13C. This behavior was also verified when processing pre-reacted acid feed as observed in runs 14A, 14B and 20A. EtOH enhanced entrainment of water in distillates while promoting esterification of esters in the reactive zone.

8.4.1.4 Operation with pre-reactor

In general higher esters yield were obtained operating with pre-reacted acid feed. Concentrations obtained after processing acid stream in the pre-reactor were close to chemical equilibrium conditions for both SA and AcOH esterification. Despite high conversion of SA in pre-reactor, selectivity to DES was around 50 to 60%. In runs 14A, 14B and 20A column operated with high concentrations of SA in the acid feed. In these experiments high concentration of succinate species were observed at the reboiler, and consequently high temperatures were obtained at bottoms. Specifically in run 14 B it was verified that the column can operate with almost complete conversion of acids, obtaining high purity of DES (> 98%) at the bottoms and recovering EtOAc in distillate stream.

8.4.1.5 Effect of water in the feed

As observed in experiments 21A, 22A and 22B operating with ethanol 190 reduces conversion of both SA and AcOH as well as the selectivity to DES. In these experiments high concentrations of MES and H_2O were found at the bottom product of the column. Conditions were even worse when reflux was used at the top of the column (run 22B). In this case separation efficiency between succinate and acetate species was affected, because major part of non-converted AcOH was entrained to the bottoms by the water recycled in the system. When operation was performed feeding aqueous acid solutions (runs 23A, 24A and 26A) low conversions were obtained. A large amount of EtOH at the bottoms was required to obtain SA and AcOH conversions of ~ 70 and ~ 60% respectively. However MES was the predominant succinate specie in the final product. In these experiments high boiling rates were used to remove major part of the water, but because reboiler power limitations it was not possible to operate under higher distillate flows. This indicates that operation of RD system with aqueous acid solutions as directly obtained from acidified fermentation broths might not be economically feasible. To extent the study of performance of RD system under different conditions, and considering the large amount of resources required in pilot plant experiments, a simulation model of the system was developed and validated with results described above.

8.4.2 Simulation of RD experiments

Steady state simulations of RD operation were performed using an equilibrium stage model (RADFRAC®) in Aspen Plus®. Phase equilibria were modeled by using NRTL equation to calculate activity in the liquid phase [22], and Hayden O-Connell (HOC) equation for the vapor phase [23]. Binary parameters were obtained from experiments or literature and were reported in previous works from our group [24-29]. Rates of reactions were described by using pseudo-homogeneous activity-based kinetics previously developed for Amberlyst 70® [29]. Kinetics for Amberlyst 15® and self-catalyzed SA esterification were fitted to activity based model from collected data in a previous work [30]. Amberlyst 70® kinetics was used to model reactive stages in the column. Self-catalyzed kinetics was included in non-catalytic stages in the stripping zone. Pre-reactor was modeled as a CSTR with 24h retention time using Amberlyst 15® kinetic model. Kinetic parameters are summarized in Table 8-4, and parameters used for simulation of pilot plant experiments are listed in Table 8-5.

Table 8-4. Parameters for activity-based kinetics used in simulation of RD experiments

Reaction	Parameter	Amberlyst 70®	Amberlyst 15®	Self-Catalytic
SA + EtOH ↔ MES + H_2O	k_0 (kmol/ kg $_{CAT}$) (1/s)	$1.04\text{x}10^4$	$5.17\text{x}10^3$	$1.57\ \text{x}10^{5\ §}$
	E_a (kJ/kmol/K)	46200	46900	57300
	K_{EQ}		48.9	
MES + EtOH ↔ DES + H_2O	k_0 (kmol/ kg $_{CAT}$) (1/s)	$2.11\text{x}10^3$	$7.0\text{x}10^4$	$17.8^{§}$
	E_a (kJ/kmol/K)	46600	61400	34400
	K_{EQ}		10.14	
AcOH + EtOH ↔ EtOAc + H_2O	k_0 (kmol/ kg $_{CAT}$) (1/s)	$1.03\text{x}10^4$	$1.28\ \text{x}10^3$	-
	E_a (kJ/kmol/K)	47600	44600	-
	K_{EQ}	12.11	2.12	-
2 EtOH → DEE + H_2O	k_0 (kmol/ kg $_{CAT}$) (1/s)	$4.99\ \text{x}10^4$	$8.06\ \text{x}10^{4\ ‡}$	-
	E_a (kJ/kmol/K)	85400	$86900^{‡}$	-

[§] Pre-exponential factor has units of $(\text{kmol/m}^3)(1/\text{s})$

[‡] Mole fraction model assuming unitary activity coefficients.

Number of stages in simulation of pilot plant column were determined taking into account the height equivalent to a theoretical stage (HETP = 0.5 m) reported for structured packing [31, 32]. Hydrodynamic conditions in the column were estimated using correlations for structured packings included in Aspen Plus. Because neither KATAPAK SP-11 or BX are included in the data base, available parameters for a structured packing (MELLAPAK-250Y®, Sulzer) with similar liquid hold-up, pressure drop and HETP [33] were used in simulations. In each case fractional approach to maximum capacity (f_{MC}) was varied to match calculated column diameter with that of the pilot plat unit.

Table 8-5. Parameters used for simulation of RD system

Parameter		
Total number of stages (N)		12
Rectifying stages		2
Reactive stages	Catalytic	3-9
	Non-catalytic	10-12
Feed Stages	Acid feed	Above 3
	EtOH feed	On 10
Column pressure drop per stage (kPa)		0.07
Murphree stage efficiency (stages 2 to 11)		0.5
Liquid holdup (cm^3) (stages 2 to N-1) (10 % vol)		98.2
Reboiler holdup (cm^3)		1500
Product removal stage	Top	1
	Bottom	12
Catalyst loading ($kg_{Catalyst} / m^3_{Column}$)		78
Catalyst loading at pre-reactor (% w/w)		2

Because in most experiments temperature at the reboiler was governed by EtOH concentration, distillate flows were adjusted in each simulation within the range of variation observed in experimental flows (~ 5%) to match both, EtOH concentration and temperature at the bottoms. Only those runs that reached steady state were evaluated by simulation.

Results obtained by simulation are summarized in Table 8-6 and 8-7, and comparing with experimental results in Table 8-3 good agreement is most runs is observed. Average deviation between predicted and experimental concentrations of DES in bottoms and EtOH on tops is less than 5 % in most experiments. Expected higher relative deviations were observed in components present at low concentrations (<5%) because at low concentrations uncertainty in analytical measurements have a major impact.

SA and AcOH conversions and selectivity to DES are slightly over predicted in simulations compared with experiments. Because intrinsic kinetics and an equilibrium stage model were used in modeling, influence of transport phenomena is not considered.

Because catalyst particle size used in RD catalytic packing (> 0.5 mm) is higher than that used in obtaining kinetic model (< 0.3 mm) [29], diffusion may affect rate of reaction as previously reported for a similar catalyst [30].

In the other hand because reaction is enhanced by water removal, separation efficiency plays an important role in the performance of the system. In simulations efficiency was assumed constant along the column using a value of HETP = 0.5 m. Because distribution of flows in the column varies from top to bottoms, in real operation different HETP and different hold-ups within the structured packing are expected [34-38].These values are also different among the variety of experimental conditions evaluated. Then these efficiency variations not considered in the simulation model can also explain over prediction of reactions extent. In addition to this hydrodynamic calculations indicated that the column operated well below maximum capacity ($f_{MC} \ll 1$) flooding conditions. Under these conditions poor liquid distribution may affect catalyst efficiency [37].

Table 8-6. Summary of results obtained by simulation of RD experiments. Compositions are in Table 8-7

Run Code	Reboiler		f_{MC}	Distillate	Bottoms		Conversion		Selectivity to DES (%)
	T (K)	Power kW		Flow (g/min)	Flow (g/min)	AV (mg KOH / g)	SA	AcOH	
12A	396.4	0.30	0.04	22.0	8.3	10.3	99.9	95.6	92.4
12B	395.8	0.45	0.06	20.5	9.8	9.2	99.9	95.9	92.3
12C	395.8	0.59	0.08	32.0	9.5	3.1	99.9	98.7	96.8
13A	400.8	0.35	0.04	25.8	4.9	13.6	99.9	96.8	93.8
13B	397.2	0.62	0.07	23.0	7.3	10.8	99.9	96.5	93.1
13C	399.6	0.83	0.10	37.4	5.6	3.9	99.9	99.1	97.5
14A	505.1	0.53	0.08	36.7	11.1	8.3	87.3† 99.9	86.6† 98.5	97.5
14B	515.7	0.69	0.10	48.9	10.8	2.4	99.9	99.1	99.3
20A	498.6	1.00	0.17	49.5	10.6	8.8	87.3† 99.9	86.6† 99.6	97.4
21A	364.0	0.90	0.13	56.5	8.5	33.4	99.3	96.6	83.3
22A	364.5	0.96	0.14	60.1	8.6	30.7	87.8† 99.6	87.1† 99.2	85.4
22B	365.7	1.22	0.18	60.0	8.7	34.5	99.4	99.5	83.4

† Data evaluated in pre-reactor.

Table 8-7. Products concentration obtained by simulation of RD experiments. Conditions are in Table 8-6.

Run Code	Distillate composition wt %								Bottoms Composition wt %							
	H_2O	DEE	EtOAc	EtOH	AcOH	MES	DES	SA	H_2O	DEE	EtOAc	EtOH	AcOH	MES	DES	SA
12A	4.5	1.3	3.8	90.1	0.0	0.0	0.3	0.0	2.0	0.0	1.2	61.8	0.2	2.2	32.6	0.0
12B	4.7	1.4	4.0	89.8	0.0	0.0	0.1	0.0	2.1	0.0	1.2	66.7	0.2	1.9	28.0	0.0
12C	3.5	1.0	2.9	92.5	0.0	0.0	0.1	0.0	0.5	0.0	0.4	68.2	0.0	0.7	30.1	0.0
13A	4.4	1.1	3.6	90.6	0.0	0.0	0.3	0.0	0.9	0.0	0.8	38.1	0.2	3.0	57.0	0.0
13B	4.6	1.3	3.8	90.2	0.0	0.0	0.1	0.0	1.5	0.0	0.9	57.4	0.2	2.2	37.8	0.0
13C	3.3	1.4	2.5	92.7	0.0	0.0	0.1	0.0	0.3	0.0	0.3	46.5	0.0	0.9	52.0	0.0
14A	7.2	0.7	3.1	87.6	0.0	0.0	1.3	0.0	0.0	0.0	0.0	1.1	0.0	2.2	96.7	0.0
14B	5.4	0.6	2.3	90.3	0.0	0.0	1.4	0.0	0.0	0.0	0.0	0.8	0.0	0.6	98.5	0.0
20A	5.0	0.1	2.2	92.2	0.0	0.0	0.6	0.0	0.0	0.0	0.0	0.1	0.0	2.3	97.6	0.0
21A	7.9	0.0	0.9	91.1	0.0	0.0	0.1	0.0	3.2	0.0	0.0	41.6	0.0	8.0	46.9	0.3
22A	8.0	0.0	0.9	90.9	0.0	0.0	0.2	0.0	2.7	0.0	0.0	38.3	0.0	7.6	51.3	0.2
22B	7.9	0.0	0.9	91.1	0.0	0.0	0.1	0.0	3.0	0.0	0.0	38.5	0.0	8.4	49.9	0.2

Temperature and concentration profiles for typical experiments (runs 13C and 14A) are presented in Figures 8-5 and 8-6. Experimental temperature profiles are well described by simulations in most experiments except for the value at the top of the column. This may be related with cooling effects of inlet streams as discussed in section 8.4.1.

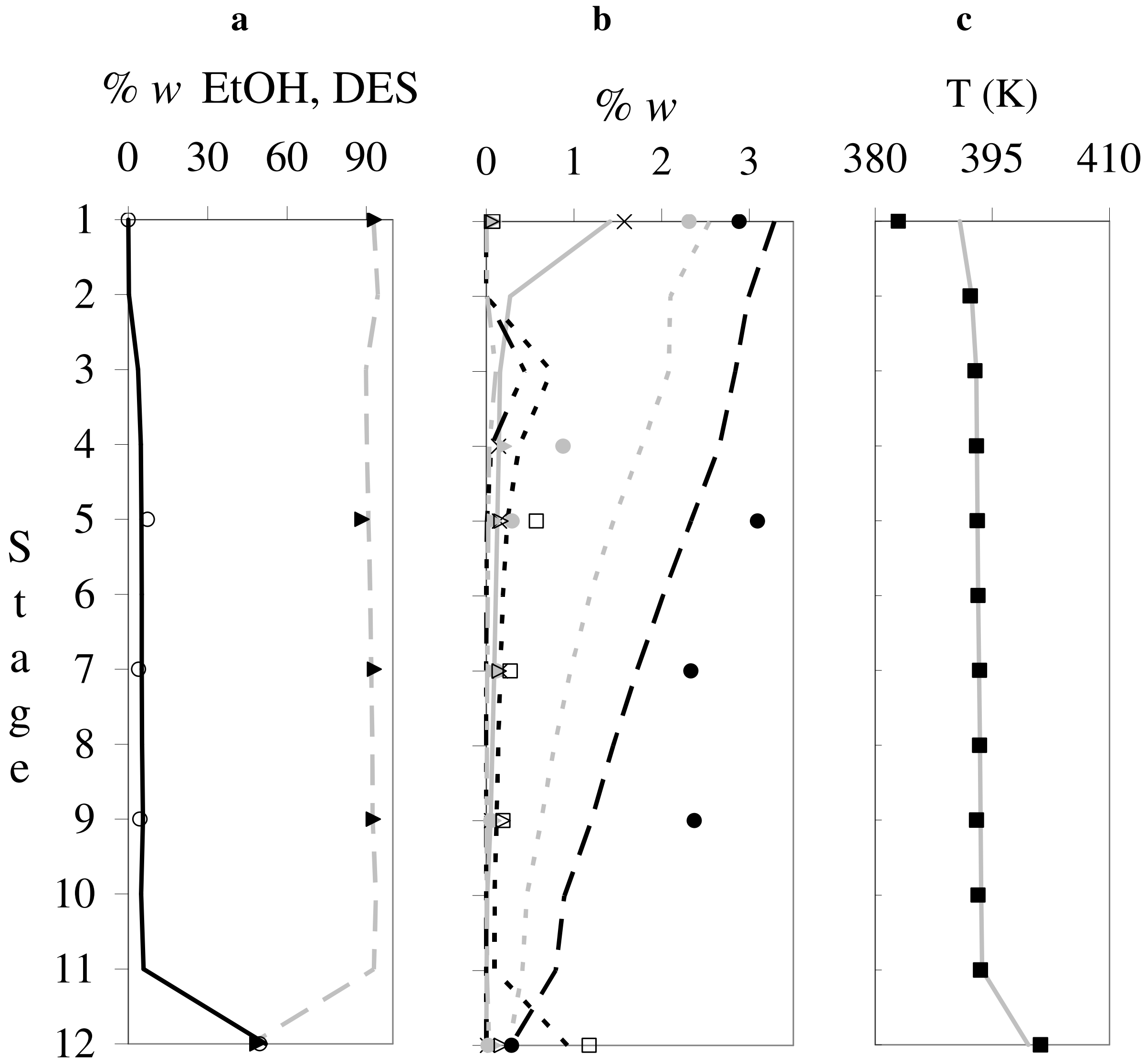

Figure 8-5. Comparison of profiles obtained by simulation (lines) and experimental data in run 13C. a) (○, ▬) - DES, (▲, ▬ ▬) – EtOH. b) (Δ, - - ▬ - -) - SA, (□, - -) - MES, (▲, - ▬ -) - AcOH, (●, - -) - EtOAc, (●, ▬ ▬) - H_2O, (X, ▬) - DEE. c) Temperature profile.

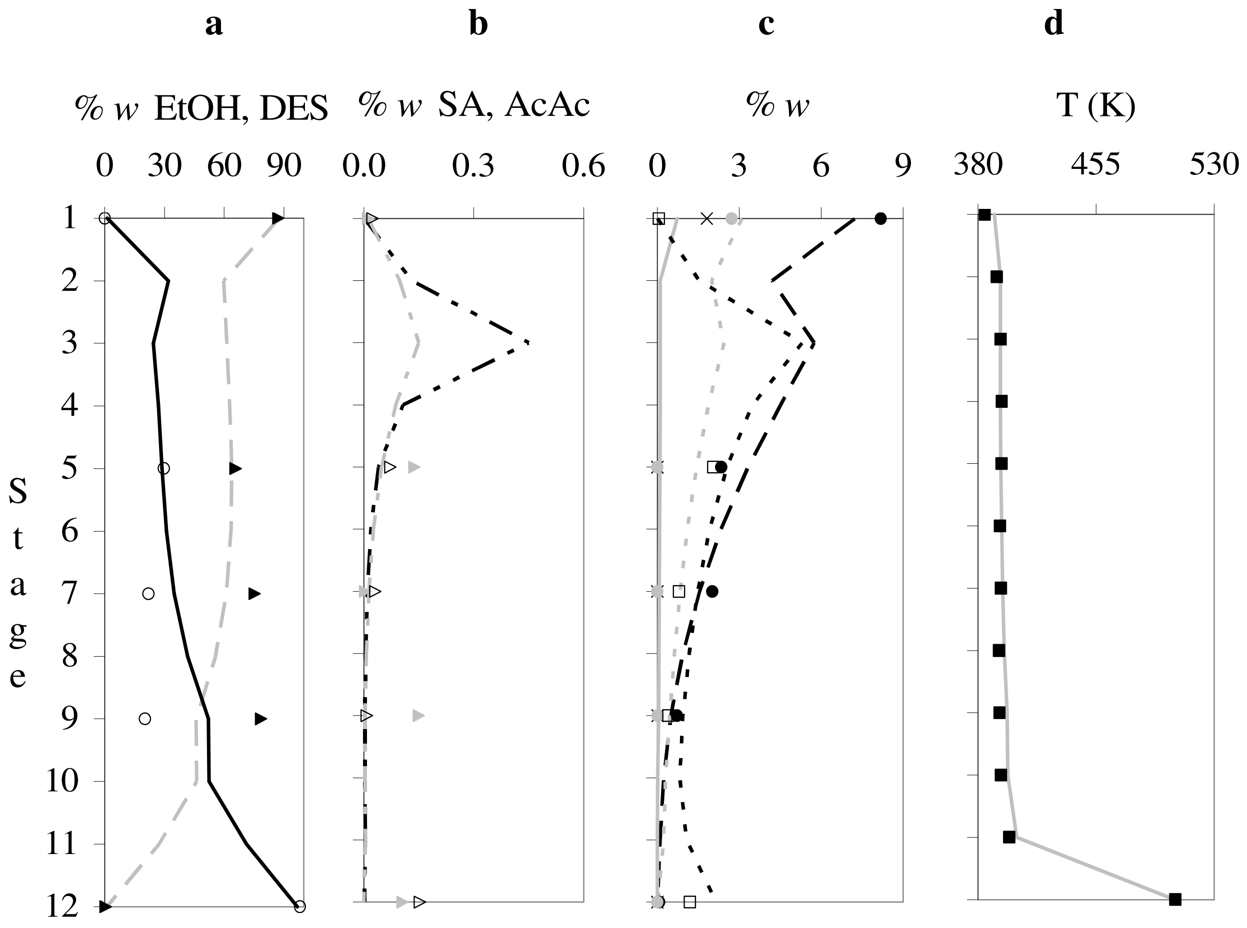

Figure 8-6. Comparison of profiles obtained by simulation (lines) and experimental data in run 14A. a) (○, ▬) - DES, (▲, ▬ ▬) - EtOH. b) (Δ, - - ▬ - -) - SA, (▲, - ▬ -) - AcOH. c) (□, - -) - MES, (●, - -) - EtOAc, (●, ▬ ▬) - H_2O, (X, ▬) - DEE. d) Temperature profile.

Composition profiles obtained by simulation described reasonably well trends observed in all experiments. However, composition profiles differ significantly mainly at the lower part of the column. Considering the uncertainty in real separation efficiencies along the column under different experimental conditions as discussed before, the number of stages used in simulations was obtained from reported HETP. Then location of sampling ports in the column does not necessarily correspond to those assigned in the model, and a mismatch between experimental and simulation profiles is expected.

Despite differences observed between experimental and simulation results, a simple equilibrium stage model is able to reproduced major trends under different conditions evaluated experimentally. Then a broader range of operation parameters not evaluated in the pilot unit can be studied with the computational model.

In next sections simulations are performed using similar conditions to those evaluated in run 14A. The same total inlet mass flow of SA (7.81 g/min) and AcOH (0.781 g/min) is used, however mixed acid solution is fed to pre-reactor as a saturated solution of SA in EtOH (40 wt %) at inlet temperature (363 K).

8.4.2.1 Effect of EtOH feed from bottoms

Figure 8-7 describes results obtained varying EtOH feed flow from bottoms. As expected increasing EtOH flow enhances both SA and AcOH conversion. In addition to the higher excess of EtOH, reaction is driven to completion because H_2O is entrained by EtOH and is removed in distillates. After certain level (~ 10 g/min) no significant improvement in SA or AcOH conversion is gained by using higher amount of EtOH. However selectivity to DES increases up to ~ 99 % by increasing EtOH flow up to 20 g/min because some MES still remains. This corresponds to a total EtOH inlet flow (including acid feed and EtOH from bottoms) of ~ 31 g/min. By Operating under these conditions similar performance of that observed in experiment 14A was obtained. However major energy and material savings are achieved by splitting EtOH inlet flow because run 14A used a total EtOH inlet flow from tops and bottoms of ~ 40 g/min. Also a lower temperature in the reboiler was obtained.

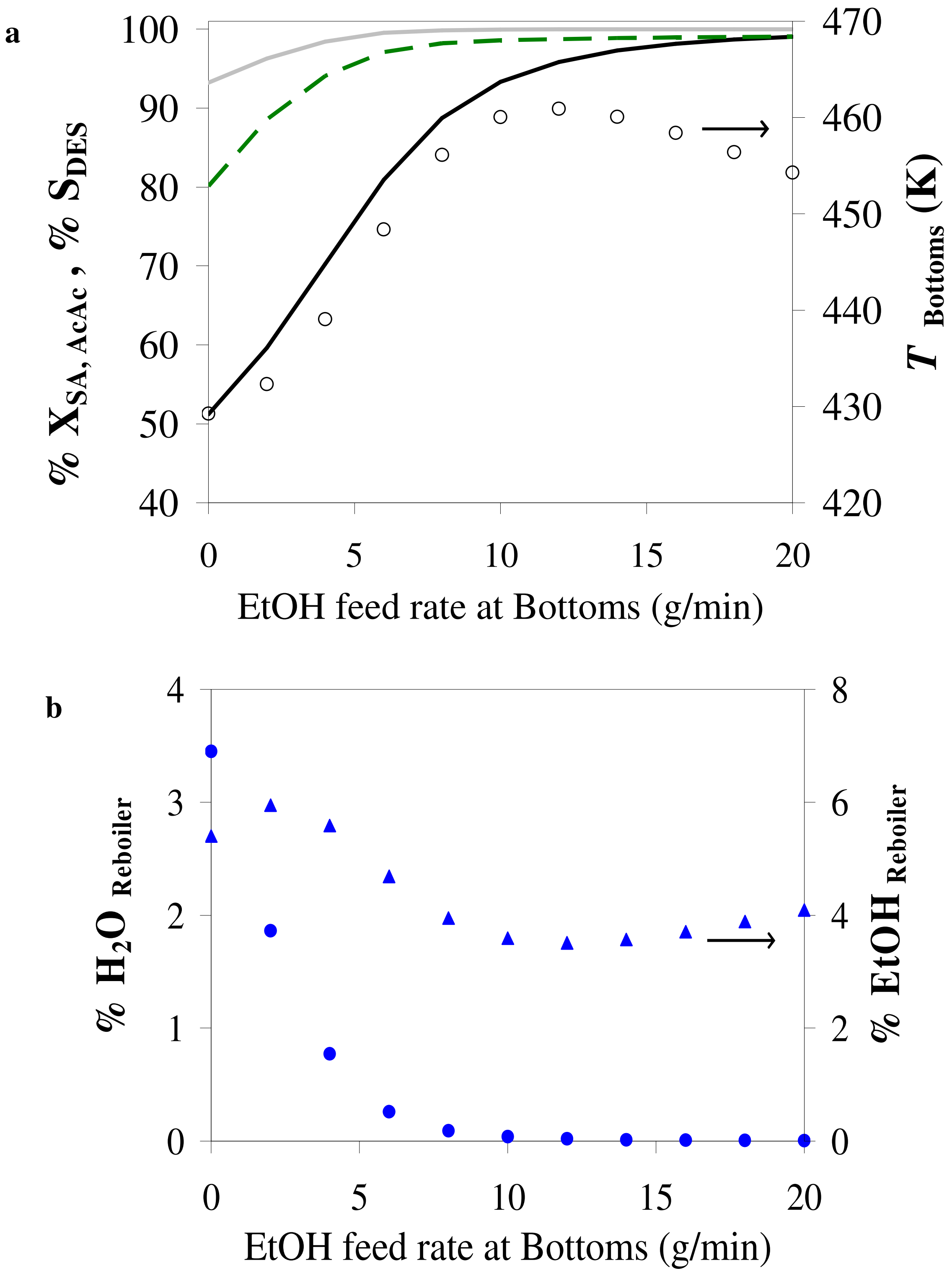

Figure 8-7. Effect of EtOH inlet flow at bottoms operating with pre-reacted mixed acids fed at the solubility limit of SA in EtOH. a) (—) - SA conversion, (– –)- AcOH conversion, (▬) - Selectivity to DES, (○) - Reboiler temperature. b) Concentrations at the reboiler, (●) - H_2O, (▲) - EtOH

The maximum observed in temperature profile in Figure 8-7a at different EtOH feed rates is explained by the accumulation of H_2O and/or EtOH in the reboiler. Operating with low boilup flows limits the extent of reaction and H_2O and EtOH accumulates at the reboiler. In the other hand, operating at high inlet flows of EtOH at bottoms enhances water separation, and excess EtOH accumulates at the reboiler decreasing boiling temperature of the mixture. As observed in Figure 8-7b a minimum concentration of EtOH at the reboiler of 3.5 wt % (with negligible amount of H_2O) corresponded to the maximum of temperature (~ 461 K) when 12 g/min of EtOH were fed from bottoms.

8.4.2.2 Effect of acid feed tray location

Simulations varying location of acid feed were evaluated using an inlet EtOH flow from bottoms of 14 g/min. As observed in Figure 8-8, by introducing the acid feed stream close to the bottom of the column selectivity to DES is severely reduced. Because the large excess of EtOH mostly all SA is converted to MES. However because MES is virtually non-volatile, esterification to DES can not take place in catalytic stages above inlet port. Then the lack of catalytic stages avoids complete esterification and EtOH accumulates at bottoms reducing boiling temperature.

In the other hand a positive effect of having catalytic stages above the mixed acids inlet port is observed for AcOH conversion. In this case, some AcOH entrained by EtOH rising to the top can be esterified in those catalytic sections, decreasing unreacted AcOH in the distillate.

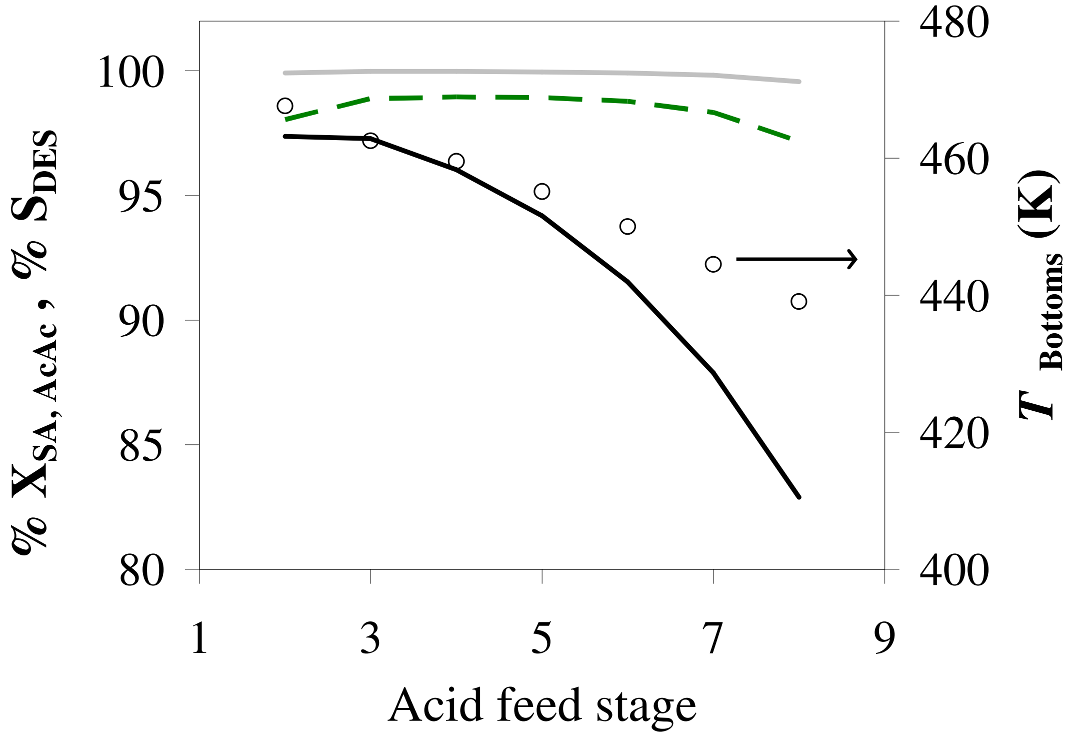

Figure 8-8. Effect of acid feed tray location operating with pre-reacted acid fed at the solubility limit of SA in EtOH. (▬) - SA conversion, (▬ ▬) - AcOH conversion, (▬) - Selectivity to DES, (○) - Reboiler temperature.

8.4.2.3 Effect of boil-up rate and reflux ratio

The effect of boiling rate was evaluated using EtOH feed from bottoms (14 g/min) and pre-reacted mixed acids feed. The boil-up ratio was evaluated at different reflux ratios up to the maximum capacity of the column (f_{MC} = 1). At a given reflux, distillate flow increases with boiling rates, so results presented in Figure 8-9 are plotted with respect to distillate flow.

As observed SA and AcOH conversion as well as selectivity to DES decrease by increasing reflux ratio, indicating the negative impact of H_2O in the reflux.

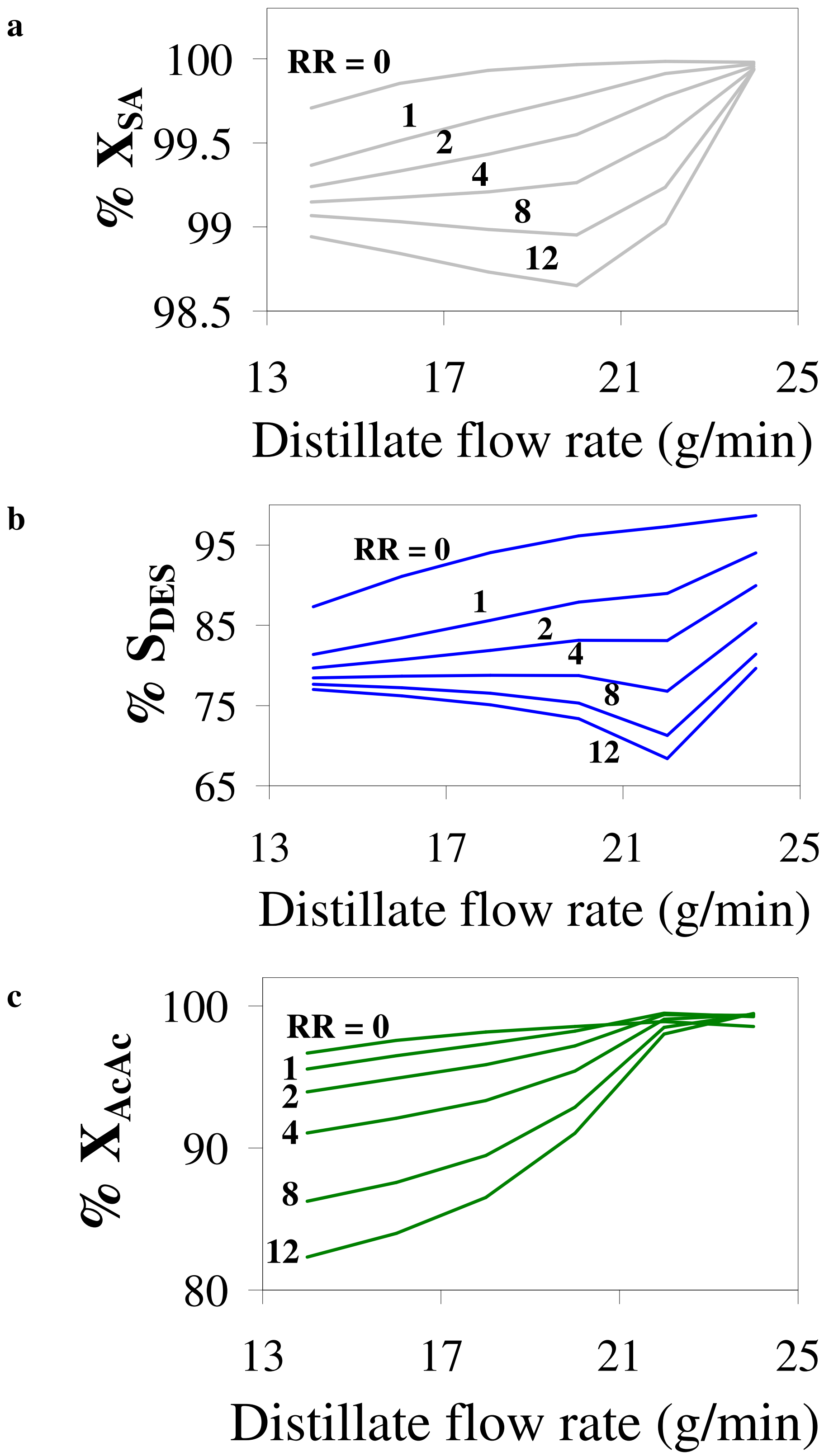

Figure 8-9. Effect of boil-up rate and reflux ratio using pre-reactor and acid feed at the solubility limit of SA in EtOH. a) SA conversion. b) Selectivity to DES. c) AcOH conversion.

When reflux is fixed, increasing boil-up rate increases the amount of EtOH in catalytic stages improving reaction performance. This also helps to entrain H_2O in the overhead, overcoming equilibrium limitations. However above a certain reflux ratio (~ 8) increasing boilup ratio has a negative effect on conversion of SA and selectivity to DES. In this case most of the EtOH is maintained in the upper part of the column and is removed from tops while H_2O is recycled and maintained in high concentrations in reactive stages limiting SA and MES esterification. Because AcOH is also recycled and maintained with EtOH in top sections, its conversion is improved by higher boiling rates even at high refluxes.

As seen in experiments and simulations, operating with a pre-reactor + column configuration can provide better performance in the mixed acid esterification system. Preferably, mixed acids must be introduced at the solubility limit of SA in EtOH to reduce energy and material consumption.The column must operate with small or no reflux and with an EtOH feed from bottoms to entrain water in distillates while maintaining low temperatures at the reboiler avoiding formation of DEE. Finally, having catalytic stages above the mixed acids stream feed port can help to enhance AcOH conversion otherwise affected by its removal in distillates.

8.5 Conclusions

Steady state RD experiments were conducted on the esterification of mixed SA and AcOH with EtOH using a pilot scale unit. Operating under different conditions it was possible to obtain almost complete conversion of both acids, with purity of DES higher than 98% as bottom product. Succinate esters were completely separated from ethyl acetate that was removed within distillate stream. This proved that simultaneous mixed acid esterification and separation of esters can be accomplished in a single RD unit.

An Aspen model was developed and validated using the experimental results. The equilibrium stage model included homogeneous kinetics and activity based phase equilibrium model (NRTL-HOC). In general, the simulation model reproduces reasonably well experimental observations and it was used to evaluate the effect of different processing variables on the performance of the system. A preferable set of operating conditions to achieve high acids conversion with high selectivity to DES was obtained. This model can be used to scale-up a process for mixed acids esterification and to perform preliminary economical evaluation.

REFERENCES

8.6 REFERENCES

[1] O. Wolf, M. Crank, M. Patel, F. Marscheider-Weidemann, J. Schleich, B. Hüsing, G. Angerer. Techno-economic feasibility of large-scale production of Bio-based polymers in Europe, European Science and Technology Observatory, EUR 22103 EN. 2005.

[2] P. Rogers, J. Chen, M. Zidwick. The prokaryotes. Chapter 3.1. Organic Acid and Solvent Production, Part I: Acetic, Lactic, Gluconic, Succinic and Polyhydroxyalkanoic Acids. 511-755. 2006.

[3] Hermann, B., Patel, M. Biochem. Biotechnol. 136 (2007) 361-388.

[4] B. Kamm, M. Kamm. Advances in biochemical engineering and biotechnology. White biotechnology, ed. R. Ulber and D. Sell, Springer, Heildelberg, vol 105, ch. 4, 175-203, 2007.

[5] M. Sauer, D. Porro, D. Mattanovich, P. Branduardi. Trends Biotechnol. 26, 2 (2008) 100-108.

[6] J. B. McKinlay, C. Vieille, J. G. Zeikus. Appl. Microbiol Biotechnol. 76 (2007) 727-740.

[7] I. Bechthold, K. Bretz, S. Kabasci, R. Kopitzky, A. Springer. Chem. Eng. Technol. 31, 5 (2008) 647-654.

[8] A. Cukalovic, C. V. Stevens. Biofuels, Bioprod. Bioref. 2 (2008) 505-529.

[9] C. Delhomme, D. Weuster-Botz, F. E. Kühn. Green Chem. 11 (2009) 13-26.

[10] J. G. Zeikus, M. K. Jain, P. Elankovan. Appl. Microbiol. Biotechnol. 51 (1999) 545-552.

[11] L. Agarwal, J. Isar, R. Saxena. J. Biochem. Biophys. Methods 63 (2005) 24-32.

[12] H. Song, S. Y. Lee. Enzyme Microb. Technol. 39 (2006) 352-361.

[13] A. Orjuela, A. Yanez, C. T. Lira, D. J. Miller. Carboxylic Acid Recovery from Fermentation Solutions. US Patent application. Filed 2009

[14] A. Tuchlenski, A. Beckmann, D. Reusch, R. Düssel, U. Weidlich and R. Janowsky. Chem. Eng. Sci. 56 (2001) 387-394.

[15] S. Schoenmakers, B. Bessling. Chem. Eng. Proc. 42 (2003) 145 -155.

[16] R. Hiwale, N. Bhate, Y. Mahajan, S. Mahajani. Recent trends. Int. J. Chem. React. Eng. Review R1. 2 (2004) 1-52.

[17] G. Jam Harmsen. Chem. Eng. Process. 46, 9 (2007) 774-780.

[18] A. A. Backhaus. (1921) Method for the production of esters. US Patent 1400852.

[19] D. Sutton, G. Reed, G. Hiles. (2005, 2007). Process for the production of esters of mono-, di or polycarboxylic acids. WO patent 051885 A1, US patent application 0129565 A1.

[20] A. Kolah, A. Orjuela, N. Hanna, C. T. Lira, D. J. Miller. Reactive distillation for the biorefinary: Pilot plant synthesis of succinic acid esters. 10AIChE - 2010 AIChE Spring Meeting and 6th Global Congress on Process Safety 2010, 13p. Mach 21-25, 2010. San Antonio, TX. USA.

[21] A. Orjuela, A. Kolah, X. Hong, C. T. Lira, D. J. Miller. Diethyl succinate synthesis by reactive distillation. In revision. 2010.

[22] H. Renon, J. M. Prausnitz. AIChE J. 14 (1968) 135-144.

[23] J. G. Hayden, J. P. O'Connell. Ind. Eng. Chem. Process Des. Dev., 14, 3 (1975) 209-216.

[24] Y. Tang, H. Huang, I. J. Chien. Chem. Eng. Japan. 36, 11 (2003) 1352-1366.

[25] A. Orjuela, A. Yanez, D. Vu, D. Bernard-Brunel, D. J. Miller, C. T. Lira. Fluid Phase Equilibr. 290 (1-2) (2010) 63-67.

[26] A. Orjuela, A. Yanez, P. Rossman, D. Vu, Bernard-Brunel, D. J. Miller, C. T. Lira. Fluid Phase Equilibr. 290 (1-2) (2010) 68-74.

[27] A. Orjuela, A. Yanez, J. Evans, D., D. J. Miller, C. T. Lira. Phase equilibria in binary mixtures with monoethyl succinate. In revision. (2010).

[28] A. Orjuela, A. Yanez, J. A. Lee, D. J. Miller, C. T. Lira. Solubility and phase equilibria for mixtures with succinic acid. In revision. (2010).

[29] A. Orjuela, A. J. Yanez, C. T. Lira, D. J. Miller. Kinetics of mixed succinic acid/acetic acid esterification with Amberlyst 70 ion exchange resin as catalyst. Submitted. Appl. Catal. A. (2010).

[30] A. Kolah, N. Asthana, D. Vu, C. T. Lira, D. J. Miller. Ind. Eng. Chem. Res. 47 (15) (2008) 5313-5317.

[31] L. Götze, O. Bailer, P. Moritz, C. von Scala. Catal. Today 69 (2001) 201–208.

[32] J. Sieres, J. Fernández-Seara. Int. J. Refrig. 30 (2007) 58-67.

[33] Sulzer Chemtech. (2010) Structured packings for distillation, adsoption, and reactive distillation. [Online]. Available: http://www.sulzerchemtech.com/ portaldata/11/ Resources//brochures/mtt/Structured_Packings_April_2010.pdf [2010, Nov 1].

[34] M. Behrens, Ž. Olujić, P. J. Jansens. Chem. Eng. Technol. 31, 11 (2008) 1630-1637.

[35] S. Ratheesh, A. Kannan. Chem. Eng. J. 104 (2004) 45-54.

[36] A. Hoffmann, C. Noeres, A. Górak. Chem. Eng. Process. 43 (2004) 383-395.

[37] A. Kolodziej, M. Jaroszyński, I. Bylica. Chem. Eng. Process. 43 (2004) 457-464.

[38] Ž. Olujić, M. Behrens. Chem. Eng. Technol. 29, 8 (2006) 979-985.

[39] A. Orjuela, A. Kolah, X. Hong, C. T. Lira, D. J. Miller. Diethyl succinate synthesis by reactive distillation. In revision.

PART 4: PROCESS CONCEPT AND PRELIMINARY ECONOMICS

9. A novel process for recovery of fermentation-derived succinic acid: Conceptual design and preliminary economics

9.1 Summary

Conceptual design of a process for recovery of bio-based succinic acid via esterification with ethanol using reactive extraction and reactive distillation is presented. The process model is based upon experiments validated at the pilot scale and it is implemented in the Aspen Plus® process simulator. Processing alternatives are developed to operate with fermentation broths containing a single acid (succinic acid) or mixed acids (succinic acid and acetic acid). Industrial scale simulations are performed varying succinic acid processing capacities (~ 13 to 52 million kilogram per year) and different concentrations of succinic acid in the fermentation broth (50, 70 and 100 kg/m^3). Preliminary process economics are evaluated for the installation of a new recovery plant within an existing fermentation facility. For a 10-year lifetime production facility processing ~52 million kg/yr of succinic acid in a broth containing 100 kg/m^3, the model predicts a capital investment of ~ $ 67 million and a process operating cost of $ 1.586 per kilogram of succinic acid. Selling price for diethyl succinate was estimated in 2.64 $/kg to achieve 30% return of investment.

9.2 Introduction

Fermentation-derived succinic acid (SA) is a valuable carboxylic acid that potentially can replace maleic anhydride as a renewable building block for many chemical commodities as 1,4 butanediol (BDO), tetrahydrofuran (THF), γ-butyrolactone (GBL), polybutilene succinates (PBS), succinimides, succinate salts, etc. As chemical platform SA has a potential market of around 1.6 million tonnes per year [1]. However current prices of petrochemical-derived maleic anhydride (1.72-1.80 $/kg) is still lower than SA obtained by fermentation (3.3 – 5.5 $/kg) which makes it unattractive as industrial feedstock.

Even though cost is still a limiting factor for the commercial success of bio-based SA, it is recognized that the fermentation route has a net fossil energy consumption of 30-40% less than the current petroleum-based route [2]. In addition to this SA can be produced with a variety of feed stocks and microorganisms, with net consumption of CO_2, making possible to integrate it within an ethanol bio-refinery. These positive attributes have been recognized by many chemical industries who envision the opportunities to obtain governmental support to assist in construction of new biobased production facilities. Currently several demonstration plants are under construction or operation [1, 3-5].

In general, in bio-based SA production 50% to 80% of processing costs are due to separation and refining of final product. Major challenges in purification are the low titer in fermentation broth (50-100 kg/m^3), the presence of various by-products including other carboxylic acids, and the nature of final product that is in the salt form due to neutralization required to control pH during fermentation.

To overcome these challenges, alternative methods have been proposed to recover SA from fermentation. After acidification of the broth to release SA in aqueous solution, selective precipitation [6-8], extraction with solvents and/or amines [9-12], ion exchange [13, 14], membrane separation [15, 16] and even esterification [17-20] have been reported. Among these the esterification route is of special interest. From a chemical production viewpoint, succinate esters are more desirable than the free acid for derivatives such as tetrahydrofuran and 1-4 butanediol [21], as the maleic anhydride route already goes through the ester. Thus, succinate recovery as esters directly from the fermentation broth would be of economic interest.

Recently our research program has demonstrated that succinic acid in salt form can be recovered directly from fermentation solids by reactive extraction with ethanol (EtOH) [22]. In this process, succinate salts from the fermentation broth are partially esterified to succinate esters in an ethanol-rich solution, from which it can be further converted into diethyl succinate using reactive distillation. Because other carboxylic acids are typically present in the fermentation broth, a mixture of different carboxylic ethyl esters is obtained as a final product. From reports on SA fermentation using different microorganisms it has been established that acetic acid (AcOH) is one of the major byproducts (5-40 kg/m^3) [23-25].

Because esterification extend is limited by chemical equilibrium, driving reaction to completion require products removal. In this direction, and specifically applied for esterification of SA and AcOH mixtures, reactive distillation has been used to simultaneously accomplish water (H_2O) removal along reaction, together with separation of diethyl succinate (DES) from ethyl acetate (EtOAc) [26, 27]. Additional advantages of RD as the reduction of capital cost and lower energy consumption have been exploited in many chemical processes some of which have been implemented at the industrial scale [28-31].

In this work the integration of a reactive extraction process to recover SA and AcOH with EtOH together with a reactive distillation system to obtain DES as the main product is presented. Conceptual design of the process was conducted using Aspen Plus® process simulation software (Version 7.1, AspenTech). Finally a preliminary economic evaluation of the process is presented including major costs components such as raw materials, equipment, utilities, labor and other economic factors.

9.3 Conceptual design of the process

9.3.1 Process concept

The process concept to recover SA from fermentative broth was by our research program and experimental validation is presented elsewhere [22, 26, 27, 32].

$$\mathrm{Na_2Succ}\ (s) + \mathrm{H_2SO_4}\ (l) + \mathrm{EtOH} \rightarrow \mathrm{SA}\ (sol) + \mathrm{Na_2SO_4}\ (s)$$

$$2\ \mathrm{NaOAc}\ (s) + \mathrm{H_2SO_4}\ (l) + \mathrm{EtOH} \rightarrow 2\ \mathrm{AcOH}\ (sol) + \mathrm{Na_2SO_4}\ (s)$$

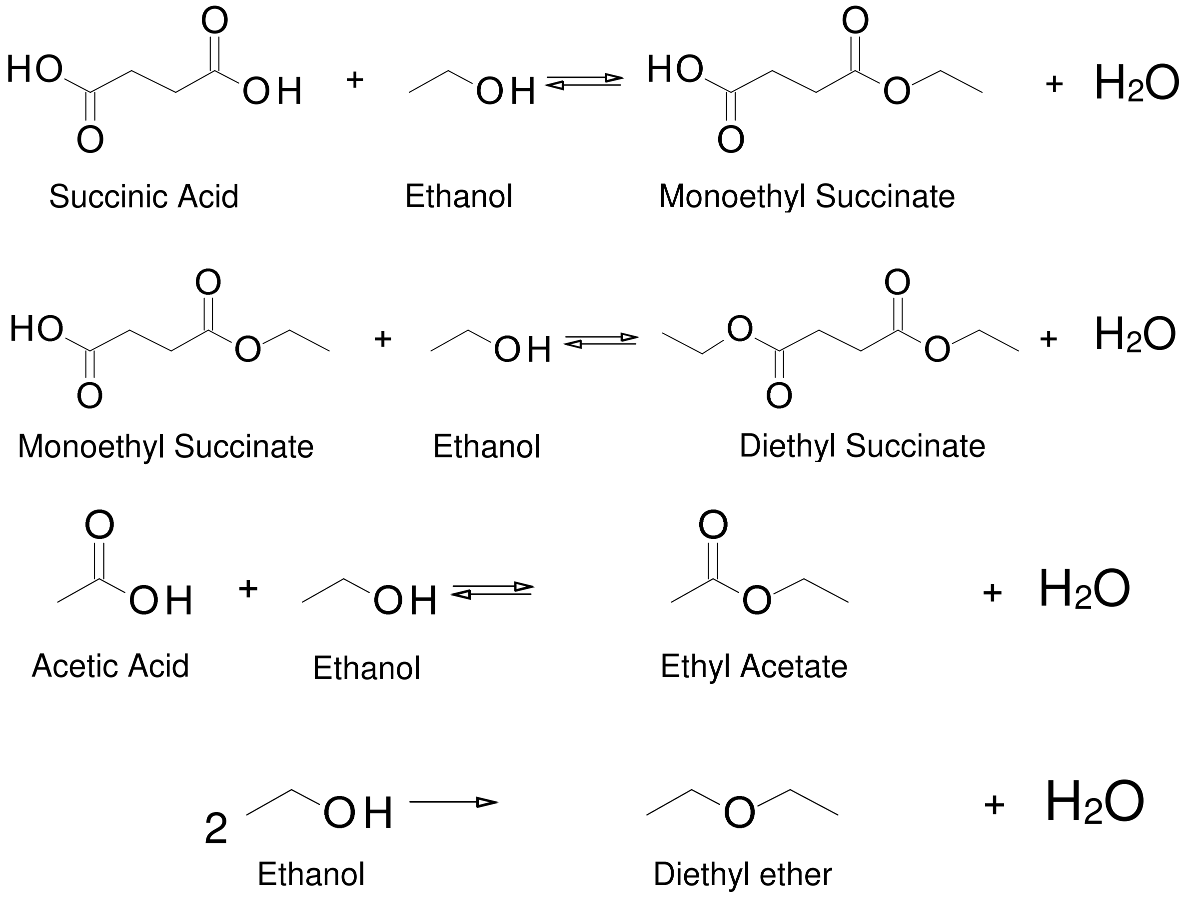

Figure 9-1. Reaction chemistry during reactive extraction of SA and AcOH with EtOH directly from sodium salts obtained by fermentation.

The overall concept involves partial esterification of the succinate salts in EtOH in a reactor, followed by reactive distillation of the mixture. Figure 9-1 describes reaction chemistry considering that both SA and AcOH are present in the fermentation broth as sodium salts: sodium disuccinate (Na_2Succ) and sodium acetate (NaOAc). Esterification of SA occurs in a series-parallel scheme of reaction with monoethyl succinate (MES) as intermediate. Etherification of EtOH is also considered in the model.

A block diagram of the process is presented in Figure 9-2. Three different sections are described. Initially the fermentation broth is treated as usual by typical centrifugation or filtration to remove cell biomass and by clarification to remove impurities and color. Water is then removed by evaporation until the succinate and acetate salts precipitate. Wet solids removed by filtration or any other method are dried to removed major part of moisture.

In the second section, extraction and pre-esterification of solid salts is performed in EtOH, adding required equivalents of sulfuric acid to acidify succinate and acetate salts. In general a slight excess of H_2SO_4 is used to ensure complete recovery. The amount of EtOH used is at least the required to dissolve SA at the temperature of extraction. Because inorganic sulfates are virtually insoluble in EtOH, they are removed by centrifugation or filtration.

Finally pre-estererified mixture is sent to a RD unit where high purity DES is obtained as bottom product. EtOAc is recovered within distillate along with excess EtOH and H_2O. In order to recovery EtOAc and recycle excess EtOH, a separation system is required for the distillate stream.

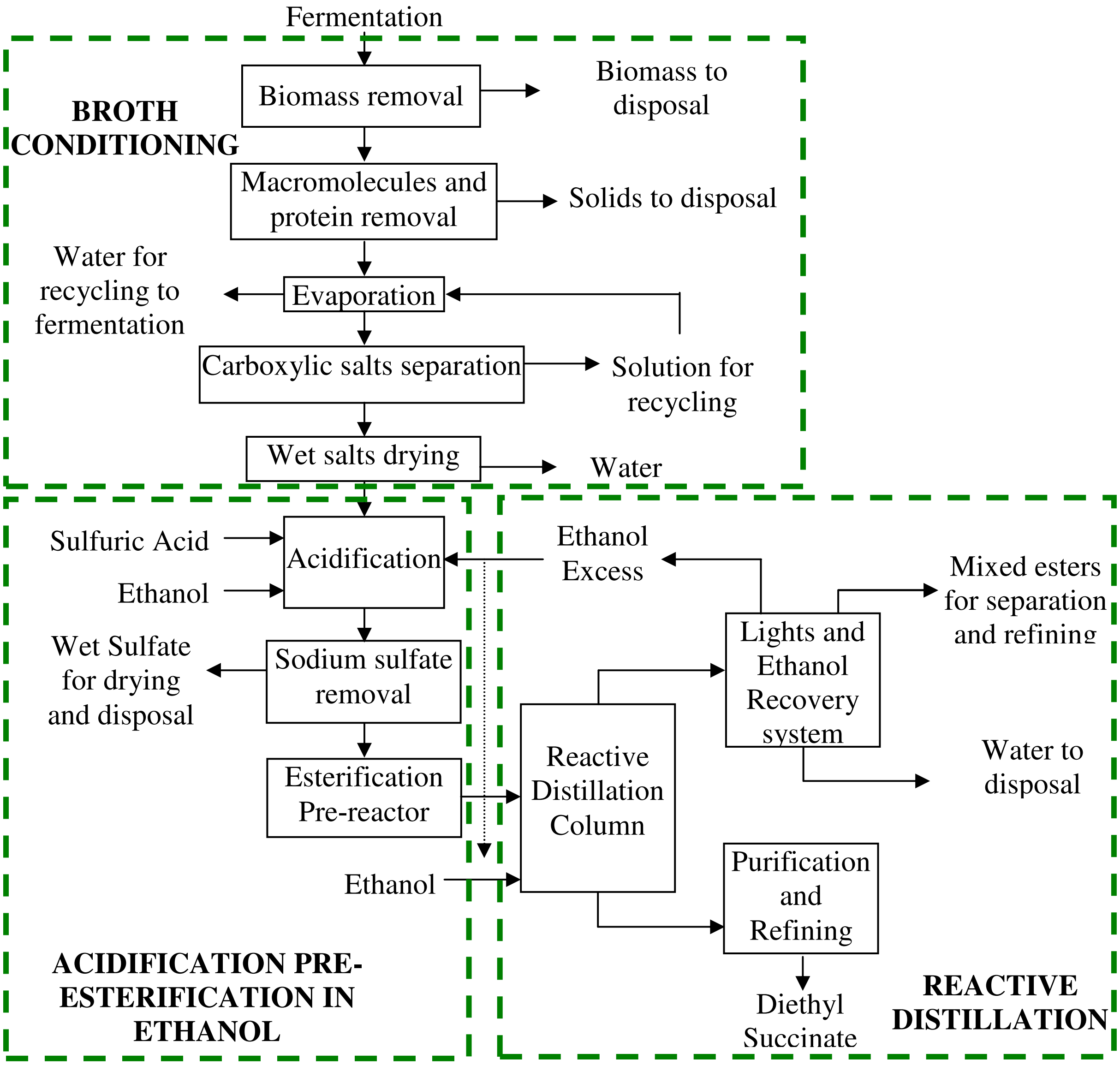

Figure 9-2. Recovery process for succinic acid form fermentation broth by esterification with ethanol.

9.3.2 Process description

The process flow diagram as a result of this study is presented in Figures 9-3 and 9-4. When AcOH is present in the broth EtOAc is recovered and additional units are required as presented in Figure 9-4. A train of three thermally integrated evaporators is used to concentrate fermentation broth. As a result of evaporation, succinate and acetate salts precipitate and are removed by centrifugation. It was assumed that dry solids were obtained here, and saturated liquor is recycled to the last evaporation stage. Dry salts are then mixed with EtOH and H_2SO_4 in two stirred reactors operating in parallel to maintain tank sizes under dimensions commercially available. After reactive extraction solid sulfates are removed and the ethanolic solution of acids and esters is sent to the RD unit.

Two inlet streams are fed into the RD unit, ethanolic acid solution from tops and recycled EtOH from bottoms. In this unit nearly pure DES is obtained from bottoms, while distillate stream reach in EtOH also removes H_2O, EtOAc, DEE and traces of DES.

In a subsequent distillation (C-1) most of the water is removed from bottoms and a top stream containing less than 10 % wt of water is obtained. Even though this top stream also contains small amounts of DEE and DES, a ternary diagram including only EtOH, H_2O and EtOAc (Figure 9-5) can help to visualize major challenges in further water removal by distillation. Top stream from column C-1 is located close to a distillation boundary (Figure 9-5) in a region where only H_2O can be obtained as pure product. Because the large excess of EtOH in C-1 distillate, a large amount of highly concentrated EtOAc or EtOH (e. i. using recycled stream after further separation) is required to move this stream to a different distillation region where other products can be obtained. In order to avoid excessive use of material and energy, a separation process including molecular sieves was used. In this case most of the water in distillates from C-1 is removed and thus moved to a region where pure ethanol can be obtained by distillation. Because saturation of molecular sieves, a common practice in the EtOH industry is recycling around 20 % of processed product into a parallel unit operating in a regeneration cycle. Then regenerating stream is sent back to column C-1.

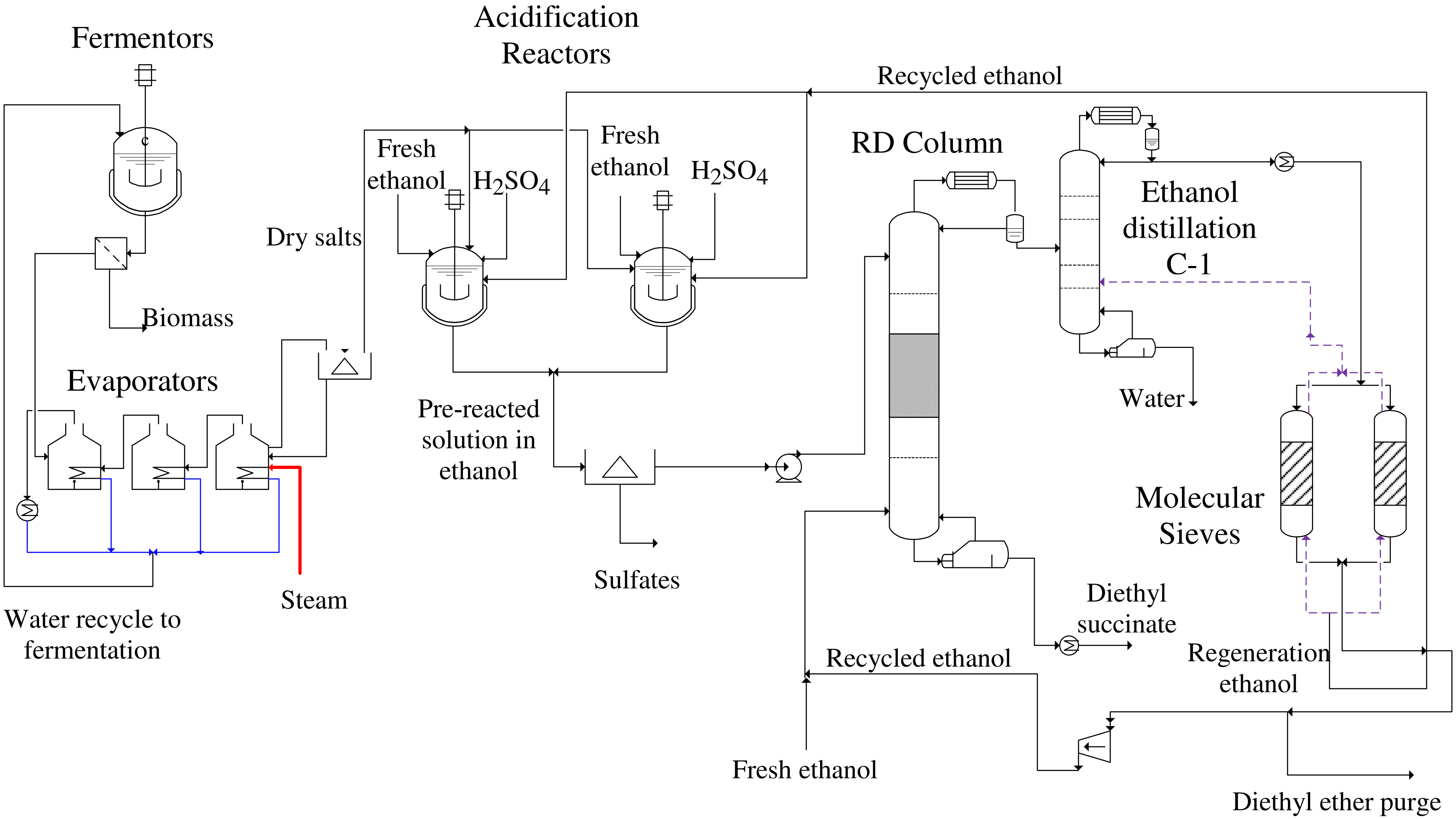

Figure 9-3. Process flow diagram for recovery of succinic acid from fermentation broths by esterification with ethanol using reactive extraction and reactive distillation.

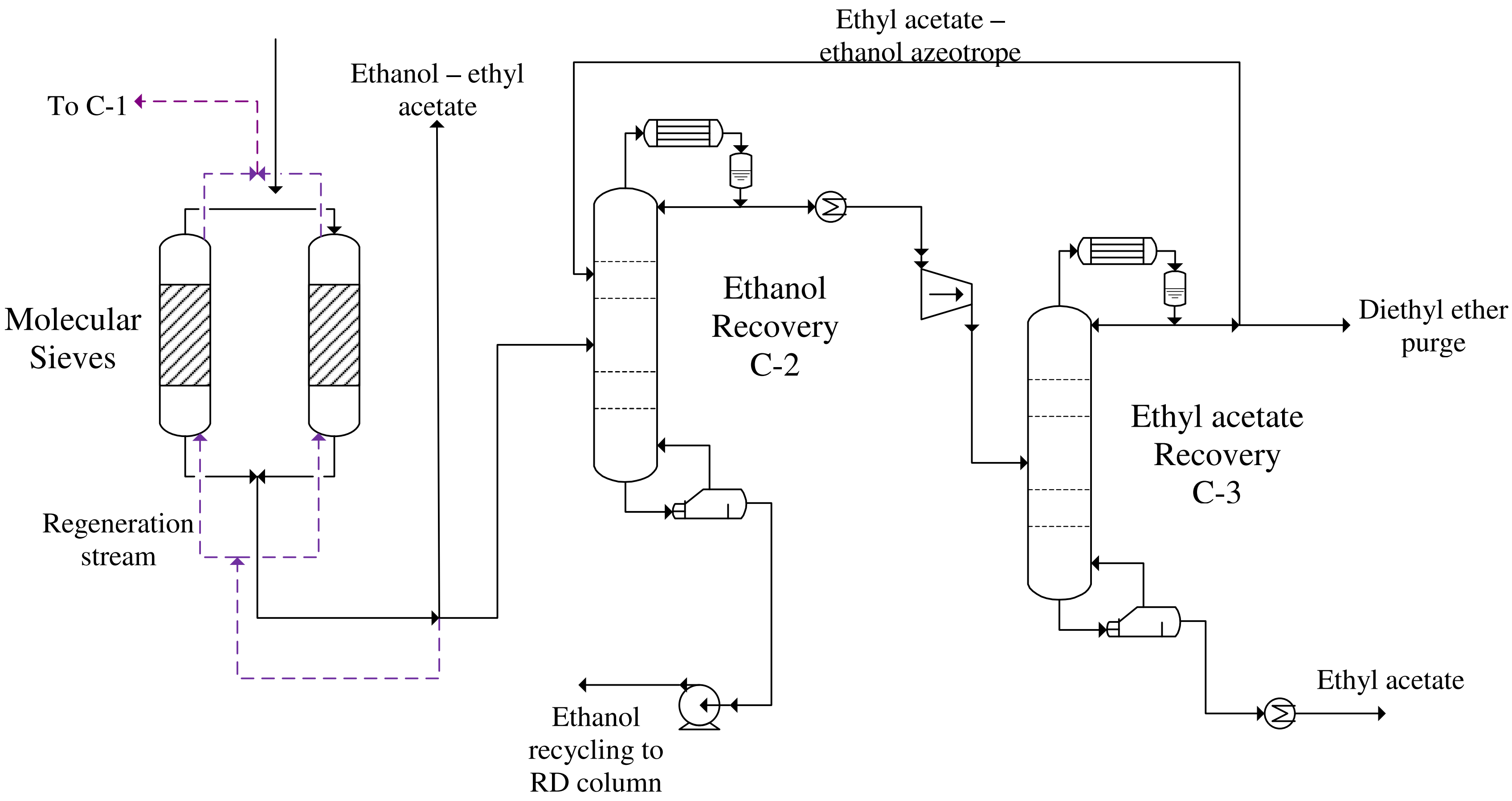

Figure 9-4. Process flow diagram for recovery of ethyl acetate.

When AcOH is not present in the broth, there is no EtOAc in the system and pure ethanol obtained from molecular sieves can be recycled to reactors or RD unit. However a purge to remove DEE must be used otherwise it will built up in the system. In the other hand if EtOAc is present in the system this must be removed.

As observed in Figure 9-5, EtOAc concentration in tops of C-1 is higher than 20 wt %. Under these conditions the use of a purge will remove substantial amount of EtOH.

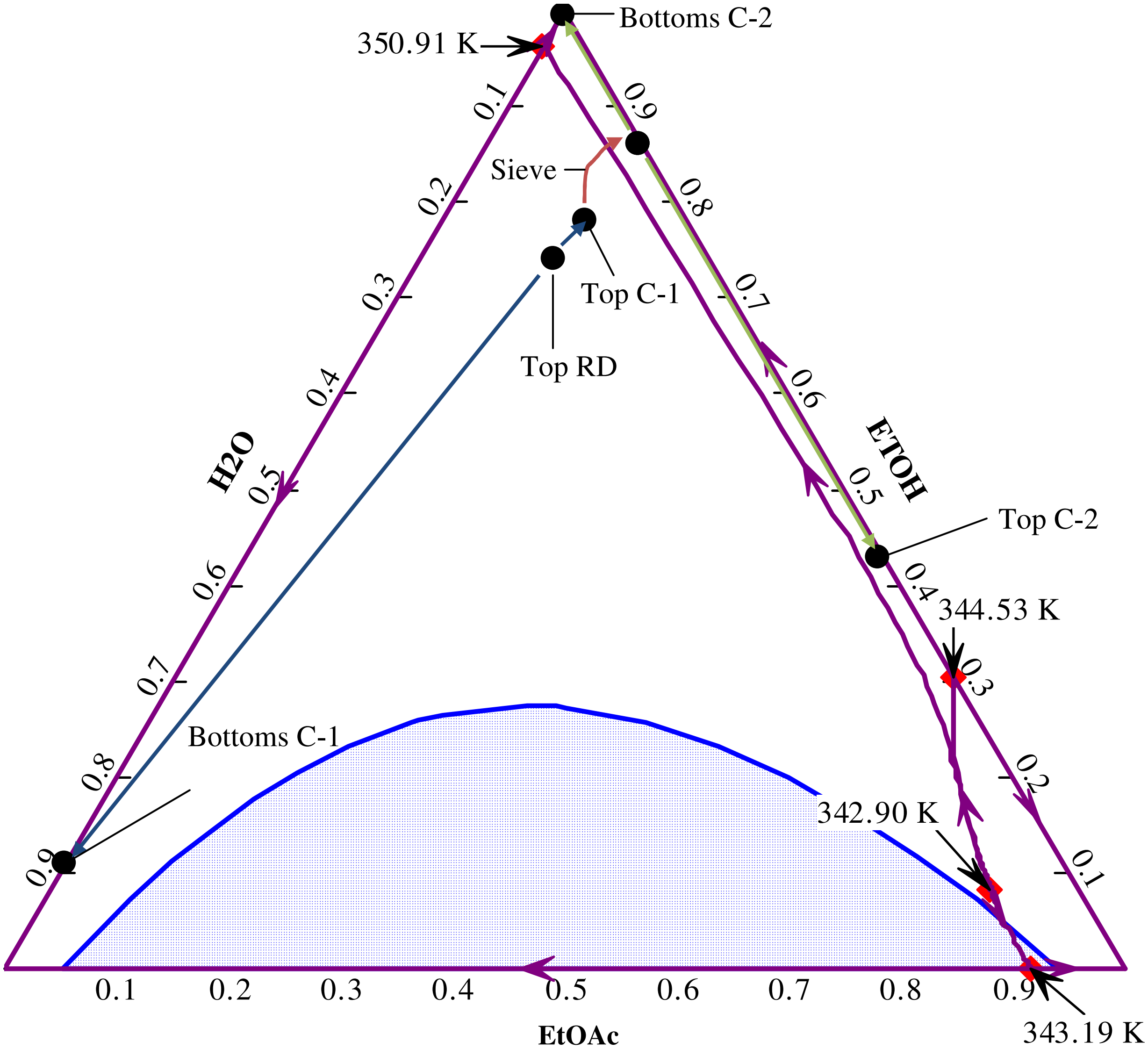

Figure 9-5. Ternary diagram for the system EtOH-H_2O-EtOAC at 101.3 kPa.

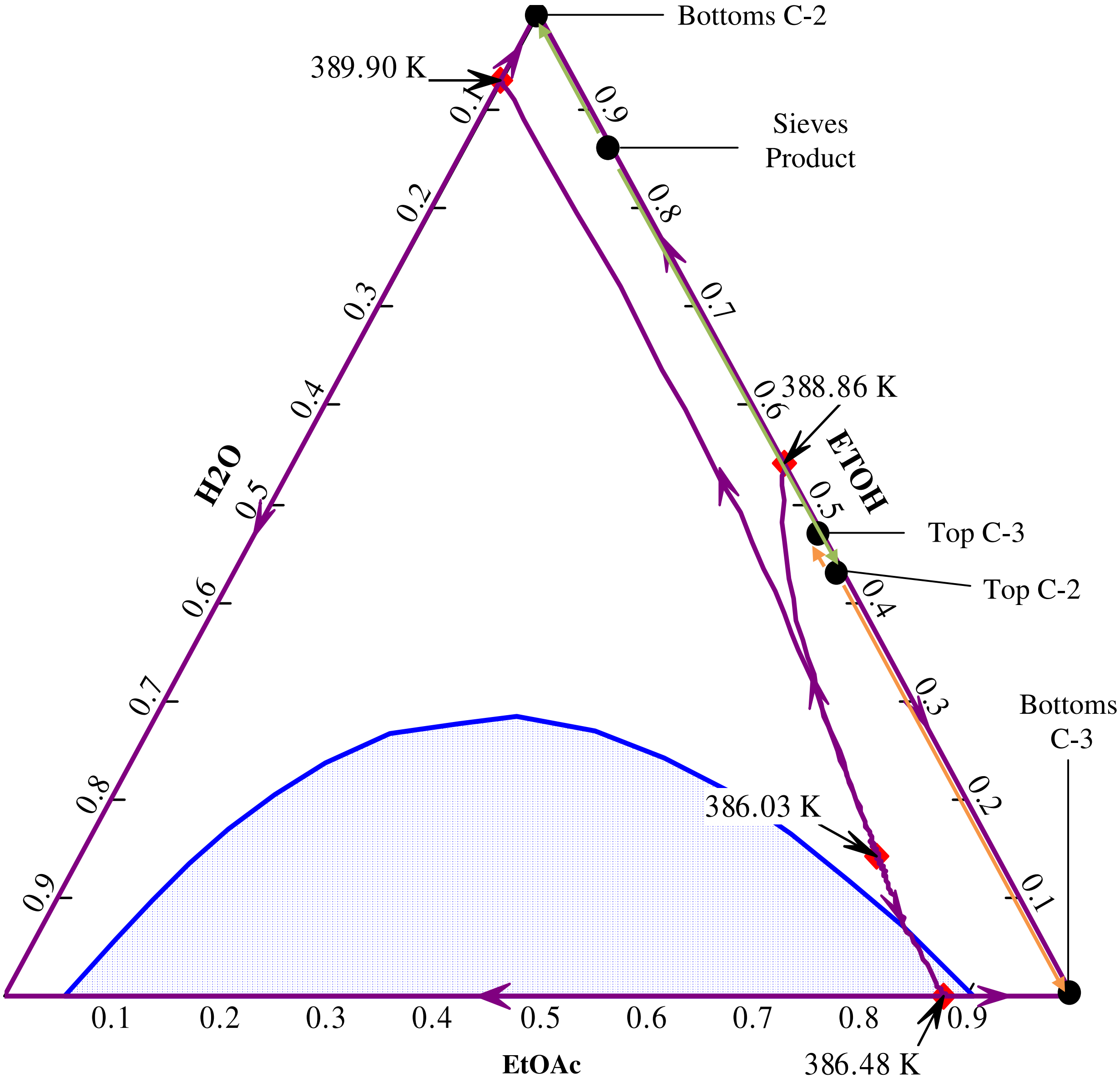

Figure 9-6. Ternary diagram for the system EtOH-H_2O-EtOAc at 404.3 kPa.

After water removal in molecular sieves, top stream from C-1 is now in a region where pure EtOH can be obtained as bottom product using column C-2 in Figure 9-4. In this case separation is limited by another distillation boundary where azeotrope EtOH-EtOAc is obtained as top product. However, as observed in Figure 9-6, a pressure shift can move distillation boundary in such a way that top stream from column C-2 can be further distilled in column C-3 to obtain pure

EtOAc as bottom product. Distillates from this last column are recycled to column C-2, but a purge is required to remove DEE out of the system

9.3.3 Process simulation

Computer simulation was carried out using steady state models in Aspen Plus® for a facility processing approximately 13, 26, 36 and 52 million kilograms of SA annually. Three different SA concentrations in the original broth were considered (50, 70 and 100 kg/m^3). When simulations were performed with broths also containing AcOH, a SA/AcOH mass ratio of 1/10 was assumed.

Required physicochemical data (e. g. vapor pressures, solubility, multicomponent phase equilibria, etc) and kinetics of reactions were evaluated experimentally by our group, or were obtained from literature [33-39].

Reactive extraction units were modeled as CSTR reactors. In a previous work it was demonstrated that acidification of salts in EtOH occurs in less than 3 hours [32], so residence time in reactors was defined as 8h. RD unit and other distillation units were modeled using an equilibrium stage approach, corrected by Murphree efficiency and height equivalent to a theoretical plate (HETP). A list of major design specifications is presented below:

- Minimum heating surface in evaporators calculated with methodology applied in sugar cane industry [40].
- Acidification reactors operated as CSTR at 363 K under 304 kPa. Kinetics of esterification was described with a model for Amberlyst 70 assuming acidity equivalents to 0.3 wt % H_2SO_4.
- Concentration of SA as free acid in EtOH in acidification reactors was 50%.

- Maximum MES concentration of 1 wt % in RD column bottom product.
- Maximum temperature of 453 K at the reboiler of RD column.
- Maximum H_2O concentration of 0.5 wt % in recycled EtOH
- Molecular sieves operated at 393 K and 152 kPa, with a recycle of 20 % of processed stream for regeneration.
- Water content of 0.3 wt % in outlet stream form molecular sieves.
- Minimum concentration of 99 wt% of ethyl acetate in bottom product of column C-3, when AcOH was considered present in the fermentation broth.
- Pressure of 404.3 kPa in EtOAc recovery column (C-3).
- Columns operated at 80% of maximum hydrodynamic capacity.
- Distillation columns operated with a constant heat transfer coefficients at reboiler (0.85 kW/m^2 K) and condensers (0.64 kW/m^2 K).
- Water was used as cooling service with a minimum temperature of 293 K.
- Compressors and pumps operated at 0.78 and 0.9 efficiency respectively.

A list of parameters used in simulation of major units is presented in Tables 9-1 to 9-3.

Table 9-1. Parameters in simulation of evaporation system

Number of effects		3
Flow arrangement		Co-current
Steam	Temperature (K)	423
	Inlet effect	1
Pressure (kPa)	Effect 1	296
	Effect 2	152
	Effect 3	35
Heat transfer coefficient (kW/m^2 K)	Effect 1	3.97
	Effect 2	2.55
	Effect 3	1.13

Table 9-2. Parameters in simulation of reactive distillation unit

Number of stages			27
Pressure (kPa)			304
Reflux ratio			0.04
Distillate/feed mass ratio			0.61
Pre-esterified acid mixture feed stage			5
Ethanol feed stage			26
Stripping zone		Stages	1
		Packing	BX®
Reactive stages	Catalytic	Stages	2-24
		Packing	KATAPAK SP-11
		Catalyst	Amberlyst 70®
		Catalyst loading (kg/m^3)	76
	Self-catalytic	Stages	25-26
Enrichment zone		Stages	25-26
		Packing	BX®
HETP (m^{-1}) [41-43]			0.5
Hold up (vol %) [41-43]			0.14
Murphree efficiency			0.5

Table 9-3. Parameters in simulation of distillation columns C-1, C-2 and C-3

Column	C-1	C-2	C-3
Number of stages	10	12	17
Pressure (kPa)	152.0	101.3	404.3
Reflux ratio	1.7	4	5
Distillate/feed mass ratio	0.875	-	-
Bottoms/feed mass ratio	-	0.221	0.023
Feed stage	9	10	10
Plate type		Sieve tray	
Murphree efficiency		0.5	

9.3.4 Preliminary economics of the process

Economic evaluation of the process is based upon results obtained from Aspen Plus® simulations. Stream flows and conditions as well as process equipment sizes and energy requirements were transferred into a spreadsheet program where economic analysis was implemented. Costs of major units were evaluated with correlations available in the literature [44]. Structured packing and catalyst costs were obtained from vendors (Sulzer, Dow Chemical Co.). Price of raw materials, products and utilities were obtained from reports as July 2010 [45, 46]. Cost of pretreated (filtered and clarified) raw fermentation broth was estimated in 0.33 $/kg of SA. Major parameters and key assumptions in economic model were obtained from literature [47] and are presented in Tables 9-4 to 9-6. A list of major equipment included in economic evaluation is presented in Table 9-7.

Table 9-4. Parameter for economic analysis

Plant location		USA - Midwest
Plant startup		2013
Plant life		10 years
Operation time		24h/day, 360 days/yr
Marshall & Swift cost index (2nd quarter 2009)		1446.5
Return of investment (ROI)		30 %
Net present worth at project end		$ 0
Combined federal/state income tax rate		35 %
Effective loan ratio		5 %
Raw materials	Broth	0.3306 $/kg SA
	Ethanol	1.72 $/gal
	Sulfuric Acid	0.23988 $/kg
Utilities	Electricity	0.0654 $/kW
	Natural Gas	5.68 $/MMkJ
Byproducts	Ethyl acetate	1.102 $/kg

Table 9-5. Parameters used in the estimation of the total capital investment

	Percentage	Calculation basis
Direct costs		
Installation	40 %	of purchased equipment cost
Instrumentation	35 %	
Piping	50 %	
Electrical	30 %	
Buildings, process, and auxiliary	60 %	
Service facilities, and yard improvements	70 %	
Land	5 %	
Direct costs	75 %	of fixed capital investment
Indirect costs	15 %	
Fixed capital investment	Direct costs + Indirect costs	
Working capital	15 %	of total capital investment
Total capital investment	Fixed capital investment + working capital	

Table 9-6. Parameters used in the estimation of the total operating costs

	percentage	Calculation Basis
Fixed Operating Costs		
Capital Cost	100 %	Of installed equipment cost
Total Labor Costs		
Plant Operators' Salaries	5.24 %	Operators / Shift at (25$/hour)
Maintenance Salaries	1.0 %	Of Capital Costs
Supervision & Administration	40.0 %	Of Operators & Maintenance salaries
Fringe Benefits	30 %	Of Operators, Maintenance & Supervision Labor
Supplies		
Operating Supplies	0.75%	Of Capital Cost
Maintenance Supplies	1.0%	Of Capital Cost
Insurance & Local Taxes	0.8%	Of Capital Cost
Depreciation		Straight line - 10 Years Economic Life
Total Operating Cost	Fixed operating costs+ variable operating costs+ Depreciation	
Process Operating Cost	Fixed operating costs+ variable operating costs (minus byproducts)+ Depreciation	

Table 9-7. Major units included in equipment cost evaluation

Equipment	Number
Evaporators	3
Reactors	2
Centrifuges	2
Reactive distillation column	1
Distillation columns	3 (1[§])
Heat exchangers (condensers and reboilers)	13 (7[§])
Molecular sieves	1
Pumps	6
Compressor	1
Fire heater	1
Cooling tower	1
Solids conveyor	1

[§] Operation without AcOH in fermentation broth

9.4 Results and discussion

Major simulation results obtained for a facility processing ~ 52 million kg/yr SA in a broth containing 100 kg/m^3 of SA with and without AcOH are presented in Table 8. Total capital investment of ~ \$ 70 million (without AcOH) and ~ \$101 million (with AcOH) was obtained. Clearly, additional distillation units required to remove and recover EtOAc increase capital investment and also processing costs. However DES prices calculated with a 30% ROI for both processing alternatives (1.21 \$/kg and 1.44 \$/kg respectively) is lower than current commercial price for diethyl maleate (2.5-2.8 \$/kg).

A breakdown of processing costs for a ~ 52 million kg/yr SA facility without AcOH in the broth is presented in Figure 9-7. As observed raw materials play a major role in determining final price for DES. Other than the broth cost that is common in any SA purification process, in our process fresh EtOH accounts for 42% of total processing costs. Nevertheless, more than 90 wt % of inlet EtOH ends up in the final product. Around 10% EtOH is lost in water stream removed from column C-1 or in purge to remove DEE (Figure 9-3). However this purge can be used as a fuel in fire heaters or further processed to obtain DEE as valuable byproduct. After global optimization of the process some EtOH savings can be obtained. It is also important to consider the opportunity of integration of this process within a bio-refinery where EtOH price can be lower than commercial price used in this study.

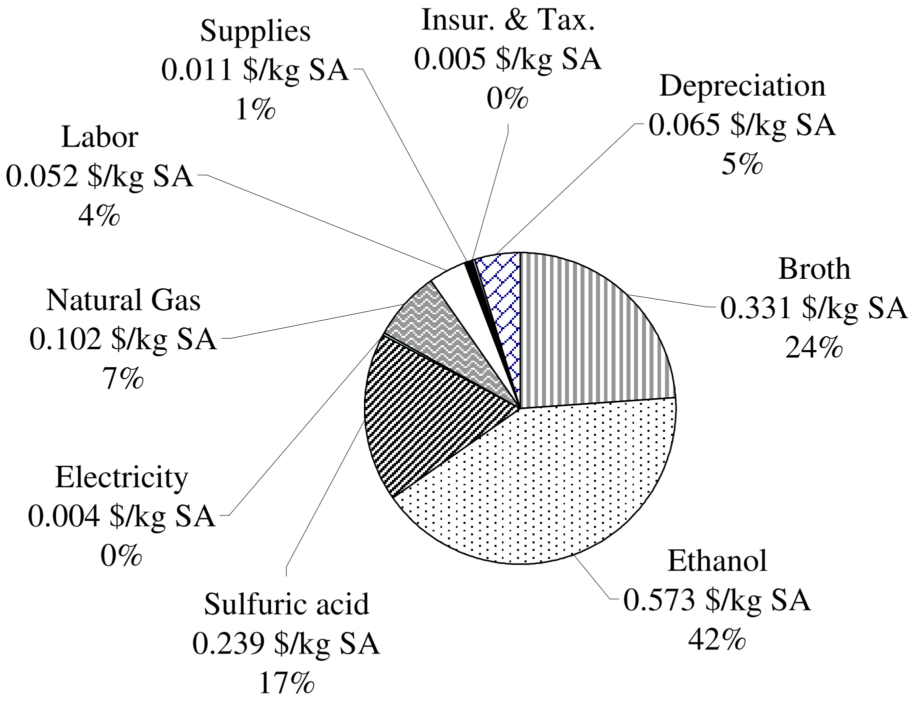

Figure 9-7. Operating costs breakdown of in the recovery of SA from fermentation broths by esterification with EtOH. Facility processing ~ 52 million kg/yr SA in a broth containing 100 kg/m^3 SA without AcOH**.**

Sulfuric acid consumption is the third major contribution to the selling price for DES. Despite in most of current technologies is a common practice to use sulfuric acid in acidification of broths; recovery from aqueous solutions is difficult. In this process sulfates precipitate because their negligible solubility in EtOH and can be easily removed. Depending on the salt form obtained in the fermentation broth (magnesium, ammonium), sulfates generated may have value as fertilizers. The value or cost of sulfates are not included in the analysis.

Table 9-8. Simulation results for a processing capacity of ~ 52 million kg/yr SA in a broth containing 100 kg/m^{3} SA with and without AcOH.

	Without AcOH	**With AcOH**
Fermentation broth feed rate, (kg/yr)	$5.25x10^{8}$	
SA feed rate, (kg/yr)	$5.25x10^{7}$	
AcOH feed rate, (kg/yr)	-	$5.25x10^{6}$
Total fresh EtOH feed rate, (kg/yr)	$5.23x10^{7}$	$5.73x10^{7}$
DES production rate, (kg/yr)	$8.03\ x10^{7}$	
EtOAc recovered, (kg/yr)	-	$3.58x10^{6}$
Electricity, (kW-h)	$3.09x10^{6}$	$1.26x10^{7}$
Natural gas, (kW)	$2.63x10^{8}$	$3.95x10^{8}$
Purchase equipment price, ($)	$1.12x10^{7}$	$1.73x10^{7}$
Direct costs, ($)	$4.63x10^{7}$	$6.74x10^{7}$
Direct costs per kg of SA, ($/kg)	0.083	0.128
Fixed capital investment, ($)	$5.81x10^{7}$	$8.98x10^{7}$
Working capital, ($)	$8.71x10^{6}$	$1.35x10^{7}$
Total capital investment, ($)	$6.68x10^{7}$	$1.03x10^{8}$
Total capital investment per kg of SA, ($/kg)	0.127	0.197
Total process operating cost, ($)	$7.26x10^{6}$	$8.15x10^{7}$
Total process operating cost per kg of SA, ($/kg)	1.382	1.552
DES price at pay back period of 10 years ($/kg)	0.967	1.066
DES price (ROI 30%) ($/kg)	1.210	1.443

Even though water removal was carried out by evaporation, energy provided by natural gas combustion corresponds only to 7% of the total operating cost. In fact 4% is due to evaporation and 3% is used in distillation systems. Considering that energy integration has not been developed here, further energy savings can be obtained. In addition to this distillated water from evaporators can be recycled into the fermentation process without further treatment. Remaining supplies, labor, depreciation and other utilities costs, play a relative minor role in this process.

In Figure 9-8 direct costs, total capital investment and operating costs are reported per mass of SA processed for all conditions evaluated. As observed the lowest costs are obtained by processing ~ 52 million kg/yr of SA at 100 kg/m^3 in the broth without AcOH. Considering that this process has been evaluated also for broths containing SA in the free acid form, [32] and also taking into account that current developments in fermentation can lead to higher concentration and high purities of SA, this processing alternative can become even more attractive in the near future.

In general directs costs and capital investment represent less than 10 % and 20 % respectively of operating costs. Above a processing capacity of ~ 36 million kg/yr of SA costs are slightly reduced because energy, broth, EtOH and H_2SO_4 consumption is proportional to the scale of production, and they account for more than 90 % of processing costs.

Selling price of DES for a 30 % ROI for all simulated cases is presented in Figure 9-9. Remarkably even at low concentrations, low processing capacities and with AcOH in the broth calculated prices are lower than diethyl maleate current price (2.5-2.8 \$/kg). This indicates that a processing alternative using recovery of SA by esterification would open new commodity-scale market for DES. However, taking into account that DES is meant to replace maleic anhydride as feed stock for major commodities, a comparison of prices in a molar basis can provide useful information.

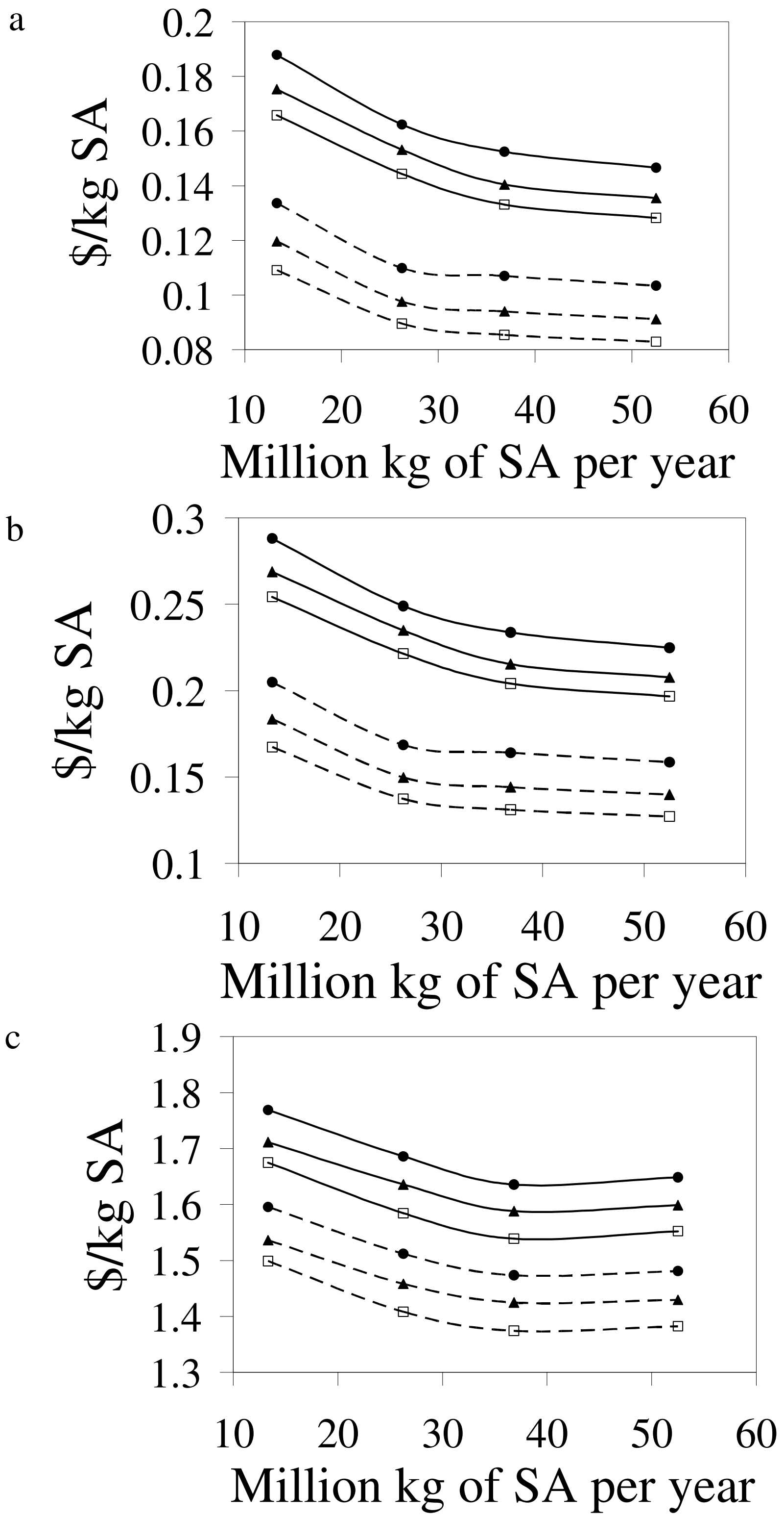

Figure 9-8. Evaluation of costs in the recovery of SA from fermentation broths by esterification with EtOH. (a) Direct costs. (b) Total capital investment. (c) Operating costs. SA concentration in the broth: (●) - 50 kg/m^3, (▲) - 70 kg/m^3, (□) - 100 kg/m^3. Fermentation broth with (continuous lines) and without (dashed lines) AcOH.

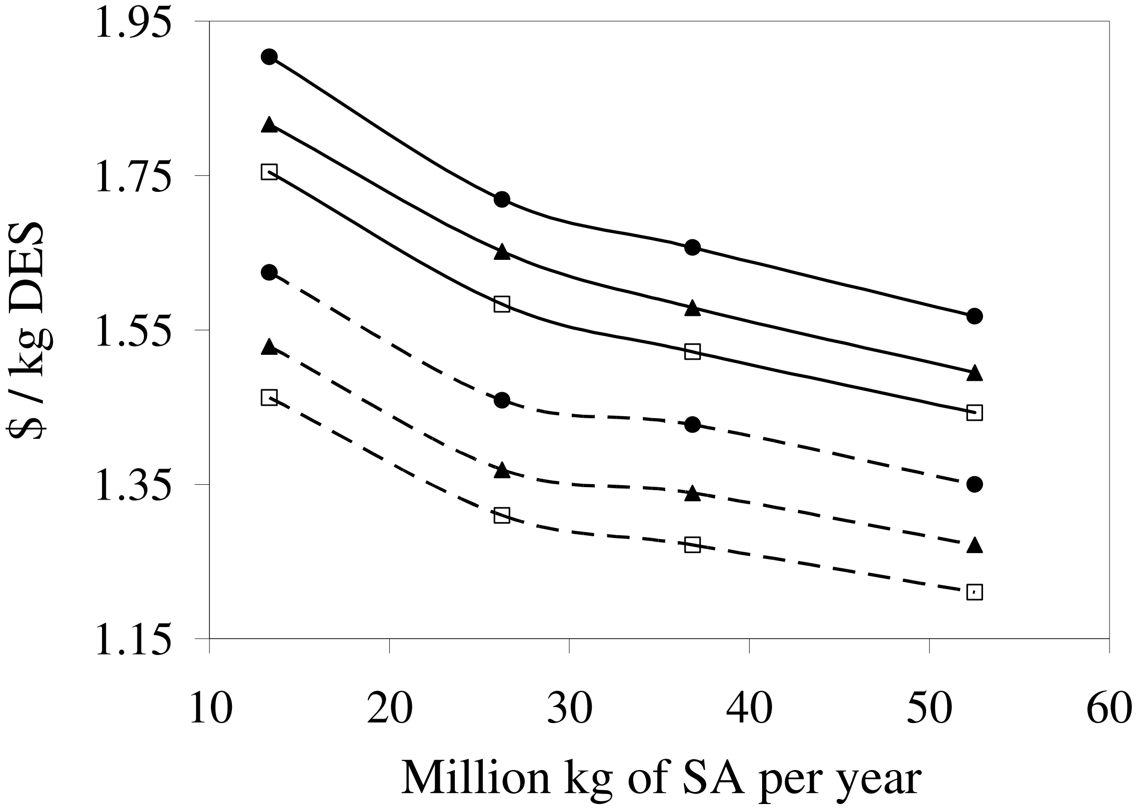

Figure 9-9. Evaluation of selling price of DES at different SA processing capacities with a ROI of 30 %. SA concentration in the broth: (●) - 50 kg/m^3, (▲) - 70 kg/m^3, (□) - 100 kg/m^3. Fermentation broth with (continuous lines) and without (dashed lines) AcOH.

For example, when DES selling price is calculated in a molar basis for a ~ 52 million kg/yr process without AcOH (1.21 $/kg = 210 $/kmol), a price slightly higher of that computed for maleic anhydride (1.78 $/kg = 174.5 $/kmol) is obtained. But taking into account that transformation of DES to other derivatives (e. g. BDO, GBL, THF) involves hydrogenolysis of the ester, two moles of EtOH are produced. Recalling that alcohol consumption plays the major role in processing costs, then EtOH liberated after hydrogenolisis can be recycled to the recovery process. This would increases efficiency and profitability of the whole process.

9.5 Conclusions

A conceptual design and economic evaluation of a process to recover SA from fermentations broths is developed. The separation involves esterification with EtOH via reactive extraction and reactive distillation to obtain DES as final product by-passing SA purification and refining. Evaluating under different production scales and considering presence of AcOH in fermentation broth, it is found that raw materials (Broth, EtOH, and H_2SO_4) are the most significant contributors to DES selling price. Even at the lower processing capacities with low concentrations of SA in the broth and including AcOH, predicted DES prices are lower than petrochemical derived diethyl maleate.

Because utilities and equipment costs have a relative minor effect in DES final price, it is expected that changes in the proposed process configuration have minor influence in overall economics. Further improvements in the model by performing energy integration and global optimization will have a positive impact on already favorable economics demonstrated for this process.

REFERENCES

9.6 REFERENCES

[1] P. Taylor. Biosuccinic acid ready for take off? Chemical world. 2010. [Online]. Available: http://www.rsc.org/chemistryworld/News/2010/January/ 21011003.asp [2010, Nov 26].

[2] D. Ruth. Bio-based succinic acid bring ‘green’ chemicals closer to the market. Medical news today. (2008) [Online]. Available: http://www.medicalnewstoday.com /articles/133890.php [Sept, 2010].

[3] M. Sauer D.Porro, D. Mattanovich, P. Branduardi. Trends Biotechnol. 26, 2 (2008) 100-108.

[4] J. Elbert. The quest to commercialize biobased succinic acid. Biomass magazine. (2007). [Online]. Available: http://www.biomassmagazine.com/article.jsp? article_id=1228 [Sept, 2010].

[5] H. Kidwell. Bio-succinic acid to go commercial. In-pharma technologist. (2008). [Online]. Available: http://www.in-pharmatechnologist.com/Materials-Formulation/Bio-succinic-acid-to-go-commercial [Sept, 2010].

[6] N. A. Collins, M. R. Shelton, G. W. Tindall, S. T. Perri R. S. O’Meadhra, C. W. Sink, B. K. Arumugam, J. C. Hubbs. Process for the recovery of organic acids from aqueous solutions. US Patent 6670505 B1. (2003).

[7] I. Fujita, K. Wada. A process for producing succinic acid. World patent application. WO 2008/010373 A1. (2008).

[8] R. Datta, D. Glassner, M. Jain, J. Vick, Fermentation and purification process for succinic acid. US Patent 5168055. (1992).

[9] C. J. King, J. Starr. Recovery of carboxylic acids from water by precipitation from organic solutions. US Patent 5104492. (1992).

[10] A. Eyal. Process and extractant composition for extracting acids. US Patent 5831122. (1998).

[11] M. Holtzapple, R. Davison, T. Luettich. Recovery of fermentation salts from dilute aqueous solutions. US Patent 6478965. (2002).

[12] D. W. Verser, T. J. Eggeman. Recovery of organic acids. US Patent Application 0256337 A1. (2005).

[13] M. Cockrem, I. Kovacs, I. Mohamednur, D. Heidel. Process for purifying an organic acid. US patent 6641734 B2. (2003).

[14] T. Kushiku, K. Fujiwara, T. Satou, C. Sano. Method for purifying succinic acid from fermentation broth. US Patent Application 0276674 A1. (2006).

[15] K. Berglund. Carboxylic acid purification and crystallization process. US patent 5034105. (1991).

[16] D. Glassner, R. Datta. Process for the production and purification of succinic acid. US Patent 5143834. (1992).

[17] R. Datta, S. P. Tsai. Esterification of fermentation derived acids via pervaporation. US Patent 5723639. (1998).

[18] M. C. Cockrem. Process for the production of organic acids and esters thereof. US Patent 6291708 B1. (2001).

[19] D. Dunuwila. Process for the direct production of esters of carboxylic acids from fermentation broths. Canadian patent application 02657666. (2009).

[20] C. Bauduin, W. Fischer, R. Pinkos, E. Scholten. Method of producing a carboxylic alkyl ester. US patent application 0137825 A1. (2009).

[21] S. Varadarajan, D. J. Miller. Biotechnol. Prog. 15, 5 (1999) 845-854.

[22] A. Orjuela, A. Yanez, C. T. Lira, D. J. Miller. Carboxylic Acid Recovery from Fermentation Solutions. US Patent application. Filed 2009.

[23] J. G. Zeikus, M. K. Jain, P. Elankovan. Appl. Microbiol. Biotechnol. 51 (1999) 545-552.

[24] L. Agarwal, J. Isar, R. Saxena. J. Biochem. Biophys. Methods 63 (2005) 24-32.

[25] H. Song, S. Y. Lee. Enzyme Microb. Technol. 39 (2006) 352-361.

[26] A. Orjuela, X. Hong, A. Kolah, C. T. Lira, D. J. Miller. Diethyl succinate synthesis by reactive distillation. In revision. 2010.

[27] A. Orjuela, A. Kolah, C. T. Lira, D. J. Miller. Mixed succinic acid/acetic acid esterification with ethanol by reactive distillation. In revision. 2010.

[28] A. Tuchlenski, A. Beckmann, D. Reusch, R. Düssel, U. Weidlich and R. Janowsky. Chem. Eng. Sci. 56 (2001) 387-394.

[29] S. Schoenmakers, B. Bessling. Chem. Eng. Proc. 42 (2003) 145 -155.

[30] R. Hiwale, N. Bhate, Y. Mahajan, S. Mahajani. Int. J. Chem. React. Eng. Review R1. 2 (2004) 1-52.

[31] G. Jam Harmsen. Chem. Eng. Process. 46, 9 (2007) 774-780.

[32] A. Orjuela, A. J. Yanez, L. Peereboom, C. T. Lira, D. J. Miller A novel process for recovery of fermentation-derived succinic acid. In revision. 2010.

[33] Y. Tang, H. Huang, I. J. Chien. Chem. Eng. Japan. 36, 11 (2003) 1352-1366.

[34] A. Kolah, N. Asthana, D. Vu, C. T. Lira, D. J. Miller. Ind. Eng. Chem. Res. 47 (15) (2008) 5313-5317.

[35] A. Orjuela, A. J. Yanez, D. Vu, D. Bernard-Brunel, D. J. Miller, C. T. Lira. Fluid Phase Equilibr. 290 (1-2) (2010) 63-67.

[36] A. Orjuela, A. J. Yanez, P. Rossman, D. Vu, Bernard-Brunel, D. J. Miller, C. T. Lira. Fluid Phase Equilibr. 290 (1-2) (2010) 68-74.

[37] A. Orjuela, A. J. Yanez, J. Evans, D., D. J. Miller, C. T. Lira. Phase equilibria in binary mixtures with monoethyl succinate. In revision. (2010).

[38] A. Orjuela, A. J. Yanez, J. A. Lee, D. J. Miller, C. T. Lira. Solubility and phase equilibria for mixtures with succinic acid. In revision. (2010).

[39] A. Orjuela, A. J. Yanez, C. T. Lira, D. J. Miller. Kinetics of mixed succinic acid/acetic acid esterification with Amberlyst 70 ion exchange resin as catalyst. Submitted. Appl. Catal. A. (2010).

[40] E. Hugot. Handbook of cane sugar engineering. 3rd, completely rev., ed. Elsevier; New York, NY, 1986, p. 588- 595.

[41] L. Götze, O. Bailer, P. Moritz, C. von Scala. Catal. Today 69 (2001) 201–208.

[42] J. Sieres, J. Fernández-Seara. Int. J. Refrig. 30 (2007) 58-67.

[43] Sulzer Chemtech. (2010) Structured packings for distillation, adsoption, and reactive distillation. [Online]. Available: http://www.sulzerchemtech.com/ portaldata/11/ Resources//brochures/mtt/Structured_Packings_April_2010.pdf [2010, Nov 1].

[44] S. M. Walas. (1990) Chemical process equipment - selection and design. Elsevier. [Online]. Available: http://knovel.com.proxy1.cl.msu.edu/web/portal/browse /display?_EXT_KNOVEL_DISPLAY_bookid=401&VerticalID=0

[45] ICIS. Chemical price reports. [Online]. Available: http://www.icispricing.com [2010, July].

[46] ICIS. ICIS Heren. [Online]. Available: http://www.icis.com/heren/ [2010, July].

[47] M. S. Peters, K. D. Timmerhaus, R. E. West. (2003). Plant design and economics for chemical engineers. 5th ed. McGraw-Hill. New York, NY.